ETHYLENE-PROPYLENE-DIENE TERPOLYMER/HEXAFLUOROPROPYLENE-VINYLIDINEFLUORIDE ELASTOMERIC COMPOSITES: THERMAL, MECHANICAL AND MICROWAVE PROPERTIES

Thesis submitted to

Cochin University of Science and Technology

in partial fulfilment of the requirements

for the award of the degree of

Doctor of Philosophy

Ajalesh B Nair

Department of Polymer Science and Rubber Technology

Cochin University of Science and Technology

Kochi- 682 022, Kerala, India

July **2013**

Ethylene-Propylene-Diene Terpolymer/Hexafluoropropylene-Vinylidinefluoride Elastomeric Composites: Thermal, Mechanical and Microwave Properties

Ph. D Thesis

Author

Ajalesh B Nair
Department of Polymer Science and Rubber Technology
Cochin University of Science and Technology
Cochin- 682 022, Kerala, India
E-mail: ajilesh4kannan@gmail.com
ajilesh@cusat.ac.in

Supervising teachers:

Dr. Rani Joseph
Professor (Emeritus)
Department of Polymer Science and
Rubber Technology
Cochin University of Science
and Technology (CUSAT)
Cochin- 682 022, Kerala, India
E-mail: rani@cusat.ac.in

Dr. Philip Kurian
Professor
Department of Polymer Science and
Rubber Technology
Cochin University of Science
and Technology (CUSAT)
Cochin- 682 022, Kerala, India
E-mail: pkurian@cusat.ac.in

July 2013

Department of Polymer Science and Rubber Technology
Cochin University of Science and Technology
Cochin- 682 022, Kerala, India

Certificate

This is to certify that the thesis entitled **"Ethylene-Propylene-Diene Terpolymer/Hexafluoropropylene-Vinylidinefluoride Elastomeric Composites: Thermal, Mechanical and Microwave Properties"** is a report of the original work carried out by **Mr. Ajalesh B Nair** under our supervision and guidance in the Department of Polymer Science and Rubber Technology, Cochin University of Science and Technology, Cochin-22. No part of the work reported in this thesis has been presented for any other degree from any other institution.

Prof. Philip Kurian   *Prof. Rani Joseph*
(Supervising Teachers)

Cochin-22
15/07/2013

Declaration

I hereby declare that the thesis entitled **"Ethylene-Propylene-Diene Terpolymer/Hexafluoropropylene-Vinylidinefluoride Elastomeric Composites: Thermal, Mechanical and Microwave Properties"** is the original work carried out by me under the supervision of **Prof. Rani Joseph** and **Prof. Philip Kurian,** Department of Polymer Science and Rubber Technology, Cochin University of Science and Technology, Cochin-22 and has never been included in any other thesis submitted previously for the award of any degree.

Cochin – 22   *Ajalesh B Nair*
15/07/2013

Dedicated to

My beloved Parents and
my teachers ....

Acknowledgements

This thesis is a culmination of a perfect working relationship with my supervisors, Prof. Rani Joseph and Prof. Philip Kurian, to whom I am eternally greatful. I specially remember Prof. Rani Joseph for her warm encouragement, precious advice and thoughtful guidance. Her dedication to research really motivated me to achieve my goals. Teacher, you have always encouraged and supported as being my mother. I wish to express my gratitude and love to you, teacher.

I will forever be thankful to Prof. Eby Thomas Thachil, former head of the Dept. of PS&RT, for his invaluable help all through this work. I am grateful to Prof. Sunil Narayanan Kutty, Head of the Department, Polymer Science & Rubber Technology, for giving necessary facilities and support during the research.

I would like to express my sincere thanks to Prof. K .E George, Prof. Thomas Kurian and Dr. Jayalatha Gopalakrishnan for their whole hearted cooperation throughout my research work. I express my gratitude to all the teaching and non-teaching staff of Department of Polymer Science & Rubber Technology for their support during these years.

My sincere gratitude is reserved for Dr. Susamma A. P (Department of Chemistry, Maharajas College, Eranakulam) and Dr. Beena T Abraham (Department of Chemistry, S N M College, Maliankara) for their support and motivation. I also convey my deep gratitude to Dr. Sreekala M S (Department of Chemistry, Sree Sankara College, Kalady) for her valuable help, support, encouragement, advice and suggestions.

I am grateful to Prof. C K Anandan, Department of Electronics, for providing necessary facilities to carry out my work there. I am greatfully indebted

Preface

In the manufacture of rubber products, blending of rubbers produces new materials with a wide range of applications because they have the potential to combine the attractive properties of both the constituents in the blend, when compared with the economical and technical uncertainties associated with synthesizing new polymeric materials. Ethylene-propylene-diene monomer rubber (EPDM) and fluorocarbon rubber (FKM) has been getting much attention over the years due to their excellent properties. In this work blends of EPDM and FKM were extensively studied in order to achieve more suitable elastomer materials which have better properties. However, the high incompatibility between FKM and EPDM make it difficult to obtain a blend with better overall properties. The properties of blends depend strongly on the compatibility of the polymers. The compatibility of EPDM and FKM rubbers is examined with the addition of maleic anhydride grafted EPDM (MA-g-EPDM) as compatibilizer.

Polymer composites find wide applications in various industrial sectors because of their light weight, design flexibility and processability. In this work, attention was paid to evaluate the effect of different flame retardant fillers on the properties like reinforcement, physico-mechanical, solvent transport properties and flammability of EPDM, FKM and their blend vulcanizates. One factor of great importance to be taken into consideration when formulating a rubber compound containing flame retardant filler is to compromise between the original physical and mechanical properties of the rubber and the modified combustion characteristics.

In the present study, an attempt has been made to prepare composites by incorporating expanded graphite fillers in insulating elastomer matrices and to study its DC electrical conductivity, dielectric properties and electromagnetic shielding characteristics, in addition to evaluating the mechanical properties. Recently, electronic devices and components have been rapidly developing and advancing. Thus, with increased usage of electronic devices, electromagnetic waves generated by electronic systems can potentially create serious problems such as malfunctions of medical apparatus and industry robots and can even cause harm to the human body. Therefore, in this work the applicable utility of the prepared composites as electromagnetic interference (EMI) shielding material are also investigated.

The dissertation includes nine chapters:

Chapter 1 gives an introduction to elastomers, fillers, polymer blends and composites, effect of fillers on vulcanizate properties and a review of the literature related to polar/non-polar rubber blends. Objectives of the present work are also discussed at the end of this chapter.

Chapter 2 is devoted to a complete description of the materials used in the present work and the experimental techniques employed for the preparation and characterization of the blends and composites. The instruments used are also discussed.

Chapter 3 describes preparation, processability and mechanical properties of non-compatibilized and compatibilized EPDM/FKM blends. The effect of blend ratio and compatibilizer loading on cure characteristics, physico-mechanical properties, dynamic-mechanical, solvent sorption, thermal analysis and phase morphology of the blends are also included.

Chapter 4 reports the effect of different fillers like aluminium hydroxide, chlorinated polyethylene, decabromobiphenyl oxide and expanded graphite on cure behaviour, reinforcement, stress-strain properties, transport mechanism of solvent, filler dispersion and morphological features of the oil-extended EPDM based composites. The thermogravimetric analysis and flammability studies of the composites are also presented.

Chapter 5 includes the preparation of elastomer composites of compatibilized and non-compatibilized EPDM/FKM blends and expanded graphite by mill mixing. The tensile properties, thermal stability, limiting oxygen index, DC electrical conductivity and morphological characteristics of the elastomer composites are described. The AC conductivity, dielectric permittivity, dielectric loss, heating coefficient, absorption coefficient and skin depth of the composites are also investigated.

Chapter 6 focused on the reinforcing effect of aluminium hydroxide in EPDM and FKM rubber. The effect of aluminium hydroxide on cure characteristics, strain-sweep studies, tensile properties (effect of aging), filler dispersion, flammability, thermal stability, kinetics of thermal decomposition and dynamic mechanical analysis of both rubbers is discussed. This chapter also examines the dielectric properties of the composites at microwave frequencies.

Chapters 7 describe the effect of chlorinated polyethylene, decabromobiphenyl oxide, aluminium hydroxide and antimony trioxide on EPDM/FKM blends respectively. This chapter describes the cure characteristics, mechanical properties, thermal stability, flammability and morphology of the composites.

Chapter 8 divided into part A and part B. The part A reports the cure characteristics, tensile properties, thermal stability, flammability and morphological features of the prepared EPDM and EPDM/FKM based profiles. The electromagnetic interference shielding efficiency of the composites is presented in part B.

Chapter 9 is the summary and conclusion, future outlook of the study.

Contents

Chapter -2
MATERIALS AND METHODS ....69 - 97

Chapter -5

EFFECT OF EXPANDED GRAPHITE ON THERMAL, MECHANICAL AND DIELECTRIC PROPERTIES OF EPDM/FKM RUBBER BLENDS

Chapter -8

Chapter -8 Part A

**APPLICATION STUDIES OF THE COMPOSITES BASED ON
EPDM AND EPDM/FKM BLENDS- INSULATION PROFILES**.................. **287 - 299**

Chapter -8 Part B
APPLICATION STUDIES OF THE COMPOSITES BASED ON
EPDM AND EPDM/FKM BLENDS- EMI SHIELDING .... 301 - 315

Chapter -9
SUMMARY AND CONCLUSIONS .... 317 - 323

List of Abbreviations and Symbols

List of Publications

Curriculum Vitae

.....౮౯.....

Chapter 1

INTRODUCTION[*]

Contents

1.1 Elastomers
1.2 Fillers in rubber industry
1.3 Effect of fillers on vulcanizate properties
1.4 Composites
1.5 Polymer blends
1.6 Review of some polar/non-polar rubber blends
1.7 Scope of the present work
1.8 Objectives of the present work

This chapter gives an introduction of the elastomers used, their blends and composites. Polymer blends are gaining technological importance due to their compromise set of properties, advantages in processing and reduction in cost. The recent developments in the blend and composite technology are included. This chapter also focuses on the effect of fillers on vulcanizate properties like reinforcement, solvent swelling and diffusion, dynamic mechanical property, thermal stability, flammability and microwave properties. The potential applications of the composites are mentioned. The scope and objectives of the present work are also presented.

---

[*] Ajalesh Balachandran Nair, Rani Joseph. Polymer blends and composites from non-polar/polar systems. *Journal of Rubber Research*, Indian Rubber Board, India (in press).

1.1 Elastomers

Elastomers form a special category of polymeric materials characterized by unique combination of useful properties such as elasticity, flexibility, toughness and impermeability. They are commonly known as rubbers and always show a large elongation at break. The most important ingredient of a polymer composite is the base polymer matrix. This may be natural or synthetic rubber or their blends depending on the service requirement of the products.

1.1.1 Ethylene-propylene-diene monomer rubber (EPDM)

In EPDM terpolymers, ethylene and propylene monomers provide a saturated backbone and non-conjugated diene monomers provide un-saturations. EPDM is an amorphous material and exhibit weak mechanical properties [1]. Mechanical properties of EPDM can be improved by the addition of reinforcing fillers [2]. One of the most important characteristic of EPDM is its ability to accept large amounts of fillers, extender oils and other additives without affecting processability with any significant tolerance to the final properties [3]. EPDM is a rapid growing synthetic rubber used in many industrial applications and it is more stable than other conventional elastomers.

Different grades EPDM are available depending on the ratios of ethylene, propylene and diene. The selection of particular grade of EPDM depends upon on the properties of the final product. Different ratios of monomers grant different characteristics to EPDM [4]. The effect of the ethylene and propylene content on the glass transition temperature (Tg) and on the crystallinity of EPDM was investigated by Berdan and Verstrata

et al. [5, 6]. They reported that Tg of EPDM varied with the content of the ethylene and propylene in a non-linear way and generally increased with increase of propylene content. Crystallinity of the EPDM increases with increase of ethylene content and decreases with that of propylene content [5-7]. High crystallinity associates with good mechanical properties and that is why high ethylene content provides good green strength to EPDM [8, 9]. On the other hand, high propylene content results low hardness EPDM, with more flexibility at low temperature and more elasticity [10]. Allen et al. reports that ethylene content also enhances the cross linking efficiency of the EPDM [11]. EPDM with high ethylene content is the best candidate for thermal insulator in space applications [12].

In EPDM, a third monomer is incorporated to add un saturation to the polymer. These are normally non-conjugated dienes. Non-conjugated dienes are incorporated for creating un saturation in EPDM are 5-ethylidene-2-norbornene (ENB), 1, 4-hexadiene (HD) and dicyclopentadiene (DCPD). These conjugated dienes take advantage of one double bond during copolymerization with ethylene and propylene while reserve the other in the side chain of EPDM for sulfur vulcanization. Generally, increase in diene content increases the rate of vulcanization. The amount of diene added ranges from 0.5 to 12 weight percentage [11]. Because of the difference in structures, different types of dienes provide different properties to EPDM. The most widely used one is EPDM with ENB as diene-monomer.

The important properties of EPDM are excellent ozone resistance, ability to accept large amounts of fillers, very good resistance to heat, oxygen and ozone. The third monomer enables EPDM to be cross linked by

conventional sulfur vulcanization, little moisture adsorption, excellent weathering resistance and resistance to polar chemicals. EPDM compounds have a low temperature flexibility compared with that of natural rubber compounds. EPDM's non-polarity gives it excellent electrical insulation. The heat resistance of EPDM compounds is much better than that of the other rubber types.

The selection of the fillers in EPDM recipe depends on the end use. Elastomers interact with fillers in presence of accelerators and curing agent. These interactions range from strong chemical reactions such as reactive grafting to weak physical interactions such as adsorption [13]. During interaction, elastomer chains adsorb on the active sites of the fillers due to covalent bonds and vander waal forces resulting a thin layer at the polymer-filler interface, which has properties different from the matrix [14]. The final properties of the composites depend on these interactions.

Generally it is accepted that the addition of reinforcing fillers results in an increase in mechanical properties of the composites if properly added [15]. The lists of properties which can be influenced by fillers are [16]: density, colour, optical properties, surface properties, thermal conductivity, electrical and magnetic properties, permeability, mechanical properties, chemical reactivity, rheology and morphology. Fillers can also influence on the compound cost.

Vulcanization of EPDM

Vulcanization produce chemical links between the polymeric chains to form a network, thereby transforming the material from a viscous liquid to a tough elastic solid of permanent shape with no plastic deformation zone [17].

Sulfur is the first and most widely used vulcanizing agent for rubber containing dienes in their structure since its discovery by Goodyear in 1839 and subsequently by John Hancock in 1843 [18]. These diene containing elastomers are vulcanized by sulfur in the presence of the organic activators and accelerators with the application of heat [18]. Two types of vulcanization systems are available for the rubber cross linking: sulfur vulcanization and peroxide vulcanization.

The choice of vulcanization system depends on the main structure of the rubber. Polymers having unsaturations in their structure can be cross linked by sulfur as well as by peroxides. However, polymers containing no unsaturation in their structure cannot be cross linked by sulfur. However, majority of rubbers are modified for sulfur cross-linking because of simplicity and ability to form cross link chains of various length and distributions [19].

Applications of EPDM

EPDM is one of the most widely used "speciality" rubber, with a variety of applications as single ply roofing, automotive parts, wire and cable covers, and in other goods that require heat and weather resistance. The main uses of EPDM are in automotive applications such as profiles, (radiator) hoses, and seals. It is used in building and construction as profiles, roof sheeting and seals, and for electrical purposes like cable insulation and jacketing. Furthermore, EPDM is used in blends with general-purpose rubbers. Considerable amounts of EPDM are also used in blends with thermoplastics, e.g; as impact modifier for polyamides, polystyrenes and particularly polypropylene. These products are used in many exterior automotive applications such as bumpers and body panels.

One of the most important applications of filled EPDM composite is to be used as internal thermal insulator for space vehicles where it protects structures from high heat flux by ablation.

1.1.2 Fluorocarbon rubber (FKM)

For more than fifty years, fluoroelstomers (FKM) have benefited the world in several ways. The FKM rubbers, though very expensive and elastomers of last resort, have been of critical importance in aerospace, automotive, chemical and petroleum industries. Their success has led to the development of related products often superior in selected special uses. The FKMs are highly specialized products that as a class show the best resistance of all rubbers to the attack of heat, chemicals and solvents. The first copolymer of FKM, VF_2 (vinylidine fluoride) with chlorotrifluoroethylene (CTFE) [20], which is later known as Kel-F. Secondly a batter copolymer was made with VF_2 and hexafluoropropylene (HFP) [21] and then an even more thermally stable and more solvent resistant terpolymer VF_2/HFP/(Tetra fluoroethylene) TFE [22]. These products are now known as 'Viton A' (copolymer) and 'Viton B' (terpolymer). After the spectacular success in military planes, the VF_2/HFP polymers gradually moved into civilian application in the petroleum and process industries, where their high value-in-use becomes apparent.

The major VF_2/HFP and VF_2/HFP/TFE elastomers are usually prepared by radical polymerization in emulsion using peroxy compounds such as ammonium persulfate as initiator, occasionally in redox systems with or without chain transfer agents such as carbon tetrachloride (CCl_4), alkyl esters, or halogen salts. Product is sold in the form of pellets, chips,

strips and slabs, which are translucent, white, or slightly coloured depending on the presence of compounding agents used.

Compounding and processing of fluoroelastomers

A typical fluorocarbon rubber formulation contains curing ingredients, acid-acceptors, fillers, processing aids, release agents, colours etc depending on the proposed applications. In general, curing is effected with agents that remove hydrogen fluoride (HF) to generate a cure site that reacts with a diamine [23], or a bisphenol [24], or with organic peroxides [25] that promote a radical cure by hydrogen or bromine extraction. Preferred amines are blocked diamines such as hexamethylene diamine carbamate (Diak No. 1) or bis (cinnamylidene) hexamethylenediamine (Diak No. 3). Preferred phenols are hydroquinone and the bisphenols such as 4, 4'-isopropylidene bisphenolmor the corresponding hexafluoro derivative, bisphenol AF. The preferred accelerator is quarternary phosphonium salt, benzyltriphenylphosphonium chloride. The crosslinking mechanism of fluoroelastomer in presence of bisphenol and phosphonium compounds is given in scheme 1 [26]. This cure system make the reaction environment highly alkaline and the alkaline environment is necessary to promote the formation of diphenolate anion as a crosslinking precursor, which is shown in scheme 1.2 [26]. Due to highly reversible nature of crosslinking reaction, there is a tendency of the crosslinking product being immediately scavenged by the calcium hydroxide (scheme 1).
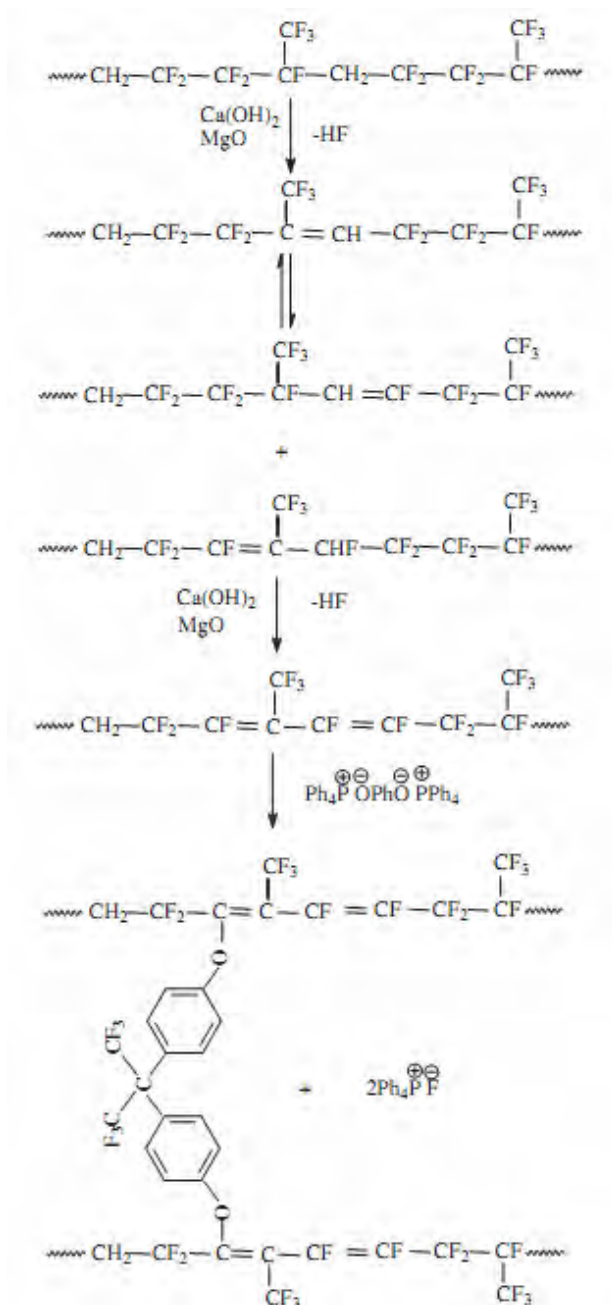
Scheme 1.1 Crosslinking mechanism of fluoroelastomers in presence of bis-phenol and phosphonium compounds [26]
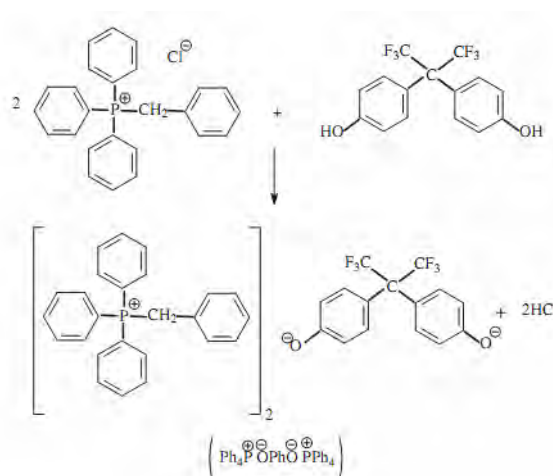
Scheme 1. 2. Formation of di-phenolate anion by the interaction of diphenol and a phosphonium salt [26].

Acid acceptors are necessary in compounded FKMs since they serve to neutralize HF generated during the cure or on extended aging at high temperatures. The most commonly used materials are magnesium oxide (MgO), calcium oxide (CaO), calcium hydroxide [$Ca(OH)_2$] etc.

Various carbon blacks and mineral fillers used in fluorocarbon elastomers to confer special properties are MT black, austin black, SRF black, barium sulphate ($BaSO_4$) etc.

The processing characteristics of fluorocarbon rubber compounds can be improved by the addition of plasticizer. Particularly effective aids are the high molecular weight hydrocarbon esters such as dioctyl phthalate (DOP), pentaerytritol stearate (PET), carnauba wax and low molecular weight polyethylene. They ensure smoother extrusions, and better die definition and mould release. The low viscosity FKM rubbers are also often used to facilitate processing without compromising properties.

Fluorocarbon elastomers may be processed using different experimental techniques like mill mixing, banbury mixing etc. Extrusion of FKM is widely practiced to produce finished goods and reforms. Most of the FKM group of fluoroelastomers (VF_2/HFP copolymers and terpolymers) can be calendared. Fluorocarbon rubbers can be easily moulded by compression, transfer or injection process.

Physical properties of FKM

The FKMs are extremely stable, excelling all rubbers in over all resistances to combinations of heat, light, ozone, solvents and aggressive chemicals. They also show low compression set at high temperature. FKM vulcanizates are considered serviceable almost indefinitely when exposed continuously up to 200^0C. The most important market for fluorocarbon elastomers is in seals and O-rings, for which compression set resistance has proved to be the best criterion of service performance. As a result of the discovery of the phosphonium chloride accelerator system for bisphenol and other phenol cures, excellent results are readily obtained with FKM. Compression set resistance is strongly affected by the filler. MT blacks provide the best overall balance of tensile properties and heat and compression set resistance. The commercial FKM elastomers have brittle points of about -25^0C to -40^0C, which are not easily improved by compounding. Plasticizers tend to harm heat stability and accelerate deterioration on aging since they are less stable than fluoropolymers. Peroxide curable fluorocarbon rubbers can be blended with fluorosilicones to improve low-temperature flexibility, but at the sacrifice of high temperature stability and solvent resistance.

Applications

Fluoroelastomers meet the need of the aerospace industry as a high-performance seal elastomer. The use of fluoroelastomers has expanded to too many other industries, especially the automotive, fluid power, appliance sectors, and many chemical fields. In general, all highly fluorinated polymers are very stable and possess exceptional resistance to oxygen, weather, flame, chemical attack and swelling in a wide range of liquids. FKM rubbers are available in various grades, which differ mainly in the polymer composition and fluorine content. In combination with the cure system (diamines, bisphenol or peroxides) the properties of the compound can be influenced to meet the requirements of the application. In general FKM has an outstanding resistance to high temperatures; its elastomeric properties in hot air are maintained up to 204°C with peak temperatures up to 300°C. FKM elastomers exhibit excellent resistance to swelling in a wide variety of oils, fuels, solvents and chemicals. The fluorocarbon rubbers are widely used in critical applications demanding their unmatched heat and fluid resistance. They also enjoy significant usage as binders for military fuels (in propellants), as processing aids for low density polyethylene, in oil-field applications, and in coatings and sealants.

1.2 Fillers in rubber industry

Fillers, especially particulate fillers are widely used in rubber industry. They are broadly classified as reinforcing and non-reinforcing depending on the properties of the final product.

1.2.1 Non-reinforcing fillers

Fillers such as calcium silicate and chalk powder, which can only lead to small increase in the viscosity of the compound and causes deterioration of the mechanical properties of the vulcanizate, and do not exhibit any reinforcing action are called non-reinforcing or inactive fillers. These are often termed as extenders, which are used to reduce the cost of production of rubber goods. Other non-reinforcing fillers are calcium carbonates, barites (barium sulphate), mica, titanium dioxide (TiO_2) and silicates of calcium and zinc.

1.2.2 Reinforcing fillers

The basic feature that distinguishes reinforcing fillers from non-reinforcing is enhancement of performance characteristics of the composite. Reinforcement in vulcanized rubber can be defined as simultaneous increase in stiffness and resistance to fracture by the addition of filler. A broader definition of reinforcement in rubber industry is "the improvement in abrasion, tear, cutting and rupture resistance, and stiffness of the vulcanized compounds". Particulates like carbon blacks and silica are the most widely used reinforcing fillers in rubber industry.

1.3 Effect of fillers on vulcanizate properties

The use of rubber is mainly dependent on its unique combination of dynamic mechanical and physical properties such as strength, flexibility, wear and tear, electrical, thermal properties, flammability etc. coupled with the fact that these properties can be varied within wide limits to suit the need. Consequently the measurement of these properties plays a vital role in the assessment of product performance and the way in which this is altered by external conditions [27].

1.3.1 Reinforcement

Reinforcement of vulcanized rubber, defined as simultaneous increase in stiffness and resistance to fracture by the addition of particulate filler, is one of the most important phenomena in material science and technology [28].

The performance and service life of rubber goods are markedly improved by the incorporation of the reinforcing fillers most notably carbon black. Stiffness at moderate strain increases with the so called structure of carbon black while fracture resistance generally increases with decreasing particle size and increased specific surface area. The mechanism of increased stiffness in carbon black filled elastomers is well understood [29, 30]. There is no clear explanation or mechanism for enhancement of the elastic modulus due to filler addition by one simple theory, since several interactions and many different length scales are involved [31].

Reinforcement of polymer nanocomposites is affected by the size, shape and spatial distribution of the filler particles. Experimental studies have shown that, while the addition of nanoparticles results in a large increase in the yield stress and the 'energy to break' for polymeric materials that are above Tg [32, 33], only very modest reinforcement is observed for polymeric materials that are below Tg [34]. These results appear to contradict existing molecular models of reinforcement of polymer matrices by conventional fillers, which assume that the reinforcing properties of the filler result only from the stiffening of the polymer matrix due to the attraction between the filler and the polymer [35, 36].

1.3.2 Solvent swelling and diffusion

Rubber, when it is in the unvulcanized form gets dissolved in a good solvent, but when it is a vulcanized or crosslinked sample it can only swell. Swelling of rubber in a solvent is affected by incorporation of filler [37]. The percentage swelling decreases with increase of filler content. In the case of reinforcing filler, strong rubber-filler interaction will have some effect on the apparent crosslink density of the system. Ratio of the restriction of swelling of the filled rubber vulcanizate to that of the gum rubber is used as a means for evaluating the reinforcing ability of filler in rubber.

Permeation is the passage of solvent substance through a non-porous solid. The permeation rate depends on the chemical structure and the morphology of the polymers, on the temperature and the size of the diffusing molecules. Observations of the physical-chemical aspects of permeation media through a polymer matrix allow the description of this process by three distinctive stages [38-40].

1)   Absorption of the permeate in the polymer matrix on the side with the higher medium concentration.

2)   Diffusion process in which the substance is transported through the polymer matrix in the direction of lower concentration.

3)   Desorption of permeates from the surface of the polymer matrix on the lower concentration side

The first stage makes evident the necessity of low swelling for low permeation. This condition is met if the chemical compatibility between

permeates and polymer matrix is low. This means that the difference in the solubility parameters of the components involved is sufficiently high and the Flory-Huggin's interaction parameter 'χ' has a relatively high value [41, 42, 43]. After swelling a state of equilibrium is reached, a stationary state with an oriented substance transport through the polymer matrix that is attained in the second stage of the permeation process. In the second stage, the transport process involves diffusion.

Diffusion is a molecular process in which the molecules float because of random thermal motion from a region with higher concentration to one of lower concentration. The transport of a solvent into a rubber is a similar process. When a piece of rubber is immersed in a solvent, the surface layers immediately absorbs the liquid in early stages and with increasing time, the solvent penetrates further and further into the bulk of the material until equilibrium is reached in which the solvent is uniform everywhere throughout the rubber. The movement of the solvent obeys the law of diffusion. The speed of movement is characterized by the diffusion coefficient of the solvent in rubber. The diffusion coefficient and the permeation rate respectively are significantly influenced by several factors like the nature of the polymer; concentration, shape and size of the penetrating molecules [44], temperature [45], filler [46] and nature of penetrate [47]. Besides its reinforcing ability, filler is founded to have a great influence on diffusion and permeation in polymers. Addition of filler in rubber compound represents a more cost effective method to reduce permeability. The transport process through fluoroelastomers indicated that the permeability and diffusivity of solvent through the polymer matrix were lowered by the addition of filler [46].

The vulcanization process involves the conversion of raw rubber into a network due to the formation of crosslinks, chemical bonds or bridges that associate the rubber macromolecules [48]. Through vulcanization the rubber elasticity is increased meanwhile its plasticity is reduced. The crosslink atoms usually employed are sulphur [49] due to its lower cost and its better control during the vulcanization process in comparison with other vulcanizing agents used such as organic peroxides [50] and metal oxides. During vulcanization with sulphur [51] crosslinks in the form of $—S_X—$ (X= 1, 2 .....) between the carbon atoms of the different rubber molecules with different length of the sulphur chains will be formed. The amount of mono, di and polysulfidic crosslinks present in the networks is calculated from the crosslink concentrations per unit volume (crosslink density). The information about the crosslink density and especially $—S_X—$ distribution offers the possibility to optimize the curing conditions, to produce new products with better mechanical and aging properties.

The experimental techniques used for the determination of crosslink density are mainly swelling studies based on the theory of Flory-Rehner [43], mechanical tests analyzed by Mooney-Rivlin method [52], magnetic resonance techniques [53], and high resolution ^{13}C-NMR MAS solid-state spectroscopy [54].

1.3.3 Dynamic mechanical properties

Dynamic mechanical analysis is used along with other techniques to measure miscibility of blends. It is thus a most powerful technique for studying the effect of molecular structure and also phase morphology on the properties required in component design. The principles and methods of investigating the dynamic mechanical properties have been discussed in

detail in many reviews [55, 56]. In a typical DMA study of polymers, the mechanical response of the specimen is tested as a function of operating variables like temperature, frequency and strain and material variables like type and extent of crosslinking, type of filler and its loading etc. In the DMA, measurements of polymers are conducted over a range of frequency at a constant temperature (isothermal) or over a temperature range at constant frequency (isochronal). The data obtained from isochronal testing is useful to study the various relaxations of the polymers. Isochronal testing also gives data regarding the storage and loss modulus which can be a direct measure of the reinforcement of filler in the polymer matrix. Rubbers are normally tested from a temperature lower than their glass transition temperature to about 100^0C. As the temperature decreases, the resistance to molecular motions in polymer increases which leads to higher storage modulus. The effect of frequency on dynamic mechanical relaxation of polymers has received attention as compared to isochronal studies, mainly due to non availability of large frequency experimental setups. The non-linear dynamic mechanical properties of elastomers filled with carbon black have been investigated by Payne [57], but the mechanisms for reinforcement and non linearity remain controversial. A widely held view is that filler agglomeration and network formation are responsible for the high levels of reinforcement and that deagglomeration and network breakdown are responsible for the nonlinearity with strain [58, 59]. There is a substantial evidence to suggest that the agglomeration and percolation do occur in filled elastomers and that the filler structures are highly dependent on the particular filler and the mixing method used for composite preparation.

1.3.4 Thermal stability and flammability

Increasing temperature of a polymer, results in the thermal excitation of the covalent bonds in polymer chains. Once a critical temperature is reached, it starts decomposing and produces small molecules in the gaseous phase. The decomposed small molecules evaporate, diffuse into the flame zone above the polymer/air interface and mix with air to form a flammable mixture. When the concentration of this mixture and the system temperature crosses the flammability limit, it starts to burn. A part of the exothermic heat that results from the burning process is fed back to the condensed phase and accelerates the degradation of the polymer, producing more volatile fragments and sustaining the combustion cycle.

The flammability of polymeric materials presents a threat to both the integrity of the product and to human health. Therefore, the search for an appropriate fire retardant or inherently non-flammable compounds represents a major scientific challenge. In this respect, it is essential to know the structural and energetic features that influence the thermal stability and flammability of polymers. Flammability is associated with the formation of flammable gaseous decomposition products during the initial decomposition. However, the decomposition rate and extent of decomposition is controlled by the amount of flame propagation. It is understood that fire resistant products might be prepared by incorporating thermally stable structural units that either do not decompose easily or even if they decompose, produce non-combustable products.

Nowadays, more and more attention is being paid to improve the flame retardant properties of polymers as it is an essential requirement for applications like wire and cables, polymer foams in different household stuffs

such as upholstered furniture and mattresses, aircraft interiors, fire-resistant coatings, profiles and clothes, etc. The driving forces for the development of flame retardant polymers include increasing safety awareness of consumers, environmental pollution generated during burning, and economic loss incurred due to burning of materials. The main approaches taken are to incorporate flame retardants either as additives or to incorporate reactive flame retardants into the rubber formulation. Additive type flame retardants are incorporated into the rubber by physical means, which may result in poor compatibility, leaching, as well as a reduction in mechanical properties. On the other hand, reactive type flame retardants are mainly organic compounds having a flame retarding moiety as well as active functional groups that can form covalent bonds with rubbers. Reactive type flame retardants have the advantages of (a) increasing compatibility between polymer and the flame retardant, (b) not degrading the mechanical properties of the rubber, (c) possessing better compatibility as the flame retardant group is a part of the binder and (d) low concentration of flame retardant is required.

Additive type flame retardants

Additive flame retardants are incorporated into the polymer by dissolving/melt compounding/blending into the polymer after the manufacture of the polymer. This method provides most economical and expeditious way of promoting flame retardancy for polymers. In general, additive flame retardants react when heated and (a) emit substances that displace the oxygen needed for a fire to burn, (b) form a protective coating on the surface of flammable substrate, thereby limiting access of the fire to fuel sources, or (c) do a combination of both. Halogenated flame retardants act in the gas phase by releasing chlorine or bromine free radicals in the gas phase.

Examples of additive type flame retardants are: halogenated paraffins, chlorofluorocarbons (CFCs), inorganic oxides and hydroxides such as antimony oxide, magnesium di-hydroxide, aluminum tri-hydroxide, mica, inorganic carbonates such as potassium carbonate, calcium carbonate, magnesium carbonate, magnesium hydroxycarbonate, boron containing inorganic compounds such as boric acid, borax, zinc borate, ammonium pentaborate, inorganic phosphorus containing compounds such as di-ammonium hydrogen phosphate, ammonium polyphosphate, melamine phosphate, triphenylphosphine oxide, red phosphorus, expandable graphite, melamine, etc. Halogenated additives such as chlorofluoro carbons (CFCs) release corrosive, obscuring, toxic and irritant halogen acids. CFCs may damage the ozone layer.

Alkyl phosphate or phosphonate: Trimethyl phosphate, triethyl phosphate, tributyl phosphate tris(monochloropropyl) phosphate, chloroalkyl phosphate such as tris(2chloroethyl) phosphate, tris(2,3-dichloropropyl) phosphate,

Aryl phosphates or phosphonates: Triphenyl phosphate, diphenyl 2-isopropylphenyl phosphate, phenyl di-(2isopropylphenyl) phosphate, diphenyl 4-isopropylphenyl phosphate,

Bromine-containing compounds: Tribromoneopentyl alcohol, dibromopentyl glycol, hexabromocyclododecane, decabromobiphenyl, decabromodiphenyl oxide (DBDPO), tetrabromobisphenol A and its derivatives, polybrominated diphenyl ethers such as pentabromodiphenyl ether, decabromodiphenyl ether, etc.

Sometimes a mixture of additive type flame retardants possess improved flame retardancy due to the synergistic mechanism involved in suppressing combustion. Additive type flame retardants are widely used in polymers; however they have several limitations such as poor compatibility, high volatility, loss of mechanical properties of polymers, and formation of increased amount of carbon monoxide (CO) and smoke during combustion.

Reactive and non reactive type flame retardants

Reactive flame retardants are chemically bound to the polymer by incorporating their chemical structure into polymer backbone during polymerization or by grafting into them. As they are chemically bonded, reactive flame retardants have greater effect on the properties of the polymer than additive flame retardants. Leaching of the flame retardant into the environment is less for reactive flame retardants when compared to additive (non-reactive) flame retardants [60]. Reactive flame retardants can be introduced by either the design of new flame retarding polymer or modification of existing polymers through copolymerization with a flame retarding unit in the chain. Covalently incorporating the flame-retarding unit in the polymer backbone imparts the flame retardancy permanently, and the original physical and mechanical properties can be maintained, or are not as greatly reduced compared to additive flame retardants.

Since they are not chemically bonded into the polymer matrix, non-reactive FR additives may be volatile and can leech out of the polymer and enter the environment under some conditions [60]. They can also have poor compatibility, and may also reduce the mechanical properties.

Mechanism of flame retardants

Depending upon the polymer, flame retardants act in one or more of the stages of the combustion process: heating, decomposition, ignition, flame spread, smoke process [61]. Flame retardants can act via physical or chemical mechanisms, and within those two general mechanisms, there are various potential ways in which flame retardants can react.

Physical

- **By cooling:** The FR additives can degrade endothermally which cools the substrate to a temperature which is below the temperature that is required for sustaining the combustion, pyrolysis, and thermal decomposition processes. Example: Metal hydroxides such as aluminum hydroxide and magnesium hydroxide.

- **By forming protective layer:** The additives can form a shield with low thermal conductivity, reducing the heat transfer from source to polymer. It further reduces the degradation rate of the polymer and decreases the fuel flow that feed the polymer. Example: Intumescent systems, expanded graphite.

- **By dilution**: The incorporation of inert fillers like talc, chalk and additives dilute the fuel so that the lower ignition limit of the gas phase is not reached.

Chemical

- **Gas phase:** The radical mechanism of gas phase during combustion is inhibited by use of FR materials, further stopping the exothermic processes occurring in the flame, cooling down the system. The supply of flammable gases is reduced and

eventually stopped. The high-reactive radicals HO· and H· can react in gas phase with other radicals formed in the degradation of FR materials [Fig. 1.1] [62]. Example: - Phosphorous based flame retardants, Halogenated flame retardants.
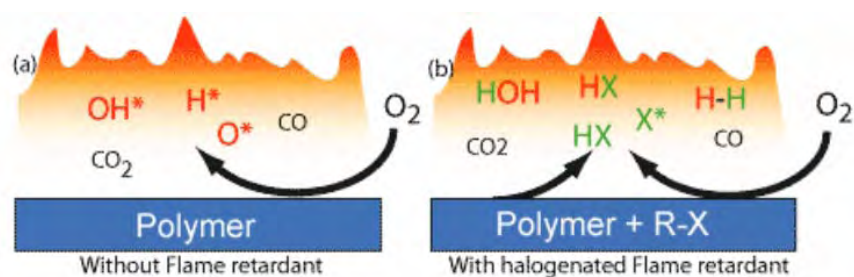
Fig. 1.1 Gas Phase mechanism of Flame Retardant [62]

▪ **Condensed phase:** Flame retardants can form a layer of carbon (charring) on the polymer surface. This is formed by dehydrating action of flame retardant. These processes form a carbonaceous layer through cross linking processes. The char barrier acts as an insulating layer to reduce the heat transfer from the flame to the combusting product. The proposed mechanism is based on the charred layer acting as a physical barrier, which slows down heat and mass transfer between the gas and the condensed phases [63, 64]. Example: - Boron based flame retardants, Phosphorous based flame retardants.
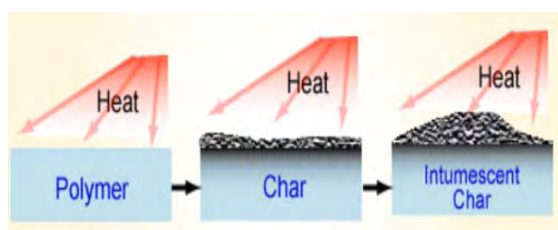
Fig. 1.2 Char Formation in the presence of flame retardant

Intumescent and nonintumescent systems

Based on the flame-retardant mechanism, polymers can be classified into either intumescent or nonintumescent types. The use of intumescent flame-retardant polymers is one of the easiest, economical and the most efficient ways to protect materials against fire. Intumescent flame retardants swell, bubble and char on exposure to a flame and the carbonaceous porous foamed mass acts as a barrier to heat, air/O_2 and pyrolysis products. At high temperature, the formed charred layer on the surface provides resistance to heat and mass transfer, giving good heat insulation to the underlying binder. Therefore, an intumescent system shields the underlying polymer from heat and fire. This lowers the temperature of the polymer surface beneath the char and causes a lag in the surface temperature rise. Additionally, the char layer hinders the diffusion of oxygen to the polymer site, i.e., the site of combustion.

1.3.5 Electrical conductivity

Conductive polymer composites containing carbonaceous fillers have been studied for years due to their ability to impart electrical conductivity, light weight, and good corrosion and ultraviolet (UV) resistance to commodity polymers. Carbonaceous fillers commonly employed for this purpose include carbon black (CB), graphite (G) and carbon fiber (CF). Conductivity may also be imparted to polymers by adding conductive metal particles (eg. copper, silver, platinum etc.). These metals, however, are more expensive and heavier than their carbon based counterparts at similar volume fraction concentrations. While less expensive metals such as steel may also be used for improving the conductivity of polymers, these metals are more prone to chemical interaction especially with oxygen, often

resulting in corrosion. High concentration of metal filler is needed to achieve good electrical conductivity which makes the system heavy and inflexible. Metal powder does not improve mechanical properties and also acts as a catalyst for oxidative degradation of matrix polymer. Carbon black powder, on the other hand reinforces the polymer especially elastomer matrix preserving its flexibility and light weight, without adversely affecting the environmental and thermal stability of the polymer matrix. Thus carbon based fillers, in addition to imparting colour and reinforcement to polymer matrix, contribute to conductivity.

1.3.6 Microwave technology

The microwave constitutes only a small portion of the electromagnetic spectrum (300 MHz to 300 GHz), but their uses have become increasingly important in investigations of material properties. Material characterization is essential for the proper selection and implementation of a substance when used in industrial, scientific and medical applications. The dielectric parameters over a wide range of temperature are needed to assess their suitability for use in telecommunications, dielectric waveguides, lenses, radomes, dielectric resonators and microwave-integrated circuits (MICs), and on lossy materials for estimating their heating response in microwave heating applications. Microwave heating is a very efficient method of heating dielectric materials and is extensively used in industrial as well as household heating applications. For design of microwave absorbers and food packages, dielectric data for lossy materials are required. The knowledge of the dielectric parameters of biological tissues is essential for the proper application of microwave diathermy. The measurement of dielectric parameters will serve as a tool for investigating the intermolecular and intramolecular mechanisms of compounds.

Hence, an in-depth study of the microwave characteristics of a material assumes significance. Determination of dielectric properties and the use of dielectric heating for polymer synthesis attribute microwaves an important status in polymer chemistry. The important application concerned with the use of microwave properties are electrostatic dissipation, microwave absorption and electromagnetic interference (EMI) shielding of sensitive electrical/ electronic circuitry and devices, antenna systems, aerospace and military equipment (e.g. lightning-protection aircraft composite panels), stealth technology, radar absorbing materials, avionics line replaceable unit (LRU) enclosures, etc., are just few of many technologies.

EMI can be shielded by the reflection and adsorption of electromagnetic radiation. In the past, metals have been primarily applied for EMI shielding by the reflection of electromagnetic radiation. However, metals have several disadvantages, including high density, proneness to corrosion and physical rigidity. As an alternative, composites with conducting fillers such as metal particles, carbon black, carbon fibers and carbon nanotubes (CNTs) have been extensively employed for EMI shielding [65–67]. Before selecting conducting fillers, three primary conditions have to be addressed. The first is that the material must have excellent electrical conductivity and magnetic properties. The second requirement is a high aspect ratio, which can provide a continuously conductive network via interconnection. The last one is excellent dispersion and adhesion in a matrix, which is a highly investigated topic that has not yet been met with a real solution [68]. Among the above three requirements, the first and second can be solved by the appropriate selection of additive materials; however, the last one remains a problem for the use of conducting fillers.

1.4 Composites

A composite material can be defined as a macroscopic combination of two or more distinct materials, having a recognizable interface between them. Composites are made up of continuous and discontinuous medium. The discontinuous medium that is stiffer and stronger than the continuous phase is called the reinforcement and the so called continuous phase is referred to as the matrix. The properties of a composite are dependent on the properties of the constituent materials, and their distribution and interaction.

1.4.1 Polymer matrix composites

Polymers are the most widely used matrix material for composites and are almost used 90% for the production of composite products. The main advantage is low cost, easy and versatile methods of processing, good chemical resistance and low density. On the other hand, low strength, low modulus and low operating temperatures limit their use.

Thermoset polymers (resins) have been used as a matrix material for reinforced composites. Starting material used in the polymerization of thermoset polymers are usually low molecular weight liquid chemicals with very low viscosity. Advantages of using thermoset polymers are their thermal stability and chemical resistance. They also exhibit much less creep and stress relaxation than thermoplastic polymers. The commonly used thermoset polymers are epoxy, unsaturated polyester, vinylester, bismaleimide resins etc.

Thermoplastic composites are those which use a thermoplastic polymer as a matrix. These composites can be reinforced with glass, carbon,

aramid or metal fibers. Thermoplastic polymer is a long chain polymer that can be either amorphous in structure or semi crystalline. Thermoplastic polymers used in thermoplastic composites can be divided into two classes, high temperature thermoplastics and engineering thermoplastics.

In elastomer matrix composites, rubber is used as the base material in a composite product if it requires rubber like elasticity and flexibility. In certain cases, rubber products require stiffness along with flexibility, often in specific directions. This can be achieved by reinforcing rubbers with filler to form composites.

1.4.2 Particulate composites

A composite whose reinforcement is a particle with all the dimensions roughly equal are called particulate reinforced composites. Particulate fillers are employed to improve high temperature performance, reduce friction, increase wear resistance and to reduce shrinkage. In many cases particulate fillers are used to reduce the cost, under these conditions the additive is filler, whereas when a considerable change in the properties of the composite occurs, the additive is reinforcement. The particles will also share the load with the matrix, but to a lesser extent than a fiber. A particulate reinforcement will therefore improve stiffness but will not generally strengthen. Hard particles in a brittle matrix will cause localized stress concentrations in the matrix, which will reduce the overall impact strength.

The reinforcements available in particulate composites do not posses any preferred directions and mainly used to improve properties or lower the cost of isotropic materials. The shape of the reinforcing particles can be

spherical, elliptical, cubic, platelet or any irregular or regular geometry. Certain particulate fillers like clay, talc etc. are non reinforcing where as carbon black is reinforcing in nature.

1.4.3 Nanocomposites

Nanocomposites are a novel class of composite materials where one of the constituents has dimensions in the range between 1 and 100 nm. Recent and ongoing research on polymer nanocomposites has shown dramatic enhancements in stiffness and thermal properties over those of polymers, without compromising on density, toughness or processability. Major differences in behaviour between conventional and nano-structured materials result from the fact that the latter have much larger surface area per unit volume. Since many important physical and chemical interactions are governed by surfaces, a nano-structured material can have substantially different properties compared to a larger dimension material of the same composition. Reinforcing efficiency requires high aspect ratios of the particulate constituent which is provided by nanofibers or nanotubes (one-dimensional) and nanofoils (two-dimensional).

1.5 Polymer blends

In recent years, polymer blends are gaining technological importance due to their variability of properties. By blending two or more elstomers, it is possible to attain properties that are not available with a single elastomer. The most important concept in polymer blends is additivity of properties. By this we mean that when a polymer is mixed with another polymer, the resulting blend has a property which is the weighted average of the properties of the individual polymers.

Polymer blends are either homogenous or heterogeneous. In homogeneous blends, both blend components lose part of their indentity and the final properties usually are the arithmetical average of both blend components. In heterogeneous blends, the properties of all blend components are present. Weakness of one polymer to a certain extent can be strengthened by the other. In some cases it is found that properties of blends are better than those of the individual components. The synergism is unfortunately hard to predict.

1.5.1 Polymer-polymer miscibility

Polymer-polymer miscibility can be visualized as equilibrium mixing at the molecular level and the formation of chemical bonds to retain this mixture at equilibrium. High molecular weight of polymers is a significant property that affects polymer thermodynamics and consequently its miscibility with other polymers. The thermodynamic expression for the free energy of mixing is:

$$\Delta G_{mix}= \Delta H_{mix}- T\Delta S_{mix} \text{ --------------------------------------- (1.1)}$$

Where ΔG_{mix} is the Gibb's free energy of mixing, ΔH_{mix} is the enthalpy of mixing, ΔS_{mix} is the entropy of mixing and T is the absolute temperature. In completely miscible blends, for which $\Delta H_{mix} < 0$ due to specific interactions, homogeneity is observed at least on a nanometer scale, if not on the molecular level.

Processability and mechanical properties of polymer blends depend mainly on their compatibility and miscibility. Miscible blends are those which are homogeneous throughout in microscopic scale. Depending on the

polymer miscibility, the blends can be classified as miscible, partially miscible, and immiscible, or in a technological sense as compatible, semicompatible and incompatible.

1.5.2 Thermodynamics of polymer blending

Flory and Huggins extended the theory of solutions, using the above equation to binary mixtures of polymers.

$$\Delta G_{mix} = (RTV/V_r)\ [(\varphi_A \ln \varphi_A/\chi_A) + (\varphi_B \ln \varphi_B/\chi_B) + (\chi_{AB}\ \varphi_A\ \varphi_B)] \ ....(1.2)$$

Where 'R' is the gas constant, 'T' is the absolute temperature, φ_A, φ_B are the volume fractions of polymers A and B, V_r is reference volume close to smallest polymer repeat unit, χ_A, χ_B is degrees of polymerization of polymer A and B, χ_{AB} is the interaction parameter [69]. The first two right hand side (RHS) terms in the equation represent the combinational entropy contribution to the free energy and the last term represents the enthalpy contribution. χ_A and χ_B represents the direct effect of component molecular weights on free energy. These terms are extremely large in polymers, and limit the entropy contribution to very small values.

The interaction parameter represents the heat of mixing of the two polymers, and was calculated by Hildebrand [70]:

$$\chi_{AB} = (\delta_A - \delta_B)^2/RT \ \text{---} (1.3)$$

where δ_A and δ_B are the solubility parameters of the polymers A and B. The heat of mixing, which is positive for endothermic systems (immiscible) and has to be negative for exothermic systems (miscible). Difference in solubility parameters of component polymers is the first, non-experimental indicator of miscibility. For miscibility in the entire

composition range, difference in solubility parameters should not exceed 0.7 at Mw= 10,000 and 0.08 at Mw= 1, 00000 [71].

Besides the criteria $\Delta G_{mix} > 0$ in polymer blends, the additional criteria for immiscibility is,

$$(\partial^2 \Delta G_{mix}/\partial \varphi^2)_{T, P} > 0 \text{ --- (1.4)}$$

Where the ΔG_{mix} values plotted against composition for a binary mixture shows a reversed curvature. The interaction parameter between two blend components directly affects the blend interfacial strength, blend morphology and consequently the properties.

1.5.3 Compatibilization

Compatible rubber blends are miscible only on a technological sense i.e, they can be co-vulcanized after blending and the properties are improved. Since most of the polymers fail to satisfy the thermodynamic criteria for miscibility the resulting blends will be heterogeneous in nature. This in turn will lead to blends with inferior properties. Owing to the lack of specific interactions between the polymer pairs, the interface formed will be very weak. In the case of polymer blends, the interface plays a important role in determining the blend properties. An interface is considered a region having a finite distance neighbouring the dispersed phase. The properties of the interfacial region can differ from those of the neat components.

For most of the polymer pairs, the interfacial width is very narrow about 1-5 nm. This implies that there is a little penetration of polymer chains from one phase into another and vice versa resulting in very few entanglements across the interface. The absence of the strong interface

between polymer pairs limits the stress transfer across the phase boundaries and requires only weak van der Waals bond during fracture. This implies that for most polymers blends which are immiscible and non compatibilized, the interface is the vulnerable location, which is most likely to fail before the component polymers on application of external stress.

Another important parameter to be addressed in polymer blending is the phase morphology development during processing. It is well established that most of the ultimate properties like toughness, strength and crack resistance, optical, rheological and dielectric properties of polymer blends are strongly influenced by the type and fineness of the phase structure. Therefore, morphology control plays a major role in the blending process. The morphology development of multicomponent polymer system is controlled by the complex interplay between viscosity and elasticity of the phases, interfacial properties, blend composition and processing conditions. Due to the high interfacial tension between the polymers blending generally leads to a poor dispersion of one polymer phase in another. As the dispersed phase entities become larger, the interfacial contacts between the two phases will be small leading to poor performance during external loading. Besides these factors, an immiscible polymer blend is thermodynamically unstable leading to phase separation. In order to restrict phase separation the interface should be modified and the phase morphology should be controlled. This can be achieved by the incorporation of suitable agents called compatibilizers. They are macromolecular species exhibiting interfacial activities in heterogeneous polymer blends. A suitably selected compatibilizer reduces the interfacial tension and enhanced the adhesion between the two phases. They are also capable to stabilize the developed

phase morphology against coalescence. The polymer blends with intentionally modified interfaces are called as compatibilized blends.

There are several methods for the compatibilization of immiscible polymer blends. Compatibilization will reduce the interfacial tension between the individual phases, permit finer dispersion during processing, provide stability against gross segregation and result in improved interfacial adhesion. The prominent mechanism of compatibilization of an immiscible polymer blend involves (i) the interfacial tension reduction at interfaces by minimising the unfavourable cross correlations and/or enhancing the favourable interactions and (ii) coalescence suppression, mainly by steric stabilization.

1.5.3.1 Physical compatibilization

It is the classical approach to compatibilizing immiscible polymer blends. In this the compatibilizing agent is chemically synthesized prior to the blending operation, and subsequently added to the blend components. The well selected copolymer bearing two distinct segments will be located preferentially at the interface owing to its chemical and molecular characteristics. Each segment will penetrate into the phase with which it has specific affinity. This will reduce the interfacial tension between the blend components and enhance the interfacial adhesion between the phases.

1.5.3.2 Reactive compatibilization

It is one of the most important cost effective mixing techniques by which one can generate new multiphase polymeric systems with stable and controlled morphologies. In recent years, more attention has been given on the reactive compatibilization technique, as it is very fast and easy. During reactive blending the interfacial chemical reaction, gives rise to *in situ*

formed copolymers, which suppress the coalescence and reduce the interfacial tension. Because of this, a stable and a fine morphology are obtained with enhanced interfacial adhesion between the phases. The stabilizing effect of a compatibilizer on blend morphology depends on its ability to lower the interfacial tension and to decrease the possibility for droplet coalescence. This in turn depends on several factors such as the type and amount of functional group present in the compatibilizer, reactive group content and end group configuration of the polymer, miscibility of the compatibilizer with one of the phases and its conformation, molecular architecture and stability at the interface.

1.5.4 Rubber blends and their characterization

Blending or mixing of two or more elastomers is carried out for three main reasons: improvement of the technical properties of an elastomer, achievement of better processing behavior, and lowering of compound cost. Blending is thus a way of obtaining optimum properties and performance at a reasonable cost, if the technical problems can be overcome.

Rubber blends, based on the miscibility of constituent polymers, can be divided into three broad classes: miscible, partially miscible and immiscible blends. A miscible blend is essentially a new single phase rubber obtained by the molecular level mixing of two or more rubbers. Such blends have the advantage of stability, easy mixing etc. But most of the properties will be a weighted average of the constituent rubbers. A totally immiscible polymer blends on the other hand will be a heterogeneous polymer blend with poor mechanical properties due to poor adhesion between the distinct phases. So, a partially miscible or compatibilized rubber blend will be the most attractive from a practical view point.

Dielectric measurements [72 – 75] have become an important tool to investigate the compatibility of different polymer blends. The dielectric properties of heterogeneous blends are greatly affected by interfacial phenomenon, which arises due to phase separation in polymer blends.

Blending of elastomers having different polarity is always a challenge due to the incompatibility, which is further aggravated by non uniform distribution of filler [76 – 78] and curatives [79–81] in the constituting elastomeric phases. Studies with non-polar/polar rubber blends have demonstrated that these materials have a range of properties which make them suitable for use in several applications. It is important to use fundamentally powerful techniques to study the structure of rubber blends. The frequently used techniques for studying rubber blends can be classified as: microscopic techniques, visco-elastic characterization and optical characterization techniques [82].

Significant improvements have been made in the analysis of elastomer blends for the determination of composition, morphology and filler inter-phase distribution. Gas chromatography (GC) [83], infrared spectroscopy (IR) [84], nuclear magnetic resonance (NMR) [85] and thermal analyses: [86] Differential thermal gravimetry (DTG), differential scanning calorimetry (DSC), thermogravimetric analysis (TGA) techniques can provide quantitative information on the composition. The latter three methods, along with small-angle X-ray scattering (SAXS) [87], small-angle neutron scattering (SANS) [88], dynamic dechanical thermal analysis (DMTA), optical microscopy [89], electron microscopy (EM) [90], transmission electron microscopy (TEM) [91], scanning electron microscopy (SEM) [92] and atomic force microscopy (AFM) [93] are also useful for

resolving differences in blend homogeneity. Time-of-flight secondary ion mass spectroscopy (ToF-SIMS) is a newly developed method to characterize elastomer blends and vulcanizates, where ToF-SIMS is applied to simultaneously map the rubber phase structure with detailed chemical information. ToF-SIMS is an extremely powerful tool for the analysis of the rubber surface structure. By scanning the surface, the top 1 to 2 nanometers are analyzed. A lateral resolution of 0.5 m can be reached. It is a unique technique which is capable to distinguish all elements of the periodic table and their isotopes as well as a vast array of organic functional groups [94].

1.5.5 Effect of fillers in rubber blends

Fillers as defined earlier are finely divided particles that are often used to enhance the performance and various desirable properties of the host matrix, depending on a typical application. The primary particle sizes of carbon black and silica fillers remain in the nanometer range. However, with these conventional fillers, the dispersion toward individual primary particles is significantly difficult to achieve. The main advantages of nanofillers are not only to reinforce the rubber matrix but also to impart a number of other properties such as barrier properties, flammability resistance, electrical/electronic and membrane properties, polymer blend compatibility, etc.

Silica is used as an important filler for rubbers to obtain highly reinforced rubber composites. The effect of silica loading on the mechanical properties like tensile strength, modulus, and hardness of binary rubber blends based on acrylonitrile-butadiene rubber (NBR)/natural rubber (NR) [95] NR/chloroprene (CR) and [96] ethylene-propylene-diene rubber

(EPDM)/NBR [97] has been well characterized in the last years. Several works were conducted to characterize the filler distribution and mechanical properties of filled binary blends in the vulcanized state [98-100].

1.5.6 Nanofillers in rubber blends

Rubbers are used in a wide range of applications and in most of them two or more rubbers are blended to optimize their all round performance in service conditions. Most of the synthetic rubbers require reinforcement with fillers for practical use. Carbon black (10-30 nm) and precipitated silica (30-100 nm) still remain the conventional fillers for this purpose. Obviously the key factors for reinforcement by fillers are good dispersion and enhanced interaction with the rubber matrix. Recently several other nanofillers have received attention for reinforcement characteristics in rubber, the most promising being organoclay, nanosilica, carbon nanotubes and nano calcium carbonate.

Nanofillers are classified into three types based on their dimensions in polymer matrices. The three dimensions of the particle can be in the order of nanometers (isodimensional nanoparticles) and hence appear as spherical particles. Carbon black, silica, aluminum oxide, titanium dioxide, zinc oxide, and silicon carbide are examples for nanoparticle fillers. Only two dimensions are in the nanometer scale and the third is larger, forming an elongated structure, as in nanotubes or whiskers or nanofibers. Examples are carbon nanotubes, carbon nanofibers, cellulose whiskers, boron nitride tubes, boron carbon nitride tubes, gold or silver nanotubes. Only one dimension of the filler is in nanometer range and hence has a layered appearance with a few nanometer thicknesses and of several hundred nanometers length. Layered silicates, layered graphite flakes and layered

double hydroxides are examples for layered nanofillers. Due to the high adsorption surface energies associated with these nanofillers, they have a strong tendency to form aggregates and agglomerates.

1.5.7 Role of nanofillers in reinforcement

The addition of general fillers to elastomer matrix affects the viscoelastic character by an increase in viscosity, limitation of chain mobility and improvement in mechanical properties. The extent to which this change occurs strongly depend on (i) particle size (ii) rubber-filler interaction (iii) filler-filler interaction (iv) filler shape and structure (v) filler concentration and (vi) filler dispersion in the matrix.

1.5.7.1 Particle size

There is a direct relation between surface area and particle size. Surface area can be expressed by m^2g^{-1} and particle diameter in nanometers. Fumed silica can have surface area of 400 m^2g^{-1} and carbon black 1000 m^2g^{-1}. Dimensions of the particulate fillers for reinforcement are generally in the range of 10 to 100 nm.

1.5.7.2 Rubber-filler interaction

Three types of interactions affect the viscoelasticity of rubber compounds. These are interactions between rubber molecules, interaction between rubber and filler and interaction between filler particles. Generally the presence of filler alters the relative segmental mobility only slightly. However, the interaction between polymer and filler strongly influences the flow behavior and mechanical properties.

The general equation for increase in viscosity, η_0 due to hydrodynamic effect of particulate fillers in real rubber filler mixes is governed by Guth Gold equation [101, 102].

$$\eta = \eta_0 (1 + 2.5\, c + 14.1\, c^2) \text{---} (1.5)$$

c = volume fraction of particulate filler

Here it is assumed that there is interaction between filler particles and they are non uniform in spherical shape. In the case of carbon black filled vulcanisate the change accompanying filler addition can be denoted by a change in Young's modulus. Thus Young's modulus of a vulcanisate containing low concentrations of spherical fillers, E, can be treated like equation (1.5) and can be modified as

$$Ef = Eg (1 + 2.5\, c + 14.1\, c^2) \text{-----------------------------------} (1.6)$$

Ef and Eg denote Young's modulii of filled and gum vulcanisates respectively.

Though equation (1.6) is valid for coarse fillers, for nano sized carbon black fillers the actual increase in modulus is much more than what the equation predicts. So equation (1.5) is modified by introducing shape factor (f) which is the ratio of longest dimension of particle to the shortest and given by

$$Ef = Eg (1 + 0.67\, fc + 1.62\, f^2\, c^2) \text{-------------------------------} (1.7)$$

The equation becomes valid when f is assumed to values close to 6 though such anisotropy is not shown by carbon black. However if it is assumed that rubber adsorbed on black surface by way of weak interactions

or mechanical entrapment (filler–rubber interaction) is a part of filler then the volume fraction of filler increases and the equation (1.7) becomes more valid. Here the effective volume fraction of filler is volume fraction of filler plus volume fraction of occluded/adsorbed rubber. Thus the actual change in modulus by addition of filler can be related to concentration of filler. The interaction between rubber and filler is quantified by bound rubber content which is the fraction insoluble in a solvent that generally dissolves NR, like toluene. An efficient method of estimating Young's modulus of a rubber vulcanisate is from measurement of hardness.

1.5.7.3 Filler-filler interactions

Filler-filler interactions play a significant role due to breakage of filler network. In the case of fillers that form aggregates there can be breakage and recovery of weak physical bonds linking adjacent filler-filler aggregates called Payne effect [103].

The Payne effect is reflected under cyclic deformations with small strain amplitudes and is manifested as a dependence of the viscoelastic storage modulus on the amplitude of applied strain. Above approximately 0.1% strain amplitude, the storage modulus decreases rapidly with increasing amplitude. At large amplitudes of about 20% the storage modulus approaches a lower bound. A pure gum vulcanisate shows a constant modulus over this range of amplitude. A similar effect called Mullins effect [104] occurs at larger deformations due to slippage of polymer chains over the surface of filler particles.

The filler particle may serve as physical cross links due to physical or chemical interactions involving filler and rubber. The filler can

physically be entrapped in the rubber and acts as a part of filler. Due to these factors fillers can share in the load bearing process when vulcanizate is strained. When fillers contribute in sharing load during deformation their presence in the matrix leads to higher strength. There is a considerable increase in modulus by incorporation of nanofilllers in rubber, which is considered to be due to the overall effect of cross linking of polymer network, hydrodynamic effect, polymer filler interactions which may be physical and chemical and formation of occluded rubber.

1.5.7.4 Shape and structure of filler

In comparison the increase in viscosity with spherical fillers (calcium carbonate) is very low. The increase in viscosity due to variation in shape factor arising from any of the factors described above can be approximated by equation (1.6) by replacing the term viscosity by modulus. Carbon black exists as aggregates which can be compact, voluminous or branched, and all these factors contribute to the definition of structure. Structure is evaluated as void volume using dibutyl phthalate (DBP). On mixing with DBP, when void volumes are filled viscosity shows a sharp increase. The shape and structure of filler also affects barrier properties. Fillers with high aspect ratio (similar to shape factor f used in equation 1.6) improves barrier properties like air permeability and solvent diffusion, more effectively than spherical fillers. The exfoliated clay layers and intercalated bundles strongly restrict the motion of polymer chains which also reduce the efficient diffusion of gas molecules. The aspect ratio exerts a stronger effect on diffusivity (D) than on permeability. In a system filled with dispersed particles of aspect ratio α, D is related to aspect ratio [105].

$$D = D_0 (1- c / (1+ \alpha/2) c) \text{ -- (1.8)}$$

where D_0 is the diffusivity of amorphous polymer and c is the volume fraction of filler.

Reinforcing fillers resemble additional chemical cross links on their effect in a rubber vulcanisate. They increase modulus and decrease swelling by solvents. However they show enhanced creep and compression set.

1.5.7.5 Filler reinforcement with respect to concentration and state of cure

Filler reinforcement is much pronounced with non crystallizing synthetic rubbers like styrene-co-butadiene (SBR) and acrylonitrile-co-butadiene (NBR) in comparison to NR. There is an optimum loading for reinforcement properties such as tensile strength, tear strength and abrasion resistance whereas stiffness increases steadily with elongation and decreases at higher loading. For example, in the case of layered clays which are used in concentrations of less than 10 parts per hundred rubber (phr) too there is an optimum concentration beyond which there is re-agglomeration of fillers leading to inferior mechanical properties and is around 5 phr in most of the polymers. There is possibility of good dispersion of nanofillers when the individual clay layers get separated leading to a structure of exfoliation. In exfoliated condition layered clays improve mechanical properties very effectively in low doses in the range 0.5-1 parts per hundred rubber.

Carbon blacks like high abrasion furnace blacks (HAF) act as a catalyst and accelerate vulcanisation reaction. In sulphur vulcanization system, usually sulphur exist as S_8 rings. These rings must be opened to form active sulphur for rubber vulcanisation Carbon black can help ring

opening process of S_8 atoms. The dissociation of an accelerator like benzothiazyl disulphide (MBTS) is faster when it is heated together with sulphur, rubber and carbon black [106]. Generally, the acidic nature of filler and a tendency for adsorption of accelerators, retard vulcanization as in the case of silica filler.

1.5.8 Methods to enhance rubber-filler interaction and reinforcement

Confinement of matrix within filler also promotes reinforcement. The reduction in filler-filler interaction and promotion of rubber filler interaction is the basic concept of reinforcement by nanofillers. They impart reinforcement as long as they are well dispersed, have polymer filler interaction and are compatible with polymer matrix. These conditions are achieved by (i) Micromechanical interlocking (ii) Physical and chemical interactions

1.5.8.1 Micromechanical interlocking

Spherical fillers like silica and carbon black exhibit structure and there is the chance for formation of immobilized rubber leading to reinforcement. In the case of layered silicate, due to intercalation of polymer molecules confined between gallery regions, rubber becomes immobilized to a small degree. In the case of tubular nanofillers like carbon nano tubes due to imperfections in the otherwise smooth surface, there can be mechanical interlocking leading to immobilization in a small degree.

1.5.8.2 Physical and chemical interactions-modification of nanofillers

The reactive sites on nanofillers both, formed during their production and introduced by suitable modification, help in reinforcement by enhancing the polymer filler interaction. The functional groups present on

fillers like carbon black and silica are able to react with functional groups present on rubbers. In the case of carbon black filler interaction is mainly of a physical nature whereas in the case of silane coupling agent chemical bond between silica and rubber is established. There can be physical adsorption of rubber on the surface of carbon black during processing operations. Polymer free radicals are formed during mixing due to the shear forces generated. Such free radicals react with carbon black to form bound rubber as carbon black acts as radical acceptors.

Nanofillers like silica and layered clays exhibit poor wettability leading to poor dispersion in rubber. This can be improved by (1) Surface modification (through introduction of suitable functional groups by chemical reactions) and (2) Surface coating. Obviously by these techniques there is introduction of functional groups on filler surface.

1.5.8.3 Surface modification of nanofillers

Surface treatment to improve filler polymer interaction has become very common in rubber industry. The material used for surface modification is one which is compatible with chemical nature of both rubber and filler. Stearic acid and their metallic salts are good examples of surface active agents. For inorganic nanofillers coating of filler surface by stearic acid or silanes reduces tendency to agglomerate and also increases compatibility with rubber matrix. Surface energy of silica can be reduced by adding glycols or amines in rubber compound. Nano zinc oxide is stabilized by hydroxyl functional oligomers. Calcium carbonate is generally coated with stearic acid or even with (γ-aminopropyl) triethoxysilane.

There are many coupling agents that can be used to enhance polymer filler interaction and include silanes, phosphorous esters, titanate coupling agents and chromium acid complexes. Organosilanes are widely used for the modification of silica surfaces. Coupling agents may be added directly to polymers or may be fixed to the fillers prior to their addition to polymers. The reaction between organosilane and silica called silanisation brings about hydrophobation of silica, reduces the filler network and makes silica compatible with polymer [107].

1.5.8.4 Role of nanofiller as compatibilizer

In rubber blends, there is uneven cross linking, heterogeneous filler reinforcement and non-uniform elastomer mixing that lead to a narrow interphase and poor physical or chemical interactions between the two phases. All these factors influence the mechanical properties of rubber blends.

Exfoliated clay layers are capable of severely reducing coalescence between dispersed domains in polymer blends due to nano level dispersion of clay layers that act as physical barriers. There are several reports to show that organoclay acts as a compatibilizer in immiscible polymer systems [108-110]. By introducing functional groups the polarity can be changed so as to have better filler dispersion and hence compatibilising action as when epoxidised natural rubber (ENR) has been used as a compatabilizer in NR clay nanocomposites. In the case of a functionalized rubber like ENR it can affect clay dispersion due to the enhanced interaction and also increased level of vulcanization by reactions involving the epoxy groups. Thus presence of polar rubbers in small proportions or in large proportions as blend components give intercalated or exfoliated structures. In the case

of rubber blends there is the possibility of interfacial cross links, and thus organoclay incorporated blend consisting of a small proportion of polar rubber shows improved mechanical properties. Here at least in a small degree layered clay acts as a compatibilizer. Rubber blends of NR/NBR [111], NR/(carboxylated styrene-co-butadiene rubber) XSBR [112] and NR/PU [113] have intercalated and exfoliated structures.

1.6 Review of some polar/non-polar rubber blends

1.6.1 NR/NBR blends

In an NR/NBR blend (ie, rubbers with different polarity), the solvent interaction parameter is very high leading to strongly phase separated blends. The comparison of the raw polymers shows that the arylonitrile content has a significant influence on the glass transition temperature (T_g) of the rubbers. An increase in ACN content results in a shift of the T_g to higher temperatures. T. Rocha etal studied [114] the dynamic mechanical investigation of all NR/NBR rubber blends shows two discrete glass transitions for both rubber phases. The T_g's of the blend are the same as the T_g's of the rubbers in the pure state.

R. Chowdhury etal. [115] studied a polyfunctional monomer, ethoxylated pentaerythritol tetraacrylate, was used as a crosslinking promoter in Natural rubber latex, acrylonitrile–butadiene rubber latex, and their 50: 50 blends.

Because of the structural dissimilarity, NR and NBR are immiscible, and compatibilizers are used during their blending. S. P Thomas et.al [116] used Neoprene or Chloroprene rubber (CR) as a compatibilizer for NBR/NR blend. A. E. Mathai et al prepared a new class of blend membranes from blends of nitrile rubber (NBR) and epoxidized natural rubber (ENR) and their

morphology, miscibility, mechanical, and viscoelastic properties have been studied. A. E. Mathai et al [117] studied the transport of a series of aromatic solvents through crosslinked nitrile rubber/epoxidized natural rubber blend membranes. This work focuses mainly on the diffusion and sorption behavior of organic solvents through crosslinked NBR/ENR blends.

H. Ismail etal. [118] studied the curing and mechanical properties of nitrile (NBR) and natural rubber (NR) blends.

A literature survey shows that studies on carboxylated nitrile rubber (XNBR)/NR blends are hardly carried out. Blending of elastomers has been often used to obtain an optimum number of desirable combinations, physical properties, processability and cost. NR shows very interesting physical properties because of its ability to crystallize under stretching. The blend vulcanizates thus produced exhibit enhanced physical properties by judicious selection of the NR: XNBR ratio [119].

N. Naskar etal studied [120] the successful use of Bis (diisopropyl) thiophosphoryl trisulfide (DIPTRI) and bis (diisopropyl) thiophosphoryl tetrasulfide (DIPTET) as a novel coupling agent and accelerator, respectively, to covulcanize an elastomer blend comprising polar XNBR and non polar NR. These compounds are capable of forming a chemical link between these dissimilar rubbers to produce a technologically compatible blend

1.6.2 NR/CR blends

Chloroprene rubber (CR) has excellent physical properties, weather resistance, thermal resistance, flame resistance and low temperature flexibility. Natural rubber is widely known to possess good mechanical

properties such as high tensile and tear strengths due to its ability to crystallize upon stretching. However, due to the existence of numerous reactive double bonds on the molecular backbone, NR is highly susceptible to degradation by thermal aging and ozone attack. In addition, oil resistance of NR is relatively poor, compared to some polar synthetic rubbers such as CR or NBR. To overcome such shortcomings, NR is frequently blended with synthetic rubbers such as NBR or CR. Recently; blends of NR/CR have been extensively studied [121-124]. The incorporation of CR into NR helps to improve oil and thermal resistance of NR. As CR and NR are cured by different techniques, careful adjustment of the cure system must be taken into account to avoid maldistribution of crosslinks within the two phases. Cure system of NR/CR blend therefore generally includes sulfur, thiourea derivatives with the addition of other conventional accelerators [125]. Apart from the curing system, the difference in polarity of the blend partners could also bring about high interfacial tension which is detrimental to the mechanical properties of the blend [126].

The use of silica as reinforcing filler in CR/NR blend and the effect of blend ratio on properties of silica-filled CR/NR blend was investigated by P. Sae-oui etal [127]. The mechanical properties as well as the resistance to aging, oil and ozone of the blends were focused.

CR is generally blended with other diene rubbers for improving the oil resistance, age resistance and flame resistance of the blend vulcanizates. But, when it is blended with diene rubbers like NR [128], SBR [129], EPDM [130] etc. the physical properties of the vulcanizates are greatly affected. In a blend of elastomers, which differ in polarity, there occurs a concentration gradient for the fillers and the curatives

which further leads to diffusion of curatives from less polar diene rubber to more polar chloroprene rubber. Earlier researchers reported several studies regarding the cure behavior of CR-EPDM [131–134] blend systems. Basu et al successfully utilized bis(diisopropyl) thiophosphoryl disulfi- de (DIPDIS) in the co-vulcanization of different rubber blends such as NR-XNBR [135], SBR-XNBR [136], EPDM-XNBR [137], EPDM- NR [138], EPDM-CR [139] and EPDM-NBR [140] using a two stage vulcanization technique. It is believed that several thiophosphoryl disulfides along with other ingredients (ZnO, sulfur, and stearic acid) are capable of building interfacial crosslinking between two different rubbers.

1.6.3 EPDM/NBR blends

The blending of NBR and EPDM rubber was performed to achieve the best properties from each component. Blending EPDM with NBR can improve the aforementioned disadvantages of EPDM because polar NBR exhibits excellent solvent resistance and adhesion properties. NBR has high resistance to swelling in oils and solvent but suffers from poor ozone resistance and heat ageing properties [141, 142]. EPDM is a saturated, nonpolar rubber (i.e., very low -c=c- content). The application of EPDM is restricted due to its poor solvent resistance and adhesion properties [143, 144]. The blend of such two polymers attracts the attentions of many researchers to tailor a blend which withstands ozone, heat aging, oil and solvents swelling with desirable mechanical characteristics. V. Jovanovic et al [145] studied cure kinetics, mechanical properties, morphology and thermal stability of composites based on carbon black reinforced NBR/EPDM rubber blends. Two separate T_g values of the CB reinforced composites based on EPDM/NBR rubber blends can be observed. The energy of activation, E_a for the NBR/EPDM/CB rubber

blend composite is lower (45.1 kJ/mol) compared to E_a for the rubber based on NBR (156 kJ/mol) and EPDM (75 kJ/mol), which indicates easier formation of rubber blend [145].

B. Jankovic et al [146] studied The non-isothermal degradation processes of NBR/EPDM rubber blends reinforced with carbon black/silica fillers were investigated with thermogravimetric analysis (TGA) and derivative thermogravimetry (DTG), using the different calculation procedures. It was found that the sample of the polymer blend, which contains the highest carbon black content (50phr carbon black), shows the greatest self-protective behavior.

S. S. Jovanovic et al studied the rheometric characteristics, curing kinetics, mechanical properties before and after thermal aging and morphology of nanocomposites based on various network precursors (i.e., NBR, EPDM and its blend reinforced of nanosilica) [147].

M Tian etal [148] studied the morphology and mechanical properties of ultra-fine full vulcanized powdered NBR rubber/ethylene-propylene-diene terpolymer (UFNBRPR/EPDM) blends were prepared by compounding ultra-fine full-vulcanized NBR particles into EPDM matrix. It is a promising method to prepare elastomer blends with excellent performances.

Grafting of maleic anhydride (MA) on olefinic polymers has been carried out in the presence of radical starters [149, 150]. The MA residue attached to EPDM rubber has been determined [151, 152]. Molded composites having good water, impact, and heat sag resistance, have been made from blends of polyamide and polyester resins and EPDM rubber modified with MA [153]. S. H. Botros et al [154] prepared of MA-g-EPDM and the testing of its action as a compatibilizer for EPDM/NBR elastomer blend.

The effect of carbon black fillers viz. semi reinforcing furnace (SRF), high abrasion furnace (HAF) and intermediate super abrasion furnace (ISAF) carbon blacks on the cure, swelling and mechanical properties of 70/30 EPDM/NBR blend have been investigated by K. C. Manoj etal [155].

To predicate and enhance the physical properties of blends, it is important to understand the atomic-scale microstructure and interactions between the two phases of blends. There exist many physical probes for characterizing the structure and properties of polymer blend [156]. Positron annihilation spectroscopy is a sensitive probe for detecting free-volume holes in polymeric materials at an atomic scale [157]. The filling effect of silica on the free-volume properties of an EPDM/NBR (75/25) blend was also examined with positron annihilation life time spectroscopy and Doppler broadening of annihilation radiation [158].

Filler distribution in the blend affects the properties of the blend, as it is controlled by the molecular weight of the polymer and filler dispersion in each phase and chemical interaction between polymer and filler [159]. Radiochemical degradation of polymer blends containing NBR/EPDM was studied by DSC [160].

Both NBR and EPDM rubbers are categorized as predominantly radiation cross-linkable type of polymers [161], which would account for the increase in tensile strength (TS) values with radiation dose up to 150 kGy. Apparently, degradation may then predominate, accompanied with restriction in reorientation, for doses higher than 150 kGy [162]. The TS measurements were carried out at comparatively large elongations and it would be expected that HAF carbon black filler exists in its particle form, that is, at its almost

accessible area. Moreover, the different type of groupings that exist on its surface, such as carboxylic, phenolic, hydroxylic, aldehydic and ketonic, would then participate in physical as well as chemical bond formation at the interface between the filler and rubber matrix, on irradiation [163].

M. M. Abou Zeid et al [164] studied the blend of NBR and EPDM (50/50) that was prepared and loaded with different concentrations of HAF carbon black up to 100 phr and subjected to gamma irradiation. The mechanical, physical, electrical and thermal properties of this blend have been studied with respect to HAF carbon black as well as irradiation dose.

1.6.4 EPDM/CR blends

As already mentioned, CR is an extremely versatile synthetic rubber with more than 75 years of proven performance in a broad industry spectrum due to its unique combination of properties: ozone resistance, oil resistance, toughness, dynamic flex life, good adhesion to other materials, and heat resistance up to 100^0C [165]. To meet the emerging needs, and for new material development for more demanding applications, improvements in resistance to heat, ozone, and cut growth of CR products are very desirable. The above requirement for CR products could be satisfied by blending with polyolefin elastomers such as ethylene–propylene rubber (EPR) or EPDM, which have better resistance to heat, ozone, and cut growth [166]. However, these CR/EPDM blends are incompatible [167].

A. Das et al studied the reinforcement and migration of nanoclay as filler in CR/EPDM rubber blends [168]. This communication demonstrates, an approach of compatibilization between CR and EPDM by using nanoclay as a compatibilizer and, simultaneously, as a very strong reinforcing nano-filler. A.

Das et al suggested a method for compatibilization of incompatible rubber blends offers routes to the design of new rubber based technical products for diversified applications [168]. The compatibilizing action of the pristine montmorillonite clay was investigated by Essawy H et al. showed the presence of clay at the interface on non-polar/polar rubber blends [169].

1.6.5 EPDM/FKM blends

Fluoroelastomers are widely used in many industrial applications due to their excellent resistance to heat, oil and solvent [170-174]. The increasing use of such polymers in automobile, aerospace, offshore, and energy-related industries imposes them stringent product performance standards under inclement temperatures and in hostile chemical environments [175-180].

Ethylene propylene diene monomer rubber (EPDM) is the material that has excellent performances in low-temperature flexibility, thermal stability, weatherability and aging resistance to oxidation and ozone [181–184]. Blending EPDM into fluoroelastomer (FKM) can be a potential measure to prepare the materials with better overall properties. However, the high incompatibility and non-co-vulcanization between FKM and EPDM make it difficult to obtain a blending material with better overall properties [185, 186]. In order to improve the compatibility and solve the co-vulcanization problem between FKM and EPDM, a polyphenol hydroxyl EPDM (PHEPDM) with pliant molecular chain and phenol hydroxyl groups is prepared. Fluorocarbon elastomer (vinylidenefluoride-co-hexafluoropropylene) can be vulcanized by bisnucleophiles such as bisphenols [180]. According to the current acceptable mechanism, the PHEPDM with phenol hydroxyl groups can act as crosslinking agent for FKM. Thus the molecules of FKM and PHEPDM are connected through

chemical bonds and some specific properties will be obtained for the vulcanized materials because of the particular structure of PHEPDM. The vulcanization procedure, low-temperature resistance, aging behavior, thermal degradation behavior and mechanical properties of the FKM/PHEPDM reactive blends have been reported by Y. Wang etal [187].

1.7 Scope of the present work

The technological importance of elastomer blends is increasing day-by-day. A detailed study of the blends of ethylene-propylene-diene rubber (EPDM) and fluorocarbon rubber (FKM) is proposed in this study. These blends may find application in the manufacture of profiles for automotive applications. Fluoroelastomers are widely used in many industrial applications due to their extreme resistance to heat, oil and solvent. EPDM is a material that has excellent performances in low-temperature flexibility, thermal stability, weatherability and resistance to oxidation and ozone aging. Blending fluoroelastomer with EPDM can be a potential measure to prepare materials with better overall properties. Literature reports only limited work on these elastomer blends and its composites. Hence in this investigation it is proposed to make a systematic study on the characteristics of these rubber blends.

The inherent heat resistance of fluorocarbon rubber identifies it as a potential polymer for high temperature profile applications. EPDM is an outstanding polymer which also meets requirements like weatherability, heat resistance etc. This work deals with the preparation and characterization of composites based on EPDM, FKM and EPDM/FKM rubber blends and the effect of blend ratio and concentration of compatibilizer on the various properties. Very little scientific information is available about the effect of fillers on the properties of EPDM/FKM blends. The effect of fillers

deserves an in-depth examination to achieve an in-sight into the mechanism and contribution of fillers in the EPDM/FKM blend. An attempt has been made to develop EPDM and EPDM/FKM products for high temperature applications and also for EMI shielding applications.

1.8 Objectives of the present work

- Preparation of EPDM/FKM rubber blends at different blend ratios

- Study the effect of MA-g-EPDM as a compatibilizer on cure characteristics, mechanical properties and phase morphology of blends

- Evaluation of dynamic mechanical properties of the above blends as a function of blend ratio and compatibilizer concentration

- Effect of aluminium hydroxide, chlorinated polyethylene, decabromobiphenyl oxide and expanded graphite on cure characteristics, mechanical and flame retardant properties of EPDM and EPDM/FKM based composites

- Solvent sorption studies of the composites based on EPDM and EPDM/FKM blends

- To analyze the thermal stability of the blends and composites

- Study of the microwave characteristics of the composites in the S- band frequencies

- Preparation and characterization of EPDM and EPDM/FKM based products for high temperature applications

- Evaluation of the electromagnetic shielding effectiveness of the composites

References

[1]   Du A, Zhang Z, Wu M, Express Polymer Letters 2009, 3, 295-301.

[2]   Su J, Chen S, Zhang J, Xu Z, Polymer Testing2009, 28, 235-242.

[3]   Gwaily SE, Abdel Aziz MM, Madani M, Composites Polymer Testing1998, 17, 265–287.

[4]   Brydson JA, Rubber Chemistry, Applied Science Publishers, London, 1978.

[5]   Baldwin FP, Ver Strate G, Rubber Chemistry & Technology1972, 45, 709-881.

[6]   Ver Strate G, Bikales NM; Over- berger CG, Menges, G (Ed), John Wiley & Sons1986, New York, 6, 522-565.

[7]   Cady L, Denton D, Edmondson S, Glass S, Mangold D, Flexpo, International conference June 1999, Houston.

[8]   Kole S, Chaki TK, Bhowmich AK, Tripathy DK, Polymer Degradation and Stability1993, 41,109-115.

[9]   Smith DBW, Laird JL, Larson SF. In paper presented at the 150 Technical Meeting, Rubber Division ACS1996, Louisville 8-9, Paper No 27.

[10]   Gamlin CD, Dutta NK, Choudhury NR, Polymer Degradation and Stability 2003, 80, 525–531.

[11]   Allen, Ralph D, Rubber World 1982, 186, 36-41.

[12]   Bhuvaneswari CM, Sureshkumar SM., Kakade SD., Gupta M, Defense Science Journal 2006, 56, 309-320.

[13]   Bart JCJ. Firenze University Press2006, Italy.

[14]   Ray S, Shanmugharaj AM, Bhowmick AK, Journal of Materials Science Letters 2004, 21, 1097-1100.

[15]   Qinfu Liu Q, Zhang Y, Xu H, Applied Clay Science 2008, 42, 232–237.

[16]   Wycyph G, Chem Tec Publishing 2000, Canada.

[17]   ASTM D1566-09, Standard Terminology Relating to Rubber.

[18]   Vulcanization from Wikipedia, www.wikpedia.org/wiki/vulcanization

[19]   Marton JM, Smith WK, 1, CBS publisher 2004, Delhi.

[20]   Conroy ME et al., Rubber Age 1955, 76, Griffis CB and Montermoso J, Rubber Age 1955, 77.

[21]   Dixon S, Rexford DR, Rugg JS, ind. Eng. Chem 1957, 49, 1687; Rexford DR (to E. I. du Pont de Nemours & Co.), U. S. Pat. 3, 1962, 051, 677.

[22]   Pailthorp JR, Schroeder HE (to E. I. du Pont de Nemours & Co.), U. S. Pat. 1961, 2, 968, 649.

[23]   Smith JF and Perkins GT, Proc. Inst. Rubber Conf. Preprints 1959, 575.

[24]   Moran AL, Pattison DB, Rubber World 197, 137 ; Schmiegel WW, Kautsch and Gummi 1978, 31, 137.

[25]   Apotheker D, Krusic PJ (to E. I. du Pont de Nemours & Co.), U. S. Pat. 1980, 4, 214, 060; Apotheker D et al., Rubber Chem Technol 1982, 55, 1004.

[26]   Schmiegel WW, Logothetis AL, ACS Symp Ser 1984,159–82.

[27]   Dutta NK, Ph.D thesis, Rubber technology centre, Indian institute of technology, Kharagpur, 1990.

[28] Shepard NA, Street JN, Park CR, "Chemistry and technology of rubber", Davis C and Blake JT, Editors, Reinhold, New York, Ch 11, 1937.

[29] Medalia A, J. Colloid. Interf. Sci. 1970, 32, 115.

[30] Kraus G. Rubber. Chem. Technol. 1971, 49, 199.

[31] Huber G, Vilgis TA, Kautsch. Gummi Kunstst. 1999, 52, 102.

[32] Rharbi Y, Cabane B, Vacher A, Joanicot M, Boue F, Europhys. Lett. 1999, 46, 472.

[33] Yuan QW, Mark JE, Macromol. Chem. Phys. 1999, 200, 206.

[34] Petrovic ZS, Zhang W, Mater. Sci. Forum 2000, 352, 171.

[35] Meissner B, J. Appl. Polym. Sci. 1974, 18, 2483.

[36] LeBlanc J, J. Appl. Polym. Sci. 1997, 66, 2257.

[37] Nakajima N, Yamaguchi Y, J. of Appl. Polym. Sci. 1997, 66, 1445-1453.

[38] Beck K, Kreiselmaier R, Peterseim V, Osen E, Kautschuk Gummi Kunststoffe 2003, 56, 657.

[39] Veranaud JM, Prentice Hall 1991, New York.

[40] Streit GP, Achenbach M, Gummi Fasern Kunststoffe 2001, 54, 816.

[41] Hildebrand JH, Scott RL, 1964, New York.

[42] Azaar K, Grang R, Rosca ID, Vernaud JM, Gummi Fasern Kunststoffe 2001, 54, 236.

[43] Flory PJ, Rehner J, J. Chem. Phys. 1945, 11, 52.

[44] Aitken A, Barrer RM, Trans. Faraday Soc. 1955, 51, 116.

[45]   Sallem M, Asfour AFA, Dekee D, J. Appl. Polym. Sci. 1989, 37, 617.

[46]   Maria GA, Sanguineti A, J. Appl. Polym. Sci 2004, 42, 1987.

[47]   [Georgoulis LB, J. Appl. Polym. Sci. 2005, 97, 775.

[48]   Coran AY, Rbber Chem. Technol. 1995, 68, 351.

[49]   Koenig JL, Rbber Chem. Technol. 2000, 73, 385.

[50]   Class JB, Processing at Meeting of the Rubber Division, 1997.

[51]   Chapman AV, Porter M, Roberts AD, " Natural Rubber Science and Technlogy", Oxford Science Publications 1988, Oxford, 511.

[52]   Cowie JMG, "Chemie und Physik der synthetischen Polymeren", Verlag Vieweg 1997, Wiesbaden.

[53]   Grinberg F, Grinberg F, Nestle N, Kuhn W, J. Polym. Sci. 2001, 39, 2207.

[54]   Simon G, Schneider H, Haeusler KG, Prog. Colloid Polym. Sci. 1988, 78, 30.

[55]   Medalia AI, Rubber Chem Technol. 1973, 46, 877.

[56]   Medalia AI, Rubber Chem Technol. 1978, 51, 437.

[57]   Payne AR, J. Appl. Polym. Sci. 1962, 6, 57.

[58]   Kraus G, J. Polym. Sci.: Appl. Polym. Symp. 1984, 39, 75.

[59]   Heinrich G, Kluppel M, Adv. Polym. Sci. 2002, 160, 1.

[60]   Rahman F, Frank Rahman, Katherine H, Langford, Mark D, Scrimshaw, John N, Lester, The Science of the Total Environment 2001,275.

[61]   Celebi F, Aras L, Gunduz G, Akhmedov IM, J. Coat. Tech. 2003, 75, 65 - 71.

[62] http://www.specialchem4polymers.com/tc/Flame-Retardants/index.aspx?id=9305

[63] Jincheng W, Shenglin Y, Guang L, Jianming J, J. Fire sci. 2003,21, 245.

[64] Mamleev V, Gibov KM, J. Elas. and Plas. 2007, 39, 33.

[65] Park KY, Lee SE, Kim CG, Han JH, Compos. Struct. 2007, 81, 401–406.

[66] Im JS, Kim JG, Lee YS, Carbon 2009, 47, 2640–2647.

[67] Huang Y, Li N, Ma Y, Du F, Li F, He X, Lin X, Gao H, Chen Y, Carbon 2007,45,1614–1621.

[68] Han MS, Lee YK, Lee HS, Yun CH, Kim WN, Chem. Eng. Sci., (in press).

[69] Paul DR, Bucknall CB (Ed), Polymer Blends, John Wiley and sons Inc. 2000, 1, New York.

[70] Barton AFM, CRC 1st ed, CRC Press 1990, Boca Raton.

[71] Billmeyer FW, 3rd Ed., Wiley Intersciences 1984, New York.

[72] Azima LG, Saad, Salwa El-Sabbagh, J. Appl. Polym. Sci. 2001, 79, 60.

[73] Younan AF, Abd-El-Messieh SL, Gas- ser AA, J. Appl. Polym. Sci. 1998, 70, 2061.

[74] George S, Varughese KT, Thomas S, J. Appl. Polym. Sci. 1999, 73, 255.

[75] Mohamed MG, Abd-El-Messieh SL, El-Sab- bagh S, Younan AF, J. Appl. Polym. Sci. 1998, 69, 775.

[76] Hess WM, Scott CE, Callan JE, Rubber Chem. and Technol. 1967, 40, 371.

[77]   Callan JE, Hess WM, Scott CE, Rubber Chem. and Technol. 1971, 44, 814.

[78]   Sirkar AK, Lamond TG, Rubber Chem. and Technol. 1973, 46, 178.

[79]   Gardiner JB, Rubber Chem. and Technol. 1968, 41, 1312.

[80]   Gardiner JB., Rubber Chem. and Technol. 1970, 43, 370.

[81]   Guillaumond FX, Rubber Chem. and Technol. 1976, 49, 105.

[82]   Van Der Velden GPM, Kelm J, Rubber Chem. Technol. 1990, 63, 215.

[83]   Kinsey R, Rubber Chem. Technol. 1990, 63, 407.

[84]   Sircar A, Lamond T, Rubber Chem. Technol. 1975, 48, 631.

[85]   Zhang Y, Macromolecules 2001, 34, 7056.

[86]   Gardiner JB, Rubber Chem. Technol. 1969, 42, 1058.

[87]   Marsh P, Voet A, Price L, Rubber Chem. Technol. 1967, 40, 359.

[88]   Binning G, Rohrer H, Gerber CH., Weibel E, Phys. Rev. Lett. 1982, 49, 57.

[89]   Hess WM, Rubber Chem. Technol. 1991, 64, 386.

[90]   Yerina N, Magonov S, Rubber Chem. Technol. 2003, 76, 846.

[91]   Knoll A, Magerle R, Krausch G, Macromolecules 2001, 34, 4159.

[92]   Ban LC, Campo KS, Rubber Chem. Technol. 1991, 64, 126.

[93]   Trent JS, Scheinbein JI, Couchman PR, Macromol. 1983, 16, 589.

[94]   US 6984450, Schill & Seilacher (GmbH & Co.), Hamburg, DE, invs.: K. Menting, C. Stone, 2006.

[95]   Poh BT, Ismail H, Tan KS, Polym. Test. 2002, 21, 801.

[96]   Sae-Oui P, Sirisinha CH, Wantana T, Hatthapanit K, J. Appl. Polym. Sci. 2007, 104, 3478.

[97]   Eid MAM, El-Nashar DE, Polym. Plast. Technol. Eng. 2006, 45, 675.

[98]   Shutilin YF, Parinova MP, Polner NN, Kaucuk i Rezina 1989, 3, 34.

[99]   Sircar A, Lamond TG, Rubber Chem. Technol. 1973, 46, 178.

[100]   Hess WM, Chirico VE, Rubber Chem. Technol. 1977, 50, 301.

[101]   Guth E, Rubber Chem. Technol. 1938, 11, 676-679.

[102]   Guth E, Rubber Chem. Technol. 1945, 18, 596-604.

[103]   Payne AR, Watson WF, Rubber Chem. Technol. 1963, 36, 147-155.

[104]   Mullins L, Rubber Chem. Technol. 1969, 42, 339-362.

[105]   Nielson LE, J. Macromol. Sci. Chem. A 1967, 1, 929-942.

[106]   Ali MS, Gholam Reza B, Massoud Ghasemzadeh-Barvarz, Iranian Polymer Journal 2005, 14, 573-578.

[107]   Negrete-Herrera N, Putaux JL, Bourgeat-Lami E, Progress in Solid State Chemistry 2006, 34, 121-137.

[108]   Voulgaris D, Petridis D, Polymer 2002, 43, 2213-2218.

[109]   Wang YQ, Zhang, Fu Q, Macromolecular Rapid Communications 2003, 24, 231-235.

[110]   Mehrabzadeh M, Musa KR, The Canadian Journal of Chemical Engineering 2002, 80, 1083-1092.

[111]   Alex R, Nah C, Plastics Rubber and Composites 2006, 35,219-225.

[112]   Stephen R, Varghese S, Joseph K, Oommen Z, Thomas S, Journal of Membrane Science 2006, 282,162-170.

[113] Psarras GC, Gatos KG, Karger- Koscis J, Journal of Appl. Polym. Sci. 2007, 106, 1405-1411.

[114] Rocha T, Rosca C, Ziegler J, Schuster RH, Kautschuk Gummi Kunststoffe 2005, 22.

[115] Chowdhury R. J. Appl.Polym. Sci. 2007, 103, 1206–1214.

[116] Shaji PT, Mathew EJ, Marykutty CV, J. Appl.Polym. Sci. 2012, 124, 4259–4267.

[117] Mathai AE, Thomas S, Polymer Engineering and Science 2003, 43, 3.

[118] Hanafi Ismail, Tan S, Poh BT, Journal of Elastomers and Plastics 2001, 33, 251.

[119] Naskar N, Debnath SC, Basu DK, J. Appl. Polym. Sci. 2001, 80, 1725.

[120] Naskar N, Debnath SC, Basu DK, J. Appl. Polym. Sci. 2001, 80, 1725–1736.

[121] Saad ALG, El-Sabbagh S, J. Appl. Polym. Sci. 2001, 79, 60–71.

[122] Helaly FM, El-Sabbagh SH, Journal of Elastomers and Plastics 2002, 34, 335–348.

[123] Das A, Ghosh AK, Basu DK, Kautschuk Gummi Kunststoffe 2005, 58, 230–238.

[124] Ramesan MT, Alex R, Khanh NV, Reactive & Functional Polymers 2005, 62, 41–50.

[125] Hofmann W, Rubber technology handbook. Hanser Publishers 1989, Munich.

[126] Tinker AJ, Jones KP, Chapman & Hall Ltd.1998, London.

[127] Sae-oui P, Sirisinha C, Hatthapanit K, eXPRESS Polymer Letters 2007,1, 8–14.

[128] Gaczynski R, Parasiewicz W, Ciechanowicz L, Polymery Tworzywa Wielkoczastecskowe 1974,19, 249.

[129] Ramesan MT, Mathew G, Kuriakose B, Alex R, European Polymer Journal 2001, 37, 719.

[130] Sutton MS, Rubber World 1964, 62, 149.

[131] Ishitobi T. and co-workers, 38th Annual Meeting Soc. Rub. Ind. Japan, May, 1971.

[132] Younan AF, Abd-El-Messieh SL, Gasser AA, J Appl. Polym. Sci. 1998, 70, 2061.

[133] Kalidaha AK, De PP, Bhattacharyya AS, Sen AK, Die Angew Makromol. Chem. 1993, 204, 19.

[134] Spenadel L, Sutphin RL, Rubber Age 1970, 102, 55.

[135] Naskar N, Biswas T, Basu DK, J Appl Polym Sci 1994, 52,1007.

[136] Biswas T, Naskar N, Basu DK, J Appl Polym Sci 1995, 58, 981.

[137] Naskar N, Debnath SC, Basu DK, Rubber Chem. and Technol. 2002, 75, 309.

[138] Ghosh AK, Debnath SC, Naskar N, Basu DK, J. Appl. Polym. Sci. 2001, 81, 800.

[139] Das A, Ghosh AK, Pal S, Basu DK, Polym. Advn. Technol. 2004, 15, 197.

[140] Ghosh AK, Basu DK, Kautsch. Gummi Kunstst. 2003, 56, 101.

[141] Mohamed GM, Abd-El-Messieh SL, El-Sabbagh SH, Younan AF. J Appl Polym Sci 1998, 69,775–83.

[142] El-Nashar DE, Turky G. Polym Plast Technol Eng 2003, 42, 269–84.

[143] Azima LG, El-Sabbagh SH, J Appl Polym Sci 2001, 79, 60–71.

[144] Ismail H, Jaffri RM, Rozman HD. J Elastom Plast 2003, 35, 181–92.

[145] Vojislav J, Suzana S-J, Jaroslava B-S, Gordana M, Milena M-C, Composites: Part B 2012, http://dx.doi.org/10.1016/ j.compositesb. 2012.05.020

[146] Bojan J, Milena M-C, Vojislav J, Suzana S-J, Gordana M. Thermochimica Acta 2012, 543 , 304–312.

[147] Suzana S-J, Vojislav J, Gordana M, Sandra K, Milena M-C. Composites: Part B 2011, 42, 1244–1250.

[148] Ming T, Yuan-W T, Yong-L LU, Jinliang QIAO, Tie LI and Li-Qun Z. Polymer Journal 2006, 38, 50–56.

[149] Viviano B, Roberto F. US Patent 4929682, 1990-05-29 [C08F255/04, C08F255/06, C08F291/02].

[150] Norbert H, Guenther S, Hans G, Rainer W, US Patent 4906690, 1990-03-06 [C08F255/04, C08F287/00].

[151] Chen D, Kennedy JP, Polymer Bulletin 1987, 17, 71–77.

[152] Coutinho FMB, Ferreira MIP, Polymer Testing 1994, 13, 25–34.

[153] Thomes YU, Thomas DJ, US Patent EP0282153, 1988-09-14 [C08L77/00].

[154] Botros SH, Tawfic ML, Journal of elastomers and plastics 2006, 38.

[155] Manoj KC, Prajitha K, Unnikrishnan G, Journal of Applied Polymer Science 2011, 120, 2654–2662.

[156] Liu J, Jean YC, Yang H, Macromolecules 1995, 28, 5774.

[157] Peng ZL, Wang B, Li SQ, Ng SJ, Liu H, Xie HQ, Phys Lett A 1994, 194, 228.

[158] Ehsan Gomaa. Journal of Applied Polymer Science 2007, 105, 2564–2570.

[159] Bandyopadhyay S, De PP, Tripathy DK, De SK, Polymer 1995, 36, 1979–84.

[160] Traian Z. Nucl Instrum Methods Phys Res B 2001, 185, 136–9.

[161] Woods RJ, Pikeav AK, New York: John Wiley & Sons, Inc., 1994, 344.

[162] Banik I, Bhowmick AK. Rad Phys Chem 1999, 54, 135–639.

[163] Franco C, Pitro R, Pandalai SG, Mater Sci 2001, 2, 253–61.

[164] Magda M, Abou Zeid, European Polymer Journal 2007, 43, 4415–4422.

[165] Das A, Naskar N, Basu DK, J Appl Polym Sci 2004, 91,1913.

[166] Deuri AS, Bhowmick AK, J Appl Polym Sci 1987, 34, 2205–2222.

[167] Ramesan MT, Mathew G, Kuriakose B, Alex R, Eur Polym J 2001, 37, 719–728.

[168] Das A, Mahaling RN, Stöckelhuber KW, Heinrich G. Composites Science and Technology 2011, 71, 276-281.

[169] Essawy H, El-Nashar, Polym Test 2004, 23, 803–7.

[170] Kader MA, Bhowmick AK, J Appl Polym Sci 2003, 89, 1442–52.

[171] Boutevin B, Caporiccio G, Pietrasanta FG, Ratsimihety A. J Fluorine Chem 2003, 124, 131–8.

[172] Maiti M, Bhowmick A, J Polym Sci Part B Polym Phys 2006, 44, 162–76.

[173] Maiti M, Bhowmick AK, Polym Eng Sci 2007, 47, 1777–87.

[174] Wang P, Schneider NS, Sung NH, J Appl Polym Sci 1999, 71, 1525–35.

[175] Mitra S, Ghanbari-SA, Kingshott P, Hvilsted S, Almdal K. J Polym Sci Part A Polym Chem 2004, 42, 6216–29.

[176] De Angelis MG, Sarti GC, Sanguineti A, Maccone P, J Polym Sci Part B Polym Phys 2004, 42, 1987–2006.

[177] Valsecchi R, Vigano M, Levi M, Turri S, J Appl Polym Sci 2006, 102, 4484–7.

[178] Ghosh A, De SK, Rubber Chem Technol 2004, 77, 856–72.

[179] Mitra S, Ghanbari-SA, Kingshotta P, Almdal K, Rehmeier HK, Christensen AG, Polym Degrad Stab 2004, 83, 195–206.

[180] Ameduri B, Boutevin B, Kostov G, Prog Polym Sci 2001, 26, 105–87.

[181] Sirqueira AS, Soares BG, Macromol Mater Eng 2007, 292, 62–9.

[182] Wu Wl, Chen DJ, Polym Compos 2006, 27, 621–6.

[183] Deniz V, Karaagac B, Ceyhan N, J Appl Polym Sci 2007, 103, 557–63.

[184] Mitra S, Ghanbari-Siahkali A, Kingshott P, Hvilsted S, Almdal K, Mater Chem Phys 2006, 98, 248–55.

[185] Kanu RC, Shaw MT, Polym Eng Sci 1982, 22, 507–11.

[186] Mathew AP, Thomas S, Polym Degrad Stab 2001, 72, 423–39.

[187] Yaming Wang, Lan Liu, Yuanfang Luo, Demin Jia. Polymer Degradation and Stability 2009, 94, 443–449.

.....ഹരി.....

Chapter 2
MATERIALS AND METHODS

Contents

2.1   *Materials*
2.2   *Preparation of EPDM based composites*
2.3   *Preparation of FKM based composites*
2.4   *Preparation of an intimate mix of EPDM and MA-g-EPDM*
2.5   *Preparation of EPDM/FKM rubber blends*
2.6   *Characterization methods*

This chapter deals with the details of materials used, experimental techniques employed for the preparation of composites from Ethylene-propylene-diene monomer rubber (EPDM), Hexafluoropropylene-vinylidine fluoride dipolymer rubber (FKM) and EPDM/FKM rubber blends. The various characterization techniques employed are also described.

2.1 Materials

The materials used in this study were EPDM and FKM. A compatibilizer MA-g-EPDM was used for the preparation of EPDM/FKM rubber blends.

2.1.1 Rubbers used

2.1.1.1 Ethylene-propylene-diene monomer rubber (EPDM)

An oil-extended EPDM rubber (Keltan 7341 A), a new conjugate long chain branching grade rubber, was obtained from DSM, Netherlands. It had the following specifications.

Mooney viscosity, ML(1+8) 150^0C	53
Ethylene content (%)	53
ENB-content (%)	7.5
Oil-content (%)	17

2.1.1.2 Hexafluoropropylene-vinylidine fluoride dipolymer rubber (FKM)

Viton A401C, a fluoroelastomer containing bisphenol curatives was obtained from DuPont Dow Elastomers. The detailed properties are listed below.

Chemical composition	Dipolymer of HFP and VF$_2$, plus cure chemicals
Specific gravity (g/cm^3)	1.82
Mooney viscosity, ML(1+10) 120^0C	42

The properties of other grades of fluoroelastomers obtained from Lanxess, Shanghai, and had the following specifications.

	ML(1+10) 121^0C	Volatile matter (%)	Fluorine content (%)
Levatherm F 6625	49	0.50	66
Levatherm F 6834	42	0.20	68
Levatherm F 7044	40	0.10	70

2.1.1.3 Maleic anhydride grafted ethylene-propylene-diene monomer rubber (MA-g-EPDM)

Maleic anhydride grafted EPDM, MA-g-EPDM (DE5005) was obtained from DSM Elastomers, Netherlands. It is a low molecular weight amorphous copolymer grafted with 2 wt% of maleic anhydride and is intended to provide improved adhesion (polar materials) or miscibility with numerous substrates and polymers. It is fully compatible with Keltan grades. It is also used for the

improved co-vulcanization of dissimilar elastomer blends. The detailed properties obtained from the technical brochure are given here.

Ethylene content (%)	49
Maleic anhydride (%)	2
Mooney viscosity, ML(1+4) 125^0C	65

2.1.1.4 Chlorinated polyethylene rubber (CPE)

Chlorinated polyethylene is a medium viscosity chlorinated polyethylene with low crystallinity. It is used as an elastomer in various formulations. It is available in powder form. Chlorinated polyethylene (Tyrin 3630) was supplied by the Dow chemical company, USA. It had the following specifications.

Apparent density (g/cm^3)	0.45
Chlorine content (%)	36
Mooney viscosity, ML(1+4) 125^0C	80

2.1.2 Fillers used

The fillers used in this work are listed below.

2.1.2.1 High furnace abrasion black (HAF-black)

High abrasion furnace black (N330) was used in the study was supplied by M/s Philips carbon black India Ltd., Kochi, India. It had the following specifications.

Appearance	Black granules
DBP absorption (cc/100g)	102
Pour density (kg/m^3)	376
Iodine number (mg/g)	82

2.1.2.2 Medium thermal black (MT-black)

MT black (N990) was supplied by Vajra rubber products, Thrissur.

2.1.2.3 Aluminium hydroxide (ATH)

Aluminium hydroxide gel dried purified was obtained from Merck Specialities Pvt. Ltd., Worli, Mumbai. The detailed technical data is given below.

Al_2O_3 (%)	47
P^H	≤ 10

Another grade of ATH was obtained from Associated Stabplast & Chemicals, Kota, Rajasthan, India. It had the following specifications.

Al_2O_3 (%)	64.5
Moisture (%)	0.2
Density (g/cm^3)	2.40

2.1.2.4 Calcium hydroxide [Ca(OH)$_2$]

Calcium hydroxide was obtained from Nice chemicals Pvt. Ltd., The detailed specification is given below.

Molecular weight	74.10
Assay (%)	95

2.1.2.5 Decabromo biphenyl oxide (DBBO)

Decabromobiphenyl oxide was produced by Hangu salt Industry (Changlu, Tianjin, China).

2.1.2.6 Expanded Graphite (EG)

Expanded graphite (Flexifoil L-200) was obtained from Metachem manufacturing company Pvt. Ltd., Pune, India. The detailed specification is given below.

Expansion at $500^0C/1g/90s$ (cc Min.)		200
pH		10
Mesh Size	85% Min.	+ 60µ
	95% Min.	+ 100µ
	05% Max.	-100µ

2.1.2.7 Antimony trioxide (Sb_2O_3)

Antimony trioxide was produced by Associated Stabplast & Chemicals, Kota, Rajasthan, India. The product specification is given below.

Purity as Sb_2O_3 (%)	99.65
Moisture (%)	0.085
Iron as Fe_2O_3 (%)	0.004
Lead as PbO (%)	0.003

2.1.3 Accelerators used

2.1.3.1 N-Cyclohexyl-2-benzothiazolesulfenamide (CBS)

CBS was obtained from Merchem Ltd., Cochin, India. It had the following specifications.

Melting point (^0C)	103
Flash point (^0C)	177
Density (at 25^0C, Kg/m^3)	1200

2.1.3.2 Tetramethylthiuram disulfide (TMTD)

TMTD was obtained from Merchem Ltd., Cochin, India. The specification of TMTD is given below.

Melting point (^0C)	142
Flash point (^0C)	150
Density (20^0C, Kg/m^3)	1425

2.1.3.3 Zinc diethyldithiocarbamate (ZDEC)

ZDEC was obtained from Merchem Ltd., Cochin, India. The specifications are given here.

Melting point (^{0}C)	172
Flash point (^{0}C)	220
Density (20^{0}C, Kg/m^3)	1480

2.1.3.4 Zinc dibutyldithiocarbamate (ZDBC)

ZDBC was obtained from Merchem Ltd., Cochin, India. It had the following specification.

Melting point (^{0}C)	108.4
Zn-content (^{0}C)	14.7

2.1.3.5 Zinc dibenzyldithiocarbamate (ZBEC)

ZBEC was obtained from Merchem Ltd., Cochin, India. The specifications are listed below.

Melting point (^{0}C)	178
Zn-content (%)	10.5

2.1.4 Plasticizers used

2.1.4.1 Paraffinic oil

M/s. Hindustan Petroleum Ltd., India, supplied paraffinic oil. It had the following specifications

Viscosity gravity constant (VGC)	0.85-0.9
Aniline point (^{0}C)	96

2.1.4.2 Dioctyl phthalate (DOP)

Dioctyl phthalate used was commercial grade supplied by Rubo-Synth Impex pvt. Ltd., Mumbai. The viscosity of the sample was 60 mPa. s.

2.1.4.3 Chlorinated paraffin wax (CPW)

Chlorinated paraffin wax used in this study was obtained from KLJ Organic Ltd., Gujarat, India. The important physical and chemical properties of CPW are given below.

Boiling point (^{0}C)	300-350
Flash point (^{0}C)	>200
Molecular weight	405-450

2.1.5 Other compounding ingredients used
2.1.5.1 Zinc oxide (ZnO)

Zinc oxide (activator) was supplied by M/s Meta Zinc Ltd., Mumbai and had the following specifications.

Specific gravity	5.5
ZnO content (%)	98
Acidity (%)	0.4

2.1.5.2 Stearic acid

Stearic acid (co-activator) was supplied by Goderej soaps Pvt. Ltd., Mumbai and had the following specifications.

Specific gravity	0.85
Melting point (^{0}C)	50-69
Acid number	185-210

2.1.5.3 Magnesium oxide (MgO)

Magnesium oxide used was commercial grade supplied by Posrec Co. Ltd., Pohang, South Korea. The detailed specification is given below.

MgO	98.80
Specific surface area (m^2/g)	150
Median particle size (μm)	2.8

2.1.5.4 Calcium oxide (CaO)

Calcium oxide (molecular weight= 56.08) was obtained from Qualigens fine chemicals, Mumbai.

2.1.5.5 Polyethylene glycol (PEG)

Polyethylene glycol was obtained from Merck Specialities Pvt. Ltd., Worli, Mumbai. The detailed technical data is given below.

Molecular weight (g/mol)	3500-4000
Hydroxyl number	25-32
Melting range (^{0}C)	54-58

2.1.5.6 Azodicarbonamide (ADC)

It is a self-dispersible universally employed chemical blowing agent in powder form for the production of cellular products, was supplied by High polymer labs Ltd., New Delhi, India. The detailed specification is given in Table.

Decomposition point (°C)	200 ± 3
Moisture content (% max.)	0.5
Average particle diameter (microns)	5.0 ± 0.5

2.1.5.7 Sulphur

Sulphur (vulcanizing agent), was supplied by Standard chemicals Co. Pvt. Ltd., Chennai and had the following specifications.

Specific gravity	2.05
Acidity, max (%)	0.01
Solubility in CS_2 (%)	98

2.1.6 Solvents used
2.1.6.1 Toluene

Toluene was supplied by Fine chemicals Ltd., Mumbai and had the following specifications.

Boiling point (^{0}C)	95
Acidity	0.012
Alkalinity	0.012

2.1.6.2 Methyl ethyl ketone (MEK)

Methyl ethyl ketone (molecular weight= 72, boiling point= 80^{0}C) was of analytical grade and is used as such without further purification and was obtained from Universal laboratories Pvt. Ltd., Mumbai.

2.2 Preparation of EPDM based composites

The compounding was done as per in ASTM D 3184-89 (2001). The fillers were incorporated into EPDM at various loadings (0, 5, 15, 25, 35 and 45 phr). The sequence of addition of compounding ingredients is given in table 2.1. After mixing the stock was passed six times through tight nip and finally sheeted out.

Table 2.1 Formulation used in the preparation of EPDM composites

Ingredients	ATH	EG	CPE	DBBO
EPDM	100	100	100	100
ZnO	4.5	4.5	4.5	4.5
Stearic acid	2.0	2.0	2.0	2.0
Flame retardant fillers (Y)*	0, 5, 15, 25,35 and 45	0, 5, 15, 25, 35 and 45	0, 5, 15, 25, 35 and 45	0, 5, 15, 25, 35 and 45
HAF black	20.0	20.0	20.0	20.0
Paraffinic oil	5.0	5.0	5.0	5.0
CBS	0.5	0.5	0.5	0.5
TMTD	0.5	0.5	0.5	0.5
Sulphur	1.50	1.50	1.50	1.50

*All the fillers were loaded at 5, 15, 25, 35 and 45 phr. Where, Y: Aluminium hydroxide (ATH), Chlorinated polyethylene (CPE), Decabromobiphenyl oxide (DBBO) and Expanded graphite (EG).

2.3   Preparation of FKM based composites

Fluorocarbon mixes were prepared on a Brabender plasticorder at room temperature. The rotor speed and time of mixing were 60 rpm and 8 min. respectively. The compounding ingredients were added as per formulation given in table 2.2.

Table 2.2 Formulation used in the preparation of FKM composites

Ingredients	phr
FKM	100
$Ca(OH)_2$	6.0
MgO	4.0
MT black	20

2.4   Preparation of an intimate mix of EPDM and MA-g-EPDM

In the compatibilized blends MA-g-EPDM was mixed with EPDM on a two-roll mill (16×33 cm^2) at a friction ratio of 1:1.25. A nip gap of 0.2 mm was set at room temperature so as to get an intimate mix of MA-g-EPDM and EPDM.

2.5   Preparation of EPDM/FKM rubber blends

Mix prepared in section 2.4 and FKM (prepared as per the formulation given in table 2.2) were blended on laboratory size two-roll mixing mill and the temperature maintained at 70 ± 5^0C. The compounding was done as per in ASTM D 3184-89 (2001).

The blends were designated as follows. E_{100} means EPDM and E_0 means FKM. E_{90} means a blend of 90 phr of EPDM and 10 phr of FKM. The binary blends were designated as E_{90}, E_{80}, E_{70}, E_{60} and E_{50}. The MA-g-EPDM, compatibilized E_{50} blends were designated as E_{50X}, where X=1, 2.5, 5, 7.5 and 10. X denotes the weight percentage of the compatibilizer in the blend. Formulations used in the preparation of EPDM/FKM blends are given in table 2.3.

Table 2.3 Formulations used in the preparation of EPDM/FKM blends

Ingredients (by weight)	E_{100}	E_{90}	E_{80}	E_{70}	E_{60}	E_{50}	E_0	E_{501}	$E_{502.5}$	E_{505}	E_{505*}	$E_{507.5}$	E_{5010}
EPDM	100	90	80	70	60	50	-	49	47.5	45	50	42.5	40
FKM (Mix.)	-	13	26	39	52	65	130	65	65	65	65	65	65
MA-g-EPDM	-	-	-	-	-	-	-	1	2.5	5	5	7.5	10
ZnO	4.5	4.05	3.6	3.15	2.7	2.25	-	2.25	2.25	2.25	2.25	2.25	2.25
Stearic acid	1.5	1.35	1.2	1.05	0.9	0.75	-	0.75	0.75	0.75	0.75	0.75	0.75
HAF	20	18	16	14	12	10	-	10	10	10	10	10	10
Paraffinic oil	5	5	5	5	5	5	-	5	5	5	5	5	5
DOP	5	5	5	5	5	5	-	5	5	5	5	5	5
CBS	1	0.9	0.8	0.7	0.6	0.5	-	0.5	0.5	0.5	0.5	0.5	0.5
TMTD	1	0.9	0.8	0.7	0.6	0.5	-	0.5	0.5	0.5	0.5	0.5	0.5
S	1.5	1.35	1.2	1.05	0.9	0.75	-	0.75	0.75	0.75	0.75	0.75	0.75

FKM Mix. = FKM -100phr, Calcium hydroxide-6phr, Magnesium oxide-4phr, MT black-20 phr.

* MA-g-EPDM as an additive (compatibilizer) at 5phr (parts per hundred rubber).

EV (E_{50} in table 2.3) means a blend of 50 phr of EPDM and 50 phr of FKM. The MA-g-EPDM (5phr) compatibilized EV blends are designated as EV* (E_{505*} in table 2.3). The 'Y' loaded uncompatibilized and compatibilized blends are represented as EVY and EVY*. In all the blends, the Y loading was 0, 5, 15, 25, 35 and 45 phr, which is represented as Y0, Y1, Y2, Y3, Y4 and Y5 respectively. Where, Y= Aluminium hydroxide (ATH), Chlorinated polyethylene (CPE), Decabromobiphenyl oxide (DBBO), Expanded graphite (G) and Antimony trioxide (S).

2.6   Characterization methods

The following characterization methods were adopted for the vulcanizates.

2.6.1 Cure characteristics

The cure characteristics of the mixes were determined using Rubber Processing Analyser RPA 2000 supplied by Alpha Technologies, USA, as per ASTM D 2084-01. Subsequently, the rubber compounds were vulcanized up to the optimum cure time at 150 ^{0}C at a pressure of 200 kg/cm^2. The moulded samples were cooled quickly in water at the end of the curing cycle and stored in cool dark place for 24 h prior to physical testing.

The instrument used has two directly heated opposing biconical dies with a die gap of 0.487mm that are designed to achieve a constant shear gradient over the entire sample chamber. The lower die is oscillated at 50 rpm and the torque transducer on the upper die senses the force being transmitted through the rubber. To determine the cure characteristics of the rubber compound, approximately 5 g of the sample was placed in a sealed

biconical cavity under pressurized conditions and submitted to harmonic torsional strain by the oscillation of the lower die through a small deformation angle about 2^0 and the transmitted torque is measured. The following data can be taken from the time-torque curves.

a) *Minimum torque (D_{min})*: Measure of the stiffness of unvulcanized test specimen. It is the torque shown by the mix at the test temperature before the onset of cure.

b) *Maximum torque (D_{max})*: Measure of the stiffness or shear modulus of the fully vulcanized test specimen at the vulcanization temperature. It is the torque recorded after curing of the mix is completed.

c) *Scorch time (T_{10})*: It is the time taken for attaining 10% of the maximum torque.

d) *Optimum cure time (T_{90})*: Time taken for attaining 90% of the maximum torque. It is the time corresponding to a torque equal to $0.9(D_{max} - D_{min}) + D_{min}$.

e) *Cure rate index (CRI)*: It is a measure of the rate of cure and was calculated using the formula, $\text{CRI} = \dfrac{100}{(T_{90} - T_{10})}$

2.6.2 Strain-sweep studies

The strain sweep measurements on green compound were conducted to study the rubber-filler interaction. Rubber Process Analyzer (RPA 2000-Alpha Technologies) is a purposely modified commercial dynamic rheometer [1]. Such instrument was modified for capturing strain and torque signals, through appropriate software. Filled rubber compounds

exhibit strong non-linear viscoelastic behaviour, the well-known Payne effect, i.e. the reduction of elastic modulus with increasing strain amplitude [2]. RPA can do strain sweep tests in which the variation of storage modulus (G'), loss modulus (G") and complex modulus (G*) with change in strain amplitude are measured. With respect to its measuring principle, the RPA cavity must be loaded with a volume excess of test material. In agreement with ASTM D 5289, the manufacturer recommends to load samples of about 5.0 g (4.4 cm^3) for a standard filled rubber compound with a specific gravity of 1.14 g/cm^3. Samples for RPA testing were consequently prepared by die cutting 46 mm diameter disks out of around 2 mm thick sheets of materials. The testing temperature was selected as 100°C; a temperature below the curing temperature and the shear strain was varied from 0.5 to 40% keeping the frequency measurements at 0.5 Hz.

2.6.3 Mooney viscosity

The mooney viscosities of the rubber samples were measured on the mooney viscometer which is designed for measuring the shearing viscosity of rubber and rubber like materials by a disc rotating (2 rpm) in a cylindrical cavity set at 100^{0}C and filled with rubber under test. In running a viscosity test, the sample was allowed to warm-up for one minute after the platens were closed and the motor was then started. Reading taken after 4 minutes was reported as the mooney viscosity of the rubber [ML(1+4) 100^{0}C]. Mooney viscosity was measured on a model Ektrontek, Taiwan.

2.6.4 Extrusion process

Extrusion was done on a two inch variable speed extruder, Plus-one machine fabric, Belgaum, India.

2.6.5 Vulcanization of extruded product

Vulcanization of the extruded product was carried out in a hot-air aging oven.

2.6.6 Stress-strain properties

The tensile tests were carried out on dumb-bell shaped specimens punched out from the vulcanized sheets. The measurements were carried out on a Shimadzu Universal testing machine (10 KN) with a grip separation of 40 mm, using a crosshead speed of 500 mm/min as per ASTM D 412.

2.6.7 Tear strength

The test was carried out as per ASTM D 624-1998 using unnicked, 90^0 angle test pieces. The samples were cut from the compression moulded sheets parallel to the mill grain direction. The measurements were carried out on a Shimadzu Universal testing machine (10 KN) with a grip separation of 40 mm, using a crosshead speed of 500 mm/min.

2.6.8 Hot air aging studies

Measuring the tensile properties after ageing at 70, 150 and 200 ^{0}C for 22 h in a hot air oven to assess resistance of the sample to aging.

2.6.9 Density

The densities of the samples were estimated by the method of displacement of liquid (ASTM D 792).

2.6.10 Hardness

The hardness (Shore A) of the moulded samples were determined using Bareiss Digital hardness tester in accordance with ASTM D 2240-03. The tests

were performed on unstressed samples of 30 mm diameter and 6 mm thickness.

2.6.11 Abrasion resistance

The abrasion resistance of the samples was determined using a DIN Abrader (DIN 53, 516). Samples having a diameter of 6±0.2 mm and a thickness of 6 mm were kept on a rotating sample holder and a 10N load was applied. Initially a pre run was given for all samples and its weight is taken. The weight after final run was also noted. The abrasion loss in cm^3/h was calculated using the formula given below (equation 2.1).

$$\text{Abrasion loss} = \frac{\text{loss of weight}}{\text{specific gravity}} \times \frac{60}{2.2} \text{ ----------------------------- (2.1)}$$

2.6.12 Rebound resilience

Rebound resilience is the ratio of energy that is given up on recovery from deformation to the energy required to produce the deformation. It is expressed as percentage and is measured using a vertical rebound resilience tester as per ASTM D 2632-01. A plunger weighing 28±0.5 g is dropped from a height of 40 cm to the sample of thickness 12.5 mm and the rebound height is measured.

2.6.13 Compression set

The samples (1.25cm thick and 2.8cm diameter) in duplicate compressed to a constant deflection (25%) were kept in an air oven at 70 ^{0}C for 22 h. (ASTM D 395-1998 Method B). The samples were taken out, cooled to room temperature for half an hour and the final thickness measured. The compression set was calculated using the equation,

$$\text{Compression set (\%)} = \frac{T_0 - T_1}{T_0 - T_s} \times 100$$

Where, T_0 & T_1 are the initial and final thickness of the specimen and T_s is the thickness of the spacer bar used.

2.6.14 Heat build-up

The BF Goodrich flexometer, conforming to ASTM D 623-1999 was used for measuring the heat build-up. A cylindrical sample of 25mm in height and 19 mm in diameter was used for the test. The oven temperature was maintained at 100^0C. The samples were preconditioned in this oven for 20 minutes. After preconditioning the test samples were subjected to a flexing stroke of 4.45 mm under a load of 10.9 Kg and the temperature rise at end of 20 minutes was taken as the heat build-up.

2.6.15 Solvent sorption experiments

Circular samples of 2 cm diameter were cut from polymer sheets by means of a standard die. The thickness and initial weight of the samples were taken. The samples were kept in diffusion bottles at constant temperature in an air oven. The samples were periodically removed from the bottles, the adhering solvent removed by using tissue paper and the samples were weighed on an electronic balance. The samples were then immediately replaced into the diffusion bottle. The experimental procedure was continued until the equilibrium swelling was attained. The solvent uptake [Q_t (%)] of the samples was computed using the equation 2.2,

$$Q_t(\%) = \frac{M_s/MM_s}{M_p} \times 100 \quad \text{-- (2.2)}$$

where M_s is the mass of solvent sorbed, MM_s is the molar mass of solvent and M_p is the mass of polymer. Swelling ratio was calculated using equation 2.3,

$$Q = \frac{W_2 - W_1}{W_1} \times 100 \ \text{--- (2.3)}$$

Where, Q is the ratio of swollen weight to original weight; W_1 and W_2 are the weights of the sample before and after swelling, respectively.

The crosslink density ($1/2Mc$, where Mc is the number-average molecular weight of the rubber chains between crosslinks) was determined with an equilibrium swelling method with toluene and methyl ethyl ketone (MEK) as solvent for EPDM, FKM and EPDM/ FKM blends. Samples approximately 1 cm in diameter, 0.2 cm thick and 2g weight were punched out from the central portion of the vulcanizate. These were allowed to swell in toluene for 24 h. The swollen samples were taken out of the solvent and weighed after drying in a vacuum oven.

The volume fraction of rubber (V_r) in the swollen network was then calculated by the method reported by Ellis and Welding from the following equation 2.4 [3],

$$V_r = \frac{(D - FT)\rho_r^{-1}}{(D - FT)\rho_r^{-1} + A_0 \rho_s^{-1}} \ \text{--- (2.4)}$$

where T is the weight of the test specimen, D is the deswollen weight of the test specimen, F is the weight fraction of insoluble components, A_0 is the weight of the absorbed solvent corrected for the swelling increment, ρ_r is the density of rubber, and ρ_s is the density of the

solvent. For blends containing HAF, the previously obtained value of V_r was converted into V_{r0} with the following equation derived by Porter [4],

$$\frac{V_{r0}}{V_r} = 0.54 \times e^{-z} + 0.44 \text{ --- (2.5)}$$

where z is the weight fraction of the filler. The crosslink density $1/2Mc$ was determined from V_{r0} using the Flory–Rehner equation [5],

$$1/2Mc = -\left[\frac{\ln(1-V_{r0}) + V_{r0} + \chi V_{r0}^{2}}{2V_s \rho_r (V_{r0})^{1/3}} \right] \text{ ------------------------------ (2.6)}$$

where ρ_r is the density of rubber, V_s is the molar volume of the solvent, and χ is the parameter characteristic of the interaction between the blend and solvent (χ of EPDM/FKM blends was found to vary linearly with their composition). V_{r0} is the volume fraction of rubber in the swollen network.

2.6.16 Limiting oxygen index

The limiting oxygen index (LOI) or oxygen index (OI) is a method for evaluation of the flammability of materials. LOI is defined as the minimum concentration of oxygen in an oxygen–nitrogen mixture, required to sustain burning of a vertically mounted specimen. The oxygen index was described as follows (equation 2.7) and oxygen index of the air is 21.

$$\text{Oxygen index} = \frac{[O_2]}{[O_2]+[N_2]} \times 100 \text{ ---------------------------------- (2.7)}$$

The flame retardancy of all the composites was evaluated by the test of LOI using an oxygen index instrument (Dynisco, Alpha Technologies, USA) according to ASTM D 2863. The experimental set up for LOI test is given in Fig. 2.1.
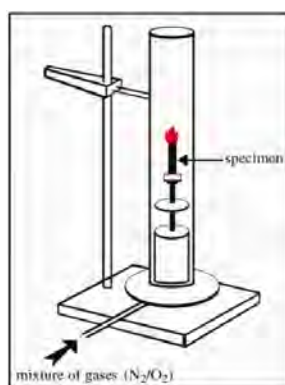
Fig. 2.1 Set up for LOI test

2.6.17 UL-94 Horizontal burning test

The composites flame resistance was evaluated by the horizontal burning test UL94 HB as per ASTM D635 & ISO 1210. This test method covers a small-scale laboratory procedure in order to gain information on the relative linear burning rate (BR) or extent and time of burning, or both, of horizontally self-supporting samples in the form of bars. Each sample is marked at 25 mm and 100 mm from one end of the test specimen. A flame with a 20 mm high blue cone is applied at 45^0 from horizontal for 30 s. When the flame passes the 25 mm and 100 mm marks, the burning time is recorded and the BR (mm/min) can be calculated. The occurrence of dripping can be visually detected; however, this method does not provide a classification system for the dripping behaviour of tested materials. The experimental set up for UL94 HB test is given in Fig. 2.2,
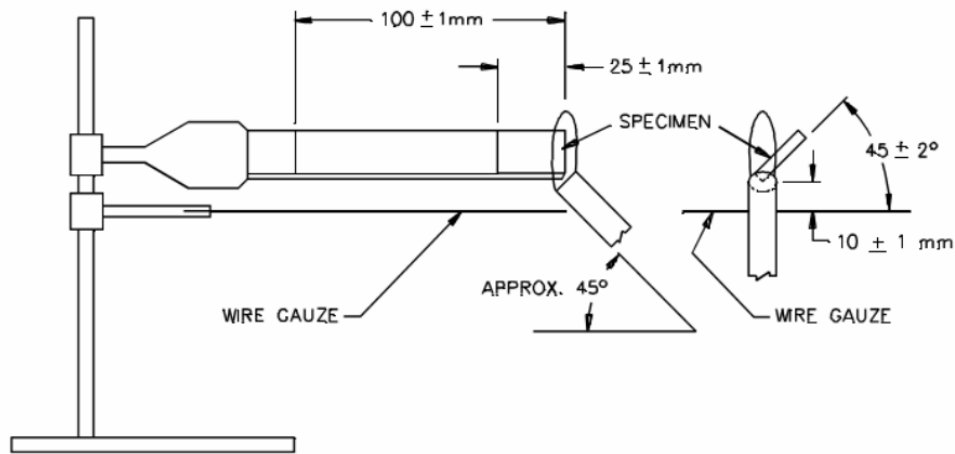
Fig. 2.2 Set up for UL-94 horizontal burning test

2.6.18 DC-Electrical conductivity

The DC electrical conductivity of the composites (rectangular strips of dimensions 4×2×2 mm) was measured by a standard two-probe electrode using a Keithley 2400 source-measure unit in dry air at ambient temperature. The sample was placed between two electrodes through which current was passed and the resistance was measured directly from the instrument. The conductivity of the samples was calculated using the formula (equation 2.8),

$$\sigma \text{ (S/cm)} = \frac{I}{V} \times \frac{l}{A} \text{ --- (2.8)}$$

Where 'σ' is the electrical conductivity, 'I' is the current through the electrode in amperes, 'V' is the voltage in volts, 'l' is the thickness of the sample in centimeters and 'A' is the area of contact of the electrodes with the sample in centimeter square.

2.6.19 Measurement of microwave properties

The determination of microwave properties was carried out by the resonance method, based on the cavity perturbation technique. In the cavity perturbation technique, generally rectangular or cylindrical wave-guide resonators are employed. When a dielectric material is introduced into a cavity resonator at the position of maximum electric field, the resonant frequencies of the cavity are perturbed. The contribution of magnetic field for the perturbation is minimum at this position. So, from the measurement of the perturbation due to the sample, the dielectric parameters can be determined. The microwave characteristics of the composites were studied using Agilent Performance Network Analyzer E8362 B. The measurements were done in S (2.44, 2.685 and 2.972 GHz) band frequencies at room temperature.

2.6.19.1 Design of rectangular wave-guide cavity

The cavity resonators are constructed from brass or copper wave-guides. The inner walls of each cavity are silvered to reduce the wall losses. Both the resonators are of transmission type, since power is coupled into/out through separate irises. The design details of S-band rectangular wave-guide used in the measurements are given below.

Dimensions of the cavity (cm)	S-band
Length	34.5
Breadth	7.2
Height	3.4

The photographs of the S-band wave-guide cavity resonators are shown in Fig. 2.3. The network analyzer is shown in Fig. 2.4.

Fig. 2.3 The S band wave-guide cavity resonator

Fig. 2.4 Setup for the measurement of microwave properties

2.6.19.2 Theory of microwave characterization

When a dielectric material is introduced in a cavity resonator at the position of maximum electric field, the field perturbation due to the sample is given (equation 2.9) by Kupfer et al. [6]

$$-(d\Omega/\Omega) \approx \frac{[(\varepsilon^* -1) \int\limits_{Vs} E.E_0^* dV]}{2 \int\limits_{Vc} |E_0|^2 dV} \quad\text{--- (2.9)}$$

where $d\Omega$ is the complex frequency shift; Vc and Vs are the volumes of the cavity and the sample, respectively. E and E_0 are the perturbed and unperturbed fields in the cavity, respectively; and ε^* is the relative complex permittivity of the sample material.

$$\varepsilon^* = \varepsilon' - j\varepsilon''$$

where, ε' is the real part of the complex permittivity and ε'' is the imaginary part of the complex permittivity. Complex frequency shift is related to the quality factor, Q is given in (equation 2.10),

$$(d\Omega/\Omega) \approx (dw/w) + j/2\,[(1/Qs)-(1/Q_0)] \text{----------------------------------- (2.10)}$$

Qs and Q_o are the quality factors of the cavity with and without sample. Quality factor; Q is given by $Q=f/\varDelta f$ where f is the resonant frequency and $\varDelta f$ is the corresponding 3 dB band width. For small samples, we assumed that $E = E_0$ and for the dominant TE_{10p} mode in a rectangular wave guide:

$$E_0 = E_{omax} \sin(\Pi x/a)\sin(\Pi p z/d),\ p = 1, 2, 3\ etc \text{----------------------- (2.11)}$$

E_{omax} is the peak value of E_0, 'a' is the broader dimension and 'd' is the length of the wave guide resonator. From equations 2.9-2.10, the real and imaginary parts of the relative complex permittivity are given by

$$\varepsilon' = 1+(f_0 - f_s)/2f_s \,.(V_c/V_s) \text{-- (2.12)}$$

$$\varepsilon'' = (V_c/4V_s)\,[(Q_o - Q_s)/\,Q_o\,Q_s] \text{--- (2.13)}$$

The real part of the complex permittivity; ε', is generally known as the dielectric constant/dielectric permittivity and the imaginary part; ε'', is the dielectric loss of the material. The dielectric constant represents the

amount of dipole alignment, both induced and permanent, and the dielectric loss represents the energy required to align dipoles or move ions.

The loss tangent (tan δ) is given by:

$$\tan \delta = (\sigma + w\varepsilon'')/ w\varepsilon' \text{-- (2.14)}$$

where $(\sigma + w\varepsilon'')$ is the effective conductivity of the medium. When the conductivity σ due to free charge is negligibly small (good dielectric), the effective conductivity is due to electric polarization and is reduced to:

$$\sigma_e = w\varepsilon'' = 2\Pi f \varepsilon_0 \varepsilon'' \text{-- (2.15)}$$

The efficiency of heating is usually compared by means of a heating coefficient: J, which is defined as [7, 8]:

$$J = 1/ \varepsilon' \tan \delta \text{-- (2.16)}$$

The absorption of electromagnetic waves when it passes through the medium is given by the absorption coefficient (α_f), is defined as [9]

$$\alpha_f = \varepsilon'' \, f \, /nc \text{-- (2.17)}$$

where $n = (\varepsilon'^2 + \varepsilon''^2)^{1/2}$ and c is the velocity of light.

Penetration depth, also called skin depth, is basically the effective distance of penetration of an electromagnetic wave into the material, given as [10]:

$$\delta f = 1/ \alpha f \text{-- (2.18)}$$

The quality factor; Q_0 of the cavity and resonance frequency; f_0 in the unperturbed conditions were measured. The samples in the form of thin

rectangular rods, the length of which equals the height of the cavity. The samples were inserted into the cavity through a slot and positioned at the maximum electric field. The resonance frequency; f_s and loaded quality factor; Q_s of the samples were measured. Permittivity values were then calculated using the above equations 2.12 and 2.13.

2.6.20 EMI shielding measurements

EMI shielding measurements were performed using a wave-guide coupled to an Agilent Performance Network Analyzer E8362 B in the X band. The two test port cables of the network analyzer were connected via two wave-guide to coaxial adapters. The network analyzer was calibrated in the X band frequency range (8-12) GHz for the thru response. The sample was placed between the two sections of the wave-guide and the transmission loss was measured. This directly gave the shielding efficiency of the sample. The samples used were rectangular slices of dimensions 2.3×1×0.18 cm. The set-up is shown in Fig. 2.5.

Fig. 2.5 Set-up for EMI shielding measurement

2.6.21 X-ray diffraction analysis

X-ray powder diffraction patterns were obtained by using a Bruker AXS D8 Advance X-ray Powder Diffractometer equipped with Cu Kα radiation.

2.6.22 Fourier transform infrared spectroscopy

FTIR spectra of the samples were recorded on a Thermo Nicolet FTIR Spectrometer Model Avatar 370.

2.6.23 Thermogravimetric analysis

Thermogravimetric analysis of the samples was carried out in TGA Q-50 thermal analyzer (TA Instruments) under nitrogen atmosphere. The samples were heated from room temperature to 800^0C at a heating rate of 20^0C/min and a nitrogen gas flow rate of 40–60 cm^3/min. The sample weight varied from 10–15 mg. The onset of degradation temperature, the temperature at which weight loss is maximum (T_{max}), and residual weight in percentage etc were evaluated.

2.6.24 Differential scanning calorimetry

The sample was first heated under vaccum for 15 minutes at 85^0C (elimination of water) before it was sealed in an aluminium pan with a perforated lid. The sample pan was placed in a differential scanning calorimetry (DSC) cell (Q-100, TA instruments calorimeter) under a dry nitrogen purge. The samples (3-6 mg) were inserted into the apparatus and immediately heated from -80^0C to 150^0C at a rate of 10^0C/min. and kept for one minute at this temperature inorder to erase thermal history. The samples were quenched to -80^0C and then heated to 150^0C at a heating rate of 10^0C/min. in nitrogen atmosphere.

2.6.25 Dynamic mechanical analysis

Dynamic mechanical analysis (DMA) was carried out on a DMA Q800 dynamic mechanical analyzer (TA instruments) using a tension film

mode. Samples for DMA measurement were cut from the vulcanized sheets. All samples were tested from -80 to 40^0C at a ramp rate of 3^0C/min and a frequency of 1 Hz. Oscillating strain was set at 0.02% for all tests.

2.6.26 Scanning electron microscopy (SEM)

Scanning electron microscopic studies of the tensile fractured surfaces of the vulcanizates was done on a Scanning electron microscope (JEOL JSM 840 A).

2.6.27 Atomic Force Microscopy (AFM)

The samples were imaged using Nanosurf easy scan 2 operating in contact mode using NSC14/Cr-Au cantilever. The representative scans of the blend surface at three different locations were obtained for each sample. Images were recorded in the constant force mode, under ambient conditions, in air. In this mode, an electronic feedback circuit maintains a constant cantilever deflection while the tip is scanned over the surface by adjusting the height of the sample. In this way, a three dimensional image is produced by recording the z-direction while scanning the sample in the x- and y-direction.

References

[1]   Jean LL, Marie C, J. Appl. Polym. Sci. 2001, 80, 2093.

[2]   Payne AR, Whittaker WE, Rubber Chem. Technol. 1971, 44, 440.

[3]   Ellis B, Welding GN, London: Soc. Chem. Ind., 1964.

[4]   Porter M, Rubber. Chem. Technol., 1967, 40, 866.

[5]   Flory PJ, Rehner J, J Chem Phys 1943, 11, 512-520.

[6]   Kupfer K, Kraszewski A, Knoochel R,   In Sensors Update, Wiley-VCH: 2000, 186, Germany,

[7]   Ku CC, Liepins R, Hansen Publishers 1987, 92, Munich.

[8]   Ezquerra TA, Kremmer F, Wegner, Progress in electromagnetic research Elsevier 1992, 6, New York.

[9]   Bradford LS, Carpentier MH, Chapman & Hall 1993, London.

[10]   Stephen CW, Frederic HL. United States Book crafters, Chelsea, 1985.

.....ഇൗ.....

EPDM/FLUOROCARBON RUBBER BLENDS: THERMAL AND MECHANICAL PROPERTIES[*]

Contents

Ethylene propylene diene rubber (EPDM) and Hexa fluoropropylene-vinylidinefluoride dipolymer, Fluoroelastomer (FKM) blends with and without compatibilizer (MA-g-EPDM) were prepared by two-roll mill mixing. The effect of blend ratio and amount of compatibilizer on mechanical properties and thermal stability were investigated. The cure characteristics and mechanical properties of EPDM, FKM and their blends of varying compositions were studied for unaged and aged samples. The 50:50 (w/w) FKM/EPDM showed the highest mechanical properties. The tensile properties of all the composites, especially those with higher proportion of FKM increased with aging. Swelling of the blends was reduced after aging. The incorporation of FKM rubber improved the thermal stability of EPDM rubber. The apparent degradation activation energy (E) of EPDM/FKM blends was calculated by using Coats–Redfern method. The results showed that the EPDM/FKM blends had higher thermal stability but lower E than FKM. The thermal degradation process of both EPDM/FKM blends and FKM were determined by nucleation and growth mechanism. The differential scanning calorimetry (DSC) results showed that glass transition temperature (T_g) peak for EPDM is shifted to higher temperature, due to improved compatibility on addition of compatibilizer. The dynamic mechanical properties such as storage modulus, loss modulus and damping properties of blends was investigated with special reference to the effect of blend ratio and compatibilizer loading. The effect of change in the composition of the polymer blends on tan δ was studied to understand the extent of polymer miscibility and damping characteristics. The morphology of blends was investigated using scanning electron microscopy (SEM) and atomic force microscopy (AFM).

[*]   1.Ajalesh Balachandran Nair, Philip Kurian, Rani Joseph. Ethylene–propylene–diene terpolymer/hexa fluoropropylene–vinylidinefluoride dipolymer rubber blends: Thermal and mechanical properties. *Materials & Design*, Volume 36, 2012, p 767-778.
2. Ajalesh Balachandran Nair, Philip Kurian, Rani Joseph. Studies on EPDM/FKM blends: Effect of MA-g-EPDM as a compatibilizer. *Journal of Polymer materials: An international journal*, Volume 30, 2013, p 37-51.

3.1 Introduction

Fluoroelastomers are widely used in many industrial applications due to their excellent resistance to heat, oil and solvent [1-5]. The increasing use of such polymers in automobiles, aerospace, off shore and energy related industries impose them stringent product performance standards under high temperatures and in hostile chemical environments [6-11]. It is also used in elastomeric sealing applications of nuclear reactors [12]. The application of fluoroether rubber was overviewed in military affairs, automobile, petroleum exploitation, semiconductor industry [13]. Ethylene propylene diene monomer rubber (EPDM) has excellent performance in low-temperature flexibility, thermal stability, weatherability and resistance to oxidation and ozone [14-17]. EPDM can also accept large amounts of filler and extender oil with no significant prejudice to the final properties [18, 19]. Different compatibilized and non compatibilized polar non-polar blends were prepared by various researchers [20, 21]. Blending of FKM into EPDM can be a potential measure to prepare materials with better overall properties. However, the high incompatibility and non-co-vulcanization between FKM and EPDM make it difficult to obtain a blend with better overall properties [22, 23]. The problem of the cure rate incompatibility in dissimilar rubbers was studied by Rao Qiuhua et al. [24]. Fluoroelastomer (FKM)/ethylenepropylene-diene rubber (EPDM) blends were prepared by static vulcanization and dynamic vulcanization by Qian Lili et al. [25]. The fluororubber/methyl vinyl silicone rubber (FKM/MVQ) blends were prepared by mechanical blending [26]. The mechanical properties and dynamic mechanical properties of fluoroelastomer (FKM)/thermoplastic polyurethane (TPU) blend compatibilized with FKM-graft-maleic anhydride (FKM-g-MA) were experimentally investigated by

Dong Lijie et. al.[27]. The thermal stability of blends depends strongly on the compatibility of the polymers [28].

Different polymers decompose over different temperature ranges yielding different proportions of volatiles and residues. One of the most accepted methods, for studying the thermal properties of polymeric materials is the thermogravimetry. Thermogravimetric curve represents the drop in the weight (W) of the sample with the temperature (T). The normal (TGA) and derivative (DTG) thermogravimetric curves provide information about the nature, number of stages of thermal breakdown, weight loss of the materials in each stage, threshold temperature, stability and extent of degradation of the polymeric material [29].

Polymer blends are generally categorized into two main classes: miscible blends that exist in a single homogeneous phase exhibiting synergistic properties and immiscible blends that have two or more different phases, showing at least two glass transition temperatures (Tgs). Apart from these two, there is a third category of blends, called technologically compatible blend, which exist in two or more different phases on micro scale, yet displays combination of properties [30,31].

Maleic anhydride (MA) modification of different kinds of rubber is a useful way of compatibilizing immiscible polymer blends as well as improving interfacial adhesion in polymeric composites. Several factors can influence mechanical properties, such as the particle size and particle size distribution of the dispersed phase, and the degree of adhesion between the two phases. The adequate chemical structure of the compatibilizing

agent can reduce the interfacial energy between the phases and finer dispersion can be achieved [32].

In this chapter, we report the evaluation of the physico-mechanical, dynamic mechanical and thermal stability of compatibilized and non-compatibilized EPDM/FKM blends at different blend ratios. SEM and AFM investigations have been carried out to study the morphology of the EPDM/FKM blends.

3.2   Experimental details
3.2.1 Materials

Detailed material description is given in section 2.1.

3.2.2 Methods

Formulation used in the preparation of EPDM/FKM blends is given in table 2.3. Experimental procedures are presented in section 2.6.

3.3   Results and Discussion
3.3.1 Cure characteristics

Fig. 3.1 represents the effect of blend ratio on the cure curves of EPDM/FKM blends. Fig. 3.2 represents the cure curves of EPDM/FKM compatibilized blends. Variation of scorch time (T_{10}) and cure time (T_{90}) is shown in table 3.1. In the case of non-compatibilized blends, the optimum cure time (T_{90}) increases with the addition of FKM. The cure time for EPDM is 11.3 min. and that for FKM is 20.4 min. All other blends show an optimum cure time between that of EPDM and FKM. In the case of the EPDM/FKM blends, E_{50} shows the highest cure time. The maximum torque values increase with increase in concentration of

FKM (Fig. 3.1). E_0 shows maximum torque value of 8.5 dNm and E_{100} the least, 3.8 dNm.
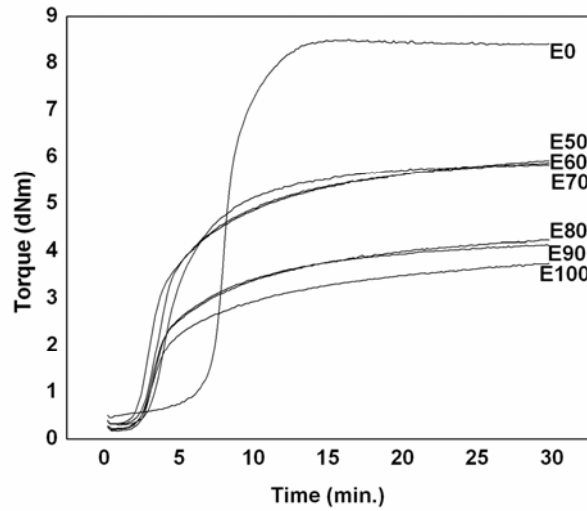

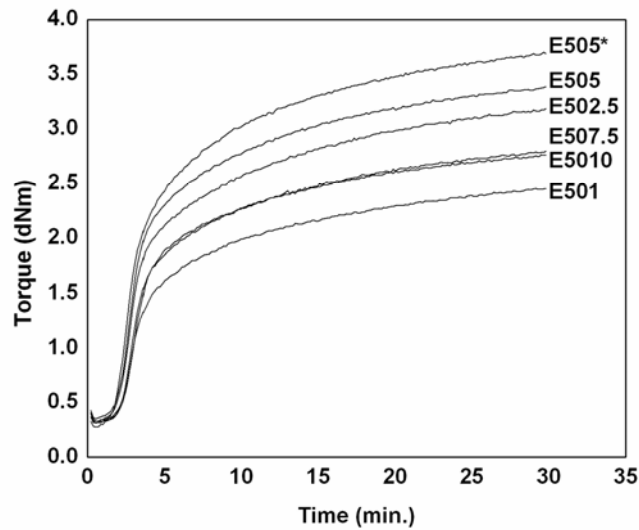**Fig. 3.1 Effect of blend ratio on the cure curves of EPDM/FKM blends**

Fig. 3.2 Cure curves of EPDM/FKM blends compatibilized with MA-g-EPDM

The increase in the cure time of the compatibilized blends may be attributed to the cure retardancy effect of maleic anhydride. The reactions between some maleic anhydride groups of the MA-g-EPDM with accelerator may cause a delay in the optimum cure time. On the other hand these reactions increase interfacial bonding between EPDM and FKM in the presence of MA-g-EPDM. In the case of 50/50, EPDM/ FKM compatibilized blends, the optimum cure time increases with increase in the amount of MA-g-EPDM. The mix containing 10 phr MA-g-EPDM shows the highest cure time. The maximum torque value is obtained for E505*. In all the blends, the scorch time (time required to reach 10 % of the maximum torque) is found to be unaltered and the mechanical properties are improved by the addition of FKM.

The mooney viscosities of the blends were determined using mooney viscometer (section 2.6.3). From table 3.1, it is found that the mooney viscosity decreases with increase in FKM content. The uncompatibilized blends were characterized by sharp interface and poor interaction between the two phases, resulting in interlayer slip between phases, which may result in the reduction of mooney viscosity.

Table 3.1 Properties of vulcanizates

Sample	Scorch time (Min.)	Cure time (Min.)	Mooney viscosity ML(1+4) 100°C	Hardness (Shore A)	Rebound resilience (%)	Abrasion loss (cm³/h)	Compression set (%)	Heat buildup (°C)	Crosslink density 10^{-5}gmolcm^{-3} in toluene	in MEK
E_{100}	2.58	11.3	60	51	61	5.21	29.68	8	9.5	-
E_0	7.00	20.4	70	72	40	3.31	10.22	19	-	3.37
E_{90}	2.68	14.1	51	53	57	4.69	27.96	14	10.2	17.8
E_{80}	2.60	15.1	49	55	55	4.36	25.20	16	11.4	14.1
E_{70}	3.23	15.5	48	56	50	3.75	25.33	17	11.6	10.3
E_{60}	2.77	16.1	47	62	51	3.36	20.42	19	12.6	7.4
E_{50}	2.37	17.6	45	65	49	3.23	16.35	21	13.6	5.8
E_{501}	2.00	16.3	49	66	46	3.20	15.29	26	14.3	6.2
$E_{502.5}$	2.13	16.3	49	65	45	3.18	15.34	29	16.4	6.5
E_{505}	2.14	17.3	50	65	43	3.16	15.92	29	18.7	7.3
E_{505*}	2.32	17.2	49	66	42	3.11	15.44	28	19.0	7.9
$E_{507.5}$	2.33	18.0	49	65	41	3.09	14.29	29	19.1	8.0
E_{5010}	2.40	18.7	49	66	40	3.12	13.52	30	18.8	8.4

The mooney viscosity of EPDM/FKM with varying compatibilizer content as shown in table 3.1, indicates that the blends become more viscous with the addition of compatibilizer during compounding. The increase in mooney viscosity indicates that there is less slippage at the interface as a result of the addition of the compatibilizer. This is because the compatibilizer decreases the interfacial tension resulting in stronger interaction between EPDM and FKM. This gives rise to an increase in mooney viscosity of the blends when MA-g-EPDM is added.

3.3.2 Effect of thermal aging on stress-strain properties

Aging of polymers normally reduces its mechanical properties. But in the case of both compatibilized and non-compatibilized EPDM/FKM blends, aging at 70 and 150^{0}C for 22 h, does not alter the mechanical properties. This is primarily because the EPDM and FKM are basically high temperature resistant material and the conditions under which aging tests are performed are not very severe. The main objective of the aging study is to determine whether the blends prepared from EPDM and FKM are resistant to standard aging tests. Aging helps the process of vulcanization of FKM and their blends to reach maximum level. During press curing of FKM blends, reaction products such as water, generated from the following reaction inhibits the vulcanization process and hence lowers the strength [33].

$$MgO + 2HF \rightarrow MgF_2 + H_2O \text{ --- (3.1)}$$
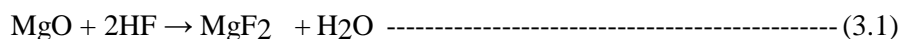
During aging process, evolved water is removed easily in an open air atmosphere. It can be seen that the effect of aging on the tensile strength is minimum for EPDM. The blends containing FKM show an increase in tensile strength because of the completion of curing during aging. Effect of

cure system affects the mechanical and physico-chemical properties of rubber vulcanizates [34].

The rubber samples under investigation, which did not contain any antioxidant, were subjected to thermal aging at 70, 150 and 200 ^{0}C for 22 h. Aging temperature play an important role in changing the mechanical behaviour of rubber [35]. The effects of thermal aging on the tensile strength, elongation at break, modulus at 100 % elongation and the equilibrium swelling of the samples were studied. Figs. 3.3, 3.4 and 3.5 show that the tensile strength, elongation at break and 100 % modulus increase at 70 ^{0}C and 150 ^{0}C aging and decrease slightly at 200 ^{0}C aging. This behaviour can be attributed to further crosslinking of the rubber vulcanizates, followed by degradation of polymer chain. But in the case of FKM all the above properties remain unaltered on aging.
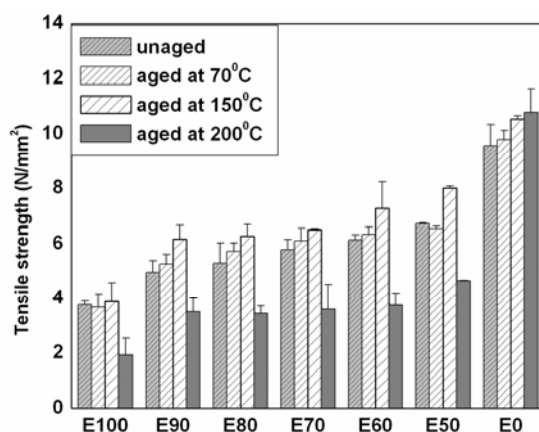

Fig. 3.3 Variation in tensile strength before and after aging for uncompatibilized EPDM/ FKM blends
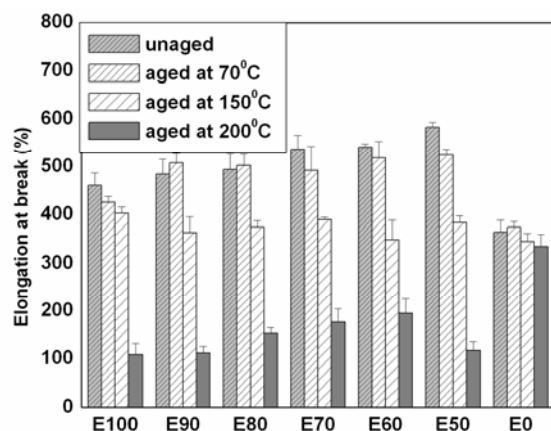
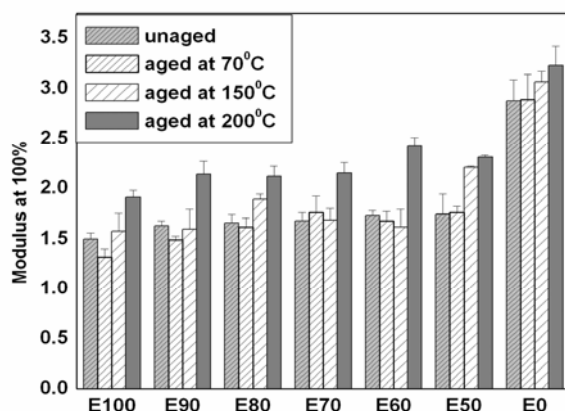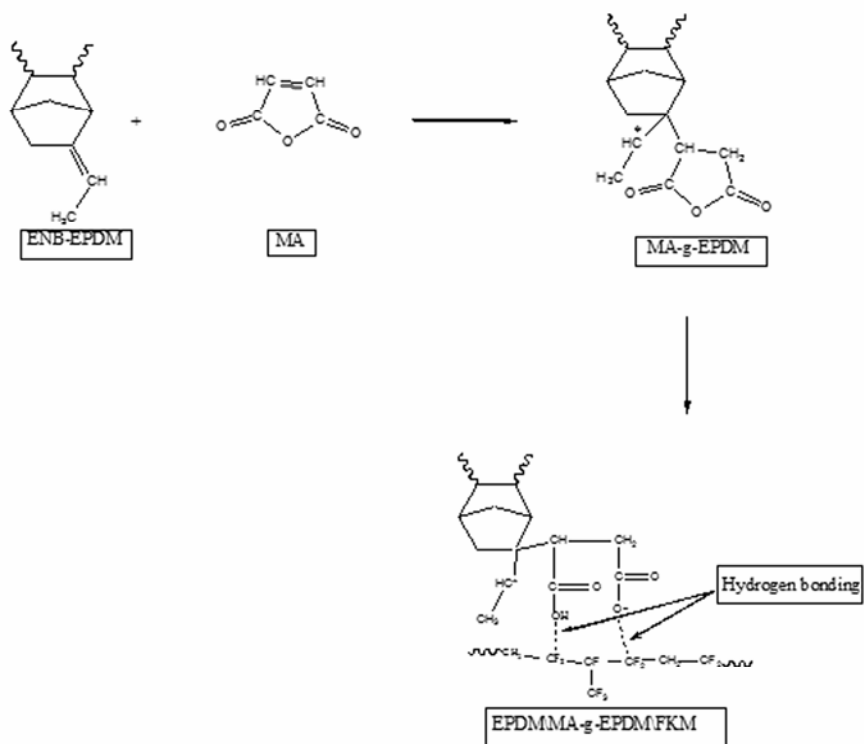**Fig. 3.4 Variation in elongation at break before and after aging for uncompatibilized EPDM/ FKM blends**

Fig. 3.5 Variation of modulus (at 100% elongation, N/mm^2) of the uncompatibilized EPDM/ FKM blends before and after aging

In compatibilized blends of EPDM/FKM, the 50/50 (w/w) blend was subjected to detailed study. Tensile strength of EPDM/MA-g-EPDM/FKM increases by compatibilization with MA-g-EPDM as shown in Fig. 3.6. The increment of tensile strength of compatibilized blend compared to uncompatibilized EPDM/FKM blends is due to the formation of hydrogen bonding (Scheme 3.1) and improvement in the interfacial interactions

between EPDM and FKM in the presence of compatibilizer, as confirmed by the morphological behavior.

Scheme 3.1 Possible interaction of compatibilized EPDM/ FKM blends
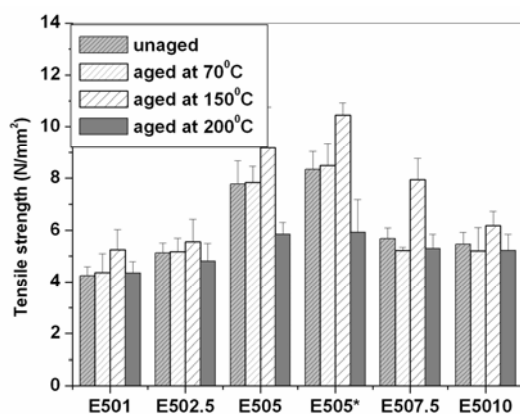

Fig. 3.6 Variation in tensile strength before and after aging in 50/50, EPDM/FKM blends with compatibilizer MA-g-EPDM

Fig. 3.7 show the variation of elongation at break (EB) of the compatibilized blends with increasing amounts of MA-g-EPDM. On addition of MA-g-EPDM, the EB of the compatibilized blends increased. E_{505*} shows maximum EB. After aging the EB value of all the blends decreases and it shows lowest value at 200 ^{0}C aging for 22 h. The tensile modulus at 100 % elongation (M_{100}) of the EPDM/FKM blends with and without MA-g-EPDM is shown in Fig. 3.8 and 3.5 respectively. The presence of maleic anhydride groups causes a stronger interaction between EPDM and FKM in comparison to the blends without MA-g-EPDM. The degree of reinforcement is much more significant in the presence of the MA-g-EPDM as compatibilizer in EPDM/FKM blends. The increase in modulus after aging is due to increase in crosslink density. The samples containing increasing concentration of FKM show better retention in properties after aging. This again shows that the introduction of FKM can improve the aging resistance of the EPDM in its blends.
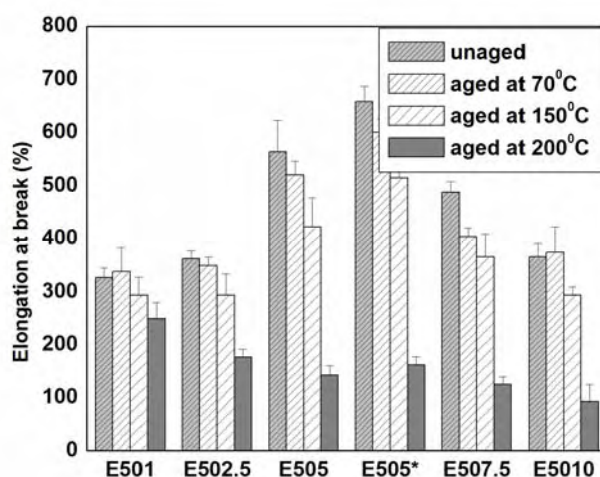

Fig. 3.7   Variation in elongation at break before and after aging in 50/50, EPDM/ FKM blends compatibilized with MA-g-EPDM
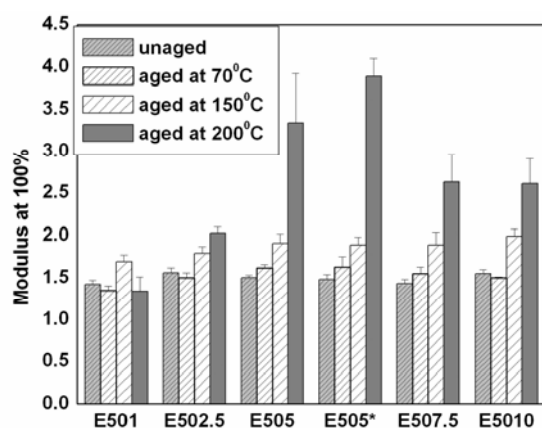
Fig. 3.8 Variation of modulus (at 100% elongation, N/mm^2) of the compatibilized EPDM/ FKM blends before and after aging

3.3.3 Other mechanical properties

Table 3.1 shows the resilience, hardness, abrasion resistance, and compression set of the vulcanizates. In all the cases the compatibilized vulcanizates show better properties confirming the effect of compatibilization. There is a gradual increase in heat generation values of all the blends (table 3.1). The energy dissipation can be through loss at filler-matrix interface, friction between the chains and break down of filler structure. Compared to uncompatibilized blends, the compatibilized blends show higher heat build-up values. This will be manifested as lower resilience values.

3.3.4 Swelling studies

The swelling percentage is the measurement of the degree of cross linking, the reduction in swelling indicating increase in cross link density and thus the reduction in solvent uptake. Fig. 3.9 gives a comparison between the swelling percentage of the compatibilized and uncompatibilized blends aged at different temperatures. After aging, the equilibrium swelling of

compatibilized blends decreases much more than that of the uncompatibilized blends. The increase in cross link density of blends after adding MA-g-EPDM may be due to the hydrogen bonding with FKM. The stress-strain properties discussed earlier also confirm these results. The addition of carbon black decreases the swelling of all the blends. This may be due to a restriction to the penetration of the solvent molecules into the bulk of the polymer by the filler-polymer network. The extent of swelling of a blend in a solvent depends on the structure of the polymer phases and can be related to the properties of the polymer chains, such as molecular mobility, phase interaction, and so on [36]. As filler preferentially reinforces the rubber phase, its introduction should reduce the volume swell of the rubber phase and, thus, reduce the overall volume swell of the blends in solvent. This phenomenon is also related to the vulcanization procedure of rubber. In the aging process, there is some unreacted anhydride groups (MA-g-EPDM) embedded in the EPDM matrix reacting with FKM because of the chain movement of MA-g-EPDM. Thus the compatibilized blends are vulcanized for the second time and equilibrium swelling ratio is reduced more after aging than that of the uncompatibilized blends. All compatibilized blends display lower solvent uptake than the non modified blend, which is an indication of increase in crosslink density (table 3.1). In Fig. 3.10, the photographs show the swelling of different samples (a) in MEK and (b) in Toluene. The difference in swelling behaviour of the samples is clearly understood from the Fig. 3.10.
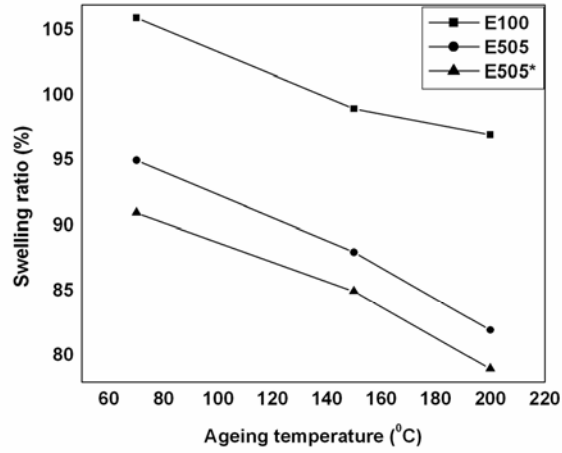
Fig. 3.9 Variation of swelling ratio (in toluene) of EPDM and EPDM/FKM blends with aging temperature
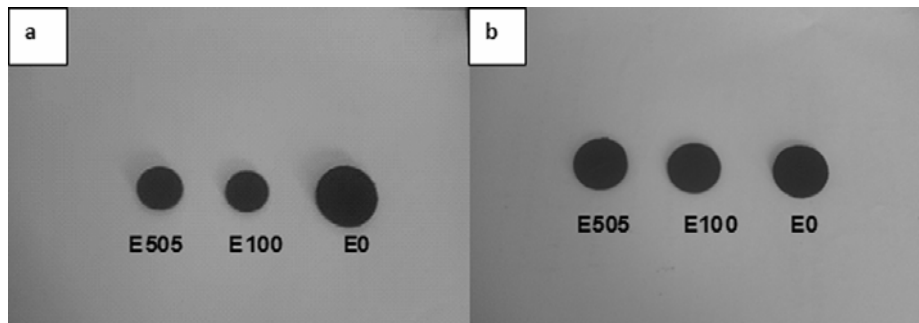
Fig. 3.10 Photographs showing the swelling of different samples (a) in MEK and (b) in toluene

3.3.5 Thermal stability of neat polymers and uncompatibilized blends

The thermal degradation temperature of EPDM, FKM and their blends with and without compatibilizer is determined by the thermogravimetric analysis. The TGA and DTG thermograms of EPDM and FKM in nitrogen atmosphere are shown in Fig. 3.11 (a) and (b). As it can be seen from Fig. 3.11 (a), in the case of EPDM, a major degradation starts at 418 ^{0}C and gets completed at 511 ^{0}C. Hence the sample can be considered as stable up to 418 ^{0}C

in nitrogen atmosphere. Above 511 ^{0}C volatilization becomes very rapid and almost complete decomposition occurs. So we could not see any appreciable weight loss in the thermogram above this temperature. The peak of the DTG curves gives the temperature corresponding to maximum degradation (T_{max}). In the DTG curve of EPDM, the peak appeared at 487 ^{0}C. The degradation of FKM (Fig. 3.11b) starts at around 438 ^{0}C and gets completed almost at 523 ^{0}C. FKM has got greater thermal stability in nitrogen atmosphere than EPDM, which is evident from the displacement of the weight loss curve to higher temperature. DTG curve also supports the thermal stability of FKM (T_{max} 502 ^{0}C), when compared to EPDM (T_{max} 487 ^{0}C).
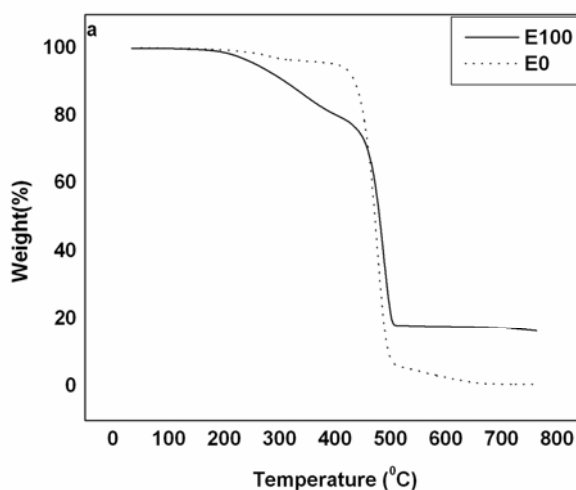

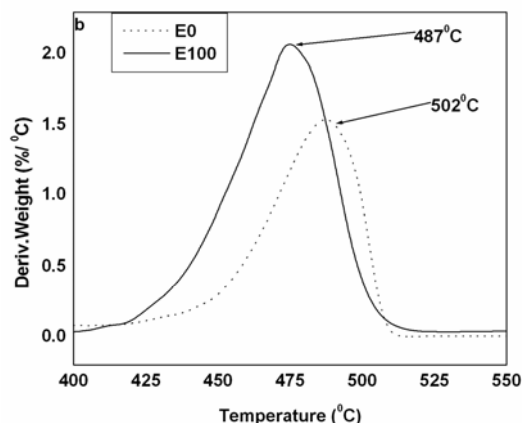**Fig. 3.11 (a) The thermograms of EPDM and FKM vulcanizates**

Fig. 3.11 (b) The derivative thermograms of EPDM and FKM vulcanizates

The thermal degradation of the rubber results in the scission of cross linking network and the chain cleavage, and the decrease of the cross linking density and molecular weight. This reduces the mechanical strength and the application value of the rubbers. It has been confirmed that the polymers like fluorocarbon rubbers [37, 38] degrade in several steps including chain cleavage, end-initiated depolymerization and random scission.

The effect of blend ratio on the TGA and DTG themograms of blends is presented in Fig. 3.12 (a) and (b) respectively. The weight loss of neat polymers and their blends at different temperatures is given in table 3.2. It can be seen from table 3.2 that degradation temperature corresponding to different percentage weight loss increases gradually by the addition of FKM rubber in blends. Table 3.2 also gives the percentage weight loss of the specimens at three different temperatures viz. 450, 475 and 500 ^{0}C. As the percentage of the FKM rubber in the blend increases, a gradual decrease of weight loss can be noticed indicating an increase in thermal stability. This indicates improved thermal stability upon incorporation of FKM. The thermal stability of the polymer blends depends mainly on the morphology and the miscibility of the

system. From Fig. 3.12(b) it is clear that among the blends E_{50} possesses highest T_{max} value, indicating highest thermal stability. E_{50} blend has got co-continuous structure. The thermal degradation results suggest that even though the EPDM/FKM blends are immiscible, the thermal stability of EPDM can be improved by the addition of FKM.
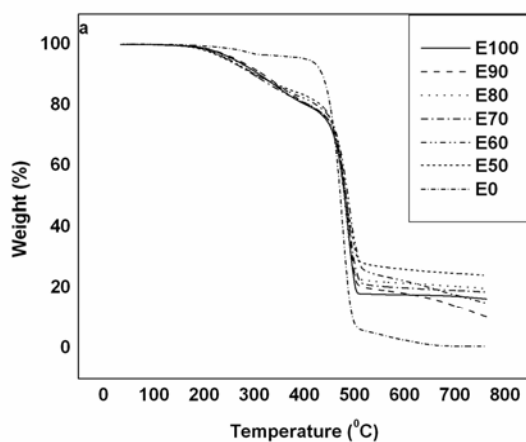

Fig. 3.12 (a) Effect of blend ratio on the thermograms (TGA) of EPDM, FKM and their blends
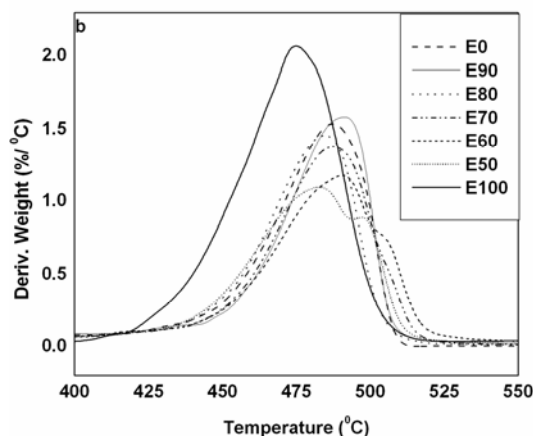
Fig. 3.12 (b) Effect of blend ratio on the derivative thermograms (DTG) of EPDM, FKM and their blends

Table 3.2 Degradation temperatures and weight loss at different temperatures of samples

Sample	Onset degradation temperature (T_0, ^{0}C)	Temperature at which 50% degradation (T_{50}, ^{0}C)	Maximum degradation temperature ($T_{max.}$, ^{0}C)	Weight loss at 450^0C (%)	Weight loss at 475^0C (%)	Weight loss at 500^0C (%)
Pure EPDM	404	463	467	24	80	99
Pure FKM	409	463	466	28	74	94
E_{100}	418	480	487	26	43	78
E_0	438	501	502	5	17	48
E_{90}	410	480	485	28	49	76
E_{80}	420	481	487	25	42	74
E_{70}	423	481	486	25	42	73
E_{60}	421	482	486	25	42	68
E_{50}	422	490	490&504	22	35	60
E_{501}	433	498	487&510	19	29	51
$E_{502.5}$	440	495	489&509	19	31	54
E_{505}	436	502	487&511	18	29	55
E_{505*}	435	498	486&506	20	32	58
E_{5010}	427	496	485&500	19	33	56

3.3.6 Thermal stability of compatibilized blends

Fig.3.13(a) and (b) shows the TGA and DTG curves for compatibilized 50/50 (w/w) EPDM/FKM blends. Compatibilizer has substantial influence on the thermal properties of the blends. The thermal stability of the blends was found to increase with the addition of MA-g-EPDM. This may be due to the physical interaction between the two constituents at the interface without influencing the bulk. So the individual components are likely to follow their own degradation route. In Fig. 3.13(b), the peak corresponding to the major weight loss is shifted to higher temperatures upon compatibilization. The addition of 1phr of MA-g-EPDM results in the improvement of the onset temperature of degradation. Interestingly, E_{505} blend system is found to possess better thermal stability compared to all other blends. The addition of 5 phr of MA-g- EPDM to E_{50} blend shows the highest degradation temperature. Further additions of the compatibilizer (10 phr) don't show improvement in the degradation temperature. It can also be seen from the table 3.2, that the degradation temperature corresponding to the major weight loss (DTG peak) increased upon compatibilization. The percentage weight loss at different temperatures decreased upon compatibilization. Thus it is clear from the table 3.2 that all blends with MA-g-EPDM are thermally more stable compared to un-compatibilized blends.
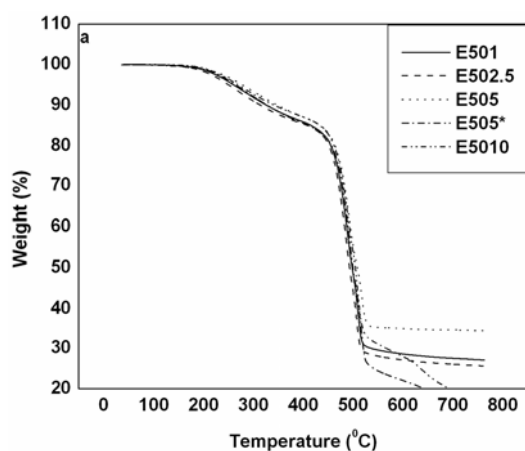
Fig. 3.13 (a) Thermograms of 50/50, EPDM/FKM blends compatibilized with MA-g- EPDM
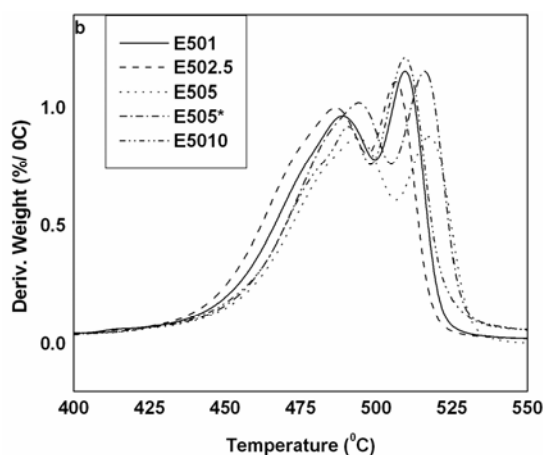
Fig. 3.13 (b) Derivative thermograms of 50/50, EPDM/FKM blends compatibilized with MA-g-EPDM

From table 3.3, the initiation of degradation ($T_{5\%}$) of EPDM is found to occur at 255^0C and that of FKM at 450^0C. In the case of uncompatibilized blends, the incorporation of FKM shows only a slight improvement in the initiation temperature of degradation. But in the case of all compatibilized E_{50} blends, the incorporation of FKM is found to shift the degradation temperature to a higher region.

Table 3.3 Initiation degradation temperatures of different samples

Sample	Temperature at which 5% degradation ($T_{5\%}$, ^0C)	Temperature at which 10% degradation ($T_{10\%}$, ^0C)	Temperature at which 15% degradation ($T_{15\%}$, ^0C)
E_{100}	255	312	355
E_0	450	464	473
E_{90}	258	311	357
E_{80}	259	314	358
E_{70}	260	318	361
E_{60}	262	321	363
E_{50}	263	323	381
E_{501}	261	327	416
$E_{502.5}$	262	326	411
E_{505}	271	342	427
E_{505*}	265	327	421
E_{5010}	260	332	424

The change in degradation temperature of compatibilized blends is due to the improved interfacial adhesion between the two components as a result of interphase linking through MA-g-EPDM. MA grafted EPDM shows interaction between the polar anhydride groups of EPDM and the C-F bonds in FKM phase as illustrated in scheme 3.1. The resulting copolymer will locate at the interface and decreases interfacial tension thus providing a good interfacial adhesion between the EPDM and FKM phases. This in turn will contribute towards the improvement of thermal stability.

3.3.7 Kinetic analysis of thermal decomposition

The degradation behavior of EPDM/FKM blends is studied by Coats–Redfern method [39]. The thermal degradation functions adopted are listed in table 3.4. The Coats–Redfern method is correlative to the thermogravimetric function $g(\alpha)$ and activation energy is obtained from the equation:

$$\ln [g(\alpha)/T^2] = \ln \{(AR/\Phi_E) (1{-}2RT/E) \} - E/RT \text{--------------------- (3.2)}$$

where α is the decomposed fraction at any temperature and is given as:

$$\alpha = C_i{-}C/C_i{-}C_f \text{ --- (3.3)}$$

where 'C' is the weight at the temperature chosen, C_i is the weight at initial temperature and C_f is the weight at final temperature, 'α' is the heating rate and 'E' is the activation energy for decomposition. The activation energy (E) is determined from the plot of ln $[g(\alpha)/T^2]$ against the reciprocal of absolute temperature (1/T). Activation energy (E) can be calculated from the slope of the curve. The order of decomposition reaction was determined from the best linear fit of the kinetic curve that gives the maximum correlation coefficient. The form of $g(\alpha)$, which best represents the experimental data gives the proper mechanism. From these calculations we find that the Mampel equation $[-\ln (1{-}\alpha)]$ fits well in the case of various uncompatibilized and compatibilized EPDM/FKM blends. The linear correlation coefficients suggest that the F_1 model is the most appropriate to describe the experimental results (Table 3.5). This shows random nucleation, as the mechanism of degradation is the rate controlling process.

Table 3.4. The mechanisms of solid-state thermal degradation reaction and corresponding thermal degradation functions g(α)

g(α) = kt	Symbol	Rate controlling process
	Deceleratory αt curves	

(a) Based on diffusion mechanism

g(α) = kt	Symbol	Rate controlling process
α^2	D_1	One-dimensional diffusion
$\alpha+(1-\alpha)\ln(1-\alpha)$	D_2	Two-dimensional diffusion
$[1-(1-\alpha)^{1/3}]^2$	D_3	Three-dimensional diffusion
$1-(2/3)\alpha-(1-\alpha)^{2/3}$	D_4	Three-dimensional diffusion (Gistling-Brounshtein equation)

(b) Based on geometrical models

g(α) = kt	Symbol	Rate controlling process
$1-(1-\alpha)^{1/n}$	R_n	Phase-boundary reaction; n=1, 2 and 3 (one, two and three dimensional, respectively

(c) Based on 'order' of reaction

g(α) = kt	Symbol	Rate controlling process
$-\ln(1-\alpha)$	F_1	First order (Mampel equation)

Table 3.5. Apparent activation energy (E) and correlation coefficients (r) for FKM and EPDM/FKM blends by Coats–Redfern method

Sample	E (kJ/mol)	r
E_{100}	111	0.9936
E_{90}	113	0.9942
E_{80}	119	0.9980
E_{70}	119	0.9934
E_{60}	120	0.9997
E_{50}	121	0.9986
E_{501}	126	0.9984
$E_{502.5}$	129	0.9989
E_{505}	131	0.9993
E_{505*}	134	0.9984
E_{5010}	126	0.9979
E_0	189	0.9985

In the case of uncompatibilized blends, the activation energy value revealed that the incorporation of FKM has resulted in slight enhancement of activation energy. From table 3.5it is clear that the activation energy is highest for FKM. Higher value of activation energy (E) indicates higher thermal stability. Representative plot of Coats– Redfern equation for E_0 and E_{100} are shown in Fig. 3.14. It is interesting to note that all the compatibilized blends show higher activation energy (E) as expected. This indicates that compatibilization using MA-g-EPDM also increases the thermal stability of E_{50} blend system. Addition of 5phr of compatibilizer shows the highest activation energy compared to other compatibilized and uncompatibilized systems. From the table 3.5 it is observed that the EPDM/FKM blends have lower apparent activation energy (E) than FKM. It means that FKM has better thermal stability than its blends with EPDM.
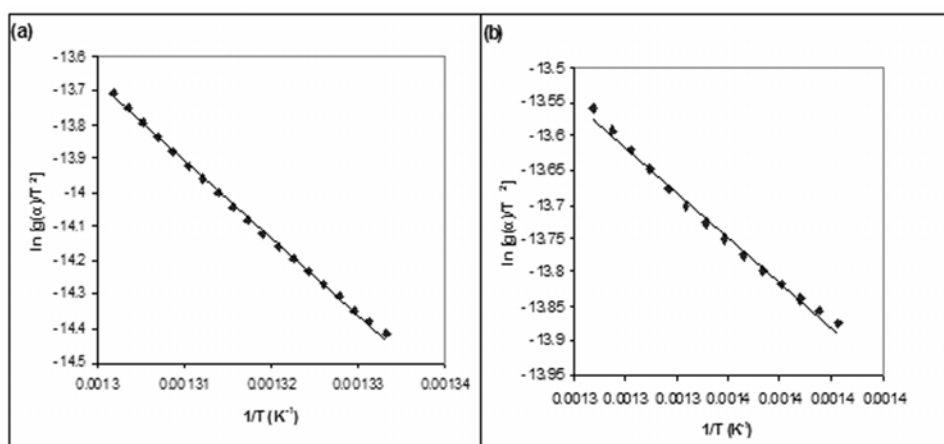

Fig. 3.14 Representative plot of Coats–Redfern equation for (a) E_0 and (b) E_{100}

3.3.8 Differential scanning calorimetry

The DSC curves of pure EPDM, FKM and its blends are shown in Fig. 3.15(a) and (b) respectively. The glass transition temperature of the polymer depends on the structure and co-operative mobility of the chain segments. This behaviour is reflected in the occurrence of a single glass transition temperature in miscible blends. In the case of partially miscible blends, the glass transition temperature gets shifted. In completely immiscible polymer blends, the T_g remains unaltered [40]. T_g value of pure EPDM is found to be -60.01^0C and that of pure FKM is $-19.25 ^0$C. In Fig 3.15(b), the uncompatibilized blend E_{50} shows that the T_g value of both components remain unaltered. But in the case of compatibilized blend E_{505*}, the T_g of EPDM phase shifted (-55.48^0C) towards FKM, indicates better interaction between the FKM phase because of the effect of the MA-g-EPDM.
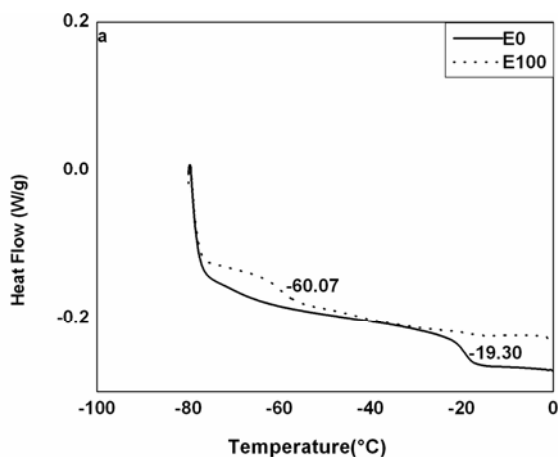

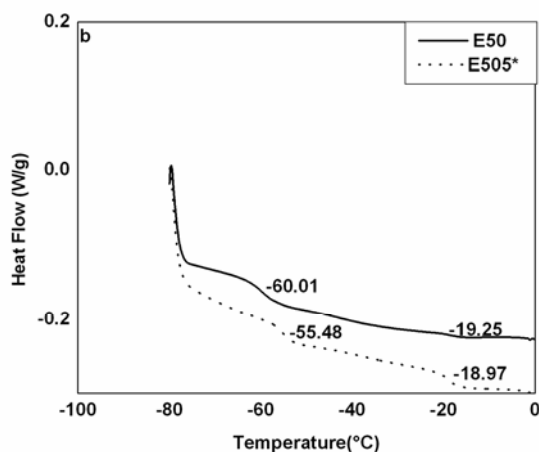**Fig. 3.15 (a) The DSC curves of EPDM and FKM vulcanizates**

Fig. 3.15 (b) The DSC curves of compatibilized and uncompatibilized 50/50, EPDM/ FKM blends

3.3.9 Scanning electron microscopy

The tensile fractured surfaces of EPDM/FKM and EPDM/MA-g-EPDM/FKM blends are presented in Fig. 3.16 and 3.17 respectively. It is evident that the morphologies of the tensile fractured surfaces of the compatibilized and uncompatibilized blends are quite different. In the case of uncompatibilized blends (Fig. 3.16), a large number of holes are clearly observed, indicating the poor interfacial adhesion between EPDM and FKM. Moreover, the fracture surface is found to be smooth resulting from a brittle matrix fracture. In the 50/50 blend containing MA-g-EPDM (Fig. 3.17), the fracture surface is rough and fractures in ductile mode. In compatibilized blends, the SEM photographs show a finer and more even dispersion of the elastomer particles. Morphology studies of the blend samples are in good agreement with the variation in mechanical properties.
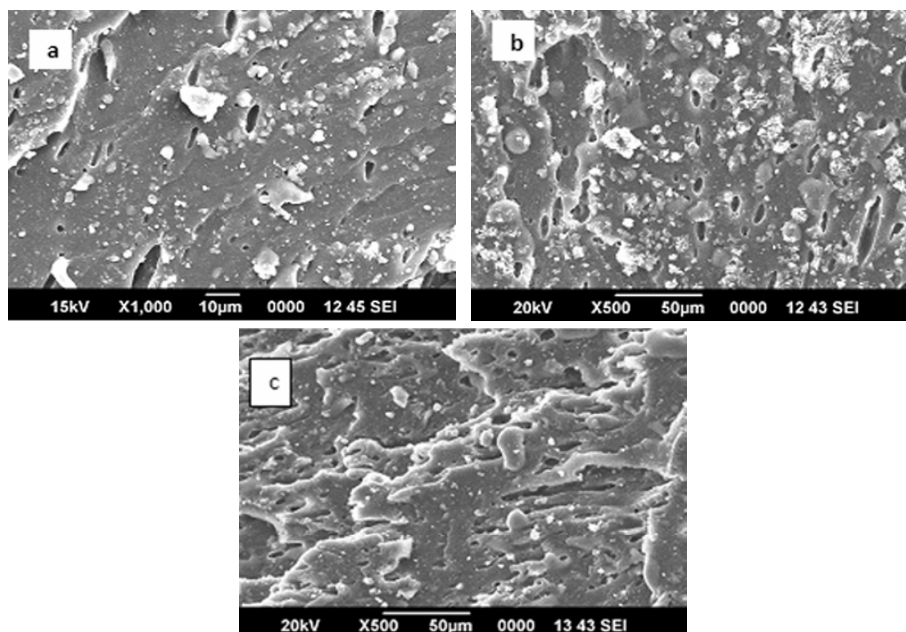
Fig. 3.16 Scanning electron photographs of EPDM/ FKM blends (a) E$_{80}$ (b) E$_{60}$ (c) E$_{50}$
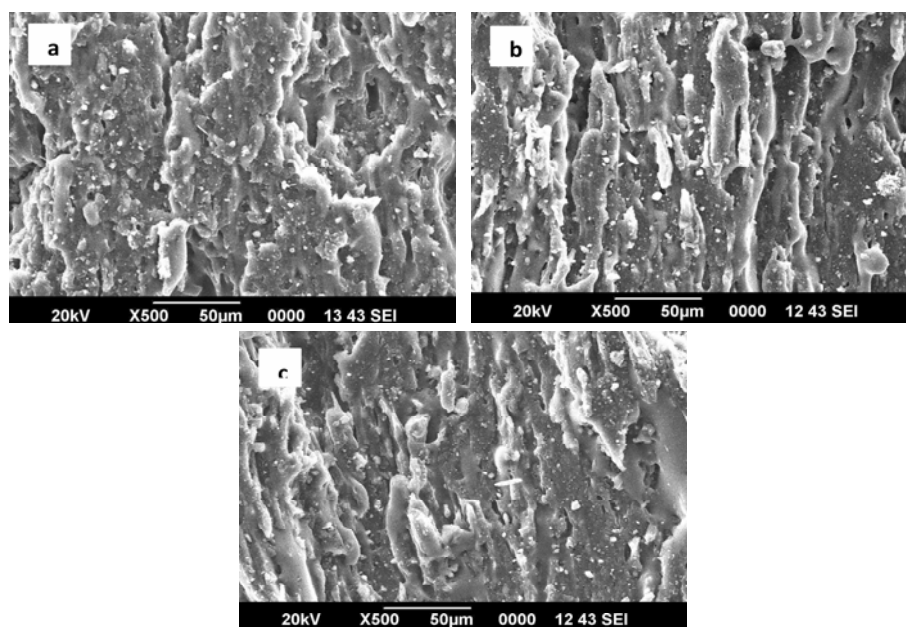

Fig. 3.17 Scanning electron photographs of 50/50 blend containing different levels of MA- g-EPDM (a) 2.5 (b) 5 (c) 10 phr

3.3.10 Dynamic mechanical analysis (DMA)

3.3.10.1 Uncompatibilized blends- effect of blend ratio

When a polymeric material is subjected to dynamic mechanical stress, the stress-strain curve is not reversible, because a part of the energy is lost due to internal friction. The energy loss is appreciable for most elastomeric material and is used for controlling fatigue and vibration isolation. Hence the dynamic modulus is expressed as complex modulus, which consists of two components, storage modulus (E') and the loss modulus (E"). The storage modulus represents the energy stored to cause subsequent deformation and loss modulus represents the energy lost due to hysteresis. The ratio of the loss modulus and storage modulus is called loss factor (tan δ) and represents internal friction or damping. Hence DMA provides information on change in internal damping as well as glass transition temperature of polymeric materials and their blends.

The characterization of rubber blends can also done with the help of dynamic mechanical analysis. It helps to study the polymer/polymer compatibility. The T_g of a polymer depends on the structure and co-operative mobility of the chain segments. Generally for incompatible system, the tan δ versus temperature curve shows two damping peaks corresponding to the glass transition temperatures of individual polymers [41]. When blend components are compatible, a single peak is found for the combined processes [42]. Broadening of the transition occurs in the case of partially compatible systems. Shift in T_g to higher or lower temperatures also indicates partial miscibility.
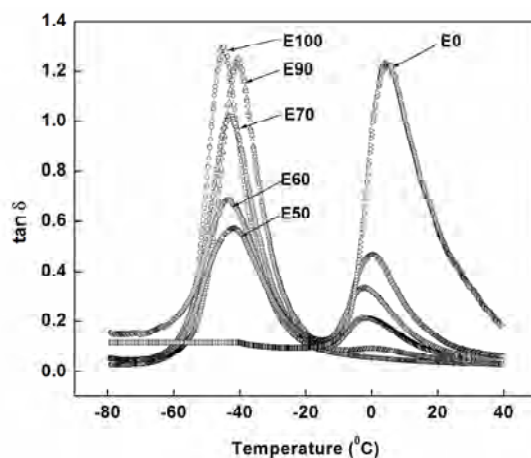
Fig. 3.18. Tan δ vs temperature curves for different composition of EPDM/ FKM blends

Tan δ vs temperature curves for different composition of uncompatibilized EPDM/FKM blends are given in Fig. 3.18. In the case of absolutely incompatible blends dynamic mechanical analysis should reveal two glass transition regions corresponding exactly to those of the original polymers, thereby indicating very small interaction at the phase boundaries and the existence of large domains. This stringent condition is not met even for the most incompatible blends considered in this investigation, EPDM/FKM. From the Fig. 3.18, it is clear that E_{100} shows a peak around -45 ^{0}C corresponding to the T_g of EPDM whereas FKM (E_0) shows a peak around +6 ^{0}C. However two distinct peaks each exactly corresponding to the glass transition temperatures of EPDM and FKM can be observed in all the blends indicating the incompatibility and immiscibility between the phases.

The Tg values of EPDM/FKM rubber blends obtained from the tan δ curves are given in table 3.6. The pure vulcanizates show a T_g at -45 ^{0}C and +6 ^{0}C respectively. As the weight percentage of FKM increases in the blend, T_g remain unaltered. This indicates the lack of compatibility between

two rubbers. In the case of compatibilized blends (5 phr), separation between the T_g peaks are slightly reduced. This is due to the interfacial interaction between the two phases. But at higher loading (10 phr) there is not significant variation.

Table 3. 6 Glass transition temperatures of EPDM/FKM rubber blends

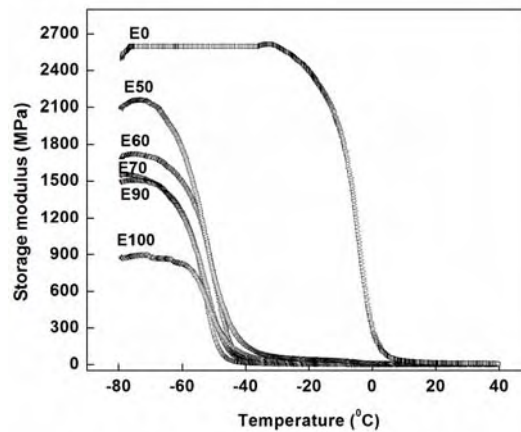| Rubber blends EPDM: FKM	Glass transition temperature (^{0}C)		Separation between two peaks
	EPDM	**FKM**	
100:0	-45	Absent	-
90:10	-41	0.58	40.42
70:30	-42	-1.98	40.02
60:40	-43	-1.78	41.22
50:50	-43	+1.18	41.82
50:50 with 5phr MA-g-EPDM	-38	-1.00	37.00
50:50 with 10phr MA-g-EPDM	-42	-0.90	41.10
0:100	Absent	+6.0	-

Fig. 3.19 Storage Modulus vs temperature curves for different composition of EPDM/FKM blends

Storage modulus vs temperature curves for different composition of uncompatibilized EPDM/FKM blends are given in Fig. 3.19. Storage

modulus increases with increase in concentration of FKM. The highest storage modulus is obtained for FKM. The E' values of the blends are found to be intermediate between those of pure components depending on the proportion of FKM. The storage modulus decreases with increase in temperature and finally levels off at high temperature.
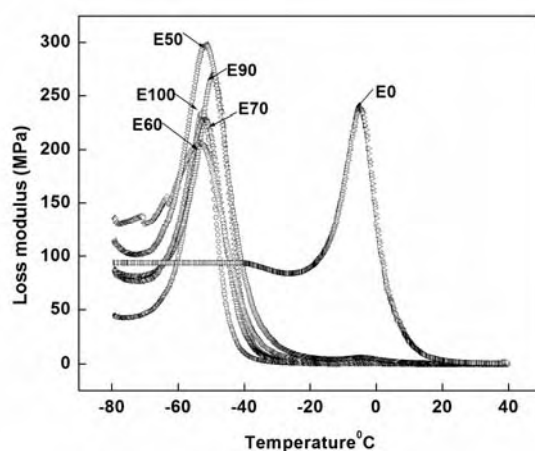
Fig. 3.20. **Loss modulus vs temperature curves for different composition of EPDM/FKM blends**

Variation of loss modulus (E") with temperature for EPDM, FKM and EPDM/FKM blends are given in Fig. 3.20. The loss modulus peak corresponds to the maximum heat dissipation per unit deformation. The loss modulus increases with increase in FKM content.

3.3.10.2 Effect of compatibilization

As discussed in the above section (3.3.10.1), the EPDM/FKM blend systems are incompatible. The incorporation of a compatibilizer into an immiscible blend reduces the interfacial energy of the phases, stabilizes the morphology against coalescence and improves the interfacial adhesion. As a result, systems with improved and reproducible properties are obtained.

Dynamic mechanical analysis (DMA), which is sensitive to molecular motions and transitions [43] has been chosen as a tool for characterizing blend compatibilisation.

The variation of tan δ as a function of temperature of the compatibilized blends is given in Fig. 3.21. The compatibilized blends also show the presence of two peaks corresponding to the T_g 's of EPDM and FKM similar to those of the uncompatibilized blends. This indicates that compatibilisation did not alter the degree of miscibility. As the compatibility increases, the interpenetration of the components increases. There is no appreciable shift in T_g towards the average value. This emphasizes that significant increase miscibility does not occur for the compatibilized blends. However, domain boundary mixing [44] or interfaces mixing [45] have been shown to cause an increased temperature dependence of storage modulus. From Fig. 3.21 it is clear that 5% compatibilizer loaded blend shows the lowest tan δ compared to other blends at various temperatures. This may be due to the maximum interfacial interaction provided by the compatibilizer. This is evident from the SEM analysis also (section 3.3.9).

With the optimum concentration of MA-g-EPDM, a slight shift in the damping maximum of the FKM phase occurs (Fig. 3.21) towards EPDM phase. This is due to an increased intermolecular interaction at the phase boundary, caused by the presence of polar groups on compatibilizer. As a result the low temperature flexibility of FKM is improved.
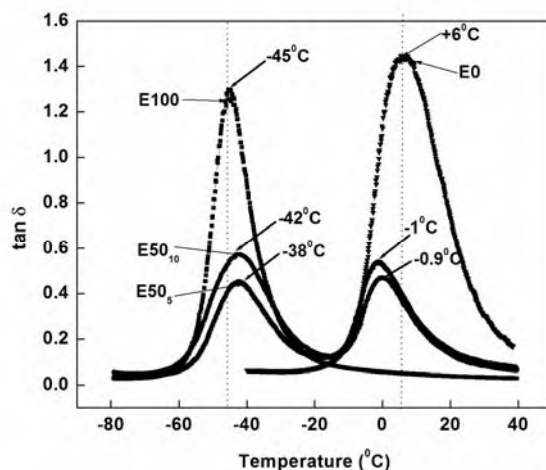
Fig. 3.21 Tan δ vs temperature curves for E_{100}, E_{5010}, E_{505*} and E_0

The variation of storage modulus as a function of temperature for 50:50 (w/w) EPDM/FKM blends compatibilized with two different concentrations of MA-g-EPDM is shown in Fig. 3.22. The E' values of compatibilized E_{50} blends are higher than that of uncompatibilized blend at the same temperature. The addition of MA-g-EPDM makes the blend technologically compatible to some extent even though molecular level miscibility cannot be achieved. Even by the addition of 5% compatibilizer, the storage modulus of the blends increases. The increase in the modulus upon the addition of the compatibilizer is due to the increase in the interfacial adhesion caused by the compatibilizing agent due to the improved adhesion between an intimate mix of MA-g-EPDM and EPDM with FKM.
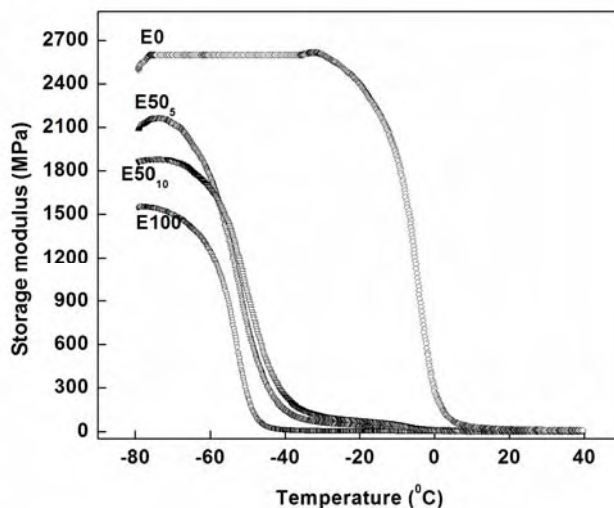
Fig. 3.22 Storage modulus vs temperature curves for E_{100}, E_{5010}, E_{505*} and E_0

The presence of compatibilizer improves the interfacial adhesion by enhancing the interfacial thickness and thereby facilitating the stress transfer between the components. Thus MA-g-EPDM, improves the interfacial adhesion. Consequently, the storage modulus of the blends is enhanced. A decrease in E' by the addition of 10 wt% MA-g-EPDM indicates the formation of micelles in the matrix. At higher compatibilizer loading, decrease in modulus value may be due to the formation of agglomerates of the compatibilizer molecule.

Fig. 3.23 depicts the change of loss modulus (E") as function of temperature for EPDM/FKM blends compatibilized by MA-g-EPDM. The shift in the Tg values of the FKM phase of the compatibilized blends compared to the uncompatibilized blends indicate the strong interaction between the EPDM and FKM as a result of reactive compatibilisation. Thus a shifting of Tg values of the components is taken as an indication of miscibility enhancement and therefore can be considered as an evidence for

compatibilization. In the case of both compatibilized and uncompatibilized blends, the loss modulus curve (Fig. 3.23) with two discrete shoulders relates to the EPDM and FKM phase respectively.
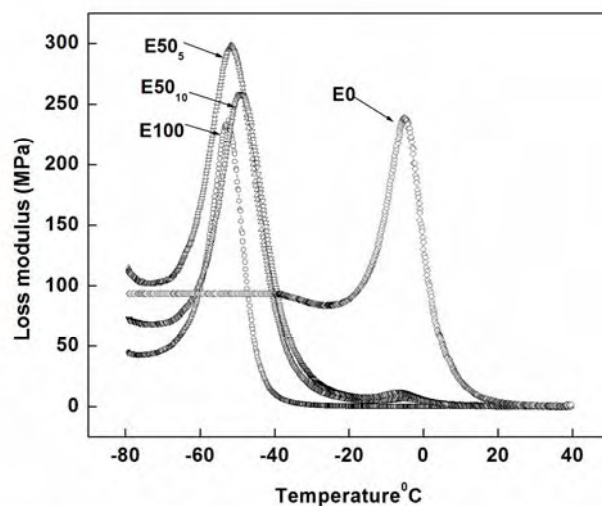
Fig. 3. 23. Loss modulus vs temperature curves for E_{100}, E_{5010}, E_{505*} and E_0

We can conclude that both electron microscopy and dynamical mechanical analysis clearly show the system is still phase separated even in the presence of the compatibilizer. Tan δ curve also indicates that compatibilizer addition could not make the system completely miscible. This is in agreement with the conclusions [46] that if two polymers are far from being miscible, then no copolymer is likely to make a single phase system. In a completely immiscible system, the main role of the copolymer is to act as an interfacial agent.

3.3.11 Atomic force microscopy

Morphology of rubber blends plays an important role in determining the dynamic and mechanical properties of the blends. Characterization of

morphology of rubber blends can be achieved by various microscopic techniques. The common techniques used are transmission electron microscopy (TEM) and scanning electron microscopy (SEM). These techniques require many steps of sample preparation, including sectioning and staining with toxic chemicals to provide the contrast. In 1981, scanning tunneling microscopy was invented and later developed to atomic force microscopy (AFM) in 1986. AFM has now become a relatively common tool, which is widely used in the study of materials. It is a powerful technique for distinguishing surface properties such as viscoelasticity, stiffness, friction and adhesion of materials. For multi-component polymers, the differences in these properties for different regions of the surface can be translated into morphology especially from phase imaging AFM. By using such a concept, AFM has been applied to the study of rubber blends [47] to investigate the morphologies of SBR/BR [48, 49], BR/IR and SBR/IR blends [50]. It can also be used for studying filled systems for the shape of filler particles [51], filler distribution and also filler aggregation.

The compatibilized and uncompatibilized EPDM/FKM blends were imaged using Nanosurf easy scan operating in contact mode using NSC14/Cr-Au cantilever. The representative scans of the blend surface at three different locations were obtained for each sample. Images were recorded in the constant force mode, under ambient conditions, in air. In this mode, an electronic feedback circuit maintains a constant cantilever deflection while the tip is scanned over the surface by adjusting the height of the sample. In this way, a three dimensional image is produced by recording the z-direction while scanning the sample in the x and y- direction.
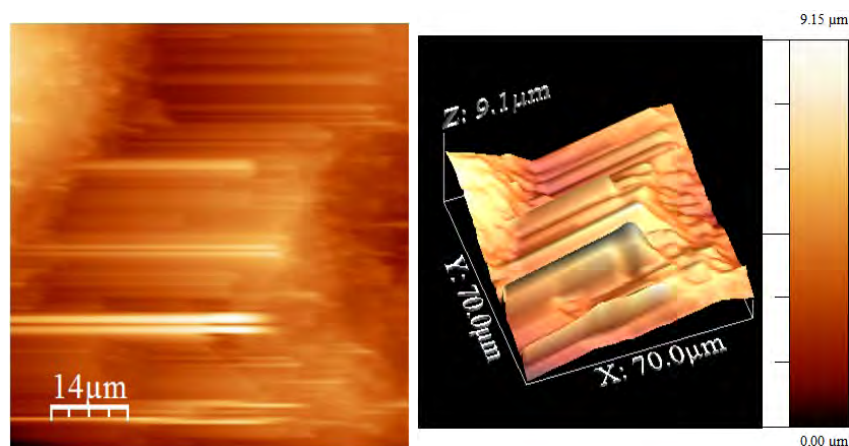
Fig. 3.24 The AFM image (left side), and corresponding three dimensional (3D) topographies (right side) of prepared uncompatibilized 50:50, EPDM/FKM rubber blend

A comparative assessment of the phase morphology and extent of comptabilization or interface characteristics of compatibilized and uncompatibilized blends are reported here. The 3D (three dimensional) topography of uncompatibilized EPDM/FKM blend clearly shows a two phase morphology (Fig. 3.24), indicating the expected immiscibility of the two components. AFM roughly confirms the micro-phase separation in these blends. The image shows the elongated rubber particles, some of which are completely surrounded by the other. It is apparent from the images that the area percentage of both phases does not match the prepared blend ratio. But it is quite impossible to determine whether the phases are co-continuous. This is a result of inhomogeneous phase separation (coexistence of an interphase) in different regions. Thus in the case of uncompatibilized binary blends phase boundary is distinctly established.
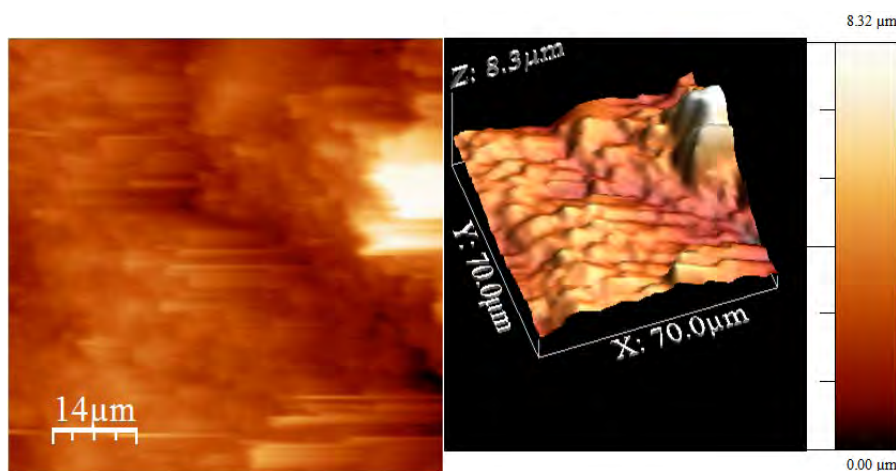
Fig. 3.25 The AFM image (left side), and corresponding three dimensional (3D) topographies (right side) of prepared compatibilized 50:50, EPDM/FKM rubber blend

It can be seen from Fig. 3.25 that the EPDM/FKM compatibilized blend presents a more even homogenous morphology with uniform contrast throughout the image compared to uncompatibilized blends. The topography image, given in Fig. 3.25 shows the occurrence of a less rough surface with fairly good homogeneity. This is due to the generation of compatibility between the two phases.

3.4 Conclusions

From the cure characteristics it is found that the maximum torque, scorch safety and the optimum cure time increase with increase in FKM content. The EPDM/MA-g-EPDM/FKM blends show high tensile strength, indicating physical interaction between two elastomers in presence of MA-g-EPDM. The thermal stability of FKM and blends containing higher proportion of FKM were not affected during aging. After aging, the equilibrium swelling ratios of EPDM/MA-g-EPDM/FKM blends decrease in comparison with that of the uncompatibilized blends.

The addition of FKM into EPDM improves the thermal stability significantly. With the incorporation of compatibilizer, MA-g-EPDM the chemical interaction and physical entanglement between the two constituents are possible at the interface only, but the bulk of the polymer remained uninfluenced. So the individual components were likely to follow their own degradation route. In the case of uncompatibilized blends, even though, they are heterogeneous with two phases morphology, the fluoro groups in FKM protects the EPDM phase from hot-air aging and thermal degradation. This is the reason why EPDM/MA-g-EPDM/FKM blends have a good hot-air aging resistance and thermal stability. The kinetic study shows that random nucleation mechanism is the rate controlling process in the degradation of the blend. The DSC studies reveal that the compatibilized blends shows shifts in the T_g value towards FKM phase indicating better polar-non polar interaction in compatibilized blends. Phase morphology obtained in the case of compatibilized blends is better than that of uncompatibilized blends. The addition of MA-g-EPDM as a compatibilizer improves the viscoelastic properties indicating improved interaction between the two components in the compatibilized system. AFM studies shows that the EPDM/FKM compatibilized blend presents a more even homogenous morphology with uniform contrast throughout the image compared to uncompatibilized blends.

References

[1] Kader MA, Bhowmick AK, J Appl Polym Sci 2003, 89, 1442–1452.

[2] Boutevin B, Caporiccio G, Pietrasanta FG, Ratsimihety A, J Fluorine Chem 2003, 124, 131–138.

[3] Maiti M, Bhowmick A, J Polym Sci Part B Polym Phys 2006, 44, 162–176.

[4] Maiti M, Bhowmick AK, Polym Eng Sci 2007, 47, 1777–1787.

[5] Wang P, Schneider NS, Sung NH, J Appl Polym Sci 1999, 71, 1525–1535.

[6] Mitra S, Ghanbari-SA, Kingshott P, Hvilsted S, Almdal K. J Polym Sci Part A Polym Chem 2004, 42, 6216–6229.

[7] De Angelis MG, Sarti GC, Sanguineti A, Maccone P. J Polym Sci Part B Polym Phys 2004, 42, 1987–2006.

[8] Valsecchi R, Vigano M, Levi M, Turri S, J Appl Polym Sci 2006, 102, 4484–4487.

[9] Ghosh A, De SK, Rubber Chem Technol 2004, 77, 856–872.

[10] Mitra S, Ghanbari-SA, Kingshotta P, Almdal K, Rehmeier HK, Christensen AG, Polym Degrad Stab 2004, 83, 195–206.

[11] Ameduri B, Boutevin B, Kostov G, Prog Polym Sci 2001, 26, 105–187.

[12] Sinha NK, Mukhopadhyay R, Dhupia D, Das Gupta S, Baldev Raj, J Mater Design 2011, 32, 5141–5153.

[13] Liu H, Wu L, You Y, Liu Y , An Z, J New Chemical Materials2007, 4.

[14] Sirqueira AS, Soares BG, Macromol Mater Eng 2007, 292, 62–69.

[15] Wl Wu, Chen DJ, Polym Compos 2006, 27, 621–626.

[16] Deniz V, Karaagac B, Ceyhan N. J Appl Polym Sci 2007, 103, 557–563.

[17] Mitra S, Ghanbari-SA, Kingshott P, Hvilsted S, Almdal K. Mater Chem Phys 2006, 98, 248–255.

[18] Madala AI, Kraus G, In: Mark JE, Erman BK, Eirich FR, editors. Science and technology of rubber 1994, New York: Academic press, 387.

[19] Yuhua L, Ao L, Weiling W, China Synthetic rubber industry 1997, 20, 12.

[20] Khalf AI, Nashar DEEl, Maziad NA, J Mater Design 2010, 31, 2592-2598.

[21] Noriman NZ, Ismail HJ Mater Design 2011, 32, 3336-3346.

[22] Kanu RC, Shaw MT, Polym Eng Sci 1982, 22, 507–511.

[23] Mathew AP, Pakirisamy S, Thomas S, Polym Degrad Stab 2001, 72, 423–439.

[24] Rao Q, Yan X, Deng S, Song Y. China Synthetic Rubber Industry 2001-04.

[25] Qian Lili, Huang Chengya, Hu Zhao, Deng Chun, China Synthetic Rubber Industry, 2009-03.

[26] Guo Jianhua, Zeng Xingrong,Luo Quankun,Song Guosheng. China Synthetic Rubber Industry, 2009-02.

[27] Dong Lijie, Wang Ying, Yang Jian, Xiong. China Synthetic Rubber Industry, 2009-03.

[28] Santra RN, Mukundo PG, Chaki TK, Nando GB, Thermochim Acta 1993, 219, 283-292.

[29] Mc Neill IC, Comprehensive polymer science. 6th ed. New York: Allen/Pergamon Press, 1989 [chapter 15].

[30] Paul DR, Mewman S, Polymer blends, vol. 1 and 2, New York: Academic press, 1978.

[31] Utracki LA, Carl Hanser Verlag, Munuch. Vol. 25. USA: Oxford University press, 1990.

[32] Newman S, Paul DR, Newman S, editors. Polymer blend. New York: Academic press, 1978.

[33] Holly HW, Mihal FF, Starer I, Rubber Age 1965, 96, 565.

[34] Khaled F, Nemr El, J Mater Design 2011, 32, 3361-3369.

[35] Mostafa A, Abouel-Kasem A, Bayoumi MR, El-Sebaie MG. J Mater and Design 2009, 30, 791-795.

[36] Klier J, Peppas NA, Polymer 1987, 28, 1851-1859.

[37] Kader MA,   Bhowmick AK, Polym Degrad Stab 2003, 79, 283–295.

[38] Banik I, Bhowmick AK, Raghavan SV, Majali AB, Tikku VK, Polym Degrad Stab 1999, 63, 413–421.

[39] Coats AW, Redfern JP, Nature 1964, 68, 201.

[40] Kolesov IS, Radusch HJ, European Polymer Journal 1999, 35, 527-541.

[41] Papke N., Karger-Kocsis J, Polymer 2001, 42, 1109–1120.

[42] Varughese KT, Nando GB, De PP, De S K, Journal of Material Science 1988, 23, 3894–3900.

[43] Murayama T, Elsevier, New York,1978.

[44] Hashimoto T, Tsukahara Y, Tachi K, Kawai H, Macromolecules 1983, 16, 648–657.

[45]   Feng D, Wilkens GL, Crivello JV, Polymer 1989, 30, 1800–1813.

[46]   Newman S (eds.: Paul D. R., Newman S.) Academic Press INC 1978, New York, 2, 63–89.

[47]   Tsukruk VV, Rubber Rev 1997, 70, 430.

[48]   Gunter M, Brandsch R, Thomas Y, Malner T, Bar G, Kautch. Gummi Kunstst. 1999, 52, 717.

[49]   Bar G, Ganter M, Brandsch R, Delineau L, Whangbo MH, Langmuir 2000, 16, 5702.

[50]   Mass S, Gronski W, Kautch. Gummi Kunstst. 1994, 47, 409.

[51]   Van Haeringen DT, Schonherr H, Vansco GJ, Van der Does L, Noordermeer JWM, Janssen PJP., Rubber Chem. Technol. 1999, 72, 862.

…..ഇൽ…..

<div align="right">Chapter 4</div>

COMPOSITES BASED ON OIL-EXTENDED EPDM RUBBER: THERMAL AND MECHANICAL PROPERTIES[*]

Contents

Oil-Extended EPDM composites with different flame retardant fillers like Aluminium hydroxide (ATH), Chlorinated polyethylene (CPE), Decabromobiphenyl oxide (DBBO) and Expanded graphite (EG) were prepared by conventional mill mixing. Thermal, mechanical and sorption characteristics of the vulcanizates were studied. The effect of different fillers on the flammability of the composites was measured using Limiting Oxygen Index (LOI) and UL-94 HB tests. Scanning Electron Microscopic (SEM) studies of the composites were also conducted. ATH and CPE improved the thermal stability of the composites substantially. Among the four fillers ATH has the highest reinforcing effect on the EPDM rubber. Sorption studies of the composite showed that ATH reduced the swelling rate of the microcomposite considerably. All the four fillers were effective in improving the flame retardant property. Filler dispersion studies and SEM images point to a uniform dispersion of filler in the matrix which is in good agreement with significant improvement in mechanical properties.

4.1 Introduction

Ethylene-propylene-diene terpolymer (EPDM) is a rubber which, when suitably formulated, shows remarkable properties such as ozone and heat resistance, good chemical resistance and excellent electrical properties [1]. Filler combinations are often used so that an adequate balance of properties can be achieved, along with good characteristics of processability and cost [1, 2].

The transport properties of organic solvents and gases through polymers are of great technological importance. The diffusion and transport properties of polymers were found to be strongly dependent on the additives and the type of crosslinking [3]. The diffusion process is a kinetic parameter depending on the free volume within the material, segmental mobility of polymer chains and the size of the penetrant molecule [4]. It is too complex to trace the reinforcement occurred in elastomers with the addition of filler. Mathai A. E [5] studied the transport properties of various rubbers and blends in the presence of fillers.

Flame retardant additives are most widely used in practice. Brominated flame retardants are the most effective flame retardants in the market and are adopted by most engineering plastics [6]. However, halogenated flame retardants release toxic gases when they are subjected to high temperatures. With the proposal of the concept of environment friendly flame retardants, some brominated flame retardants are replaced by halogen free flame retardants, particularly metallic hydroxide such as magnesium hydroxide [7], aluminium trihydrate [8], hydrotalcite [9] etc. An extensively used halogenated flame retardant is decabromobiphenyl

oxide (DBBO). The flammability characteristics of SBR which is compounded with different mixtures of decabromobiphenyl oxide and aluminum hydroxide as flame retardants and the effect of the added compounds on some of the physical and mechanical properties were studied by M. A. Khattab [10]. ATH is a well known flame retarder which is also a smoke suppressor. The main advantages of ATH over other similar agents are its low cost and low toxicity. On burning, no toxic or corrosive substances are evolved and they can be used in combination with other flame retardants [11].

Chlorinated polyethylene (CPE), another flame retardant possesses high resistance to hydrocarbon oil, heat and weathering, attributed to the chlorine atoms added to the polyethylene backbone [12].

Expanded graphite (EG) maintains the layered structure of natural graphite flakes but with larger layer spacing. Moreover the multi-pores, functional acids (-COOH) and the -OH groups will enhance the physical and chemical adsorption between the EG and the polymer solution. EG has been applied widely as a functional carbon material, used in sealing, catalyzing mechanism, space flight military affairs, environmental protection etc. [13].

In this part of the study ATH, CPE, DBBO and EG were used as fillers in oil extended EPDM were prepared. The sorption properties of organic solvent (toluene) through EPDM containing these micron sized fillers were investigated. The thermal, mechanical and flame retardant properties of the prepared composites were also evaluated. SEM investigations were carried out to study the morphology of these composites.

4.2 Experimental details

4.2.1 Materials

The specification of the materials used is given in section 2.1.

4.2.2 Methods

Formulation used in the preparation of EPDM composites is given in table 2.1. The methods used in this work are given in section 2.6.

4.3 Results and Discussion

4.3.1 Cure characteristics

The cure curves of compounds containing ATH, CPE, DBBO and EG filled EPDM are shown in Figs. 4.1 to 4.4. The cure parameters of EPDM filled with ATH, CPE, DBBO and EG are given in table 4.1. Maximum torque (D_{max}) increases with increased filler loading in all cases except CPE. Increase in D_{max} indicates higher degree of crosslinking. In CPE filled systems the maximum torque value decreases with increase in concentration of CPE. The decline in D_{max} of the EPDM/CPE blend is due to the comparatively low viscosity of CPE leading to softening of blend on heating. The cure time T_{90} increased on adding ATH, CPE and DBBO. In the case of EG, cure rate is accelerated after 25 phr loading. The reason for the lower cure time at higher loading of EG is due to the increase of thermal transition of EPDM in presence of EG which promotes the vulcanization process. EG have increased specific surface by acid treatment, which results in improved thermal transition, filler-filler and filler-matrix interactions. Within the composite system, there could be two paths of thermal transition. In one path, heat can pass from EG flakes-polymer-EG flakes and in the other path through direct contact between the EG flakes. The second path of thermal conduction will be more effective for

higher filler concentration which increases the interaction between the fillers which in turn increases the process of vulcanization.
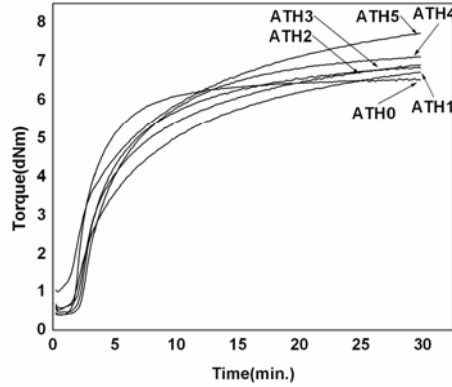

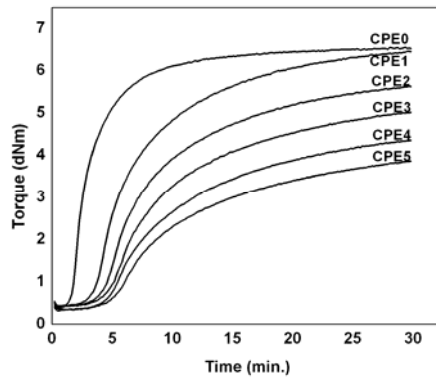**Fig.4.1 Cure curves of ATH filled EPDM composites**

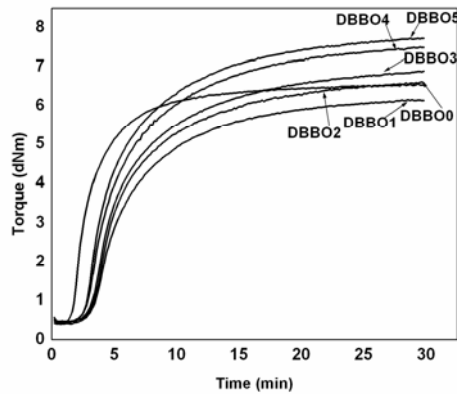**Fig. 4.2 Cure curves of CPE filled EPDM composites**

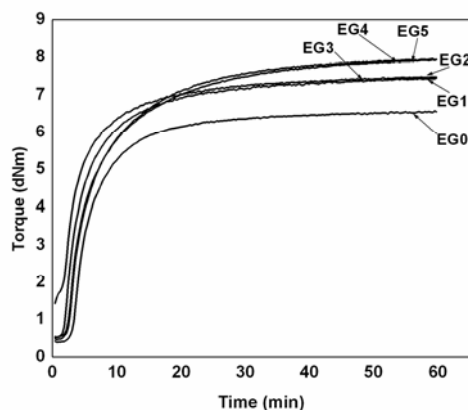**Fig. 4.3 Cure curves of DBBO filled EPDM composites**

Fig. 4.4 Cure curves of EG filled EPDM composites

Table 4.1 Cure characteristics and filler dispersion parameters of EPDM composites

Sample name	$D_{min.}$	$D_{max.}$	T_{10}	T_{90}	M_f/M_p	α_f	η_r	M_r	L
Unfilled	0.395	6.583	3.40	15.89	-	-	-	-	-
ATH1	0.396	6.740	2.50	14.45	0.05	0.51	1.00	1.02	0.02
ATH2	0.454	6.874	2.32	14.59	0.15	0.25	1.15	1.04	0.11
ATH3	0.565	6.920	2.20	17.58	0.25	0.11	1.43	1.05	0.38
ATH4	0.523	7.129	1.96	18.79	0.35	0.19	1.32	1.08	0.24
ATH5	0.984	7.737	1.61	19.07	0.45	0.20	2.49	1.17	1.31
CPE1	0.428	6.468	3.77	17.19	0.05	0.48	1.08	0.98	0.10
CPE2	0.415	5.652	4.46	19.12	0.15	1.02	1.05	0.86	0.19
CPE3	0.415	5.027	4.84	20.54	0.25	1.02	1.05	0.76	0.29
CPE4	0.314	4.367	4.92	21.08	0.35	0.99	0.79	0.66	0.13
CPE5	0.343	3.870	5.31	21.92	0.45	0.96	0.87	0.59	0.28
DBBO1	0.392	6.171	3.48	14.94	0.05	1.32	0.99	0.93	0.05
DBBO2	0.431	6.613	3.44	15.12	0.15	1.07	1.09	1.00	0.09
DBBO3	0.454	6.890	3.36	15.22	0.25	0.16	1.14	1.05	0.10
DBBO4	0.434	7.505	3.01	14.95	0.35	0.41	1.09	1.14	0.04
DBBO5	0.437	7.737	2.94	14.23	0.45	0.40	1.11	1.18	0.07
EG1	0.366	7.080	3.00	18.98	0.05	1.70	0.93	1.08	0.15
EG2	0.464	7.463	2.79	21.65	0.15	0.87	1.17	1.13	0.04
EG3	0.533	7.495	2.65	17.55	0.25	0.50	1.34	1.14	0.21
EG4	1.118	7.525	2.07	16.57	0.35	0.10	2.83	1.14	1.69
EG5	1.520	7.966	1.63	16.21	0.45	0.09	3.84	1.21	2.64

4.3.2 Strain-sweep studies

The strain sweep measurements of the compounds were carried out to study the rubber-filler interaction. The testing temperature was selected as 100^0C, a temperature below the curing temperature and the shear strain was varied from 0.5 to 40% keeping the frequency measurement at 0.5 Hz.

From Figs. 4.5 to 4.8, it is found that the complex modulus (G*) values increase with loading for all the composites except EPDM/CPE. The increase in modulus is due to the inclusion of rigid filler particles in the soft rubber matrix and hydrodynamic effect. The elastic modulus of a filled rubber is strongly dependent on the deformation, and it decreases substantially with strain. The high values of G* is due to higher filler-filler or filler-polymer interactions. Among the composites G* value (Fig. 4.5) is maximum for EPDM/ATH system.

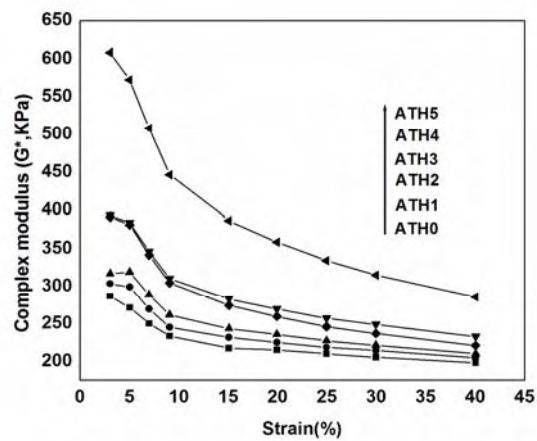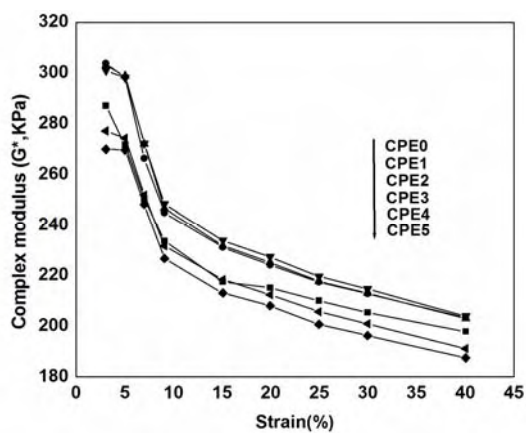**Fig. 4.5 Strain sweep curves of ATH filled EPDM composites**

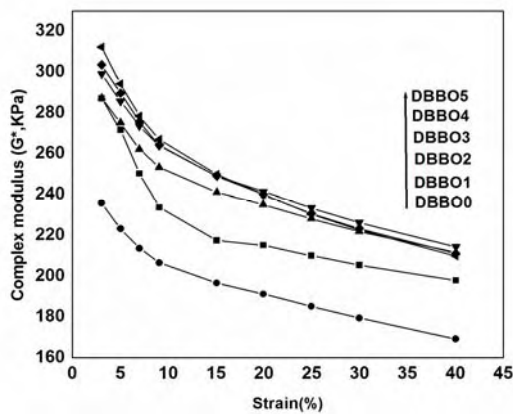**Fig. 4.6 Strain sweep curves of CPE filled EPDM composites**

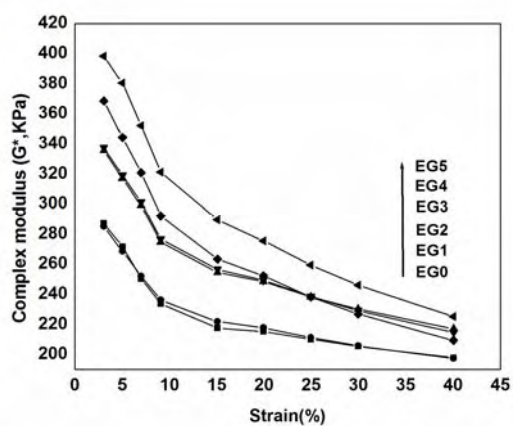**Fig. 4.7 Strain sweep curves of DBBO filled EPDM composites**

Fig. 4.8 Strain sweep curves of EG filled EPDM composites

4.3.3 Filler dispersion

The detailed description regarding the theory of filler dispersion will be discussed later in section 5.3.2. Table 4.1 presents the computed η_r, M_r and L values. In ATH filled composites the filler particles are well dispersed in the matrix except at higher loading. Both η_r and M_r values increase with loading indicating an increase in relative viscosity and relative modulus of the elastomer. In CPE, DBBO and EG filled systems, there is much difference between η_r and M_r values. The index 'L' increases with filler loading pointing to the agglomeration of the filler in the elastomer.

In ATH and DBBO filled composites the value of α_f is found to decrease up to 25 phr loading and then increases due to the agglomeration. This is in good agreement with the variation in tensile properties. In the case of other systems a regular trend in α_f is not observed.

4.3.4 Swelling behavior

The diffusion curves for the ATH, CPE, DBBO and EG filled oil-extended EPDM composites are given in Figs. 4.9, 4.10, 4.11 and 4.12. The curves are plotted as the fractional uptake of penetrant against $t^{1/2}/h$, where h is the thickness of the sample. These types of plots are referred as reduced sorption curves [14], because the sample thickness is included in the abscissa. ATH filled EPDM exhibits reduced swelling than other systems. Initial swelling is very high for all the systems due to large concentration gradient and the severe solvent stress of the polymer sample. The swelling rate attains equilibrium when the concentration gradient becomes zero. The low swelling rate of ATH/EPDM is in good agreement with its improved mechanical properties. The increased swelling in the case of other systems

may be due to the large particle size of the fillers as is evident from the SEM photographs (section 4.3.12) to be discussed later. The increase in solvent uptake (%) at equilibrium swelling of filler reinforced samples can be expressed in terms of the decrease in contact surface area between polymer and filler. The diffusion of penetrant depends greatly upon the concentration of available space that is large enough to accommodate the penetrant molecule. A penetrant molecule may exist in a hole of sufficient size and can jump into a neighboring hole once it acquires sufficient energy. Addition of fillers of large particle size will increase the availability of spaces and enhance the mobility of chain segments. In the case of all filled systems, the addition of polar filler decreases the swelling rate in non-polar solvent.

In ATH filled EPDM composites, the equilibrium toluene uptake decreases with increase in concentration of ATH except at lower loadings. This can be explained in terms of the filler dispersion and also due to the polarity of the hydroxyl groups present on the filler surface, which resists the non-polar solvent uptake. The uneven distribution of other fillers in the EPDM phase results in rather complex behavior.
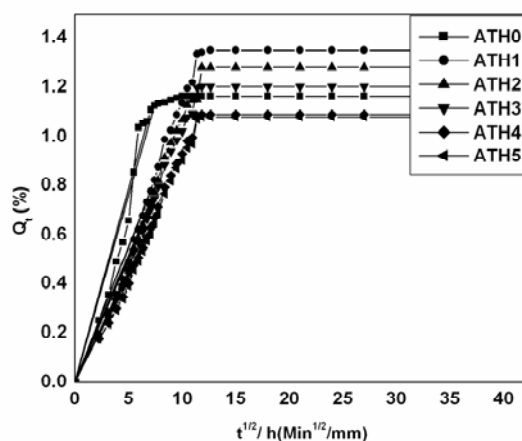

Fig. 4.9 Q_t Vs $t^{1/2}$/h plots of ATH filled EPDM composites
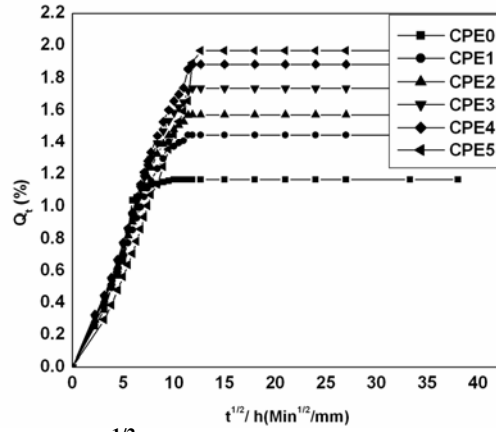
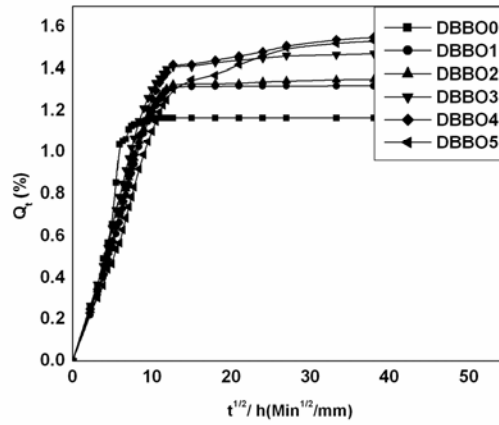**Fig. 4.10 Q_t Vs $t^{1/2}$/h plots of CPE filled EPDM composites**

Fig. 4.11 Q_t Vs $t^{1/2}$/h plots of DBBO filled EPDM composites
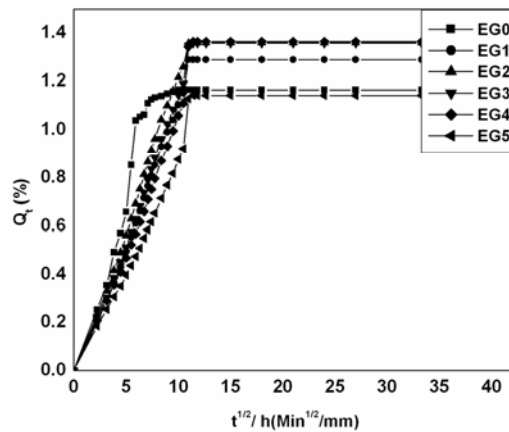

Fig. 4.12 Q_t Vs $t^{1/2}$/h plots of EG filled EPDM composites

The process of diffusion is a kinetic parameter related to the penetrant size and to the polymer segment mobility. The diffusion coefficient of a polymeric sample immersed in an infinite amount of solvent can be calculated using the equation 4.1 [15],

$$Q_t/Q_\infty = 1-(8/\Pi^2) \sum_{n=0}^{n=\infty} \Sigma \, [1/(2n+1)^2 \exp(-D(2n+1)^2 \, \Pi^2 t/h^2) \text{ --------------- (4.1)}$$

where t is the time, h is the initial thickness of the sample, D is the diffusion coefficient and n is an integer. From this equation it is understood that a plot of Q_t vs. $t^{1/2}$ is linear at short time and D can be calculated from the initial slope. The equation 4.2 for short time limiting is [15],

$$Q_t/Q_\infty = (4/h) \, (D/\Pi)^{1/2} \, t^{1/2} \text{ -- (4.2)}$$

By rearranging this equation, the diffusion coefficient (D) can be calculated using the equation 4.3 [16],

$$D = \Pi \, (h\theta/4Q_\infty)^2 \text{ --- (4.3)}$$

where θ is the slope of the initial portion of the plot of Q_t vs. $t^{1/2}$ and Q_∞ is the equilibrium mole percentage uptake. The liquid sorption tends towards an equilibrium value, which depends upon the nature of the material. The permeability (P) is given by the equation 4.4,

$$P = DS \text{ --- (4.4)}$$

Where D and S are the diffusion and sorption coefficient respectively.

Table 4.2 gives the variation in D, S and P as a function of filler loading. The diffusion coefficient decreases dramatically on the addition of ATH filler. The ATH filled composite exhibits lower diffusivity value indicating resistance to non-polar solvents.

Table 4.2 Variation of Diffusion coefficient (D), Sorption coefficient (S), Permeation coefficient (P) and Variation of n, k and crosslink density (CLD) values of EPDM composites

Sample	$DX10^{-7}$ (cm^2/s)	S	$PX10^{-7}$ (cm^2/s)	n	k (min^{-2})	CLD $(10^{-5}gmolcm^{-3})$
Without filler	1.01	1.07	1.08	0.39	8.28	9.47
ATH1	2.12	1.22	2.58	0.55	14.83	10.1
ATH2	1.92	1.25	2.39	0.52	12.99	7.61
ATH3	2.10	1.36	2.86	0.53	13.51	5.24
ATH4	1.58	1.44	2.28	0.52	14.78	3.89
ATH5	2.19	1.41	3.09	0.46	14.15	3.35
EG1	6.46	1.19	7.69	0.56	15.97	12.9
EG2	7.32	1.25	9.18	0.57	14.59	9.52
EG3	5.55	1.25	6.95	0.52	14.47	7.54
EG4	4.42	1.26	5.56	0.49	14.70	5.62
EG5	4.44	1.05	4.67	0.47	13.27	6.24
CPE1	7.34	1.33	9.79	0.60	14.99	10.6
CPE2	5.97	1.45	8.64	0.56	13.62	7.45
CPE3	5.75	1.60	9.20	0.57	14.58	4.91
CPE4	4.82	1.73	8.36	0.54	14.19	4.62
CPE5	3.95	1.81	7.16	0.49	15.16	2.99
DBBO1	7.21	1.24	8.97	0.57	17.53	9.32
DBBO2	6.96	1.18	8.21	0.55	16.63	7.55
DBBO3	6.68	1.10	7.39	0.53	15.09	6.47
DBBO4	6.36	1.00	6.39	0.51	14.22	5.48
DBBO5	5.94	0.99	5.93	0.49	13.85	4.85

The reinforcement of fillers is predicted by using Kraus equation [17]. The equation is,

$$V_{r0}/V_{rf} = 1 - m [f/ (1-f)]$$ .... (4.5)

where V_{rf} is the volume fraction of rubber in the solvent swollen filled sample and is given by,

$$V_{rf} = [(d-fw)/\rho_p] / [d-(fw/\rho_p) + (A_s/\rho_s)]$$ ----------------------------- (4.6)

where d is the deswollen weight, f is the volume fraction of the filler, w is the initial weight of the sample, ρ_p is the density of the polymer, ρ_s is the density of the solvent, and A_s is the amount of solvent absorbed.

$$V_{ro} = (d/\rho_p)/ [(d/\rho_p)+ (A_s/\rho_s)] \text{ -- (4.7)}$$

A plot of V_{ro}/V_{rf} as a function of f/(1- f) should give a straight line with slope m. The value of m is a direct measure of the reinforcing ability of the filler used. According to this theory, reinforcing fillers have negative slope, indicating better polymer/filler interaction.

Kraus plot slopes of ATH, CPE, DBBO and EG filled oil-extended EPDM are shown in table 4.3. The values indicate poor reinforcement effect due to the aggregation of filler. The linear relation in accordance with the Kraus plot is not obeyed in these systems. The deviation from linearity may be due to the aggregation of filler in the EPDM matrix, resulting in increased solvent penetration. Consequently, the decrease in the value of V_{rf} is more than the expected value. The slope obtained with different fillers is in the order CPE>DBBO>EG>ATH which shows that ATH offers better reinforcement. Deviation from linearity may also be due to the interaction between the filler and the curing agents.

Table 4.3 The slope m values obtained from Kraus plot for microfillers reinforced EPDM

Reinforcing Fillers	Kraus equation slope (m)
ATH	1.09
CPE	2.67
DBBO	1.24
EG	1.21

The crosslink density (CLD), $1/2M_c$ was determined using the Flory–Rehner equation [18].

Swelling measurements are useful in characterizing the network degradation. In the case of unfilled rubbers, the swelling restriction is due to the crosslinks connecting the polymer chains, but in filled systems filler-polymer interaction also may interfere. The variation of CLD with filler loading for the composites is shown in table 4.2. The CLD is found to decrease slightly with filler loading. The amount of solvent absorbed by the sample increases leading to reduction in CLD. The decrease in CLD may also be due to the aggregation of filler. The crosslink density of EPDM with different fillers (5phr) followed the order ATH>EG>DBBO>CPE.

4.3.5 Transport mechanism

The transport properties of polymeric membranes can be followed by using the empirical equation [19, 20],

$$\text{Log}(Q_t/Q\infty) = \log k + n \log t \text{ -- (4.8)}$$

The slope of the plot $\log(Q_t/Q_\infty)$ vs. log t gives the value of n, and its y-intercept is the value of k, which depends upon the structural significance of polymer as well as its interaction with the solvent. According to the n values obtained from the above equation, three basic modes of transport are distinguished [20]. Table 4.2 presents the 'n' and 'k' values of composites of oil-extended EPDM reinforced with ATH, CPE, DBBO and EG fillers, in toluene. From the 'n' and 'k' values it is inferred that EPDM/ATH system exhibits Fickian behaviour while CPE filled EPDM composite exhibits anomalous behaviour. The 'k' values of ATH filled systems were lowest indicating poor polymer/solvent interaction.

4.3.6 Effect of thermal aging on stress-strain properties

Fig. 4.13 shows that addition of even 5 phr ATH produces marked increase in tensile properties of EPDM. Maximum values of tensile strength and elongation at break are observed at 25 phr ATH loading. In the case of CPE filled composites, the maximum tensile strength and elongation at break are obtained at 45 phr loading (Fig. 4.14). From Fig. 4.15 it is evident that the tensile strength and elongation at break of EPDM are improved by 45% and 36% respectively, on adding 25 phr DBBO. Fig. 4.16 shows the variation of tensile properties of EPDM composite with EG loading. The maximum tensile strength 9.01 MPa is obtained at 25 phr EG loading. Elongation at break also shows an increasing trend initially. It is seen that the four fillers under study, decline the mechanical properties of EPDM at higher loading due to filler aggregation. The molecular segmental motion is restricted because of the physical interaction between the filler aggregates and polymer chains resulting in reduction of properties. Modulus at 100% elongation increases with filler loading for all the composites. Graphite is known for its self-lubricating and dry-lubricating behaviour, which arises from the weak binding between the graphene sheets and the possibility of interlayer sliding.
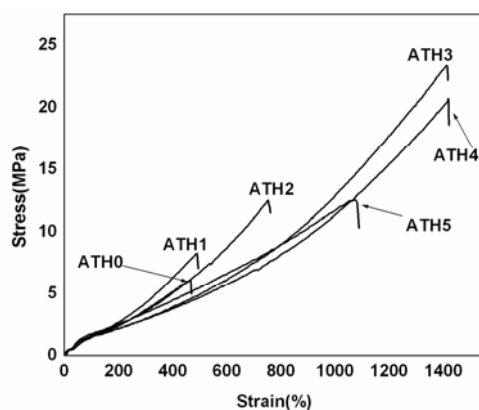

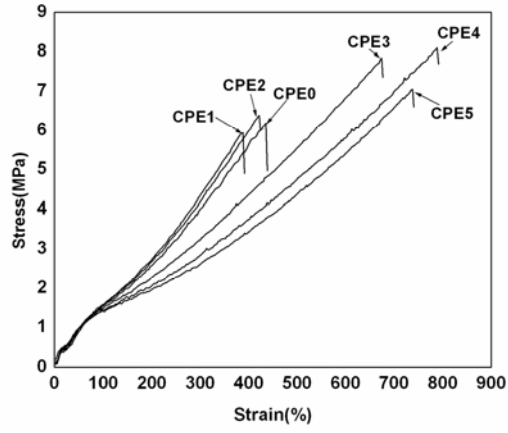**Fig. 4.13 Stress-strain behaviour of ATH filled EPDM composites**

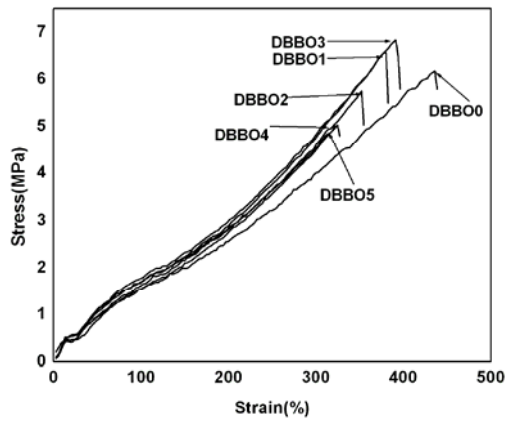**Fig. 4.14 Stress-strain behaviour of CPE filled EPDM composites**

Fig. 4.15 Stress-strain behaviour of DBBO filled EPDM composites
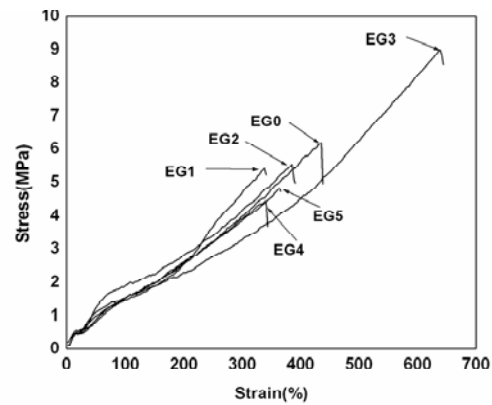

Fig. 4.16 Stress-strain behaviour of EG filled EPDM composites

4.3.7 Other mechanical properties

Table 4.4 shows the hardness, resilience, tear strength, abrasion resistance and compression set of the vulcanizates. The hardness values increased with increase in filler loading. This will be manifested as lower resilience values. In the case of tear strength, ATH filled EPDM vulcanizates show better properties compared to the other systems. The maximum tear strength (55.39 N/mm) is obtained for 35 phr ATH loaded EPDM rubber. Incorporation of the other three fillers brings about only a marginal increase in tear strength.

Table 4.4   Mechanical properties and limiting oxygen index values of the composites

Sample name	Hardness (Shore A)	Rebound resilience (%)	Tear strength (N/mm)	Abrasion loss (cm^3/h)	Compression set (%)	Limiting oxygen index (%)
Unfilled	51	66	21.91	2.24	15.57	20
ATH1	54	65	24.50	2.86	16.92	20
ATH2	55	62	34.58	2.98	21.09	21
ATH3	56	58	42.71	3.07	25.19	22
ATH4	56	56	55.39	3.30	32.83	23
ATH5	60	54	53.50	3.41	34.81	24
CPE1	52	65	22.43	2.36	15.20	21
CPE2	53	63	24.26	2.49	22.12	21
CPE3	54	64	29.21	2.53	25.00	21
CPE4	55	64	27.64	2.77	33.84	22
CPE5	57	62	23.04	2.85	36.28	22
DBBO1	52	65	15.60	2.97	07.31	22
DBBO2	53	62	15.75	3.86	07.43	23
DBBO3	56	62	20.17	4.78	09.40	24
DBBO4	58	60	21.97	5.18	11.40	25
DBBO5	59	59	22.32	5.70	11.76	26
EG1	52	64	17.90	2.36	16.03	22
EG2	55	63	18.63	2.46	20.63	23
EG3	56	63	20.95	4.96	26.36	23
EG4	60	60	31.62	8.59	26.98	25
EG5	61	60	25.68	10.17	27.41	26

4.3.8 Thermal stability of composites

The thermal degradation behavior of the EPDM containing various flame retardant materials can be clearly read from the thermograms and differential thermograms.

4.3.8.1 Thermal stability of EPDM/ATH composites

As can be seen from Fig. 4.17, in the case of EPDM a major degradation starts at 418 ^{0}C and gets completed at 511 ^{0}C. The T_{max} of EPDM appears at 487 ^{0}C. The weight loss of composites at different temperatures is given in table 4.5. It can be seen that degradation temperature corresponding to different percentage weight loss increase gradually with the addition of ATH. Table 4.5 also gives the percentage weight loss of the samples remained at three different temperatures viz. 425, 450 and 475 ^{0}C. As the percentage of the ATH increases, a gradual increase in weight loss is observed. This may be due to the percentage increase in filler. The initiation of degradation ($T_{5\%}$) of compounds without ATH was found to occur at 255 ^{0}C and that for 45 phr ATH loaded compounds is 287 ^{0}C. This shows improved thermal stability of EPDM/ATH system.
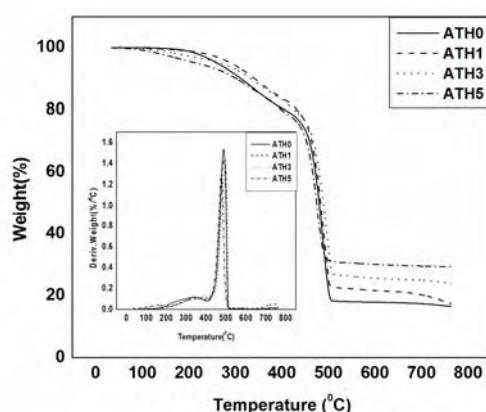

Fig. 4.17 The thermograms of ATH filled EPDM composites. The inset is the derivative thermograms

4.3.8.2 Thermal stability of EPDM/CPE composites

Fig. 4.18 shows the TGA and DTG curves of CPE filled EPDM. Weight loss observed in the temperature range 200-300^{0}C (T_{max}^1), is due to the dehydrochlorination of CPE. Apart from HCl, other volatile substances such as H_2, CO, CO_2, CH_3OH, etc. are also released. The major degradation (second stage) due to EPDM matrix occured at 487^{0}C (T_{max}^2).
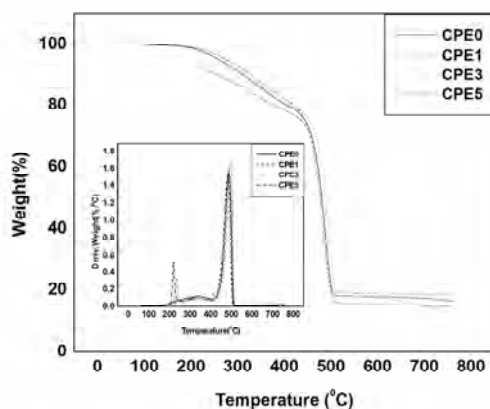
Fig. 4.18 The thermograms of CPE filled EPDM composites. The inset is the derivative thermograms

4.3.8.3 Thermal stability of EPDM/DBBO composites

In nitrogen atmosphere, DBBO filled EPDM composites exhibit two major weight losses [Fig. 4.19]. The first weight loss (T_{max}^1=370-400^{0}C) is due to the decomposition of C-Br bonds or the evaporation of DBBO. Another major weight loss (second stage) at 487^{0}C (T_{max}^2) is of EPDM matrix. Addition of DBBO improves the onset of degradation (T_0). The relative mass loss at stage 1 of DBBO based composites increases and is proportional to its concentration.
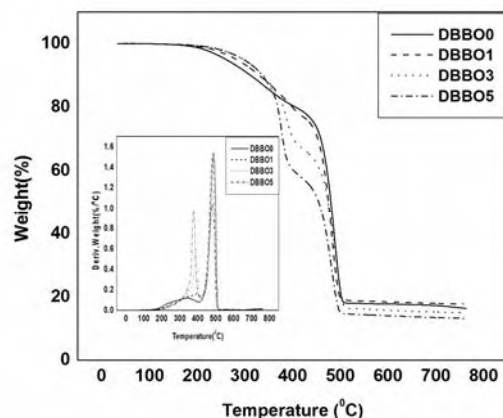
Fig. 4.19. The thermograms of DBBO filled EPDM composites. The inset is the derivative thermograms

The DBBO flame retardant used in this work does not increase char formation. This is as would be expected. It is known that the brominated flame retardants are gas phase active producing bromine atoms or hydrogen bromide that interrupts the flame propagation reactions.

4.3.8.4 Thermal stability of EPDM/EG composites

Fig. 4.20 demonstrates the TGA and DTG plots of EG filled composites carried out under nitrogen atmosphere. Addition of EG does not change the nature of degradation but alters the maximum degradation temperature. The first phase degradation (minor degradation) is due to EG. The second stage degradation (major degradation) is due to EPDM matrix. The peak heights of the DTG plots at higher temperature range are dropped noticeably with the addition of EG, due to the intumescent char formation on the matrix surface.
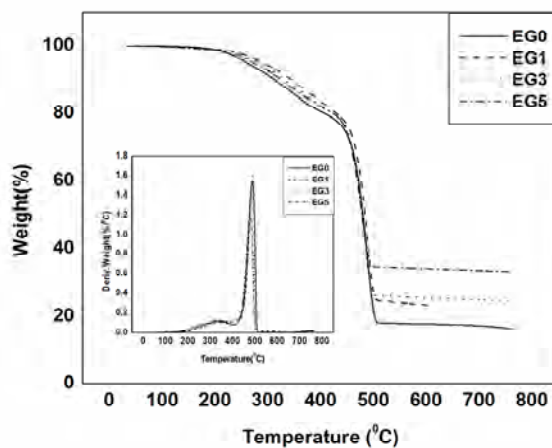
Fig. 4.20 The thermograms of EG filled EPDM composites. The inset is the derivative thermograms

Table 4.5 Degradation temperatures and weight loss at different temperatures of composites

Sample Name	T_0 (^{0}C)	T_{50} (^{0}C)	T_{max}^1 (^{0}C)	T_{max}^2 (^{0}C)	Weight loss at 425^{0}C (%)	Weight loss at 450^{0}C (%)	Weight loss at 475^{0}C (%)	Residue (%)
unfilled	418	480	-	487	26	43	78	16
ATH1	417	480	-	491	19	25	44	17
ATH3	416	483	-	492	21	25	40	23
ATH5	418	488	-	490	21	25	36	29
CPE1	431	482	225	489	20	25	41	12
CPE3	432	481	228	490	21	26	42	16
CPE5	433	480	226	488	24	28	44	18
DBBO1	442	480	389	487	23	27	44	17
DBBO3	430	470	383	485	34	39	54	14
DBBO5	431	457	378	482	43	48	62	13
EG1	434	478	341	485	20	26	46	23
EG3	432	481	341	484	20	24	42	24
EG5	433	484	338	483	20	24	40	33

4.3.9 Differential scanning calorimetry

DSC measurements were carried out to evaluate the influence of ATH, CPE, DBBO and EG (25 phr) on the chain flexibility of EPDM. Compared to unfilled sample, all filled samples exhibit an increase in T_g from -60 to -55 (Fig. 4.21). This shows an increment in Tg, which may be due to the stiffening of the chain due to the presence of filler.
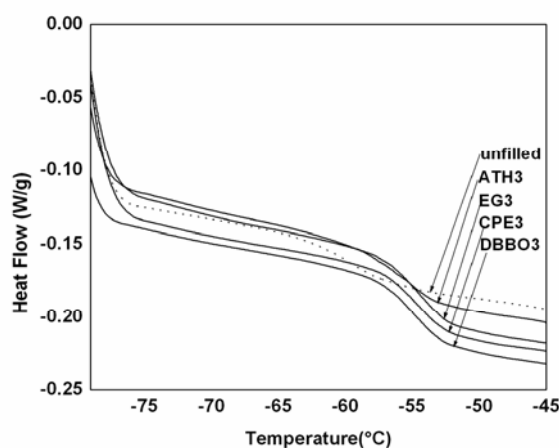
Fig. 4.21 The DSC curves of unfilled and 25phr ATH, CPE, DBBO and EG filled EPDM

4.3.10 UL-94 HB test

When a polymer burns horizontally, the dripping of polymer onto underlying materials, may promote the propagation of fire, where as the formation of char layer allows the obstruction of combustible gases and the formation of barrier against heat, reducing the burning rate (BR) of the polymer and dripping of flaming material. Table 4.6 gathers the results of UL-94 HB characterization. Accordingly, composites without ATH show a relatively high BR. The addition of ATH to EPDM significantly modifies the process of burning.

The "worm" like structure that is formed by the graphite expansion suffocates the flame and the compact char layer that is formed limits the transfer of heat and mass from the polymer to the heat source, preventing the decomposition of the material [21]. EG can prevent combustible gases from feeding the flame, and separates oxygen from the burning material more efficiently. In UL-94 HB studies, the addition of EG also significantly modifies the process of burning. The volume of the resulting carbonaceous char increases, with the increase in percentage of EG.

Table 4.6 Results of horizontal burning test UL94 HB for EPDM composites

Sample Name	BR (mm/min)	Observations
unfilled	55	Intense dripping, Charring
ATH1	54	Intense dripping, Charring
ATH2	49	Burning with drips, Charring
ATH3	47	Burning with drips, Charring
ATH4	46	Burning with drips, Charring
ATH5	44	Burning with drips, Charring
CPE1	54	Intense dripping, Charring
CPE2	52	Intense dripping, Charring
CPE3	50	Intense dripping, Charring
CPE4	50	Burning with drips, Charring
CPE5	48	Burning with drips, Charring
DBBO1	45	Burning with drips, Charring
DBBO2	42	Burning with drips, Charring
DBBO3	39	Burning with drips, Charring
DBBO4	36	Burning with drips, Charring
DBBO5	34	Burning with drips, Charring
EG1	45	Burning with drips, Charring
EG2	44	Burning with drips, Charring
EG3	42	Drips with the formation of carbonaceous mass
EG4	39	Drips with the formation of carbonaceous mass
EG5	41	Formation of carbonaceous mass with the thickness correlated to the EG amount

4.3.11 Limiting oxygen index (LOI)

The results of LOI for the ATH filled EPDM composites are presented in table 4.4. An increase in concentration of ATH from 0 to 45 phr, increases the LOI from 20 to 24. The flame retardancy mechanism of ATH is based on its thermal decomposition between 200-400^{0}C. During this energy consuming process or endothermic reaction, ATH releases its chemically bonded water (34.6 wt. %), while the corresponding aluminum oxide remains as char residue. CPE filled systems shows only a marginal effect on flame retardancy. The LOI value of EG filled EPDM composites increases with increasing amount of EG, the LOI value of an EPDM/EG composite that contains 45phr EG is 26, which is much higher compared to 20 of unfilled EPDM, suggesting that the EG is an efficient flame retardant for EPDM. In DBBO/EPDM composites, the LOI results showed that the unfilled EPDM had low resistance to combustion. With increasing amounts of DBBO the LOI raised from 20 to 26. Important problem in the use of organic halogen compounds is that they promote heavy smoke production during combustion and also produces toxic and highly corrosive hydrogen halide gases.

4.3.12 Scanning electron microscopy

The tensile fractured surface morphology of the composites with varying amounts of ATH, CPE, DBBO and EG are shown in Fig. 4.22, 4.23, 4.24 and 4.25 respectively. ATH is found to have smaller and much more homogeneous in size. Addition of 25 phr ATH improves the mechanical properties of EPDM (section 4.3.6). In CPE/EPDM systems also, the morphology is related to the variation in mechanical properties. Particle size distribution was broader, in DBBO filled systems. At higher

DBBO loading, the particle was pulled out from the matrix, due to the weak interface between the matrix and the filler.
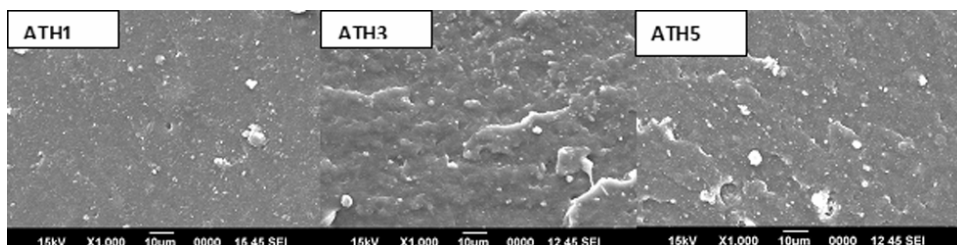

Fig. 4.22 Scanning electron photographs of ATH filled EPDM composites
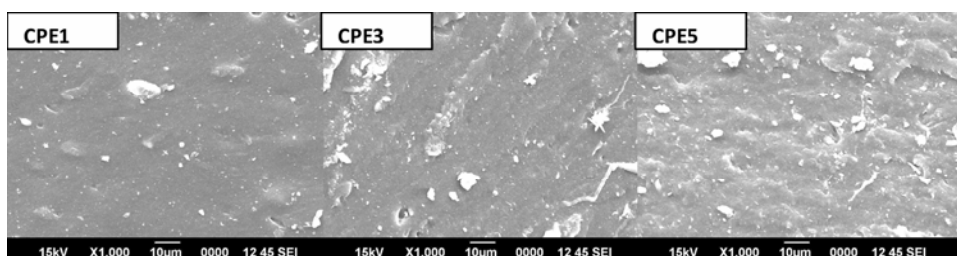

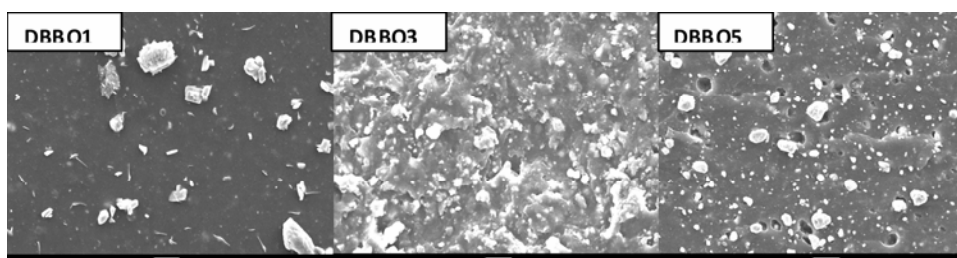**Fig. 4.23 Scanning electron photographs of CPE filled EPDM composites**

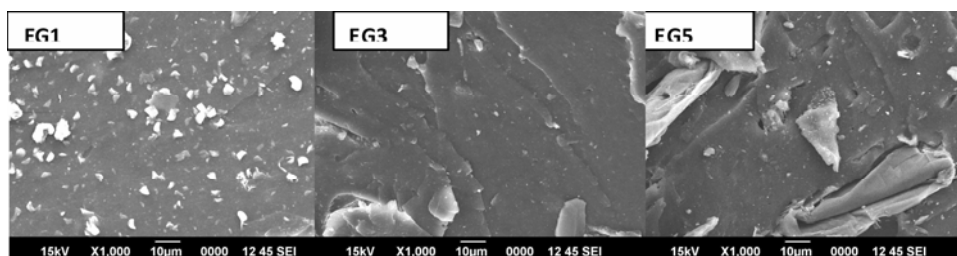**Fig. 4.24 Scanning electron photographs of DBBO filled EPDM**

Fig. 4.25 Scanning electron photographs of EG filled EPDM composites

As discussed above, the micropores in EG have good affinity to polymer. The polymers are absorbed in pores and galleries of EG, which gives the composite without distinguishing the individual inter layer plane. At higher EG loading the agglomeration is clearly observed which is in good agreement with the mechanical properties.

4.4 Conclusions

The cure characteristics of EPDM remain unaffected on addition of ATH, CPE, DBBO and EG. Strain sweep measurements reveal that the complex modulus of composites decreased in the order ATH>EG>DBBO>CPE. EPDM vulcanizates containing 25 phr ATH showed increase in tensile strength which indicates the high reinforcing effect of ATH on EPDM matrix. ATH filled microcomposites exhibited reduced swelling compared to other systems. From the thermal analysis it is evident that ATH and CPE impart maximum thermal stability to the composites. Flame retardant studies reveal that all fillers significantly retard the process of burning. EG and DBBO are better flame retardants compared to ATH and CPE. SEM analysis reveals even distribution of ATH fillers in the EPDM matrix which contributes to improvement in mechanical properties.

References

[1]   Bhowmick AK, Stein C, Stephens HL, Handbook of elastomers. New York: Marcel Dekker 1981, 729.

[2]   Ahamad RSA, Arash R, Massoud F, Saeed R. J Mater Des 2008, 29, 1051-1056.

[3]   Pomerantsev AL, J Appl Poly Sci 2005, 96, 1102–14.

[4]   Begum M, Siddaramaiah B, Kumar H, Aminabhavi TM, J Appl Polym Sci 2003, 90, 739–46.

[5]   Mathai AE. Ph.D thesis, Mahatma Gandhi University, Kottayam, Kerala, India, 2002.

[6]   Tai CM, Robert KY Li, J. of Appl. Polym. Sci 2000, 80, 2718-2728.

[7]   Ahmet A, Enver D, J Mater Des 2008, 29, 1376-1379.

[8]   Pinto UA, Visconte LLY, Nunes RCR, Eur Polym J 2001, 37, 1935-7.

[9]   Du L, Qu B, Xu, Polym Degrad stab 2006, 91, 995-1001.

[10]   Khattab MA. J. of Appl. Polym. Sci 2000, 78, 2134–2139.

[11]   Ramazani SAA, Rahimi A, Frounchi M, Radman S. Mater Des 2008, 29, 1051-1056.

[12]   Koscielecka A. J. Eur. Polym. 1993, 29, 23-26.

[13]   Renguang Yu, Xiaojing QIAO. Chin. J. Mater. Rev 2003, 17, 125-126.

[14]   Aminabhavi TM, Phayde HTS, Polymer 1995, 36, 1023–33.

[15]   Crank J. The mathematics of diffusion. 2nd ed. Oxford: Clarendon Press, 1975.

[16]   Aithal US, Aminabhavi TM, Cassidy PE. J Mem Sci 1990, 50, 225–47.

[17]   Kraus G. J Appl Polym Sci 1963, 7, 861.

[18] Flory PJ, Rehner J. J Chem Phys 1943, 11, 512-520.

[19] Chiou JS, Paul DR. Polym Eng Sci 1974, 18, 867.

[20] Lucht LM, Peppas NA. J Appl Polym Sci 1987, 33, 1557.

[21] Modesti M, Lorenzetti A, Simioni F, Camino G, Polym Degrad Stab 2002, 77, 195-202.

…..౸౷…..

EFFECT OF EXPANDED GRAPHITE ON THERMAL, MECHANICAL AND DIELECTRIC PROPERTIES OF EPDM/FKM RUBBER BLENDS[*]

Contents

Expanded Graphite (EG) filled with compatibilized and uncompatibilized EPDM/FKM (50/50, w/w) blends were prepared by two-roll mill mixing. Maleic anhydride grafted EPDM (MA-g-EPDM) is used as a compatibilizer. The cure characteristics, filler dispersion, mechanical properties and DC electrical conductivity of the composites were evaluated. The thermal stability of the EG loaded EPDM/FKM blends was studied using thermogravimetric analysis (TGA). The activation energy of the composites was evaluated by the Coats–Redfern method. The microwave properties like dielectric permittivity, dielectric loss, conductivity, dielectric heating coefficient and absorption coefficient were evaluated. At higher EG loading, the optimum cure time (T_{90}) decreases due to the increased thermal transition of the blends in presence of EG. The tensile properties of all the composites, especially those with compatibilizer, increased with aging. The AC and DC conductivities increase with increase in EG loading, due to the formation of enhanced conductive networks by EG platelets. The flammability and thermal characteristics are improved by the addition of EG. The morphology of the composites was investigated using scanning electron microscopy (SEM).

5.1 Introduction

Expanded graphite (EG) is a product made by subjecting graphite intercalation compounds (GICs) to rapid thermal treatment. EG maintains the layered structures similar to natural flake graphite but produces tremendous difference in average pore diameter [1]. EG can be mass-produced and used in many applications such as gaskets, seals, batteries, substratum for adsorption, etc. However, relatively a little is reported of EG serving as conductive fillers in polymer composites [2].

Blending a polymer with conducting fillers, such as natural graphite flake, carbon black, and metal powders, to prepare electrically conducting composites has been extensively investigated in the past few decades. Among the various conducting fillers, naturally abundant graphite, which possesses good electrical conductivity of about 10^4 S/cm at ambient temperature, has been widely used [3, 4]. In most cases, relatively large quantities of graphite were needed to reach the critical percolation value, as the graphite particle size is in micrometer and millimeter scale. Too high concentrations of the conductive filler could lead to reduction in mechanical properties [5].

Microwave absorbing materials have received increasing attention and interest in electronic and communication industries. The importance of these materials relates to the high demand for the reliability of electronic devices, and also rapid growth of radio frequency (RF) sources and interference of various electronics by radio frequency radiation [6, 7]. Microwave absorbing materials are usually supported on a metal surface to prevent the reflection of the incident wave. These materials are used as internal lining of the walls of an

echoic rooms to prevent the interference of the wave reflected from the room walls with that emitted from the device under test. Moreover, needs for light weight broad band microwave absorbers which can be used outdoors or in numerous applications where the absorber comes in contact with water or should withstand severe vibrations and/or mechanical impacts arise in airborne, automotive and marine applications [8].

Microwave absorbers have electromagnetic impedance in between the emission environment (usually air) and the incidence surface that they are put over and hence they prevent reflection that is caused by sudden impedance change. As the wave impedance in absorbing lining is a function of the lining thickness and permittivity, the material permittivity and hence, wave impedance in a defined frequency range can be adjusted so that minimum reflection occurs [9].

Ethylene propylene diene monomer rubber (EPDM) is the material that has excellent performance in thermal stability, aging resistance etc. [10-13]. Fluoroelastomers are widely used in many industrial applications [14-18]. The increasing use of such polymers in automobiles, aerospace, and in hostile chemical environments [19-24]. Blending of FKM into EPDM can be a potential measure to prepare materials with better overall properties. In order to improve the compatibility, a compatibilizer MA-g-EPDM, is used. The thermal stability of blends depends strongly on the compatibility of the polymers [25]. The adequate chemical structure of the compatibilizing agent can reduce the interfacial energy between the phases and finer dispersion can be achieved [26].

In order to achieve an acceptable degree of flame retardancy, expanded graphite has been extensively used as smoke and toxic-free additive in halogen free flame-retardant (HFFR) polymeric materials. However, their fatal disadvantages are low FR efficiency and very large usage amount, which cause the mechanical properties of the FR polymeric materials to decrease sharply. Among the FRs, intumescent flame retardants (IFRs) have aroused great attention in recent years because they are more environment friendly than the traditional halogen containing FR. Expandable graphite (EG), developed in recent years, is being used in a growing number of applications as an intumescent flame retardant additive, as a char-forming agent, as a blowing agent and as a smoke suppressant [27–29].

In this part of the study, the thermal stability and limiting oxygen index of the compatibilized and uncompatibilized EG loaded EPDM/FKM blends are evaluated. Kinetic studies of thermal degradation are also carried out. The dielectric properties at microwave frequencies of the prepared composites are measured in the S-band (2-4 GHz) frequency using the cavity perturbation technique. SEM investigations have been carried out to categorize the morphology of the composites.

5.2 Experimental details

5.2.1 Materials

The specifications of the materials used are given in section 2.1.

5.2.2 Methods

The formulation used for the preparation of EPDM/FKM blend based composites is given in section 2.5. The methods used in this work are given in section 2.6.

5.3 Results and Discussion

5.3.1 Cure characteristics and cure kinetics

The cure curves of EG filled uncompatibilized and compatibilized EPDM/FKM blends are given in Fig. 5.1 and Fig. 5.2 and some parameters of the curing properties are reported in table 5.1.

Table 5.1 Properties of composites

| Sample	Scorch time (min)	Cure time (min)	Hardness (Shore A)	Rebound resilience (%)	Compression set (%)	Abrasion loss (cm³/h)	Heat build up (⁰C)	LOI (%)
EVG0	2.37	17.60	65	49	16	3.23	21	26
EVG1	1.79	16.03	61	48	32	6.83	28	26
EVG2	1.71	15.31	63	48	30	7.84	36	27
EVG3	1.34	15.34	66	46	31	6.35	37	28
EVG4	1.24	15.70	67	46	34	7.09	42	30
EVG5	1.15	15.75	69	42	35	8.38	44	30
EVG0*	2.32	17.20	66	42	15	3.11	28	26
EVG1*	1.98	16.15	61	41	31	5.72	26	26
EVG2*	1.80	16.40	65	40	34	6.76	28	27
EVG3*	1.60	16.08	67	38	36	7.19	33	29
EVG4*	1.47	15.91	69	38	35	7.30	34	30
EVG5*	1.35	15.20	71	39	37	7.63	44	31
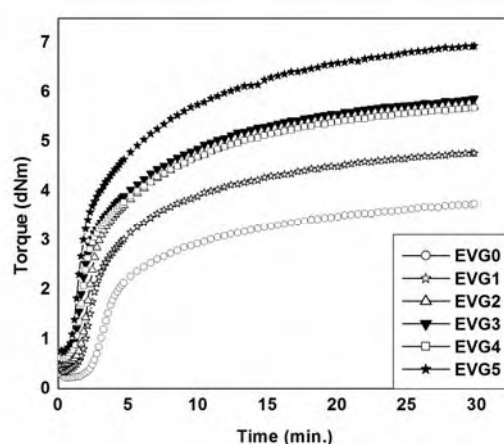
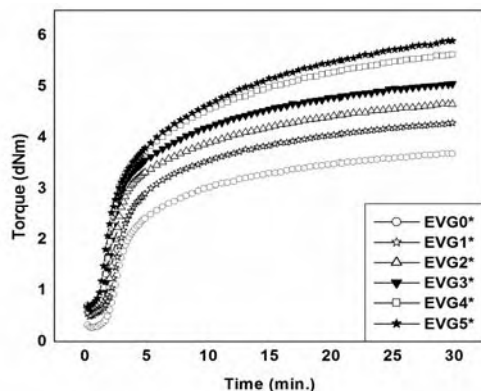**Fig. 5.1 Cure curves of EG loaded EPDM/FKM blends**

Fig. 5.2 Cure curves of EG loaded EPDM/FKM blends compatibilized with MA-g-EPDM

The minimum torque, D_{min}; which is a measure of the viscosity of the compound, is found to increase with filler loading for both series as expected. The increase in viscosity with the addition of filler suggests a reduced mobility of the rubber chains caused by the incorporation of these fillers.

The maximum torque, D_{max} increases with increase in EG loading. The maximum torque, D_{max}, is an index of the extent of crosslinking reactions and represents the shear modulus of the fully vulcanized rubber at the vulcanization temperature. It is also a measure of the filler–polymer interaction. $D_{max} - D_{min}$ represents the crosslink density of vulcanizates. It slightly increases with EG loading in both series (Fig. 5.3 and Fig. 5.4). This indicates that the addition of EG has marginal effect on the crosslink density of rubber vulcanization.

Scorch time (T_{10}) is the time required for the torque value to reach 10% of maximum torque. It is a measure of the scorch safety of the rubber compound. For the EVG and EVG* series, T_{10} slightly decreased with filler loading. Such a decrease is attributable to the heat of mixing resulting in the premature curing of the compounds.

The optimum cure time (T_{90}) increases initially and then decreases where as T_{10} shows a regular decrease. The reason for the lower T_{90} at higher loading is due to the increase of the thermal transition of the matrix in presence of EG, which promotes the vulcanization process. EG have increased specific surface area by acid treatment, which results in improved thermal transition, filler-filler and filler-matrix interactions. Generally, the cure characteristics depend on the filler properties such as nature of the filler, surface area, surface reactivity, aspect ratio and particle size. In general, a faster cure rate is obtained with fillers having lower surface area [30].
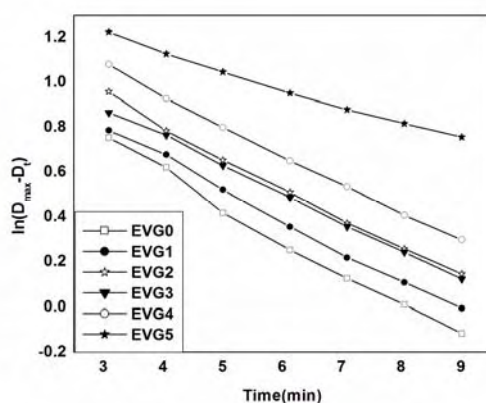

Fig. 5.3 Plot of ln (D_{max} - D_t) vs time of the composites (EVG series)
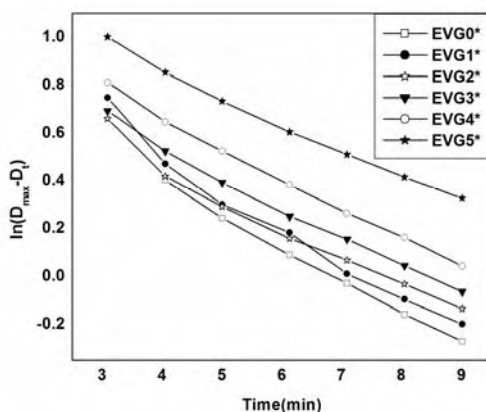

Fig. 5.4 Plot of ln (D_{max} - D_t) vs time of the composites (EVG* series)

The vulcanization kinetics were studied by the method [31, 32] are given below.

The general equation for the kinetics of a first-order chemical reaction is given in equation 5.1,

$$\ln (a-x) = -kt + \ln a \quad \text{-- (5.1)}$$

Where 'a' is the initial reactant concentration, 'x' is the reacted quantity of reactant at time 't' and 'k' is the first-order rate constant. For the vulcanization of rubber, measuring the torque developed during vulcanization monitors the rate of crosslink formation. The torque obtained is proportional to the modulus of rubber. Thus, the following substitutions can be made.

$$(a-x) = (D_{max}-D_t) \quad \text{-- (5.2)}$$

$$a = D_{max}-D_{min}$$

where D_t is the torque at time 't'. Therefore, the equation can be written as

$$\ln (D_{max}-Dt) = -kt + \ln (D_{max}-D_{min}) \quad \text{------------------------------- (5.3)}$$

Therefore, if a plot of $\ln (D_{max}-D_t)$ against time 't' is a straight line, then the cure reaction follows first-order kinetics. The cure reaction rate constant can be obtained from the slope of the corresponding straight lines.

The plot of $\ln (D_{max}-D_t)$ against time 't' of the EVG* series and EVG* series at 150^0C is presented in Fig. 5.3 and Fig. 5.4 respectively. The plots are found to be linear which proves that the cure reactions proceed according to first-order kinetics.

5.3.2 Filler dispersion

Lee has studied the filler dispersion and formation of filler agglomerates in polymer matrices in detail [40]. He assumed that $\eta_r > M_r$, where η_r and M_r are the relative viscosity and the relative modulus respectively. The paper also proposed that η_r and M_r could be determined from rheometric data by using the expression (equation 5.4),

$$\eta_r = D^f_{min}/D^0_{min} \text{ and } M_r = D^f_{max}/D^0_{max} \text{ ----------------------------- (5.4)}$$

where D denotes the torque and the superscripts 'f' and '0' are related to the loaded and the unloaded polymer, respectively. Lee introduced a new parameter 'L', which is defined as:

$$L = \eta_r - M_r \text{ --- (5.5)}$$

For ideal dispersions, $\eta_r = M_r$. This happens when the individual particles are well dispersed in the matrix. In the case of non-ideal dispersions, the value of 'L' changes slowly at low filler loadings, but above a certain limit, it increases sharply. The abrupt rise of the index 'L' at high filler loadings may be due to poor dispersion. In such a situation, it is assumed that the filler concentration has now reached the point where there is not enough rubber to fill the available voids in the filler.

Another mathematical expression has been proposed by Wolf in terms of rheometric data to characterize the filler structure present in rubber vulcanizates [41, 42]. When a filler is incorporated into a compound, the maximum torque varies and $\Delta D^f = D^f_{max} - D^f_{min}$ as observed during vulcanization increases. The ratio between D^f and D^0, the torque variation for the loaded and unloaded compounds, respectively, is directly proportional to

filler loading. By plotting the relative torque as function of filler loading, a straight line is obtained whose slope was defined by Wolf as α_f [43-46].

$$[(D^f_{max} - D^f_{min})/ (D^0_{max} - D^0_{min})] - 1 = \alpha_f (m_f/m_p) \text{------------------------- (5.6)}$$

Where m_p is the mass of polymer in the compound, m_f is the mass of filler in the compound and α_f is a specific constant for the filler, which is independent of the cure system and closely related to the morphology of the filler. The parameter α_f represents the final structure of the filler as it exists in the vulcanizates after all possible structure breakdowns that occurred during mixing and vulcanization. The reinforcement build up and crosslinking reaction takes place during curing without affecting each other. The application of the above equation allows the definition of a filler specific constant, related to the filler structure, and also predicts whether or not crosslink density is affected by the presence of the filler, in which case a straight line is obtained. The equation 5.6, also shows that based on a single test, α_f can be calculated from the changes in the torque which occur during vulcanization of the two compounds, the loaded and unloaded composition. Table 5.2 presents the computed η_r, M_r and 'L' values. In the EVG series, it is observed that $\eta_r > M_r$ which means that the filler is not well dispersed in the matrix. But in EVG* series, the filler particles are well dispersed in the matrix except at higher loading. Both, η_r and M_r values, increase slightly with loading indicating an increase in relative viscosity and relative modulus of the elastomer. The index 'L' increases with filler loading pointing to the agglomeration of the filler in the elastomer. In table 5.2, the Wolf equation is applied for all the composites. Table 5.2 shows a sharp increase in the value of 'L' with filler loading for the EVG series indicating predominance of agglomerates in the matrix. In EVG and EVG*

series, the α_f is dependent on filler loading, the value decreasing with loading. These observations are in agreement with those obtained from Lee's approach.

Table 5.2 η_r, M_r, L and α_f values of the composites

Sample	η_r	M_r	L	α_f
EVG1	1.04	0.81	0.23	15.920
EVG2	1.45	0.97	0.48	6.250
EVG3	1.86	0.99	0.87	3.780
EVG4	1.87	1.13	0.74	0.254
EVG5	2.32	1.18	1.14	0.246
EV G1*	1.53	1.30	0.23	5.444
EV G2*	1.98	1.41	0.57	2.351
EV G3*	1.99	1.53	0.46	1.917
EV G4*	2.00	1.65	0.35	1.755
EV G5*	2.05	1.79	0.26	1.680

5.3.3 Effect of thermal aging on stress-strain properties

Aging helps the process of vulcanization in FKM and their blends. Aging of polymers normally reduces its mechanical properties. But in the case of EG loaded compatibilized and uncompatibilized EPDM/FKM blends aging does not alter the mechanical properties to a great extent. During press curing of blends, water is generated as reaction product which inhibits the vulcanization process and results in lower strength [40]. EG does not enhance the mechanical properties of the polymers due to poor dispersion of the graphite, voids trapped in the composites and weak interfacial adhesion [41-48].

The rubber samples under investigation, which do not contain any antioxidant, were subjected to thermal aging at 70, 150 and 200 ^{0}C for 22 h.

Fig. 5.5, 5.6 and 5.7 show that the tensile strength, elongation at break and 100 % modulus (EVG series). It is found that the tensile strength, elongation at break and 100% modulus increase at 70 ^{0}C and 150 ^{0}C aging and decrease slightly at 200^{0}C aging. This behaviour can be attributed to further cross-linking of the rubber vulcanizates at temperatures like 70 ^{0}C and 150 ^{0}C, while degradation of polymer chains occurs at 200 ^{0}C aging.
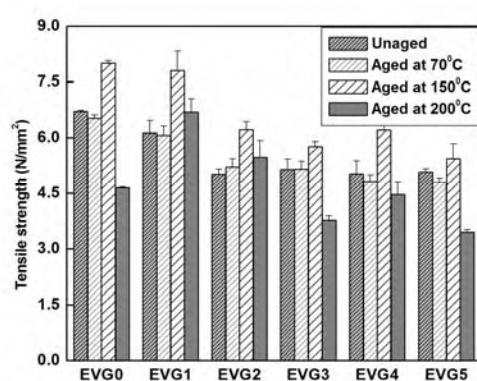

Fig.5.5 Variation in tensile strength before and after aging for uncompatibilized EG loaded EPDM/FKM blends
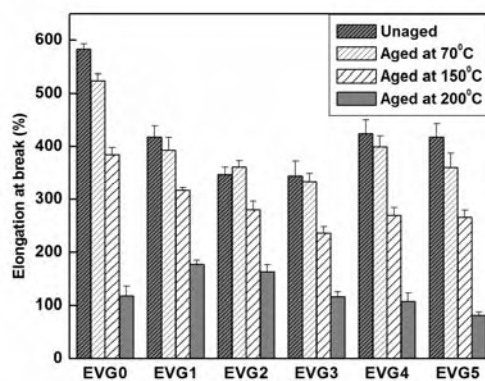

Fig.5.6 Variation in elongation at break before and after aging for uncompatibilized EG loaded EPDM/FKM blends
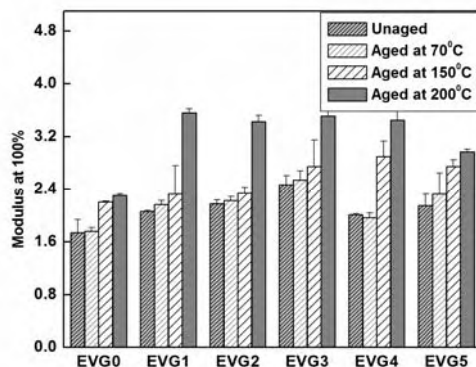
Fig. 5.7 Variation in modulus at 100 % elongation before and after aging for uncompatibilized EG loaded EPDM/FKM blends

The tensile strength of EVG* series increased by compatibilization with MA-g-EPDM as shown in Fig. 5.8. The increment in tensile strength of compatibilized blends compared to uncompatibilized blends is due to the formation of interfacial interactions between EPDM and FKM in the presence of the compatibilizer. The presence of polar groups (eg. –OH and –COOH), interacting physically and chemically with polymer matrix may also be a reason for strong interfacial interaction [49, 50]. At higher loading the values decrease due to agglomeration of the filler particles.
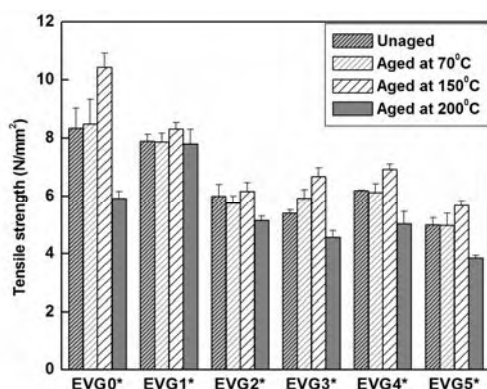

Fig. 5.8 Variation in tensile strength before and after aging for compatibilized EG loaded EPDM/FKM blends
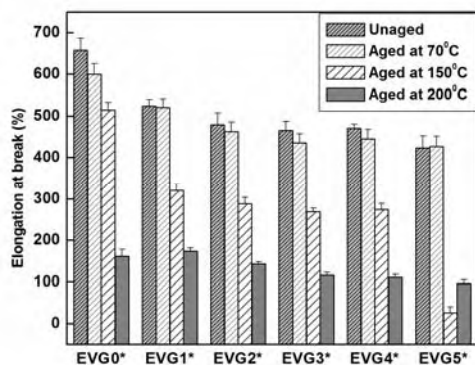
Fig. 5.9 Variation in elongation at break before and after aging for compatibilized EG loaded EPDM/FKM blends
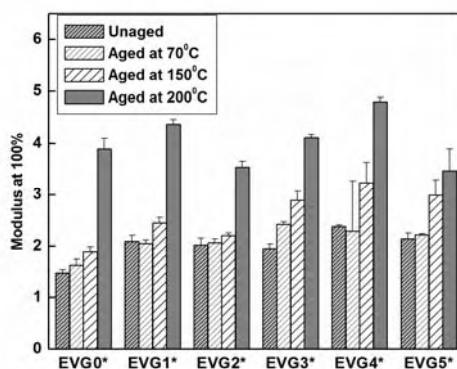
Fig. 5.10 Variation in modulus at 100 % elongation before and after aging for uncompatibilized EG loaded EPDM/FKM blends

Fig. 5.9 shows the elongation at break (EB) of the EG loaded compatibilized blends. EB values of the compatibilized blends are higher than that of the EVG series. After aging the EB value of all the vulcanizates decreased and the lowest value were observed after aging at 200^{0}C. In EVG series, the decrease in elongation at break with filler loading is due to the decrease in the stress bearing capacity of the filler–matrix interface. Compared to EVG series, the higher values in compatibilized blends is due to the sliding effect of fine graphite particles, giving a plasticizing effect.

The tensile modulus at 100 % elongation (M_{100}) of the EVG* series is shown in Fig. 5.10. The increase in modulus after aging is due to an increase in crosslink density. Incorporation of the filler particles in the soft matrix reduced the elasticity of the polymer chains.

5.3.4 Other mechanical properties

Table 5.1 shows other mechanical properties like hardness, rebound resilience, compression set, abrasion resistance and heat build-up of the vulcanizates. The hardness which depends on the distribution of the rigid filler in the host matrix increases by increase in the filler content. In compatibilized blends, the hardness increases from 66 to 71 Shore A. The reverse trend is obtained in the case of rebound resilience. The resilience values show a linear decrease with increase in EG content in both series. The compression set at constant strain increases with increase in EG loading. The abrasion loss of the blends containing different amounts of EG also shows an increase with increase in EG content. There is a gradual increase in heat generation values of all the blends. The energy dissipation can be caused by energy loss at the filler-matrix interface, friction between the chains and break down of filler structure. Compared to EVG series, compatibilized blends show higher heat build-up values. This will be manifested as lower resilience values. All the cases, the EVG* series shows comparatively better properties. This can be attributed to better interfacial adhesion between EPDM and FKM bringing about compatibility in the binary blend.

5.3.5 Thermal stability of composites

TGA is one of the most accepted techniques for evaluating thermal stability of various polymers. The TGA and DTG thermograms of EPDM

and FKM in nitrogen atmosphere are shown in Fig. 5.11. In the case of EPDM a major degradation peak (T_{max}) appears at 487^0C and that for FKM is 502^0C. FKM has got greater thermal stability in nitrogen atmosphere than EPDM, which is evident from the displacement of the weight loss curve to higher temperature.
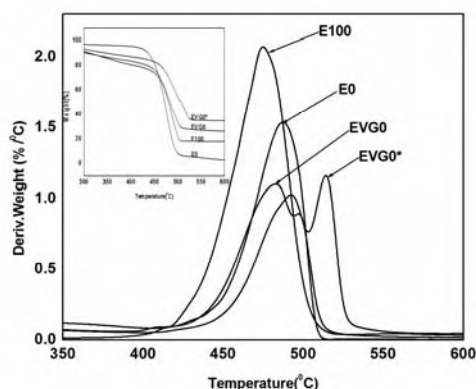

Fig. 5.11   The derivative thermograms of E100, E0, EVG0 and EVG0* vulcanizates. The inset shows the respective thermogram

Effect of compatibilization of EPDM/FKM blends with MA-g-EPDM on the thermal stability can be derived from the TG and DTG curves given in Fig. 5.11. The thermal stability of the blends is found to increase by the incorporation of MA-g-EPDM. This may be due to the chemical and physical interaction between the two constituents at the interface without influencing the bulk. So the individual components are likely to follow their own degradation route. Table 5.3 gives the onset of degradation (T_0), maximum degradatiom (T_{max}) and residue (%). Thus it is clear from the table that all blends with MA-g-EPDM are thermally more stable compared to those without compatibilizer. The increase in degradation temperature of compatibilized blends is due to the improved interfacial adhesion between the two components as a result of interface linking through MA-g-EPDM.

The thermal stability of the polymer blends depends mainly on the morphology and the miscibility of the system.

Table 5.3 Thermal characteristics of the composites

| Sample	Onset degradation temperature (T_0, ^0C)	Peak degradation temperature (T_{max}, ^0C)	Residue at 800 ^0C (%)	Apparent activation energy E (kJ/mol)	Correlation coefficient (r)
EVG0	422	490 and 504	12	121	0.9986
EVG1	426	486 and 507	30	121	0.9991
EVG3	429	483 and 507	33	122	0.9978
EVG5	428	457 and 503	38	119	0.9995
EVG0*	435	486 and 506	13	133	0.9984
EVG1*	436	486 and 506	30	131	0.9989
EVG3*	437	482 and 506	36	130	0.9971
EVG5*	429	480 and 506	40	126	0.9992
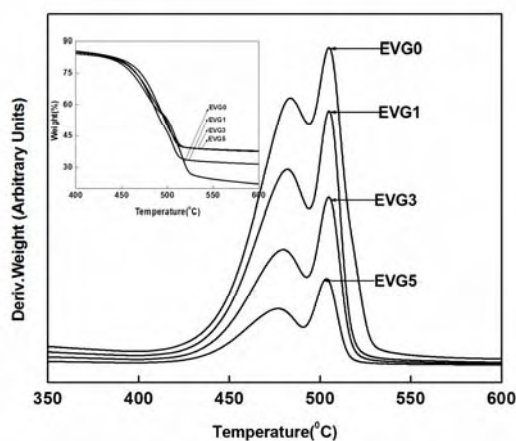
Fig. 5.12 The derivative thermograms of EVG series. The inset shows the respective thermogram
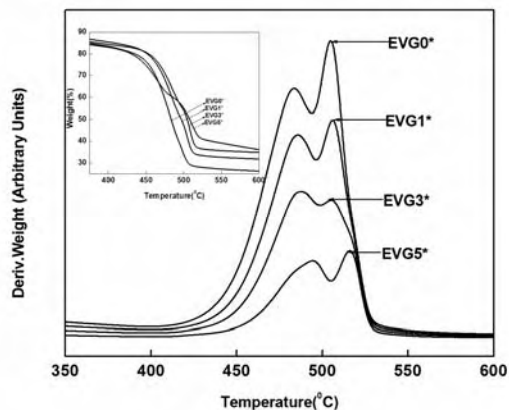
Fig. 5.13 The derivative thermograms of EVG* series. The inset shows the respective thermogram

Fig. 5.12 and Fig. 5.13 demonstrates the TGA and DTG plots of EG filled EVG and EVG* composites under nitrogen atmosphere. Addition of EG slightly improves the thermal stability of EVG and EVG* series. Finer dispersion of EG could act as "efficient heat sinks", which consumes more heat than the matrix and does not allow the accumulation of heat within the latter, and thereby preventing oxidation. But at higher loading the maximum degradation temperature does not improve much, rather exhibits a slight decrement. This may be due to the agglomeration of EG within the matrix resulting in poorer interaction. The peak heights of the DTG plots at higher temperature range are dropped noticeably with the addition of EG due to the intumenescent char formation on the matrix surface.

5.3.6 Kinetic analysis of thermal decomposition

In the case of the EVG and EVG* series, the activation energy (E) value reveals that the incorporation of EG has resulted in slight increase of the activation energy. The highest 'E' is obtained in the case of FKM [51]. Higher values of 'E' indicate higher thermal stability. From Table 5.3 it is

observed that the EPDM/FKM blends have lower apparent activation energy 'E' than FKM. It means that FKM has a better thermal stability than its blends with EPDM. In the case of compatibilized EPDM/FKM blends, the recrosslinking reaction easily takes place at high temperature leading to higher thermal stability. At higher EG loadings the 'E' of both series decrease.

5.3.7 DSC studies

The DSC curves of pure EPDM, FKM and its blends are shown in Fig. 5.14. The glass transition temperature of the polymer depends on the structure and co-operative mobility of the segments. This behavior is reflected in the occurrence of a single glass transition temperature in miscible blends. In the case of partially miscible blends, the glass transition temperature gets shifted. In completely immiscible polymer blends, the T_{gs} remain unaltered. T_g value of pure EPDM is found to be -60.01^0C and that of pure FKM is -19.25^0C. The uncompatibilized blend (EV) shows that the T_g value of both components remain unaltered. But in the case of compatibilized blend EV*, the T_g of EPDM phase shifted (-55.48^0C) towards FKM, indicates better interaction between the FKM phase because of the effect of the MA-g-EPDM. Compared to unfilled sample, filled samples (EVG3 and EVG3*) exhibit an increase in T_g (Glass transition temperature) from -60 to -55 (Fig. 5.14). This shows an increment in T_g, which may be due to the stiffness of the chain by the presence of filler. The increase of T_g can be attributed to the restricted segmental motion of molecular chains at the polymer-filler interface.
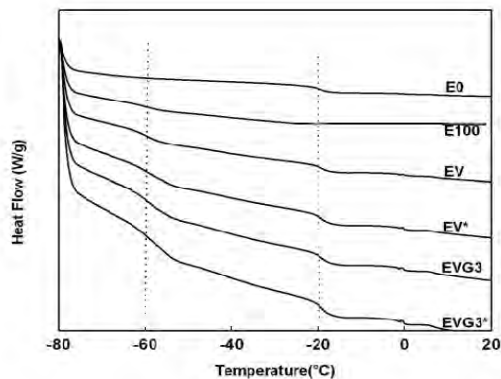
Fig. 5.14 The DSC curves of EPDM (E$_{100}$), FKM (E$_0$), compatibilized (EV*) and uncompatibilized 50/50, EPDM/FKM (EV) blends and 25 phr EG filled blends (EVG3 and EVG3*)

5.3.8 DC-electrical conductivity

The DC electrical conductivity of the composites is shown in Fig. 5.15. There is an increase in conductivity on addition of EG. In the EVG series, a conductivity of 1.92 X 10^{-4} S/cm is obtained at a loading of 45 phr EG. But the 45 phr EG loaded compatibilized blend shows a conductivity 5.6 X 10^{-4} S/cm. This may be due to the enhanced bonding between the two matrices (polar and non-polar) in presence of the compatibilizer.
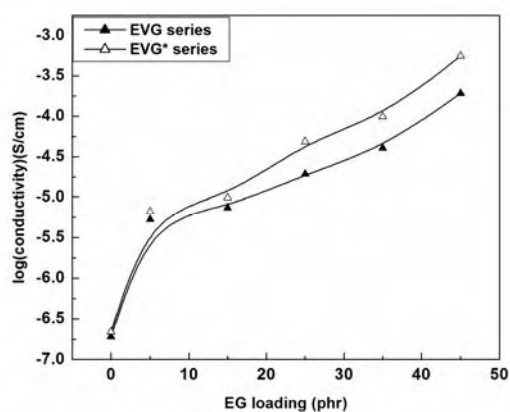

Fig. 5.15 Variation of log conductivity with EG loading

At a lower loading (5 phr), the electrical conductivity is of the order of 10^{-6} in both series. At high filler loading, the EG forms large agglomerates. Then the conducting networks are established connecting the agglomerates as shown in Fig. 5.16.
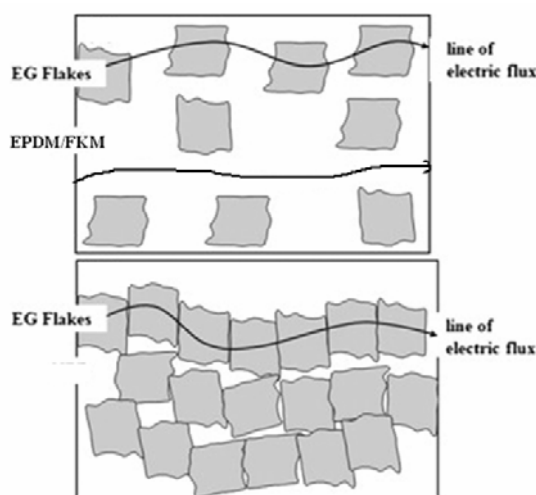
Fig. 5.16 Schematic representation of the graphite particles on the formation of conducting network (for clarity rubber blends were omitted)

The enhanced chemical and physical interactions between the graphite surface and polymer matrix resulted in improved conductivity by eliminating unbonded gaps or micro voids that are highly resistant to electrical conduction and are detrimental to the formation of a conductive network by EG. At lower loadings, there are only a few continuous conduction paths throughout the bulk of the composite. It follows that any unbonded interface with the conductive graphite particles may break up the electrical pathway, causing a significant reduction in the overall electrical conductivity. The addition of EG significantly lowers the resistivity of the polymer with a sharp transition from an electrical insulator to an electrical semiconductor. The augmentation of the electrical resistivity can be

attributed to the dispersion of EG in the polymer matrix and the formation of conductive network.

5.3.9 Dielectric properties of the composites
5.3.9.1 Variation of AC-conductivity and skin depth

The skin depth, also called the penetration depth, is basically the effective distance of penetration of an electromagnetic wave into the material [52], it can be applied to a conductor carrying high frequency signals. The self-inductance of the conductor effectively limits the conduction of the signal to its outer shell and the thickness of the shell is the skin depth which decreases with increase in frequency. When the material has good conductivity, it effectively reduces the depth of penetration of the signal. The microwave conductivity is a direct function of dielectric loss. Variation of the conductivity (S/cm) of composites with different proportions of EG with different frequency has the same nature as that of the dielectric loss factor. The highest value of conductivity and the lowest value of skin depth (Figs. 5.17 and 5.18) for the 45 phr EG loaded EVG and EVG* series are recorded at 2.972 GHz. The interfacial linking between EPDM and FKM in the presence of MA-g-EPDM is apt to form a compact and coherent rubber blend. Within the composite system, there could be two paths of electromagnetic propagation. In one path, the line of microwave can pass through EG flakes-polymer-EG flakes, and in the other path through direct contact between the EG flakes.
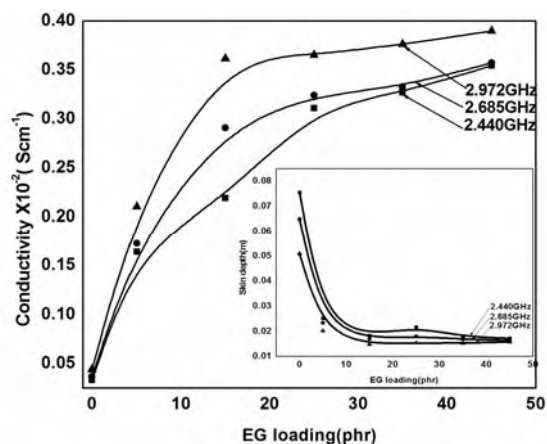
Fig. 5.17 Variation of AC-conductivity with EG loading for EVG series. The inset shows the variation of skin depth of the composites
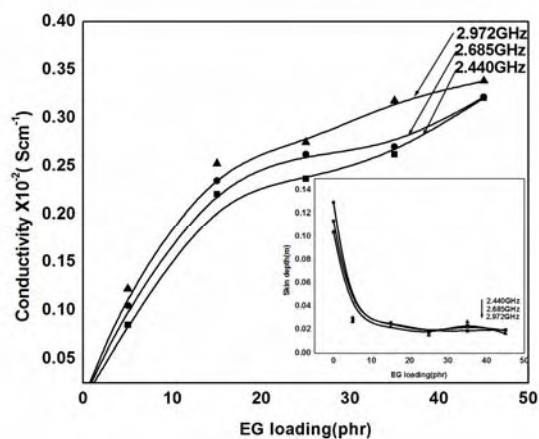
Fig. 5.18 Variation of AC-conductivity with EG loading for EVG* series. The inset shows the variation of skin depth of the composites

5.3.9.2 Variation of dielectric permittivity and loss

Figs. 5.19 and 5.20 show the variation of the dielectric permittivity of the EVG and EVG* series with loading. The variation of the dielectric loss with loading in the case of the EVG and EVG*series are given as insets in Figs. 5.19 and 5.20 respectively.
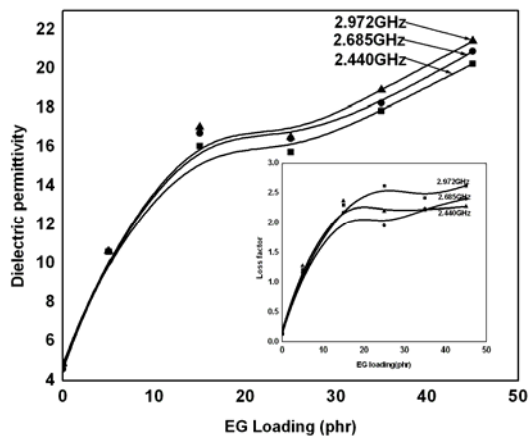
Fig. 5.19 Variation of dielectric permittivity with EG loading for EVG series. The inset shows the variation of loss factor of the composites
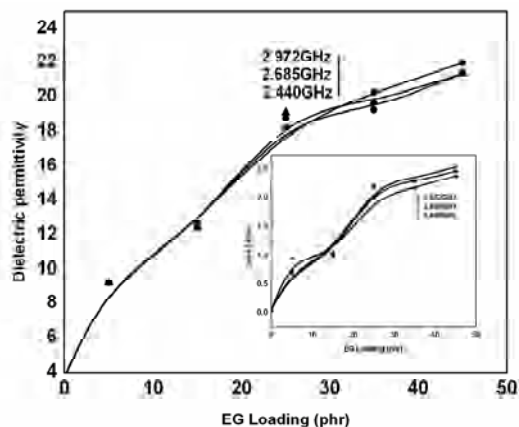
Fig. 5.20 Variation of dielectric permittivity with EG loading for EVG* series. The inset shows the variation of loss factor of the composites

The dielectric permittivity and dielectric loss are found to increase with loading in both series. The increase in dielectric permittivity with EG content may be due to the increase of conducting path formed in the matrix. Increase in dielectric loss with loading may be due the increased mobility of charge carriers. Frequency has little effect on dielectric permittivity and dielectric loss. This indicates that the polarization mechanism contributing

to the dielectric permittivity in these cases may be electronic or ionic. As the frequency is increased, the inertia of the molecule and binding forces become dominant and it is the basis for dielectric loss at higher frequencies. The relative dielectric constant and loss factor are used to characterize molecular relaxations. The relative dielectric constant is a measure of the energy stored in a sample during a cyclic dielectric relaxation, while dielectric loss is a measure of the energy lost [53]. This would be explained by the increase in the dipole polarity of the composite in the interfacial region by the addition of filler. Therefore the increase of filler loading would make dipole polarity to increase and boost dielectric constant and loss [54]. In addition, FKM is a polar rubber and its presence always enhances the dielectric constant values of a blend containing non-polar rubber. The presence of distinct phase separation and impurities in the interfacial region [55, 56] of the blend causes higher dielectric loss than that of the blend with compatibilizer. These observations support the idea that phase separation has been minimized in the compatibilized blend since MA-g-EPDM provides interfacial crosslinking between EPDM and FKM. In the EVG series, there is a large interface due to phase separation, which evidently becomes responsible for a higher dielectric loss [55].

The dielectric permittivity and loss values of the 50:50 (w/w) EPDM/FKM blends with and without compatibilizer are given in table 5.4. The dielectric permittivity and loss values have only slight variation with frequency. Dielectric permittivity and loss of blends may be attributed to the higher polarity of the FKM matrix and EG incorporation.

Table 5.4 The dielectric permittivity and dielectric loss of the 50:50 (w/w) EPDM/FKM blends with and without compatibilizer

Sample Name	Dielectric permittivity			Dielectric loss		
	2.440 GHz	2.685 GHz	2.972 GHz	2.440 GHz	2.685 GHz	2.972 GHz
EVG0	4.2751	4.2795	4.2802	0.2439	0.2454	0.2462
EVG0*	4.3971	4.4079	4.4147	0.2076	0.2108	0.2168

5.3.9.3 Variation of heating and absorption coefficient

Figs. 5.21 and 5.22 show the variation of the heating coefficient of the EVG and EVG* series with loading. The variation of the absorption coefficient with loading in the case of the EVG and EVG* series are given as insets in Figs. 5.21 and 5.22 respectively. It is observed that the heating coefficient decreases with increase in EG loading. The heat developed is proportional to both frequency and the product of 'ε' and 'tan δ'. The higher the 'J' value, the poorer will be the polymer for dielectric heating purpose. The heat generated in the material comes from the tangent loss, but the loss may not come entirely from the relaxation loss. Rather, conductivity of the material may also contribute to 'tan δ' [57].
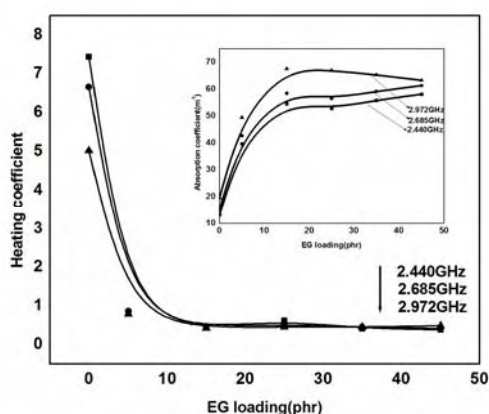

Fig. 5.21 Variation of heating coefficient with EG loading for EVG series. The inset shows the absorption coefficient of the composites
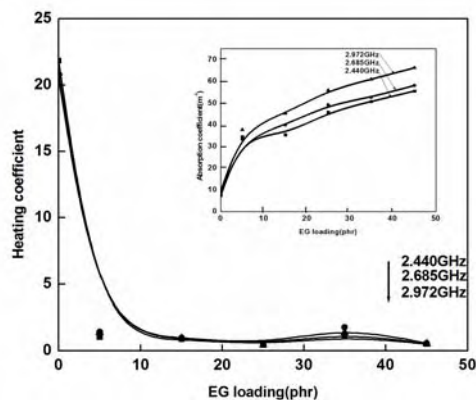
Fig. 5.22 Variation of heating coefficient with EG loading for EVG* series. The inset shows the absorption coefficient of the composites

As the absorption coefficient is derived from the complex permittivity and is a measure of propagation and absorption of electromagnetic waves when it passes through the medium, the dielectric materials can be classified in terms of this parameter indicating transparency of waves passing through it [58]. The microwave conductivity and absorption coefficient are direct functions of dielectric loss. It is clear that the absorption coefficient increases with increase in EG loading and it reaches a maximum at 45 phr EG loading at frequency 2.972 GHz as in the case of dielectric loss.

5.3.10 Limiting oxygen index

Limiting Oxygen Index (LOI) is the minimum concentration of oxygen, determined in a flowing mixture of oxygen and nitrogen that will just support flaming combustion of the material. Generally, different flame retardants exhibit different mechanisms of flame resistance. The results of oxygen index (ASTM D 2863) for the EG filled composites are presented in table 5.1.

EG is a kind of intumescent flame retardant that can effectively improve the flame resistance of EPDM/FKM blends. EG has a flake-like

graphite structure, i.e., stacked layers of hexagonal sp^2 hybridized carbon structures, which is treated with sulfuric, nitric or acetic acids which are intercalated into the graphite crystal structure (Fig. 5.23).
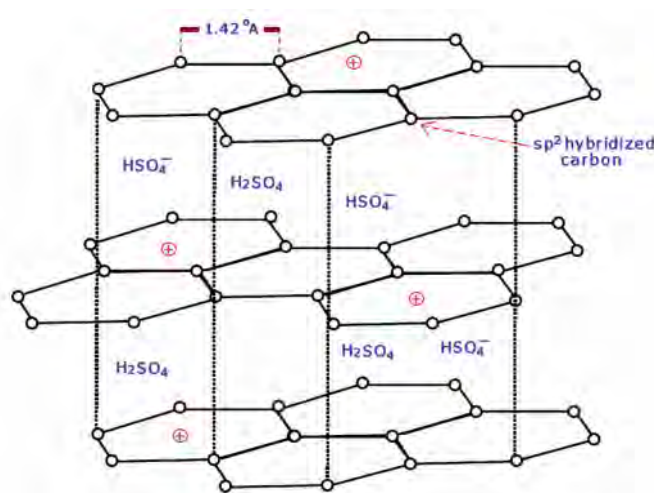
Fig. 5.23 Structure of expandable graphite intercalated by H$_2$SO$_4$

The EG structure consists of layers of hexagonal C-structures within which a chemical compound (H$_2$SO$_4$) can be intercalated. The chemical reaction of formation of EG is expressed as follows [59].

$$24n\ C + m\ H_2SO_4 + \tfrac{1}{2}\ O_2 \rightarrow C_{24n}(HSO_4^-)\ (m\text{-}1) \times (H_2SO_4) + \tfrac{1}{2}\ H_2O + [O] \text{ -- } (5.7)$$
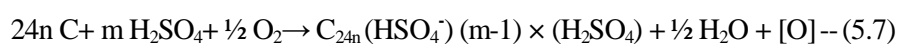
EG expands due to a redox process between H$_2$SO$_4$ and the graphite that forms the blowing gases on the reaction [60]

$$C + 2\ H_2SO_4 = CO_2 + 2\ H_2O + 2SO_2 \text{ --------------------------------------- } (5.8)$$
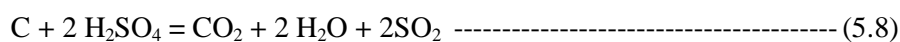
The blowing effect increases the volume of the materials by a factor of about 300 times when they are heated above 200^{0}C. The gases escape through the edges of the graphite particles, causing irreversible expansion.

When expandable graphite is exposed to heat, it expands to more than 100 times its original volume and covers the entire burning surface by a "worm" like structure. Expanded graphite acts as a char former and also as an insulating agent due to the formation of small air gaps between the graphite layers. The "worm" like structure formed by the graphite on expansion suffocates the flame and the compact char layer formed limits the transfer of heat and mass from the polymer to the heat source, preventing the decomposition of the material [61]. The LOI value of EG filled blends in both series increases with increasing amount of EG; in particular, the LOI value of an EVG5* composite containing 45phr EG is 31, which is much higher compared to unfilled EVG0*, suggesting that the EG is a very efficient flame retardant in EPDM/FKM blends. EG can prevent combustible gases from feeding the flame, and separates oxygen from the burning material more efficiently. In all EG filled composites, the burning rate is higher than that of unfilled blend due to the formation of intumescent char on the polymer surface. The volume of the resulting carbonaceous char increases, being in direct correlation with the percentage of EG added. The amount of char residue formed on the thermal degradation of a polymer is a measure of its flame resistance [62]. EG is halogen-free and works mainly in the condensed phase thereby strongly reducing the smoke density. In addition, the expanded carbon layer works as an insulating layer to reduce the heat transfer.

5.3.11 Scanning electron microscopy

The morphology of the blend vulcanizates arising from polar and non-polar rubber is greatly influenced by the compatibilizing agent, which is capable of modifying the rubber matrix through the formation of

interface crosslinking. The tensile fractured surfaces of EVG0 and EVG0* are presented in Fig. 5.24. In the case of uncompatibilized blends, a large number of holes are clearly observed, indicating poor interfacial adhesion between EPDM and FKM. Moreover, the fracture surface is found to be smooth resulting from a brittle matrix fracture. In the 50/50 blend containing MA-g-EPDM (EVG0*), the fracture surface is rough and fractures in ductile mode. In compatibilized blends, the SEM photographs shows, more homogeneous and compact surface. The SEM photographs of the tensile fractured surfaces of 25 phr EG loaded compatibilized (EVG3*) and uncompatibilized (EVG3) blends are given in Fig. 5.24. It can be observed that the incorporation of compatibilizer has led to more uniform dispersion of graphite flakes in the matrix.
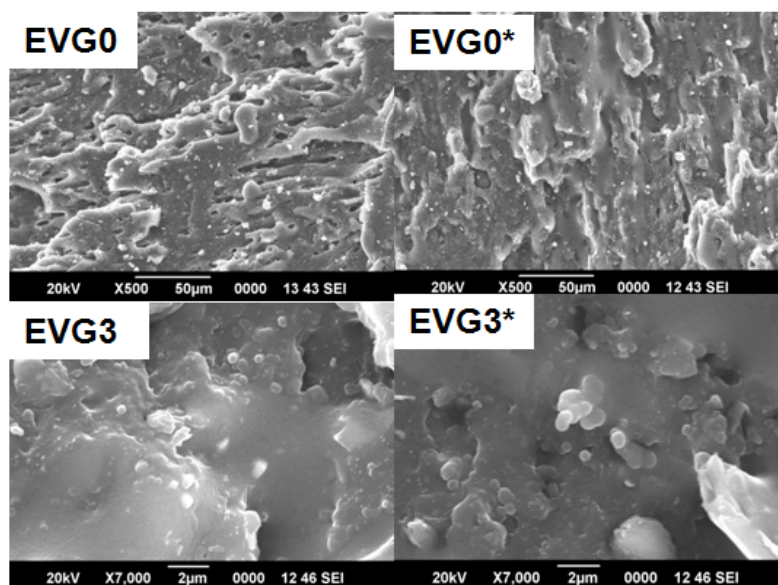
Fig. 5.24 Scanning electron photographs of EVG0, EVG0*, EVG3 and EVG3* blends

5.4   Conclusions

The cure time at higher loading decreases due to the increased thermal transition of a matrix in presence of EG. First-order kinetics is observed for the cure reactions as indicated by the cure kinetics. The tensile properties of all the composites, especially those with a compatibilizer, increases with aging. The addition of EG considerably improves flame retardant properties of EPDM/FKM blends. Expanded graphite is very effective in enhancing the AC and DC conductivity of blends due to the formation of enhanced conductive networks by EG platelets. The dielectric permittivity and loss of the composites increase with increase in frequency and with EG loading.

References

[1]   Celzard A, Mareche JF, Furdin G, Puricelli S. J Phys D: Appl Phys 2000, 33, 3094–3101.

[2]   Zheng W, Wong SC, Sue HJ, Polymer 2002, 73, 6767–6773.

[3]   Saunders DS, Galea SC, Deirmendjian GK, Composite 1993, 24, 309–321.

[4]   Ezquerra YA, Kulescza M, Alta-Calleja FJ, Synth Met 1991, 41–43, 915–920.

[5]   Pinto G, Jimenez-Martin A. Polym Compos 2001, 22, 65–70.

[6]   De Rosa IM, Dinescu A, Sarasini F, Sarto MS, Tamburrano A. Compos Sci Technol 2010, 70, 102-109.

[7]   Park KY, Lee SE, Kim CG, Han JH. Compos Sci Technol 2006, 66, 576-584.

[8]   Jonson RN, van Haaster P, US patent 7, 338, 547 B2: 2008.

[9]   Sengupta DL, Liepa VV. New York: Wiley, 2006.

[10]   Sirqueira AS, Soares BG, Macromol Mater Eng 2007, 292, 62–69.

[11]   Weili Wu, Chen Dajun. Polym Compos 2006, 27, 621–626.

[12]   Deniz V, Karaagac B, Ceyhan N, J Appl Polym Sci 2007, 103, 557–563.

[13]   Mitra S, Ghanbari-Siahkali A, Kingshott P, Hvilsted S, Almdal K, Mater Chem Phys 2006, 98, 248–255.

[14]   Kader MA, Bhowmick AK, J Appl Polym Sci 2003, 89, 1442–1452.

[15] Boutevin B, Caporiccio G, Pietrasanta FG, Ratsimihety A. J Fluorine Chem 2003, 124, 131–138.

[16] Maiti M, Bhowmick A. J Polym Sci Part B Polym Phys 2006, 44, 162–176.

[17] Maiti M, Bhowmick AK. Polym Eng Sci 2007, 47, 1777–1787.

[18] Wang P, Schneider NS, Sung NH, J Appl Polym Sci 1999, 71, 1525–1535.

[19] Mitra S, Ghanbari-Siahkalia A, Kingshott P, Hvilsted S, Almdal K, J Polym Sci Part A Polym Chem 2004, 42, 6216–6229.

[20] De Angelis MG, Sarti GC, Sanguineti A, Maccone P, J Polym Sci Part B Polym Phys 2004, 42, 1987–2006.

[21] Valsecchi R, Vigano M, Levi M, Turri S, J Appl Polym Sci 2006, 102, 4484–4487.

[22] Ghosh A, De SK, Rubber Chem Technol 2004, 77, 856–872.

[23] Mitra S, Ghanbari-Siahkalia A, Kingshotta P, Almdal K, Rehmeier HK, Christensen AG, Polym Degrad Stab 2004, 83, 195–206.

[24] Ameduri B, Boutevin B, Kostov G, Prog Polym Sci 2001, 26, 105–187.

[25] Santra RN, Mukundo PG, Chaki TK, Nando GB, Thermochim Acta 1993, 219, 283-292.

[26] Newman S. Paul DR, Newman S, editors. New York: Academic press, 1978.

[27] Kenji I, Masakij T and Bunji Y, Jpn patent 09 208 731, 1997.

[28] Kazuyoshi I, Masakij T and Kenji I, Jpn patent 08 295 753, 1996.

[29] Bell RWH, UK patent application, 2 168 706, 1986.

[30]   Wagner M, Reinforcing silicas and silicates, Rubber Chem Technol 1976, 49, 703–774.

[31]   Mathew G, Nah C, Rhee JM, Singh RP. J Elastomers Plast 2006, 38, 43–63.

[32]   Mathew G, Singh RP, Nair NR, Thomas S. J Mater Sci 2003, 38, 2469–2481.

[33]   Lee BL. Rubber Chem Technol 1979, 52, 1019-1029.

[34]   Costa HM, Visconte LLY, Nunes RCR, Furtado CRG, Int J Polym Mat 2004, 53, 475-479.

[35]   Wolf S. Rubber Chem Technol 1996, 69, 325-346.

[36]   Kraus G. Rubber Chem Technol 1978, 51, 297-321.

[37]   Sobhy MS, EI-Nashar DE, Maziad NA, Egypt J Sol 2003, 26, 241-257.

[38]   West linning H, Wolf S, Kautsch Gummi Kustst 1966, 19, 470.

[39]   Wolf S, Meng-Jio Wang, Rubber Chem Technol 1992, 65, 329-342.

[40]   Holly WH, Mihal FF, Starer I, Rubber Age, 1965, 565.

[41]   Jia W, Tchoudakov R, Narkis M, Siegmann A, Polym Compos 2005, 26, 526.

[42]   Chen GH, Wu DJ, Weng WG, Yan WL, J Appl Polym Sci 2001, 82, 2506-2513.

[43]   Chen GH, Wu DJ, Weng WG, He B, Yan WL, Polym Int 2001, 50, 980-985.

[44]   Pan YX, Yu ZZ, Ou YC, Hu GH, J Polym Sci Part B Polym Phys 2000, 38, 1626-1633.

[45] Drzal LT, Fukushima H, Polym Prep 2001, 42, 42.

[46] Yasmin A, Daniel IM. Polymer 2004, 45, 8211-8219.

[47] Yasmin A, Luo JJ, Daniel IM, Compos Sci Technol 2006, 66, 1182–9.

[48] Liu DW, Du XS, Meng YZ. Polym Polym Compos 2005, 13, 815.

[49] Chen G, Wu C, Weng W, Wu D, Yan W, Polymer 2003, 44, 1781.

[50] Zheng W, Wong SC, Composites Sci. Technol. 2003, 63, 225.

[51] Nair AB, Kurian P, Joseph R. Materials and Design 2012, 36, 767–778.

[52] Stephen CW, Frederic HL, United States Book cratters 1985, Chelsea.

[53] Twombly B, Shepard DD, Instrum. Sci. Technol. 1994, 22, 259.

[54] George S, Varghese KT, Thomas S, J. Appl. Polym. Sci. 1999, 73, 255.

[55] Zaikin AY, Nigmatullin VA, Kautsch. Gummi. Kunsts. 1994, 47, 709.

[56] Sircar AK. Rubber Chem. Technol. 1981, 54, 820.

[57] Ku CC, Liepins R. Hansen Publishers 1987, Munich, 92.

[58] Bradford LS, Carpentier MH. Chapman and Hall 1993, London.

[59] Delobel R, Le Bras M, Ouassou N, Alistiqsa F, J Fire Sci 1990, 8, 85.

[60] Camino G, Duquesne S, Delobel R, Eling B, Lindsay C, Roels T, Nelson GL, Eds., Washington DC, ACS Pub 2001, 90-109.

[61] Modesti M, Lorenzetti A, Simioni F, Camino G, Polym Degra Stab 2002, 77, 195-202.

[62] Turi EA. Academic press, Orlando, FL, 1981, 800-803.

…..ഇൽ…..

Chapter 6

EFFECT OF ALUMINIUM HYDROXIDE: IN EPDM AND IN FLUOROCARBON RUBBER[*]

> ## Contents
>
> 6.1 Introduction
> 6.2 Experimental details
> 6.3 Results and Discussion
> 6.4 Conclusions

Ethylene-propylene-diene terpolymer/aluminium hydroxide (EPDM/ATH) and fluorocarbon rubber (FKM/ATH) composites were prepared by two-roll mill mixing. ATH nano particles were incorporated at different loadings (phr), to study the effect of filler loading on the cure characteristics, mechanical properties, dynamic mechanical properties and thermal stability. The viscoelastic properties such as storage modulus, loss modulus, damping behavior and glass transition temperature of the composites were investigated by dynamic mechanical analyzer (DMA). The thermal stability of the composites was studied using thermogravimetric analysis (TGA). The dispersion of the ATH nanoparticles was studied using scanning electron microscopy (SEM). The mechanical properties of FKM/ATH composites were better than medium thermal (MT) black filled vulcanizates. The effect of ATH in combination with high abrasion furnace (HAF) black was studied in oil extended EPDM rubber. ATH was found to behave as reinforcing filler in EPDM. Upon the addition of filler, the storage modulus (E') of the composites was found to increase due to the enhancement in stiffness of the material. An investigation of the viscoelastic properties revealed that there is a strong interaction between the polymer and the filler. The incorporation of ATH improved the thermal stability of EPDM while a reduction occurred for FKM rubber. Microwave characteristics of the composites were also studied.

6.1 Introduction

Polymer composites have an important role in electrical engineering in recent years. The application of polymeric materials in this field however requires special precautions because they can catch fire easily. In comparison to traditional inorganic materials such as glass, ceramics and mica, they offer considerable advantages including excellent insulation properties, low electric losses, ease of fabrication and processing. To be useful in electrical applications, the polymeric material should have good electric insulation characteristics, in addition to flame resistance [1]. The studies on flame-retarding polymeric materials have become indispensable since these materials are widely used. There are four factors affecting the process of combustion, which are oxygen, heat, flammable materials and thermal degradation [2].

Brominated flame retardants, which stop the thermal degradation of composites by reacting with polymers, are the most effective flame retardants in the market that are adopted for most engineering plastics [3]. However, halogenated flame retardants release toxic gases when they are subjected to high temperatures. With the proposal of the concept of environmental friendly flame retardants, some brominated flame retardants are replaced by halogen free flame retardants, particularly metallic hydroxide such as magnesium hydroxide [4], aluminium trihydrate [5] etc.

In these metallic hydroxide flame retardants, aluminium trihydrate (ATH) is one of the most popular, safe, halogen free and smoke suppressants flame retardant. Other benefits include low material cost, elimination of heavy metal promoters (e.g. antimony oxide), and absence of toxic fume generation [6].

The main reason for the predominant use of carbon black in elastomers is the reinforcement that it imparts to the vulcanized rubber [7]. The effect of reinforcing carbon black on network structure, technical properties, failure mode and dielectric properties of natural rubber have been reported [8]. The dielectric properties of some synthetic rubbers, mixed with different types of carbon black in increasing quantities, over a wide range of frequencies were investigated and numbers of relaxation mechanisms were deduced [9].

Over the past fifty years, fluoroelastomers (FKM) have benefited the world in several ways. Fluoroelastomer products are a family of specialty materials appreciated for their elastic behavior under comparatively harsh conditions [10]. These elastomers are largely used in seals and other fabricated components to afford barriers against a broad range of fluids under severe conditions. Majority of the fluoroelastomers products are utilized in automotive applications, mainly in fuel and high pressure sealing application. Amounts of fluoroelastomers consumed per vehicle are small compared to natural and synthetic rubber within the tires of a vehicle, but the fluoroelastomer parts are extreme crucial for safety reason, reliable operation and environmental protection. Other application areas of fluoroelastomers include aerospace appliances, fluid power, chemical industry, oil field, semiconductors and high pressure seals for plasma coating [11]. It is a common tradition to incorporate some filler into the rubber matrix in order to obtain the ultimate properties out of it and fluoroelastomers are also not an exception. To improve their performance, various fillers have been examined, including carbon black [12], and recently nanofillers like layered silicates [13, 14], carbon nanotube [15], polyhedral oligomeric silsesquioxane (POSS) [16], etc.

EPDM terpolymers are versatile materials since their physical properties strongly depend on their composition, the copolymer microstructure and the nature of the diene. Dienes are used to introduce crosslinking sites in EPDM rubber. EPDM can be incorporated in different formulations for improving properties like resistances to ozone, heat, moisture, low temperature flexibility etc. Because of their excellent electrical insulating properties, EPDM is well-suited for wire insulation and sheathing of cables used in nuclear power plants or in low to intermediate voltage applications. In such cases, a flame-retardant compound is usually incorporated to enhance the rather low ignition resistance of the polymer matrix. In recent years, halogen-free flame retardants have been more and more widespread in cable industry, mainly for environmental reasons. Materials such as ATH are good alternative for halogen compounds since they do not give rise to toxic or corrosive substances when burning. One of the drawbacks when using metal hydroxides as flame retardants is the need for high dosage compared to other fillers (60 wt % typically), to achieve the required efficiency of flame retardancy. Due to their saturated backbone, EPDM elastomers are rather resistant to degradation by heat, in comparison to other conventional rubbers such as polybutadiene or polyisoprene, for instance [17-19].

In this study, ATH filled nanocomposites based on EPDM and FKM, were prepared. The effect of ATH loading on the cure, mechanical, dynamic mechanical, thermal properties and flammability of the nanocomposites was evaluated. The dielectric properties at microwave frequencies of the prepared composites were measured in the S-band (2-4 GHz) frequency using the cavity perturbation technique. The properties

like dielectric permittivity, dielectric loss, conductivity, dielectric heating coefficient and absorption coefficient were evaluated. SEM studies were carried out to visualize the dispersion of ATH particles in the elastomer matrix.

6.2 Materials and methods

6.2.1 Materials

The detailed description of the materials used is given in section 2.1. The FKM/ATH composites are designated (Table 6.3) as 'V_X', where X represents the ATH loadings varying from 0 to 50 phr. Vhalf (Table 6.4) stands for FKM/ATH composites containing 20 phr ATH and half the amount of acid-acceptors and Vno stands for the same mix without acid-acceptors [$Ca(OH)_2$ and MgO].

6.2.2 Experimental details

The experimental methods used are given in section 2.6.

6.3 Results and Discussion

6.3.1 Characterization of ATH

6.3.1.1 Fourier transform infrared spectroscopy
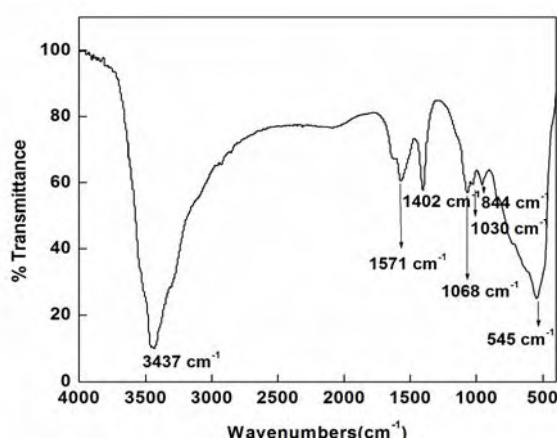
Fig. 6. 1 FTIR spectrum of ATH nanoparticles

FTIR spectrum of ATH is given in Fig.6.1. A peak is obtained in the range, 4000-2500 cm^{-1} (with the max. of 3437 cm^{-1}) due to hydroxide stretching vibration. Band at 1030 cm^{-1} and shoulder at 1068 cm^{-1} is due to symmetric and asymmetric Al-O-H bending. Shoulder at 844 cm^{-1} and a band at 545 cm^{-1} is due to the vibration mode of Al-O.

6.3.1.2 X-ray diffraction
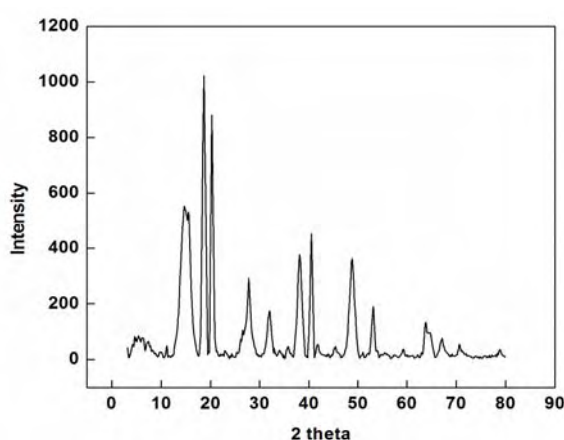
Fig. 6.2 X-ray diffractogram of ATH nanoparticle

The XRD pattern for the ATH particle is shown in Fig. 6.2. It shows sharp peaks indicating high crystallinity of the material. From Debye-Scherrer formula, d= 0.9λ/β cosΘ [Where 'λ' is the wavelength of X ray 1.5418 A^0 and 'β' is full width at half maximum of diffraction peak (FWHM) and 'Θ' is the angle corresponding to the peak], average size of crystallites (d) is found to be 13.70 nm.

6.3.1.3 Thermogravimetric analysis
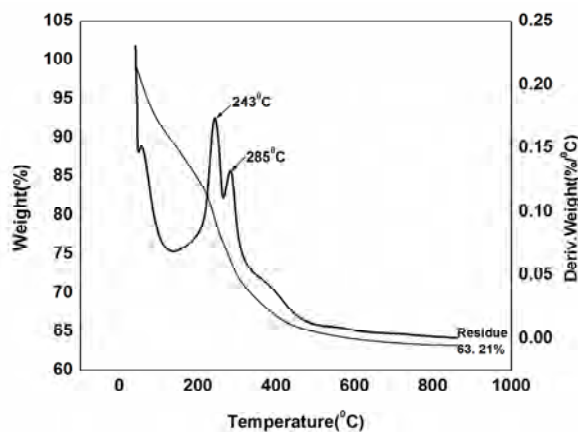
Fig. 6. 3 Thermal degradation of ATH particles

Fig. 6.3 shows the degradation behavior of ATH particle. The experimental weight loss of ATH filler (35 wt %) is in agreement with stoichiometric calculation (release of three water molecules), and confirms observations from the literature [20]. ATH looses weight from 190^0C to 800 ^{0}C according to a three-step degradation scheme: the first step proceeds very slowly from 190 ^{0}C to 220 ^{0}C (hardly visible on TG curve), the second step (strong) from 220 ^{0}C to 380 ^{0}C, and the third step from 380 ^{0}C to 800 ^{0}C (very slow). And the residue obtained is 60 %.

6.3.1.4 Scanning electron microscopy
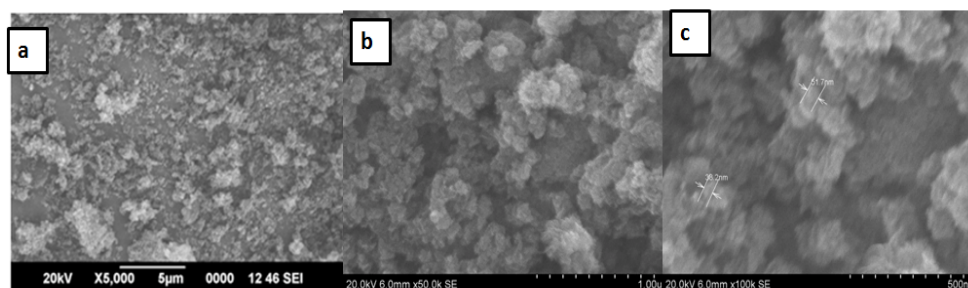
Fig. 6.4   SEM images of ATH nanoparticles at three different magnifications [(a) 5,000 (b) 50, 000 and (c) 1, 00000]

The morphology of ATH (Fig. 6.4) shows homogeneous plate-like structure with large surface area. Some bigger particles are found due to agglomeration.

6.3.2 Cure characteristics of EPDM/ATH composites

The cure curve and cure parameters of ATH filled EPDM composites are discussed in section 4.3.1.
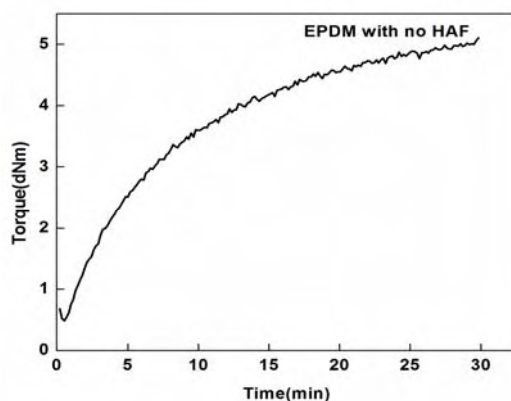
Fig. 6.5 Cure curve of 25 phr ATH loaded EPDM

The cure curve of 25 phr ATH loaded EPDM without HAF black is shown in Fig. 6.5. And the important curing parameters are given in table 6.1. Compared to EPDM filled with mixed ATH/HAF formulations (section 4.3.1), there is no significant variation in cure characteristics, except that the optimum cure time (T_{90}) is less for the present case.

Table 6.1 Cure parameters of 25 phr ATH loaded EPDM

Min. torque (D_{min}).	Max. torque (D_{max}).	Scorch time (T_{10})	Cure time (T_{90})
0.483	5.10	1.27	20.44

6.3.3 Cure characteristics of FKM/ATH composites

Table 6.2 Formulations used for the preparation of FKM/ATH composites (series 1)

Ingredients	V2	V+20phr MT black	V+ 20phr ATH and 20phr MT black
FKM	100	100	100
ATH	20	-	20
MT black	-	20	20
Ca(OH)$_2$ -6.0, MgO- 4.0			

Table 6.3 Formulations used in the preparation of FKM/ATH composites (series 2)

Ingredients	V0	V1	V2	V3	V4	V5
FKM	100	100	100	100	100	100
ATH	-	10	20	30	40	50

Ca(OH)$_2$ -6.0, MgO- 4.0

Table 6.4 Formulations used in the preparation of FKM/ATH composites (series 3)

Ingredients	FKM	Ca(OH)$_2$	MgO	ATH
V half	100	3	2	20
V no	100	-	-	20

The crosslinking of fluoroelastomers is usually carried out at moderately elevated temperature. The fluoroelastomer composites used in this study have a two-stage curing process including a initial curing stage for optimum cure time at 150 ^{0}C and a post curing stage for 6 h at 160 ^{0}C. Fig. 6.6 describes the improvement of torque against time at 150 ^{0}C of the FKM composites in the presence of ATH and curing parameters are tabulated in Table 6.5. It is found that the highest torque value is obtained for 20 phr MT black filled systems. This may be due to the higher particle size of MT black compared to ATH. Generally large particle sized MT black is used for FKM formulations because

of its large inter chain distance. It is also observed that the T_{90} value of 20 phr ATH filled composites has been decreased to 8.18 min from 26.02 min of the gum compound.

Fig. 6.6 Cure rheographs of FKM composites (series 1)

Table 6.5 Cure characteristics of FKM composites (series 1)

Sample name	Min. torque (D_{min}).	Max. torque (D_{max}).	Scorch time (T_{10})	Cure time (T_{90})
V0	0.44	5.76	13.1	26.02
V+20phr ATH	0.73	4.54	1.18	8.18
V+ 20phr MT	0.48	8.7	7.0	19.63
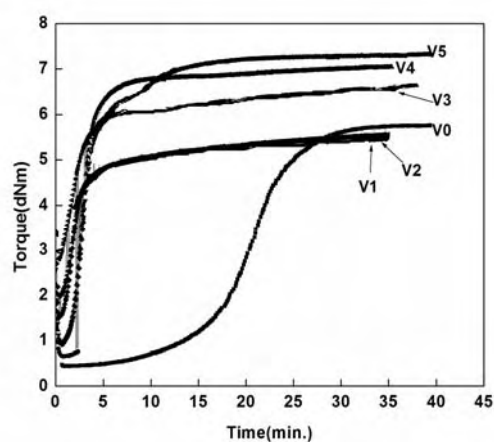
Fig. 6.7 Cure rheographs of FKM composites (series 2)

Fig. 6.7 shows that at higher loadings, D_{max} value increases with increase in ATH loading, due to the viscosity increase of the elastomer by the addition of nanofiller. It is also interesting to note that in the present study a rather small amount of ATH (10 and 20 phr) reduced the T_{90} value abruptly (table 6.6). But increased addition of filler increased T_{90} value.

Table 6.6 Cure characteristics of FKM at varying ATH loading (series 2)

Sample name	Min. torque (D_{min}).	Max. torque (D_{max}).	Scorch time (T_{10})	Cure time (T_{90})
V0	0.44	5.76	13.1	26.02
V1	0.66	7.33	4.28	9.85
V2	0.73	4.54	1.18	8.18
V3	1.52	5.47	1.10	10.8
V4	1.98	5.56	1.10	14.05
V5	2.80	6.65	0.86	16.51

From table 6.6, it is clear that the scorch time (T_{10}) decreases tremendously with the addition of ATH. This may be due to the participation of ATH filler in the curing cycle of FKM. This makes it possible to reduce the concentration of acid-acceptors considerably in the composite formulation. (table 6.4) The time-torque curves and the curing parameters of the FKM based composites are given in Fig. 6.8 and table 6.7 respectively.
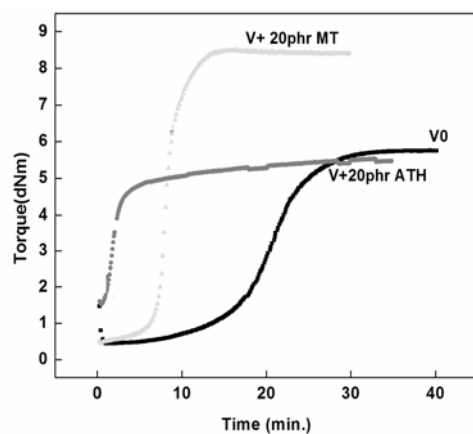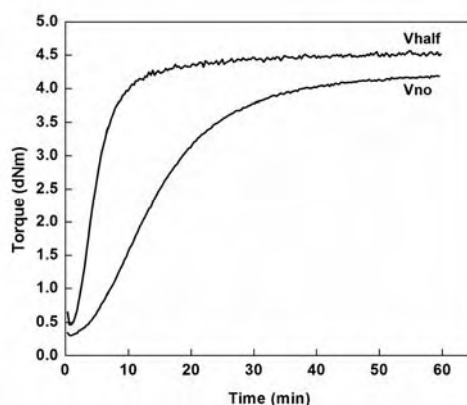

Fig. 6.8 Cure rheographs of FKM composites (series 3)

Table 6.7 Cure characteristics of FKM composites (series 3)

Sample name	Min. torque (D_{min}).	Max. torque (D_{max}).	Scorch time (T_{10})	Cure time (T_{90})
V half	0.45	4.59	2.3	12.3
V no	0.30	4.20	5.7	30.5

Table 6.7 shows that there is not much variation in minimum and maximum torque. Optimum cure time is highest (30.5 min) for formulation containing no acid-acceptors. But in the case of half acid-acceptor formulation (V half), the value is 12.3. From this it is clear that, ATH has some effect on the curing behavior of FKM.

6.3.4 Stress-strain properties of ATH filled EPDM rubber

The stress-strain properties of the unaged EPDM based composites are shown in Fig. 6.9.
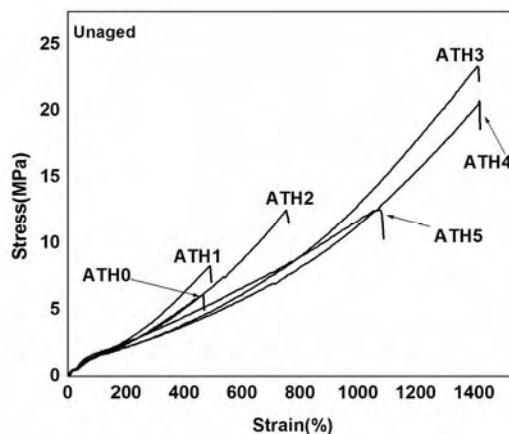
Fig.6.9 Stress-strain properties of EPDM/ATH unaged samples

The tensile properties (table 6.8) improve tremendously, even at 5 wt % addition of ATH to EPDM. In all the composites, the EB values are higher for unfilled EPDM. The 300 % modulus values are lower for

unfilled system when compared to ATH loaded systems. The platelet like filler particles also has some influence on tensile properties of composites. The elongation at break is the most affected property, when the small sized aluminium hydroxide fillers are used. The highest EB value is obtained for 25 phr ATH loaded EPDM (ATH4), which may be due to the plasticization effect of ATH particles. Higher loadings do not produce an increment in EB and TS. The reinforcement imparted by ATH brings about a segmental immobilization of polymer chains at higher loadings.

Table 6.8 Tensile properties of unaged EPDM/ATH composites

Name	Max. stress (MPa)	Max. strain (EB, %)	Modulus at 300%
ATH0	6	430	1.6
ATH1	8	487	4.0
ATH2	12	752	3.6
ATH3	23	1413	2.9
ATH4	20	1427	2.9
ATH5	12	1076	3.5

Hot air aging normally reduces the tensile properties. The rubber samples under investigation, which do not contain any antioxidant, were subjected to thermal aging at 70 and 150 ^{0}C for 22 h. The effects of thermal aging on the tensile strength, the elongation at break and modulus at 300 % elongation of the samples were studied.
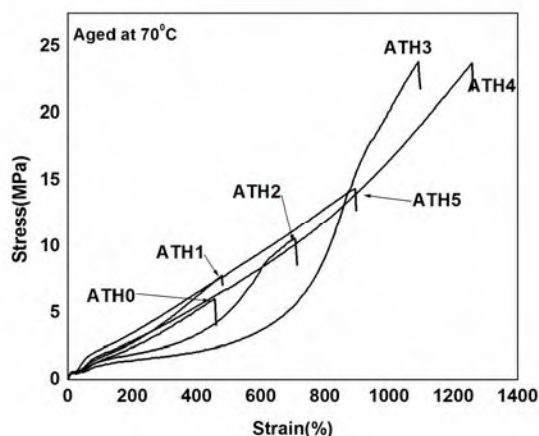
Fig. 6.10 Stress-strain properties of samples aged at 70 ^{0}C for 22 h

The stress-strain properties of EPDM/ATH composites aged at 70 ^{0}C are given in Fig.6.10. From this it clear that the tensile properties (given in table 6.9) are not reduced even after 22 h aging at 70 ^{0}C. Variation with loading is similar to that of unaged samples. The maximum tensile strength is obtained at 25 phr ATH loaded EPDM. But at higher loading of ATH was not able to produce an enhancement in tensile properties. It is also clear that the addition of ATH do not affect the aging resistance of EPDM.

Table 6.9 Tensile properties of EPDM/ATH composites aged at 70 ^{0}C for 22 h

Name	Max. stress (MPa)	Max. strain (%)	Modulus at 300%
ATH0	6	423	2.0
ATH1	8	478	4.31
ATH2	11	707	4.43
ATH3	24	1091	4.74
ATH4	23	1222	4.09
ATH5	14	894	4.96
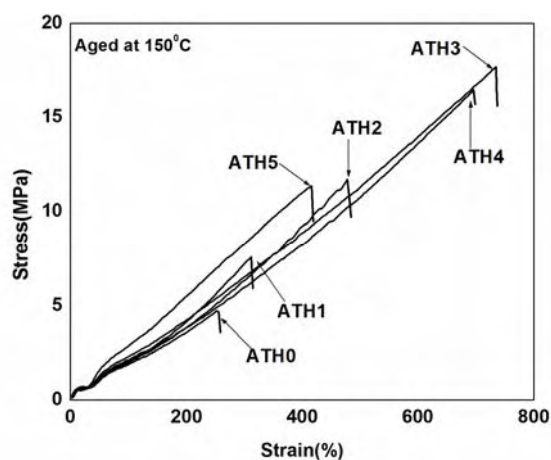
Fig. 6.11 Stress-strain properties of EPDM/ATH composites aged at 150 ^{0}C for 22 h

The stress-strain properties of EPDM/ATH composites aged at 150 ^{0}C are given in Fig.6.11. There is a decline in properties at 150 ^{0}C. But the trend is almost same as that of unaged composites.

Table 6.10 Tensile properties of EPDM/ATH composites aged at 150 ^{0}C for 22 h

Name	Max. stress (MPa)	Max. strain (%)	Modulus at 300%
ATH0	5	216	5.80
ATH1	7	312	6.23
ATH2	10	478	6.00
ATH3	16	695	6.58
ATH4	15	675	6.74
ATH5	11	416	8.27

Table 6.10 shows that after aging at 150 ^{0}C, the tensile strength of ATH3 is decreased from 23 to 16 MPa and elongation at break is decreased from 1413 to 695 %. Higher loadings of ATH produce no substantial increase in EB and TS. Compared to unaged samples, modulus at 300 % shows an increase. Increased loading also increases the modulus values.

Increase in modulus on aging and with loading is due to the increased stiffness of the polymer chain, resulting from decrease in the inter-aggregate distances with rising filler content forming a filler network. Here the filler–polymer interaction is mainly of physical nature (physisorption).
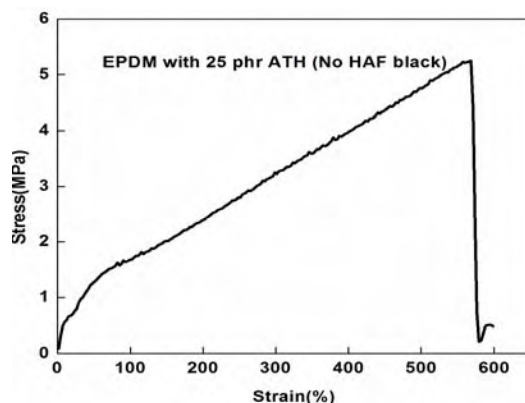
Fig. 6.12. Stress-strain curve of EPDM with 25 phr ATH and no HAF black

To confirm the synergistic effect of ATH and carbon black in EPDM rubber, the tensile properties of EPDM having 25 phr ATH and no HAF were evaluated. Fig. 6.12 depicts the stress-strain curve. By comparing table 6.11 with 6.8 it is evident that ATH, in the absence of HAF black does not reinforce EPDM. This is supported by other evidences [21-23] in the literature showing the synergistic effect of carbon black along with other fillers.

Table 6.11 Tensile properties of EPDM with 25 phr ATH and no HAF black

Max. stress (MPa)	Max. strain (%)	Modulus at 300%
5.3	573	1.2

6.3.5 Stress-strain properties of ATH filled FKM rubber

It should be remembered here that unlike other rubbers, post curing (at 160 ^{0}C for 6 h) of the FKM compounds is a very essential step to get desirable performance in the ultimate vulcanizate. The FKM compounds

after post curing show better stress–strain properties. However, the change in molecular rearrangement during the post curing is still unknown. Efficient scavenging of hydrofluoric acid (HF) by MgO and $Ca(OH)_2$ during post curing might be the reason for the formation of a stable crosslinked FKM matrix.
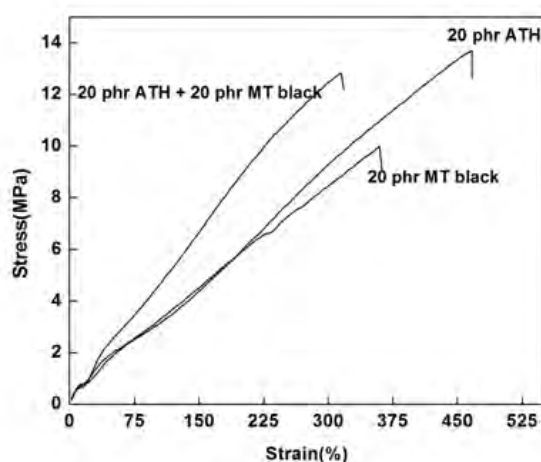
Fig. 6.13 Stress-strain curves of FKM/ATH composites (series 1)

Table 6.12. Tensile properties of FKM/ATH composites (series 1)

Properties	V+ 20 phr ATH	V+ 20 phr MT black	V+ 20 phr ATH and 20 phr MT black
Max. stress (MPa)	14	9	10
Max. strain (%)	435	358	294
Modulus at 100%	3	3	4

The stress-strain curves and the tensile properties are given in Fig. 6.13 and in table 6.12 respectively. It is understood that 20 phr ATH loaded FKM exhibits maximum tensile strength (14 MPa) and EB (435 %) when compared to MT black and ATH/MT (20/20 phr) black combinations. There is not much variation in modulus values.
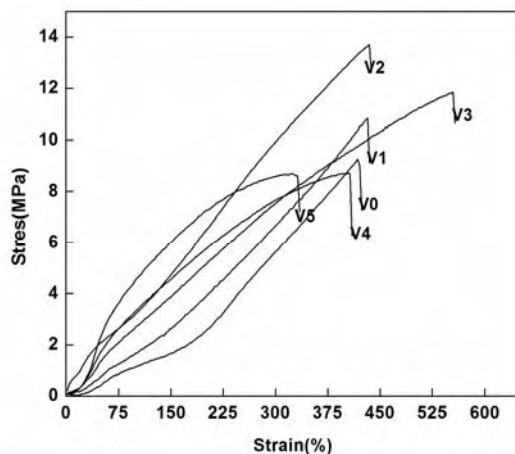
Fig. 6.14 Stress-strain behavior of FKM at varying ATH loading (series 2)

Representative stress–strain curves for the pure FKM and FKM at varying ATH loading are given in Fig. 6.14 and the tensile properties obtained from these curves are given in table 6.13. The ultimate tensile properties reflect the reinforcing effect owing to the presence of ATH in FKM matrix. It can be seen from table 6.13 that with the inclusion of only 10 phr ATH, the tensile strength and EB are increased to considerable extent compared to gum FKM. It is found that tensile strength increases from 9 MPa to 14 MPa (20 phr ATH loading) while the maximum EB (554 %) is obtained at 30 phr loading of the ATH filler. Therefore, a noteworthy enhancement in the magnitude of modulus at 100% elongation for the nanocomposites is observed as compared to unfilled compound. The improvement in tensile strength indicates homogeneous dispersion of the nanofillers and strong interfacial bonding (polar-polar interaction) between the fillers and the polymer matrix. Higher ATH loadings do not enhance the stress–strain properties due to the agglomeration of the filler particles.

Table 6.13 Tensile properties of FKM at varying ATH loading (series 2)

Name	Max. stress (MPa)	Max. strain (%)	Modulus at 100%
V0	9	418	1.15
V1	11	432	1.68
V2	14	435	2.00
V3	12	554	2.60
V4	8	404	3.3
V5	7	323	4.2
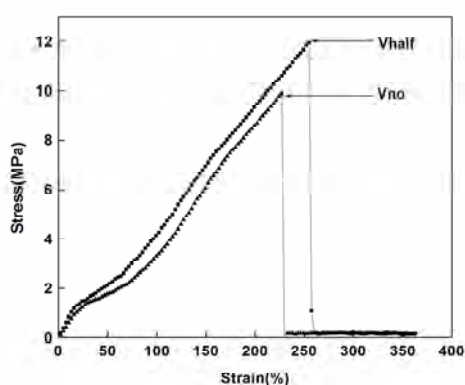
Fig. 6.15 Stress-strain behavior of FKM composites (series 3)

Fig. 6.15 and table 6.14, show that 100 % modulus is the same for half acid-acceptors case and no acid-acceptor case. Variation in tensile strength and EB are better for formulation containing half acid-acceptors (V half).

Table 6.14 Tensile properties of FKM composites (series 3)

Name	Max. stress (MPa)	Max. strain (%)	Modulus at 100%
V half	12	735	2
V no	10	722	2

6.3.6 Thermogravimetric analysis EPDM/ATH composites

The thermogravimetric analysis of ATH filled EPDM composites are discussed in section 4.3.8.1.

6.3.7 Thermogravimetric analysis FKM/ATH composites
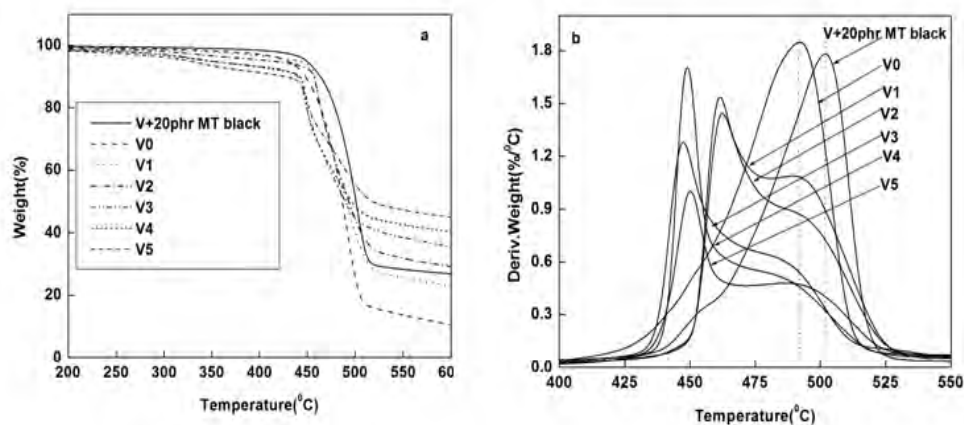
Fig. 6.16 (a) Thermogram and (b) derivative thermogram of ATH filled FKM composites

The thermogram and derivative thermogram of ATH filled FKM composites is given in Fig. 6.16 (a) and (b) respectively. Thermal characteristics are given in table 6.15. The dependence of degradation of the composites on ATH loading is better visualized in the DTG (Fig. 6.16 b). The addition of ATH caused a remarkable decrease in the thermal stability of the elastomer, as is evident from TGA thermograms.

Table 6.15 Thermal characteristics of ATH filled FKM composites

Sample name	Onset of degradation (T_0, ^{0}C)	Max. degradation(T_{max}, ^{0}C)		Residue (%)
		T_{max}^1	T_{max}^2	
V+20phr MT	424	-	502	24
V0	426	-	498	15
V1	423	456	485	19
V2	422	455	486	22
V3	420	447	484	23
V4	418	445	481	32
V5	416	439	475	36

From table 6.15, gum FKM rubber vulcanizates exhibit maximum degradation (T_{max}) at 498 ^{0}C. And 20 phr MT black loaded FKM exhibit T_{max} at 502 ^{0}C. All other ATH filled systems exhibits two T_{max} (T_{max}^1 and T_{max}^2). The initial degradation is mainly due to the filler particles and the second degradation due to rubber. The maximum degradation temperature decreases and residue increases with increase in ATH loading. This may be due to the filler particle, which decomposed at elevated temperature and the decomposition products may catalyze the thermal decomposition of the elastomer.

6.3.8 Dynamic mechanical analysis of ATH filled EPDM

The dynamic mechanical response of the composites is measured to examine the degree of filler-matrix interaction. The storage modulus (E') vs temperature curves of ATH filled EPDM is shown in Fig. 6.17. It is found that the storage modulus of the filled EPDM is higher than that of unfilled system due to the interaction of polymer chain with filler. The mechanical performance of polymer composites is highly dependent on the interfacial morphology, such as the filler shape, size, size distribution, adequacy of dispersion, and degree of adhesion between the filler and polymeric matrix. However, at higher loading the storage modulus decreases owing to the aggregation of filler.
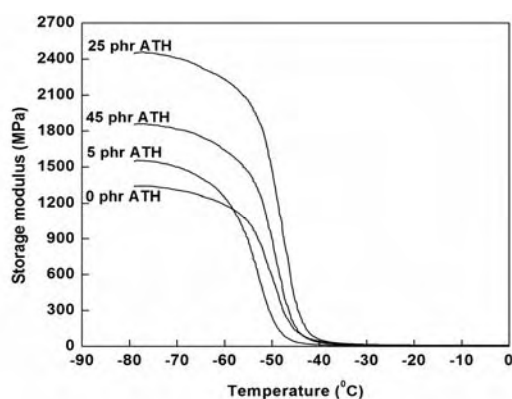
Fig. 6.17 Storage modulus vs temperature curves of ATH filled EPDM

Fig. 6.18 show the loss modulus (E") vs temperature curves of ATH filled EPDM. The E" is related to the energy loss due to viscous dissipation and is the viscous modulus of the polymeric material. The increase in E" upon the addition of filler can be explained in terms of the friction between the filler particles and the matrix molecules when the filler particles are uniformly dispersed in the rubber matrix. At higher concentration of filler, (45 phr) a decrease in E" can be observed which is due to the aggregation of filler and decrease in frictional contribution.
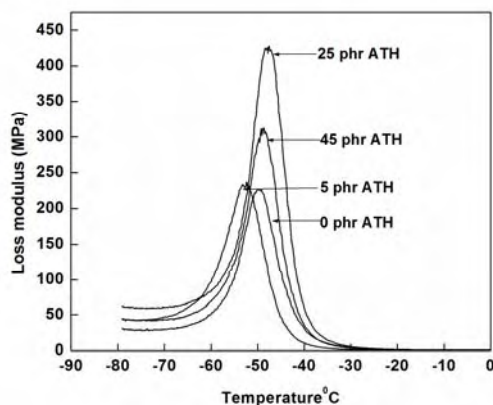
Fig. 6.18 Loss modulus vs temperature curves of ATH filled EPDM

The damping behavior of nanocomposites is displayed in Fig. 6.19. It can be seen that the nano filler reinforcement causes dramatic decrease in tan δ values; increase in concentration of ATH results in a consistent increase in the storage modulus. This can be interpreted in terms of restricted mobility of polymer chains due to their confinement in the ATH particles. The decrease in tan δ suggests a strong adhesion between rubber and the ATH filler.
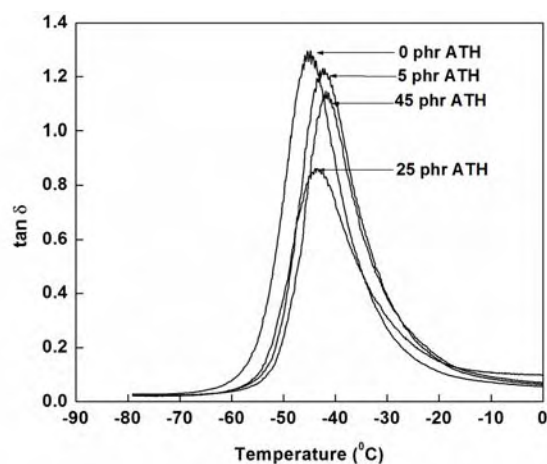
Fig. 6.19 Tan δ vs temperature curves of ATH filled EPDM

Table 6.16 displays the change in tan δ_{max} values of ATH filled EPDM as a function of concentration of filler. It is observed that the damping decreases with increase in filler content. It can be explained in terms of the restricted segmental mobility of EPDM chains due to the strong interaction between filler and the matrix.

Table 6.16 Tan δ_{max} of EPDM nanocomposites with filler loading

ATH loading (phr)	tan δ_{max}
0	1.29
5	1.23
25	0.86
45	1.15

The glass transition temperature (T_g) obtained from tan δ and E" peak are given in table 6.17. The ATH filled EPDM system shows no change in Tg (measured from tan δ and E" curves) with increase in concentration of filler.

Table 6.17 Glass transition temperature (T_g) from tan δ and $E^{"}$

ATH loading (phr)	T_g from tan δ (^{0}C)	T_g from $E^{"}$ (^{0}C)
0	-44.80	-50.13
5	-43.64	-52.33
25	-44.55	-49.76
45	-44.24	-49.72

6.3.9 Dynamic mechanical analysis of ATH filled FKM

DMA measurements are often used to evaluate polymer stiffness under dynamic mode. The glass transition temperature, T_g represents the temperature at which physical properties change drastically when the material transit from a hard glassy state to a rubbery state. Large segments of polymer chains start cooperative movement when the polymer reaches its glass transition temperature.
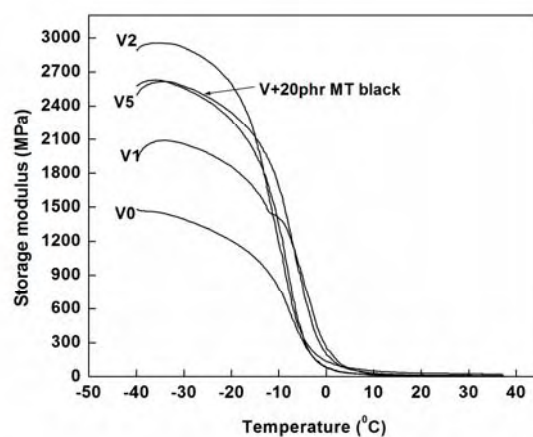
Fig 6.20 Storage modulus vs temperature curves of FKM composites

Dynamic mechanical properties were measured to examine the extent of filler–matrix interaction of the FKM/ATH nanocomposites. Fig 6.20 shows the effect of ATH on storage modulus of the FKM nanocomposites

as a function of temperature. From Fig. 6.20, it is clear that the storage modulus (E') of the FKM/ATH composite with 20 phr ATH loading was greater than the E' of both pure FKM and FKM/ATH composites containing different amounts of ATH.
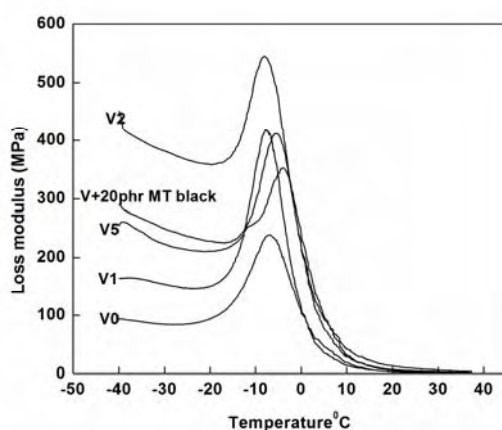
Fig. 6.21 Loss modulus vs temperature curves of FKM composites

Fig. 6.21 show the loss modulus (E") vs temperature curves of ATH filled FKM. 20 phr ATH loaded FKM shows higher loss modulus value when compared to MT black filler formulations. Gum vulcanizate shows lower E" compared to filled FKM vulcanizates. The Tan δ vs temperature curves of FKM/ATH composites is given in Fig. 6.22. Addition of the ATH results in a reduction of the maximum value tan δ up to 20 phr loading. This observation can be correlated to the strong interfacial interaction between the rubber matrix and the filler surface, which are normally noticeable in rubber nanocomposites. By the addition of organo-modified layered silicate in polychloroprene rubber, carboxylated nitrile rubber [24], acrylonitrile butadiene rubber [25] the tan δ_{max} was found to be decreased

to a considerable extent and this finding can be related to the strong interfacial interaction between the rubber matrix and the layered silicate.
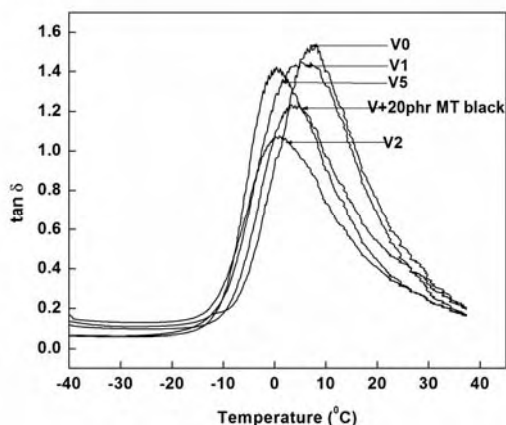
Fig. 6.22 Tan δ vs temperature curves of FKM composites

Usually, due to the strong interfacial interactions between the rubber matrix and filler surface, the glass transition temperature (T_g) is shifted to higher temperature. But it can be seen from table 6.18 that T_g of the FKM/ATH nanocomposites is shifted to lower temperature (from +4 ^{0}C for gum to -0.6 ^{0}C for 20 phr ATH loading). Analogous observation has been recently reported by Pasbakhsh et al. [26] in EPDM–HNT nanocomposites. There are numerous other references stating identical observations [27, 28]. Approximately 12 ^{0}C dwindle of T_g in case of silica-filled epoxy nanocomposites compared to unfilled gum compound was reported by Preghenella et al. [29]. Koerner et al. have also shown a decrease of T_g with increased amount clay mineral dispersion in the case of clay–epoxy nanocomposites [30] which has been attributed to two competitive effects such as rigid phase reinforcement, and destruction and plasticization of the network structure.

Table 6.18 Tan δ_{max} and glass transition temperature (T_g) from tan δ of FKM nanocomposites

Sample name	tan δ_{max}	T_g from tan δ (^{0}C)
V0	1.53	4.3
V1	1.44	4.2
V2	1.07	-0.6
V5	1.42	-1.7
V+ 20 phr MT	1.23	0.9

6.3.10 Dielectric properties of EPDM/ATH composites

The microwave characteristics of the composites were studied using cavity perturbation technique. The detailed description of the theory of microwave characterization and the experimental method used are given in section 2.6.19.

Fig. 6.23 shows the variation of the dielectric loss factor of the composites with varying amounts of ATH with frequency.
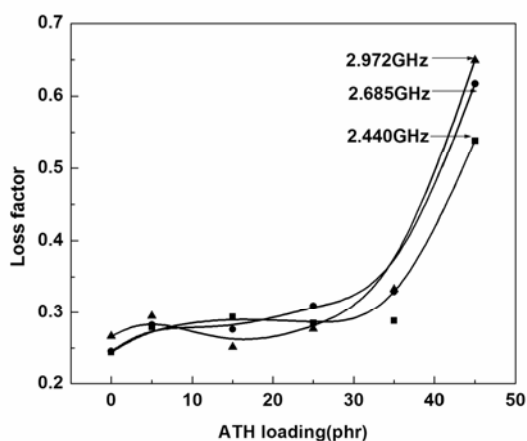
Fig. 6.23 Variation of dielectric loss with ATH loading of EPDM composites

The dielectric loss is found to increase with increase in frequency and the highest value of dielectric constant is obtained at 45 phr ATH loading. This

is because ATH fillers will yield a percolation threshold at higher loadings due to more interparticle contacts. As the frequency is increased, the inertia of the molecule and binding forces become dominant and it is the basis for dielectric loss at higher frequencies. The microwave conductivity is a direct function of dielectric loss. Variation of the conductivity (S/m) of composites with different proportions of ATH at different frequencies has the same nature as that of the dielectric loss factor as is shown in Fig. 6.24.
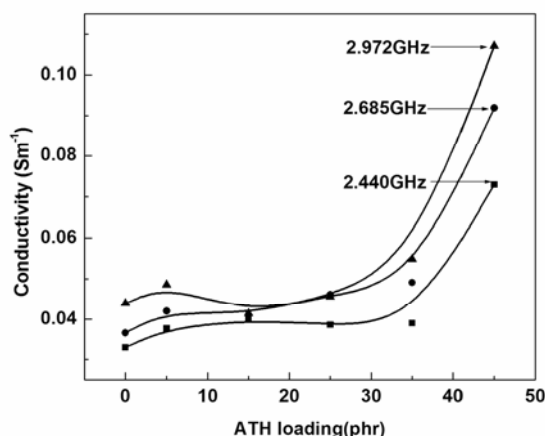
Fig. 6.24 Variation of conductivity with ATH loading of EPDM composites

At lower loading, ATH particles are randomly distributed within the matrix. But at higher loading, the filler-filler contact forming a conductive pathway within the matrix. Several studies have shown that the addition of fillers like carbon black, graphite powder etc. can increase the conductivity of the polymers [31].

The relative dielectric constant and loss factor are used to characterize molecular relaxations. The relative dielectric constant is a measure of the energy stored in a sample during a cyclic dielectric relaxation, while dielectric loss is a measure of the energy lost [32].
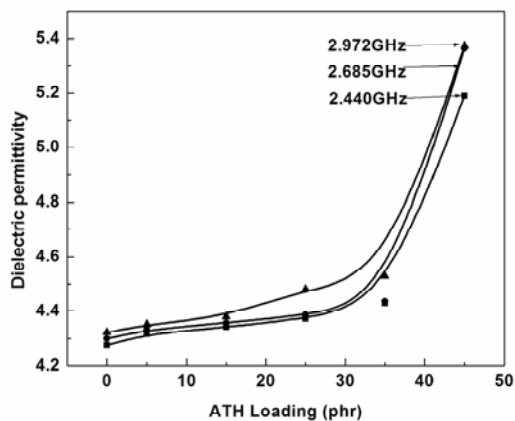
Fig. 6.25 Variation of dielectric permittivity with ATH loading of EPDM composites

Fig. 6.25 shows that the dielectric constant increases with frequency and the percolation threshold is obtained at higher loading (45 phr). This can be explained by the fact that the addition of filler increases the dipole polarity of the composite in the interfacial region, because fillers generally possess higher polarity than polymer. Therefore the increase of filler loading would make dipole polarity to increase and boost the dielectric constant and loss [33]. The prepared composites showed good conductivity and dielectric loss, which indicated that the compound dissipated current as heat energy. Therefore the developed EPDM based composites can be used in various applications, including antistatic coatings, antistatic chapels, and anticorrosion applications. In future plan, we shall include the application aspects of the composites.
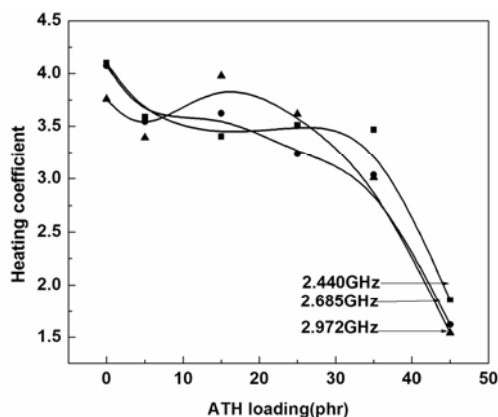
Fig. 6.26 Variation of heating coefficient with ATH loading of EPDM composites

Fig. 6.26 shows the variation of the dielectric heating coefficient (J) with frequency. It is observed that the heating coefficient decreases with frequency and also ATH loading. The heat developed is proportional to both, frequency and the product of ε and tan δ. The higher the 'J' value, the poorer will be the polymer for dielectric heating purpose. The heat generated in the material comes from the tangent loss, but the loss may not come entirely from the relaxation loss. Rather, conductivity of the material may also contribute to tan δ [34].

As the absorption coefficient is derived from the complex permittivity and is a measure of propagation and absorption of electromagnetic waves when they passes through the medium, the dielectric materials can be classified in terms of this parameter indicating transparency of waves passing through it [35]. The microwave conductivity and absorption coefficient are direct functions of dielectric loss. It is clear that the absorption coefficient increases with increase in frequency (Fig. 6.27) and also with ATH at higher concentration, and it reaches a maximum at 45 phr ATH at a frequency of 2.972 GHz as in the case of dielectric loss.
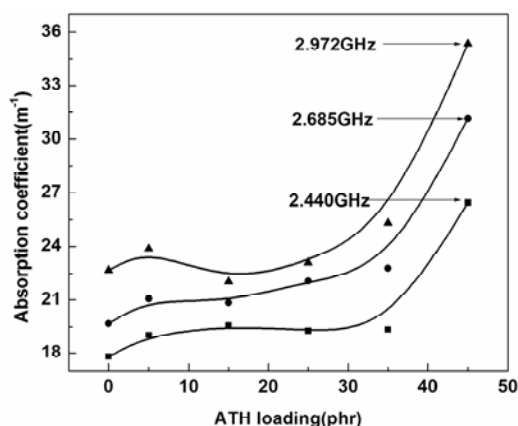
Fig. 6.27 Variation of absorption coefficient with ATH loading of EPDM composites

The skin depth, also called the penetration depth, is basically the effective distance of penetration of an electromagnetic wave into the material [36]. It can be applied to a conductor carrying high frequency signals. The self-inductance of the conductor effectively limits the conduction of the signal to its outer shell and the shell's thickness is the skin depth which decreases with increase in frequency and is shown in Fig. 6.28.
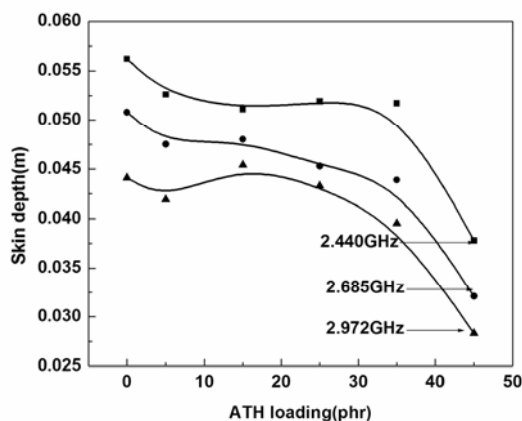
Fig. 6.28 Variation of skin depth with ATH loading of EPDM composites

When the material has good conductivity, it effectively reduces the depth of penetration of the signal. The highest value of conductivity and of

the absorption coefficient and the lowest value of skin depth were found for the 45 phr ATH loaded EPDM recorded at 2.972 GHz.

6.3.11 Dielectric properties of the FKM/ATH composites

The dependence of the imaginary part of the complex dielectric permittivity (dielectric losses) on the amount of the ATH filler and the frequency is shown in Fig. 6.29.
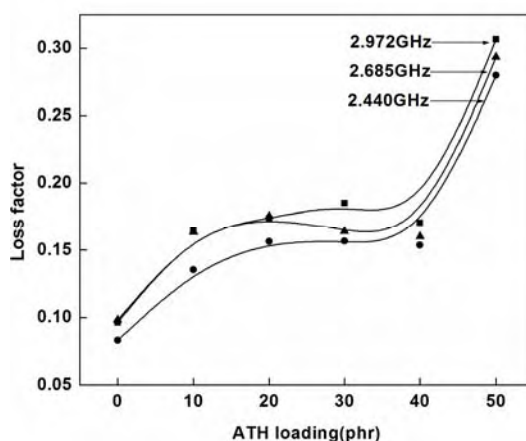
Fig. 6.29 Variation of dielectric loss with ATH loading of FKM composites

As seen from Fig. 6.29 the values of dielectric loss increase with the increasing content of ATH filler in fluorocarbon rubber. The increase is the lowest for the least filled sample while the highest increase is observed for the sample filled with 50 phr of ATH. The samples could be divided into three groups: in the first group is the non filled sample with the lowest dielectric constant value; to the second group belong the composites comprising 10, 20, 30 and 40 phr of ATH having very close dielectric loss values; the composite filled with 50 phr of ATH is in the third group which dielectric loss value is the highest. Obviously, filling FKM rubber with a significant amount of ATH (e.g., 50 phr) could be used to obtain FKM rubber

composites possessing considerable dielectric loss values. The grouping of the composites (observed in the case of the dielectric permittivity as well) might be related to reaching and passing the percolation threshold, and to the formation of conductive paths. The statement is based on the comparison dependences of the relative dielectric permittivity on filler content and the mechanism of dielectric loss occurrence [37] related mostly to the nature of dielectric polarization.

With the increase of ATH loading, there is no significant variation in the dielectric losses, but at 45 phr ATH loading there is an increase in the loss factor. The dielectric loss of a composite is affected by extrinsic factors such as porosity, microstructure, moisture content, and interface between the polymer and the filler. A dense composite with low moisture content is needed for obtaining a low loss composite. With increase in filler volume fractions the space charge getting accumulated in the interfacial area increases, leading to an increase in dielectric loss. However, this interfacial effect is effective only at low frequencies [38].
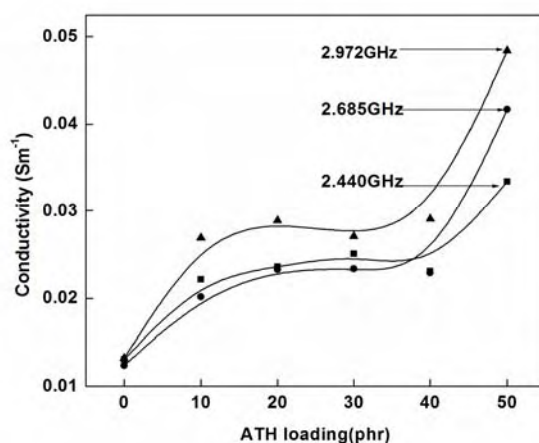
Fig. 6.30 Variation of conductivity with ATH loading of FKM composites

The microwave conductivity is a direct function of dielectric loss and hence the Fig. 6.30, showing the variation of the AC conductivity (S/m) of composites. Conductivity of the matrix at lowest loading of filler is affected by three parameters viz. the intrinsic conductivity of the filler, the shape of the filler and also the surface tension of the matrix and filler [39]. Maximum conductivity 0.05 S/m is obtained for higher ATH loading at 2.972 GHz.
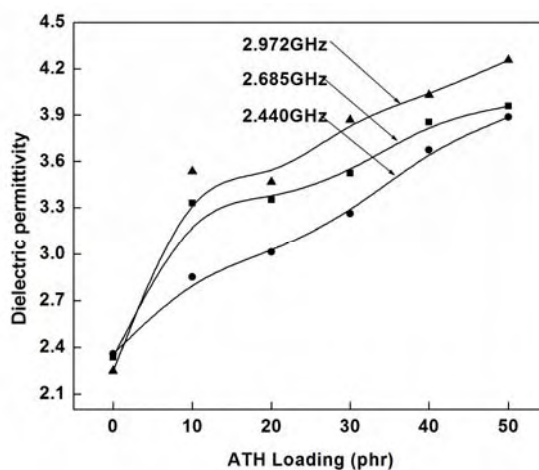
Fig. 6.31 Variation of dielectric permittivity with ATH loading of FKM composites

The dielectric relaxation and polarization processes in these copolymers are still not clearly understood. The addition of inorganic materials, the chain polar segment motion in copolymer system occurs at a relatively low frequency range. The influence of the frequency and amount of the second filler is significantly pronounced in this frequency range. The polarization mechanism operating in the giga hertz (GHz) frequency is purely electronic or orientational with relaxation times smaller than the time period of the applied signals. Interfacial polarization, which is the basic reason for the dispersion in dielectric permittivity at radio frequency region, has no role to play in microwave frequencies as it does not produce

dispersion in dielectric permittivity because of its much smaller relaxation time. But dielectric permittivity is found to increase with the increase of phr of ATH nano platelets in the composite as it is evident from Fig. 6.31. This phenomenon of increase in dielectric permittivity with the increase in filler concentration can be attributed to the enhancement of electrical conductivity of the composites. Fig. 6.31 shows the change in dielectric constant of FKM rubber measured at 2.440, 2.685 and 2.972 GHz, with various ATH loading. It can be seen that the dielectric constant increases with increasing ATH loading and also with frequency. In a copolymer system, the CF_2 dipoles are combined together by strong covalent bonds, and so, the orientation changes in the dipole moments require cooperative motion of the neighboring CF_2 groups through the large-scale trans-gauche conformation change [40].

The tendencies of the changes in dielectric constant with filler content (Fig.6.31) are analogous to those observed in the case of dielectric loss. The dielectric permittivity of the composites is also affected by a number of factors such as the porosity, size and shape of the filler particles, interface between the components and the effective dipole moment of the composites [41]. At lower loadings, since the filler is a minor dispersed phase, the major contribution to the dielectric response comes from the continuous rubber matrix. As the filler loading increases the filler particles form continuous networks and the dipole–dipole interaction increases. Consequently there will be a rise in dielectric permittivity of the composite [42].
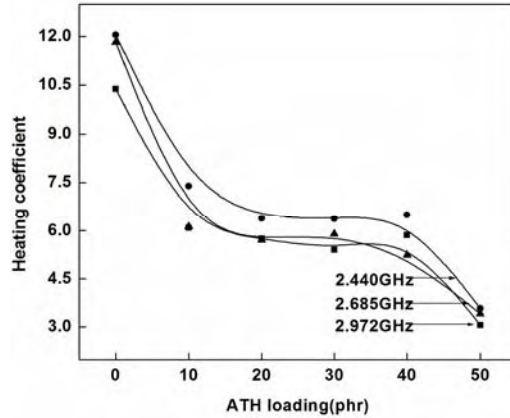
Fig. 6.32 Variation of heating coefficient with ATH loading of FKM composites

Fig. 6.32 shows the variation of dielectric heating coefficient (J) with frequency and with loading. It is observed that the heating coefficient decreases with frequency and also with filler loading. In the present study 'J' value is found to be the lowest for 50 phr ATH loaded FKM at 2.972 GHz frequency. At 2.972 GHz the heating coefficient of gum vulcanizate is 10 while at 50 phr loading it is as low as 3.
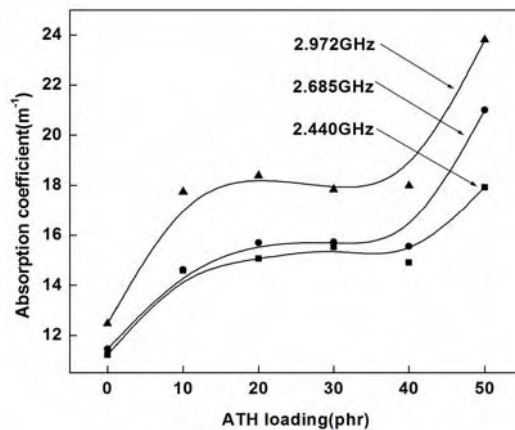
Fig. 6.33 Variation of absorption coefficient with ATH loading of FKM composites

The variation of absorption coefficient with ATH filler loading is same as that for AC conductivity in Fig. 6.33. It is clear that the absorption coefficient

increases with increase in filler loading and maximum absorption coefficient value is obtained for 50 phr ATH loaded FKM rubber at 2.972 GHz.
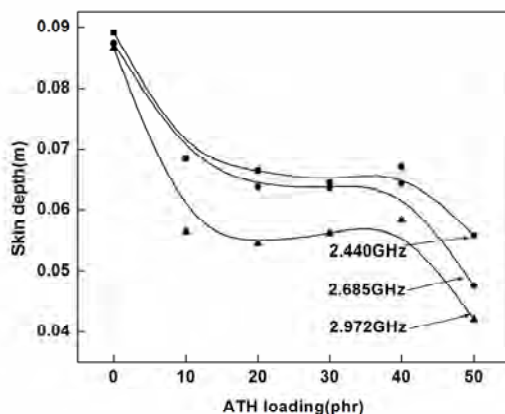
Fig. 6.34 Variation of skin depth with ATH loading of FKM composites

From Fig. 6.34 it is clear that the lowest value of skin depth is for the rubber containing 50 phr ATH loading at 2.972 GHz frequency.

6.3.12 Scanning electron microscopic studies of EPDM/ATH composites

The morphology studies of the ATH filled EPDM composites are discussed in section 4.3.12.

6.3.13 Scanning electron microscopic studies of FKM/ATH composites
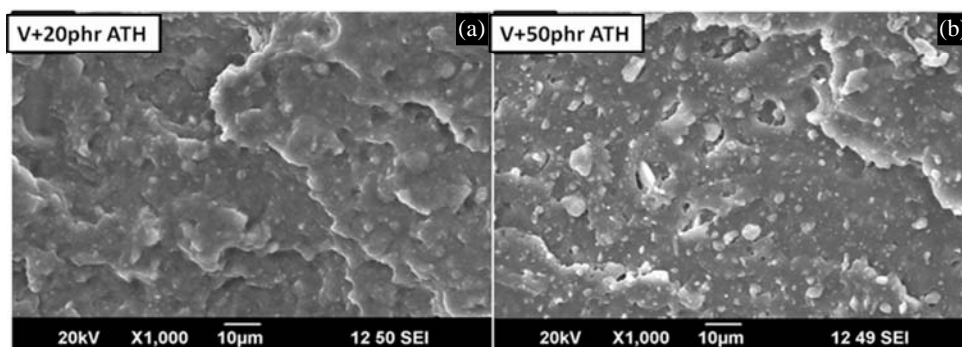
Fig. 6.35 SEM photographs of tensile fractured surfaces of (a) 20 phr ATH and (b) 50 phr ATH filled FKM composites

Generally, the dispersion state of the nanofillers in a polymer matrix is one of the decisive factors in determining the ultimate properties of nanocomposites. Uniform and homogeneous dispersion of filler especially in nanoscales leads to high mechanical properties of the resulting composites. On the contrary, the aggregated fillers in the polymer matrix act as the stress–concentration points, leading to deterioration of mechanical properties. Fig. 35 shows the state and degree of dispersion of the ATH particles into the FKM matrix. It can be seen from the SEM micrographs (Fig. 6.35 a) that ATH particles are well dispersed in the FKM matrix for the sample containing 20 phr ATH loading. As the concentration of ATH is increases the dispersion of the filler becomes hindered. Large particles are embedded in the FKM matrixes which act as stress concentration points. It can also be observed from Fig. 6.35 (b) that ATH particles are forming a local filler–filler network in the rubber matrix and due to the existence of such clusters, the 'Payne effect' has been found to be pronounced in these systems. This is in good agreement with the observed mechanical properties.

6.4 Conclusions

The addition of ATH does not affect the cure characteristics of EPDM. Rate of curing increases with increase in concentration of ATH in FKM rubber. Tensile properties increase by the addition of ATH to both EPDM and FKM. The degree of improvement depends on their interactions with the elastomer matrix and their effects on elastomer vulcanization. The thermal degradation stability of EPDM increased with the addition of ATH but decreased in the case of FKM. Storage modulus increased with the addition of ATH and reached a maximum and then decreases in both cases.

The dielectric permittivity and loss of the composites increase with increase in frequency and also with ATH concentration. The microwave conductivity of all the composites is highly dependent upon the frequency and the percolation threshold is observed at high ATH loading. The dielectric heating coefficient is found to be minimum for higher filler loading. The absorption coefficient is high and the skin depth or the penetration depth is low for samples with high ATH loading. Morphology of fracture surfaces shows better state of dispersion of nanoparticles and it is in good agreement with the observed tensile properties.

References

[1]   Younam AF, Polym. Degrad. Stab. 1995, 49, 215.

[2]   Rosa ADL, Recca A, Carter JT, McGrail PT, Polymer 1999, 40, 4093.

[3]   Smith R, Georlette P, Finberg I, Reznick G, Polym. Degrad. Stab. 1996, 54, 167.

[4]   Hippi U, Mattila J, Korhonen M, Seppala J, Polymer 2003, 44, 1193.

[5]   Pinto UA, Visconte LLY, Nunes RCR, Eur. Polym. J. 2001, 37, 1935.

[6]   Zilberman J, Hull TR, Price D, Milnes GJ, Keen F, Fire Mater 2000, 24, 159.

[7]   Sellers JW, Toonder FE, ed. Kraus G, Wiley Interscience 1965, New York.

[8]   Hanna FF, Ghoneim AM, Z. Phys. Chemie. 1970, 245, 236.

[9]   Abdel-El-Nom KN, Hanna FF, Abdel-Messieh SL, Polym. Deg. Stab. 1992, 35, 121.

[10]   Logothetis AL. Prog Polym Sci 1989, 14, 251–96.

[11]   Moore AL. Norwich: William Andrew Publishing, 2006.

[12]   Kojima G, Wachi H, Rubber Chem Technol 1978, 51, 940–7.

[13]   Maiti M, Bhowmick AK, Compos Sci Technol 2008, 68, 1–9.

[14]   Kader MA, Nah C, Polymer 2004, 45, 2237–47.

[15]   Endo M, Noguchi T, Ito M, Takeuchi K, Hayashi T, Kim YA, Adv Funct Mater 2008, 18, 3403–9.

[16]   Seurer B, Coughlin EB, Macromol Chem Phys 2008, 209, 2040–8.

[17]   Cheremisinoff NP, Marcel Dekker, New York, 1989.

[18]   Schowob Y, Caoutchoucs & Plastiques 1994, 72,733.

[19]   Arnold LK, Unwin Ltd 1969, London.

[20]   Hancock M, Rapra Technology Ltd. 1995, United Kingdom.

[21]   Qu L, Huang G, Zhang P, Nie Y, Weng G, Wu J. Polym Int 2010, 59, 1397–402.

[22]   Liu Y, Li L, Wang Q, J Appl Polym Sci 2010, 118, 1111–20.

[23]   Rattanasom N, Saowapark T, Deeprasertkul C, Polym Test 2007, 26, 369–77.

[24]   Das A, Stokelhuber KW, Heinrich G, Macromol Chem Phys 2009, 210, 189–99.

[25]   Das A, Jurk R, Stoekelhuber KW, Heinrich G, Macromol Mater Eng 2008, 293, 479–90.

[26]   Pasbakhsh P, Ismail H, Ahmad Fauzi MN, Bakar AA. Appl Clay Sci 2010, 48, 405–13.

[27]   Liu X, Wu Q, Polymer 2001, 42, 10013–9.

[28]   Shelley JS, Mather PT, DeVries KL, Polymer 2001, 42, 5849–58.

[29]   Preghenella M, Pegoretti A, Migliaresi C, Polymer 2005, 46, 12065–72.

[30]   Koerner H, Misra D, Tan A, Drummy L, Mirau P, Vaia R. Polymer 2006, 47: 3426–35.

[31]   Dervos CT, Mergos JA, Iosifides AA, Mater. Lett. 2005, 59, 2842.

[32]   Twombly B, Shepard DD, Instrum. Sci.Technol.1994, 22, 259.

[33]   George S, Varghese KT, Thomas S, J.Appl.Polym.Sci. 1999, 73, 255.

[34]   Ku CC, Liepins R, Hansen Publishers, 1987.

[35]   Bradford LS, Carpentier MH, Chapman & Hall, 1993.

[36]   Stephen CW, Frederic HL, United States Book crafters: Chelsea, 1985.

[37]   Niedermeier W, "Degussa," Technical Reports TR 832.

[38]   Smaoui H, Mir LEL, Guermazi H, Agnel S, Toureille A, J Alloys Comp 2009, 477, 316.

[39]   Skotheim TA, Vols 1 and 2, Marcel Dekker 1986, New York.

[40]   Tashiro K, Nalwa H, Ed. Marcel Dekker: New York, 1995, Ch. 2, 63.

[41]   Chen YC, Lin HC, Lee YD, J Polym Res 2003, 10, 247.

[42]   Kuo DH, Chang CC, Su TY, Wang WK, Lin BY, Mater Chem Phys 2004, 85, 201.

…..ഇരു…..

EFFECT OF ALUMINIUM HYDROXIDE, CHLORINATED POLYETHYLENE RUBBER, DECABROMOBIPHENYL OXIDE AND ANTIMONY TRIOXIDE ON THERMAL, MECHANICAL AND FLAME RETARDANT PROPERTIES OF EPDM/FKM RUBBER BLENDS

Contents

7.1   Introduction
7.2   Experimental details
7.3   Results and Discussion
7.4   Conclusions

Aluminium hydroxide (ATH), chlorinated polyethylene (CPE) rubber, decabromobiphenyl oxide (DBBO) and antimony trioxide (Sb_2O_3) filled fluoroelastomer (FKM)/ethylene-propylene-diene monomer rubber (EPDM) blends with and without compatibilizer (MA-g-EPDM) were prepared by mill mixing. Blends with compatibilizer showed better physical properties compared to that without compatibilizer. The scanning electron microscopic studies support this. The effect of different loadings of these fillers on cure characteristics, tensile properties, thermal stability and flame retardancy of EPDM/FKM blends in both series were studied. Cure studies showed that the maximum torque increased with increase in the weight percent of filler in both compatibilized and uncompatibilized blends. The filled uncompatibilized polymer blends generally exhibited poor mechanical properties due to incompatibility and phase separation. Maleic anhydride grafted EPDM was used to enhance the properties and to create good adhesion at the polymer/polymer and polymer/filler interfaces. These improvements can mainly be attributed to the compatibilizing effect of MA-g-EPDM, resulting in the more homogeneous phase distribution.

7.1   Introduction

Polymer blends are gaining technological importance due to their modest set of properties, advantages in processing and reduction in cost. By blending two or more elastomers, it is possible to attain properties that are

not available in a single elastomer. Many polymer blends show additive property. That is when a polymer is mixed with another polymer, the resulting blend has a property which is the weighted average of the properties of the individual polymer.

Elastomer blends are of great importance in rubber industry. Almost all important rubber products use polymer blends. In recent years, research and development activities in the field of polymer science and technology have been concentrated more on the modification of existing polymeric materials rather than on synthesizing new polymers [1, 2]. Compounding with blends of two or more elastomers is an effective method for attaining properties better than a single elastomer. A wide range of properties can be achieved by blending, which includes mechanical, electrical and chemical properties along with good processability [3, 4].

There are mainly three reasons to blend or mix rubber. It is to improve the mechanical properties and processability and to reduce the cost of the compound. There are one or more defects in every rubber, and to blend with other rubber is a method to achieve an optimal condition [5, 6]. Rubber blend methods include a latex blend, solution blend, mechanical blend, mechano-chemical blend, and a powder type rubber blend [7, 8]. The mechanical blend is the most widely used method to manufacture rubber blend in industry. Although two high molecular weight materials may not be compatible, a blend of micro homogeneity and useful characteristics can be generated if the viscosity after mixing by the mechanical blend is high enough to prevent phase separation.

Viton is a fluorocarbon rubber (FKM), manufactured and marketed by DuPont. It is made by typical emulsion polymerization and by copolymerization

of tetrafluroroethylene and hexafluoropropylene. Generally, high molecular weight polymer with high fluorine levels is very stable and has a higher C-F synthetic intensity than C-H intensity. It is very expensive, but the rubber is highly durable. It is mainly used in special areas such as military machines, advanced industrial machines, and satellites. DuPont, 3M in the US and DAIKIN in Japan are some representative manufacturers [9, 10].

EPDM is one of the most widely used and the fastest growing synthetic rubbers having both specialty and general purpose applications. The mechanical properties of EPDM are poor and hence fillers are added for reinforcement. EPDM have a fully saturated backbone giving excellent resistance to ozone and oxygen and hence excellent weatherability even without anti-oxidants. EPDM composites are good internal insulating material for solid rocket motors by virtue of various advantageous, such as low density (0.87-0.89 g/cm^3), low ablation rate, high thermal decomposition temperature, high specific heat, low brittle temperature, good aging resistance and good air-tightness, and its tensile strength and elongation are in full accordance with those required for this application [11]. However, EPDM matrix itself does not meet the requirements for the environment of gas flow at high temperature and high speed with high-pressure eroding in a solid rocket motor, and so various fillers have to be added to enhance its properties [12, 13].

Fluorocarbon elastomers are copolymers of various combinations of monomers. Formulations can be chosen to get a desired combination of properties. Fluoro elastomers have been widely used in automotive parts due to their superior thermal and fluid resistance. However, modern automotive operating environments require high performance materials having versatile properties. Therefore blending of EPDM with FKM may

be attractive if satisfactory net work structure develops in each of the phases and at the inter phase.

Thus a blend of EPDM and FKM could provide a new material with several desired properties. However, EPDM being non-polar and FKM being polar the resulting blend may be immiscible. Several factors can influence mechanical properties, such as the particle size and particle size distribution of the dispersed phase, and the degree of adhesion between the two phases. The adequate chemical structure of the compatibilizing agent can reduce the interfacial energy between the phases and finer dispersion can be achieved [14].

Fillers have important roles in modifying the properties of various polymers and lowering the cost of their composites. The effect of fillers on properties of composites depends on their level of loading, shape and particle size, aggregate size, surface characteristics and degree of dispersion. The homogeneous dispersion of nanoparticles in polymer matrix is very difficult because they have a strong tendency to agglomerate [15].

Flame retardation is a technology by which the normal degradation or combustion of polymers is altered by addition of certain chemicals. Some polymers are fire retardant or smoke retardant and their fire performance is acceptable for certain applications. However, for many polymers, it is necessary to improve their fire performance by incorporating commercially available flame retardants. Flame retardants are substances that can be chemically inserted in to the polymer molecule or physically blended in the polymers after polymerization to suppress, reduce, delay or modify the propagation of a flame through polymeric materials. There are several

classes of flame retardants; non-halogenated/halogen-free flame retardants (e.g. expanded graphite, ammonium polyphosphate etc.), halogenated hydrocarbons (e.g. chlorine and bromine containing compounds and reactive flame retardants), inorganic flame retardants (boron compounds, antimony oxides, aluminium hydroxides etc.).

In this part of the work is to study the effect of addition of different fillers at varying compositions into EPDM/FKM blends to improve mechanical and thermal properties. Moreover, an attention has been given to study the effect of these fillers on the flame retardant nature of EPDM/FKM blends.

7.2 Experimental details

7.2.1 Materials

The materials used are given in section 2.1.

7.2.2 Methods

The detailed experimental procedure is given in section 2.6.

7.3 Results and discussions

7.3.1 ATH filled EPDM/FKM rubber blends

7.3.1.1 Cure characteristics

Fig. 7.1 shows the torque-time graphs of ATH filled compatibilized and uncompatibilized EPDM/FKM blends obtained during the cure analysis using Rubber Process Analyzer (RPA). The initial decrease in torque observed can be attributed to the softening of the matrix. Torque then increases due to the formation of crosslinks between the macromolecular chains and then levels off as an indication of completion of curing process.
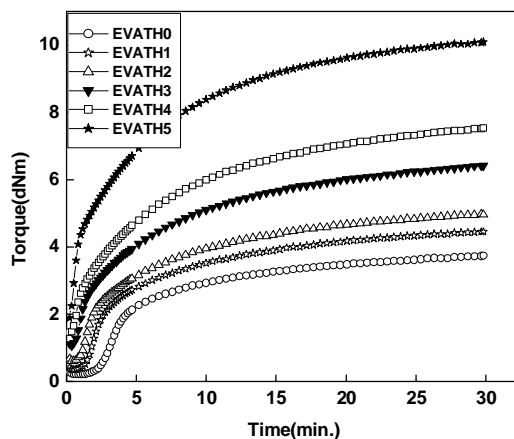
Fig. 7.1 Cure curves of ATH loaded EPDM/FKM blends

It can be seen from Fig. 7.1 and Fig. 7.2 that unfilled EPDM/FKM blends; both compatibilized and uncompatibilized, show a lower torque value compared to filled blend systems. The cure characteristics of unfilled uncompatibilized and compatibilized EPDM/FKM blends are discussed in section 3.3.1. The rheometric torque increases with increase in the weight percentage of filler successively. This indicates that as the amount of filler increases in the blend system, the shear modulus increased.
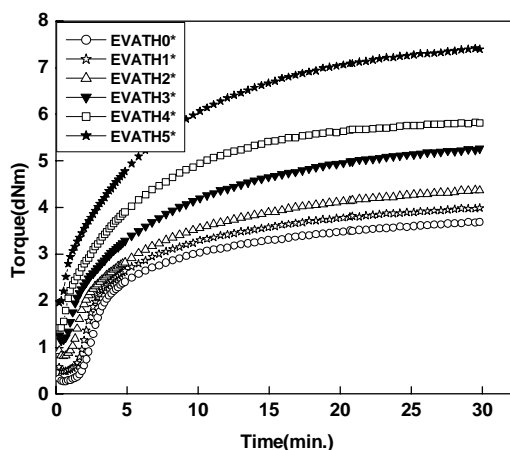
Fig. 7.2   Cure curves of ATH loaded EPDM/ FKM blends compatibilized with MA-g-EPDM

Regular variations in maximum torque and optimum cure time have been observed for the blends. It is found that unfilled blend systems, compatibilized and uncompatibilized (section 3.3.1) shows minimum optimum cure time in both the cases. Optimum cure time increased with an increase in weight percentage of filler in the blends. The optimum cure time values have been found to be highest for the blends having higher weight percentage of filler. This shows that the rate of vulcanization was more in blends containing less filler content.

Table 7.1 Cure characteristics of ATH filled EPDM/FKM blends

Sample name	D_{min} (dNm)	D_{max} (dNm)	T_{10} (min.)	T_{90} (min.)
EVATH1	0.34	4.46	1.61	16.26
EVATH2	0.61	5.00	1.23	17.27
EVATH3	1.06	6.41	0.88	17.79
EVATH4	1.44	7.53	0.73	17.87
EVATH5	1.89	10.10	0.50	18.00
EVATH1*	0.48	4.00	1.70	16.39
EVATH2*	0.80	4.38	1.30	17.27
EVATH3*	1.14	5.27	1.03	17.32
EVATH4*	1.37	5.84	0.73	17.86
EVATH5*	1.94	7.41	0.69	18.12

Scorch time (T_{10}) is usually taken as the time reach 10 % of the maximum torque. It is a measure of the premature vulcanization of the material. As shown in the table 7.1, the maximum T_{10} among the compatibilized and uncompatibilized blend systems is for unfilled blends (section 3.3.1). This shows that the scorch safety is highest for the blends without filler. Maximum torque (D_{max}) which is a measure of crosslink density is also given in the table 7.1. It is found that for the uncompatibilized blend, the highest D_{max} value is obtained for unfilled

blend which indicates better crosslinking while among the compatibilized blend systems; the D_{max} is highest for the blend with highest weight percentage of filler which indicates the enhancement in crosslinking of the compatibilized blends.

7.3.1.2 Stress-strain properties

The mechanical properties, especially the tensile strength are not governed by overall crosslinking, but it depends on the crosslink distribution and phase size as well.
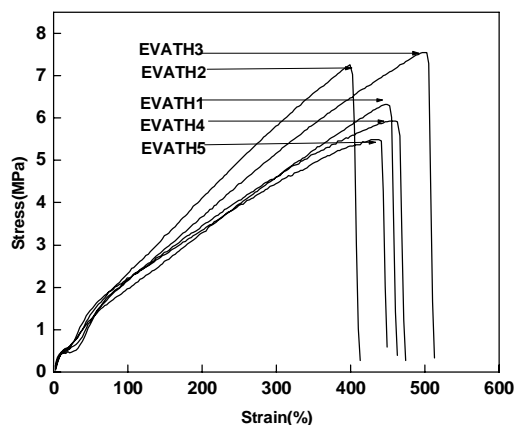
Fig. 7.3   Stress-strain behaviour of ATH filled EPDM/ FKM blends (EVATH series)

The stress-strain graph of ATH filled EPDM/FKM blends is given in Fig. 7.3. Tensile strength gradually increases with loading, pointing to the reinforcing character of the filler particles in the rubber matrix. Both surface area and surface activity of the filler are important factors in reinforcement. Particle size contributes physically and surface activity contributes chemically towards reinforcement. As the particle size decreases, the interfacial area between the filler and the elastomer increases which lead to better reinforcement.
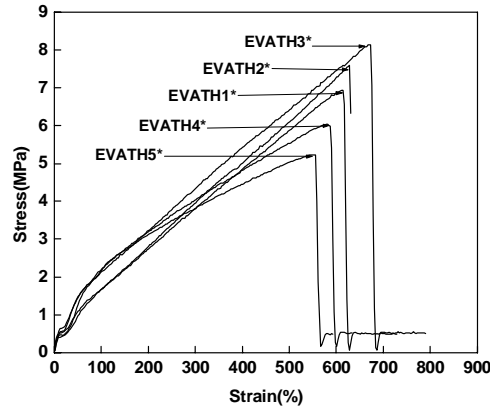
Fig. 7.4   Stress-strain behaviour of ATH filled EPDM/ FKM blends compatibilized with MA-g-EPDM (EVATH* series)

Compared to the uncompatibilised blends (Fig. 7.3), the compatibilised (Fig. 7.4) blends show slight increase in the tensile properties, confirming the effect of compatibilization.

7.3.1.3 Thermogravimetric analysis
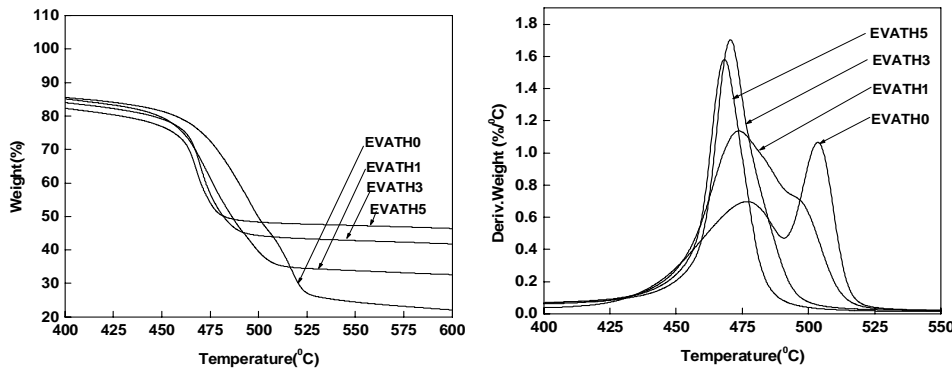
Fig. 7.5 The thermogram and derivative thermogram of EVATH series

The thermograms and derivative thermograms of ATH filled uncompatibilized and compatibilized blends are given in Fig. 7.5 and 7.6 respectively. The important thermal characteristics are reported in table 7.2. It is observed that the addition of ATH does not improve the thermal stability of blends.
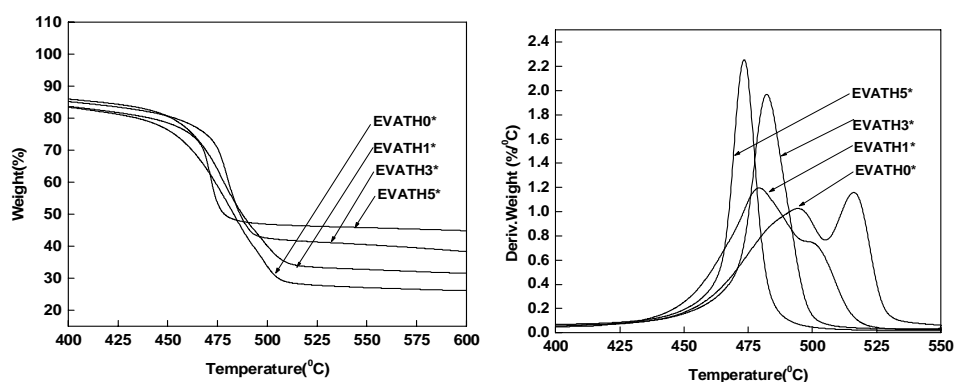
Fig. 7.6 The thermogram and derivative thermogram of EVATH* series

Pure blends in both series show two separate thermal degradation peaks due to the ability of different polymers within them to show their own degradation route. But in ATH filled systems, there is only one degradation peak due to the miscibility of EPDM and FKM. The residue percentage increases with increase in ATH loading. There is a slight improvement in the onset of degradation (table 7.2) an adding ATH. The compatibilized blend systems are found to be thermally more stable due to the action of compatibilizer. This is because miscibility is an important factor determining the thermal stability.

Table 7.2 Thermal characteristics of ATH filled EPDM/FKM blends

Sample name	Onset of degradation (T_0, ^{0}C)	Max. degradation (T_{max}, ^{0}C)	Residue (%)
EVATH0	422	490&504	24
EVATH1	429	479	30
EVATH3	432	471	38
EVATH5	440	470	41
EVATH0*	435	486&506	26
EVATH1*	427	481	31
EVATH3*	434	475	38
EVATH5*	445	472	43

7.3.1.4 Morphological studies
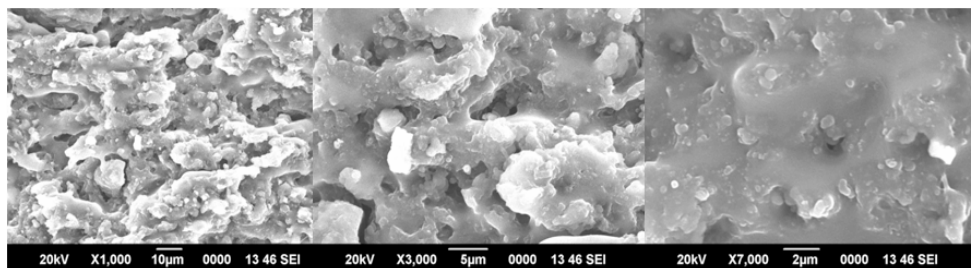
Fig. 7.7 SEM photographs of EVATH3 (25 phr ATH filled blends at three different magnifications)

Fig. 7.8 SEM photographs of EVATH3* (25 phr ATH filled blends at three different magnifications)

The morphology of the tensile fractured surface of 25 phr ATH filled uncompatibilized and compatibilized EPDM/FKM blends are given in Fig. 7.7 and Fig. 7.8 respectively. Large number of holes and weak interface are clearly observed in Fig. 7.7 (at three different magnifications). This may be due to the immiscibility of EPDM and FKM and also due to the difference in filler dispersion in the two phases. But, better interfacial adhesion is visualized in compatibilized blends (Fig. 7.8) due to the action of compatibilizer.

7.3.2 CPE filled EPDM/FKM rubber blends

7.3.2.1 Cure characteristics

The cure curves of CPE filled uncompatibilized and compatibilized EPDM/FKM blends are given in Fig. 7.9 and Fig. 7.10 and cure parameters are reported in table 7.3.
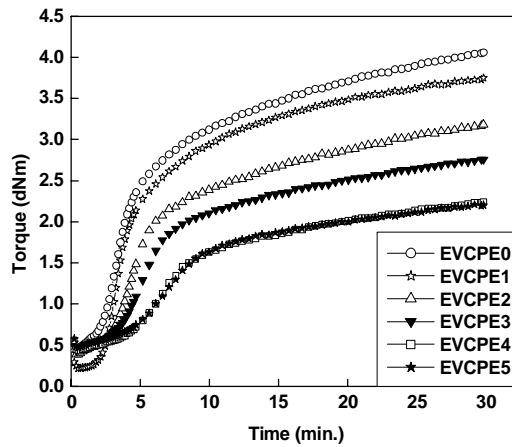
Fig. 7.9 Cure curves of CPE loaded EPDM/FKM blends
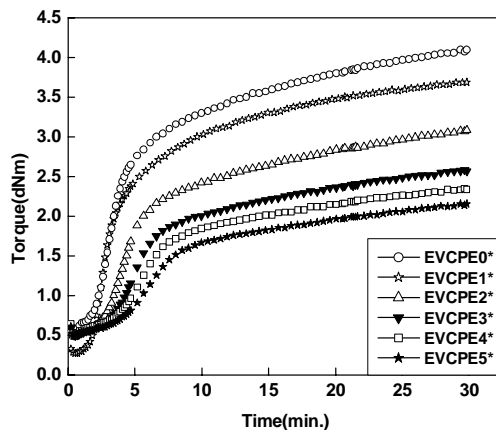
Fig. 7.10 Cure curves of CPE loaded EPDM/FKM blends compatibilized with MA-g-EPDM

It can be seen that maximum torque value decreases with increase in CPE loading. This is due to the comparatively low viscosity of CPE leading to softening of blend on heating. There is not much variation in the minimum torque values. As the CPE loading in the blend increases, vulcanization speed (optimum cure time, T_{90}) decreases. The scorch time (T_{10}) shows a slight increase with increase in CPE loading.

Table 7.3 Cure characteristics of CPE filled EPDM/FKM blends

Sample name	D_{min} (dNm)	D_{max} (dNm)	T_{10} (min.)	T_{90} (min.)
EVCPE1	0.43	4.06	2.32	19.42
EVCPE2	0.38	3.19	2.96	20.93
EVCPE3	0.43	2.77	3.11	20.50
EVCPE4	0.42	2.24	3.60	21.65
EVCPE5	0.46	2.22	3.48	21.09
EVCPE1*	0.54	4.10	2.12	18.29
EVCPE2*	0.48	3.09	2.70	19.64
EVCPE3*	0.48	2.59	3.00	20.23
EVCPE4*	0.52	2.36	3.07	20.63
EVCPE5*	0.49	2.16	3.44	21.51

7.3.2.2 Stress-strain properties
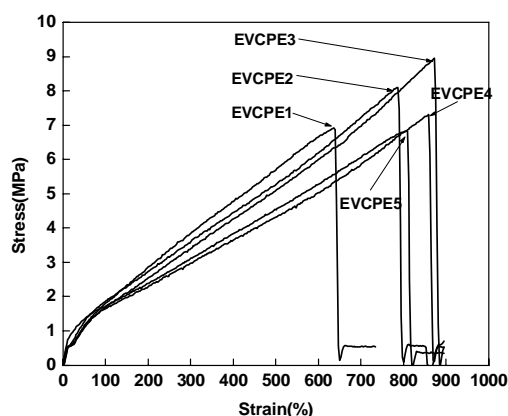
Fig. 7.11 Stress-strain behaviour of CPE filled EPDM/FKM blends (EVCPE series)

It can be seen from Fig. 7.11 and 7.12 that the increase in tensile strength with loading is not regular in both series. Tensile strength increases with filler content up to the point at which there is sufficient rubber to bind the filler and thereafter decreases. The initial increase in tensile strength is attributed to the fact that the filled polymer allows the load to be distributed among chains. This increases the resistance of rubber to failure. The compatibilized blends show comparatively higher tensile strength and elongation at break. This is due to the action of compatibilizer.
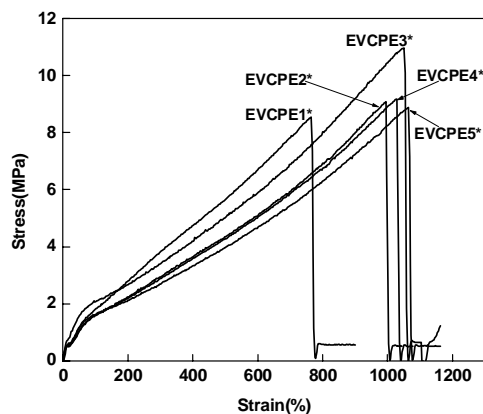
Fig. 7.12 Stress-strain behaviour of CPE filled EPDM/FKM blends compatibilized with MA-g-EPDM (EVCPE* series)

7.3.2.3 Thermogravimetric analysis
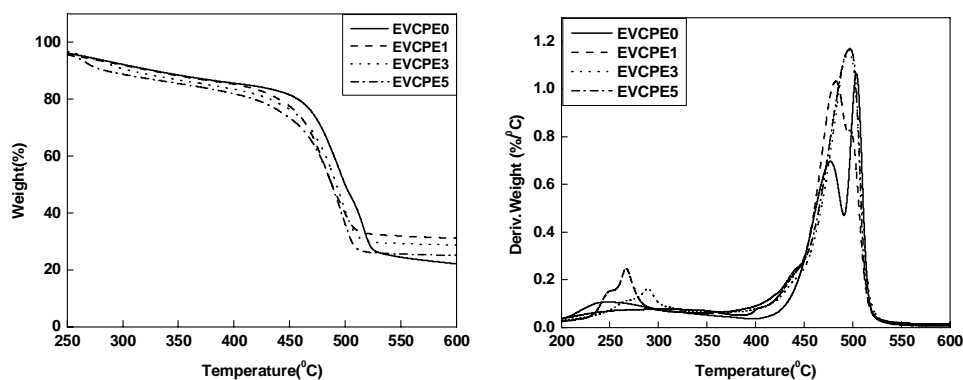
Fig. 7.13 The thermograms and derivative thermograms of EVCPE series
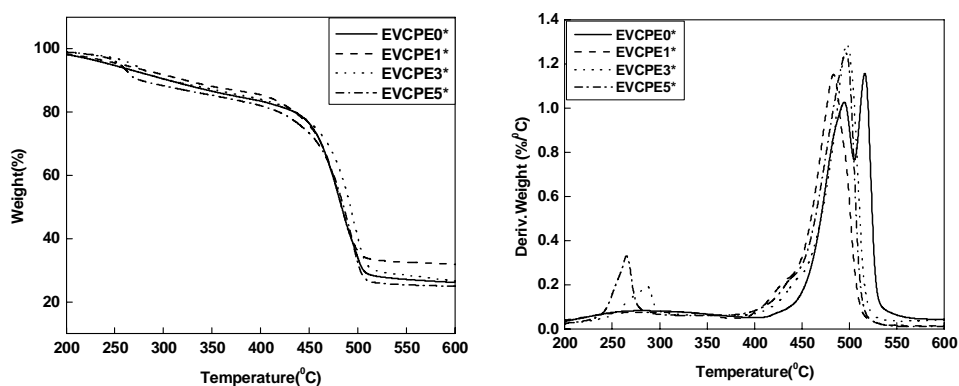
Fig. 7.14 The thermograms and derivative thermograms of EVCPE* series

The TGA curves of both uncompatibilized and compatibilized CPE loaded blends are given in Fig. 7.13 and 7.14 respectively and some of the important thermal characteristics in table 7.4. Two separate degradation peaks are obtained for unfilled blends (EVCPE0 and EVCPE0*). This is due to the separate degradation routes of individual rubbers. But in filled systems, only one maximum degradation peak is obtained. It may be due to improved miscibility in the presence of CPE. In CPE filled formulations, an initial degradation peak observed in the range 200-300^{0}C, due to the dehydrochlorination of CPE. The increased addition of CPE increases the maximum degradation temperature but it is still lower than unfilled systems. The decline in the amount of residue is due to the initial degradation of the additive.

Table 7.4 Thermal characteristics of CPE filled EPDM/FKM blends

| Sample name	Onset of degradation (T_0, ^{0}C)	Max. degradation (T_{max}, ^{0}C)	Residue (%)
EVCPE0	422	490&504	24
EVCPE1	408	280& 488	30
EVCPE3	409	284&490	27
EVCPE5	400	263&493	24
EVCPE0*	435	486&506	26
EVCPE1*	400	281&489	31
EVCPE3*	405	278&490	19
EVCPE5*	401	263&495	24

7.3.2.4 Morphological studies

Fig. 7.15 SEM photographs of EVCPE3 (25 phr CPE filled blends at three different magnifications)
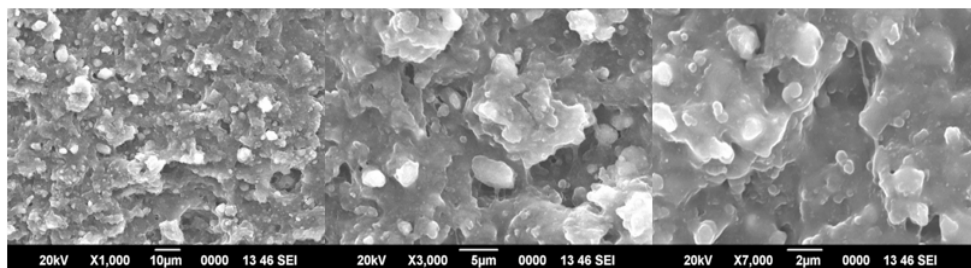
Fig.7.16. SEM photographs of EVCPE3* (25 phr ATH filled blends at three different magnifications)

The morphology of the tensile fractured surfaces of 25 phr CPE loaded blends in both series at three different magnifications is given in Fig. 7.15 and Fig. 7.16. The filler particle distribution is clearly observed from the SEM picture and is in good agreement with the tensile properties.

7.3.3 DBBO filled EPDM/FKM rubber blends

7.3.3.1 Cure characteristics
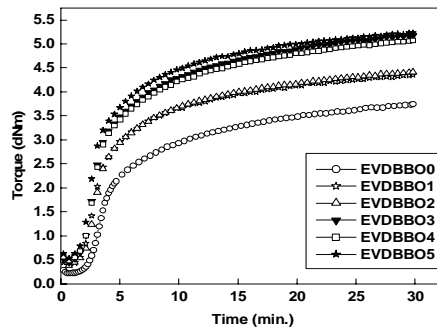
Fig. 7.17 Cure curves of DBBO loaded EPDM/FKM blends
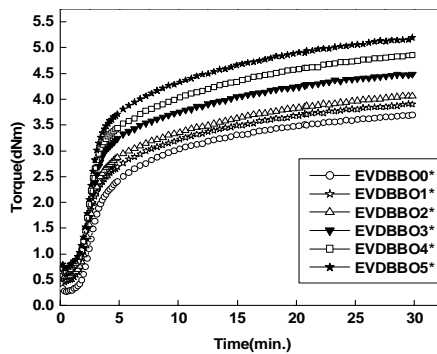
Fig. 7.18 Cure curves of DBBO loaded EPDM/FKM blends compatibilized with MA-g-EPDM

The cure curves of DBBO filled series are given in Fig. 7.17 and 7.18. and the cure characteristics are reported in table 7.5. The D_{min} is increased with loading in both series showing that DBBO and it may affect the processability of rubber blends. The D_{max} also increases with increase in DBBO concentration. The maximum D_{max} is obtained for 45 phr DBBO filled systems. The optimum cure time (T_{90}) is increased with increase in loading in both series, may be due to the adsorption of curatives on the surface of the filler particles.

Table 7.5 Cure characteristics of DBBO filled EPDM/FKM blends

Sample name	D_{min} (dNm)	D_{max} (dNm)	T_{10} (min.)	T_{90} (min.)
EVDBBO1	0.37	4.36	2.03	14.83
EVDBBO2	0.38	4.42	2.17	15.48
EVDBBO3	0.43	5.08	2.04	15.52
EVDBBO4	0.47	5.18	2.06	15.54
EVDBBO5	0.52	5.24	1.90	16.09
EVDBBO1*	0.45	3.92	1.73	16.88
EVDBBO2*	0.55	4.07	1.87	16.73
EVDBBO3*	0.63	4.51	1.84	16.76
EVDBBO4*	0.65	4.86	1.81	16.87
EVDBBO5*	0.72	5.20	1.82	17.01

7.3.3.2 Stress-strain properties

Halogenated organic compounds have been used as fire retardant additives. In general, flame retardant causes a reduction in the mechanical properties. In order to assess the effect of the flame retardant on mechanical properties of EPDM/FKM blends, the tensile strength and elongation at break were measured. Fig. 7.19 and 7.20 list the results of stress-strain measurements of the samples.
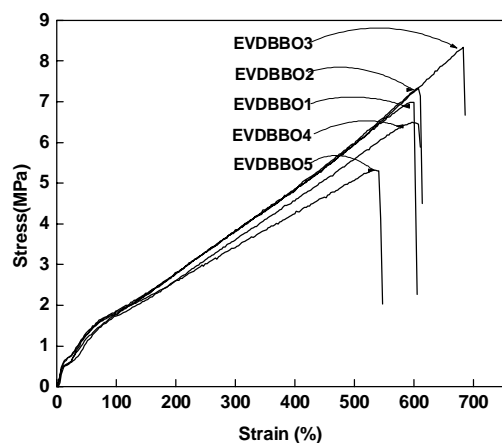
Fig. 7.19 Stress-strain behaviour of DBBO filled EPDM/FKM blends (EVDBBO series)
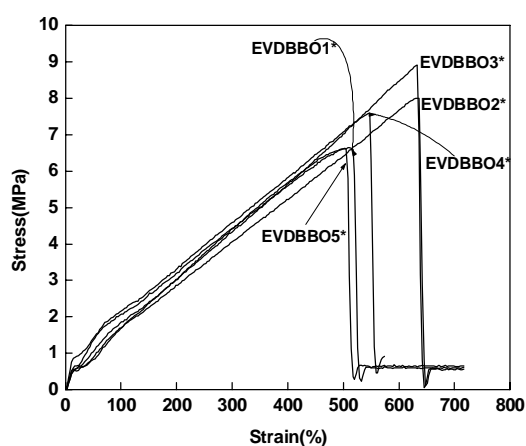
Fig. 7.20 Stress-strain behaviour of DBBO filled EPDM/FKM blends compatibilized with MA-g-EPDM (EVDBBO* series)

It is evident that addition of DBBO to EPDM/FKM rubber blends slightly increases the tensile properties. Similar trend is observed in the case of DBBO filled EPDM/PP blends [16]. The marked effect of compatibilizer is not clearly here. This is supported by SEM studies (section 7.3.3.4). Increased addition of DBBO decreases the tensile strength and elongation at break. As the filler concentration increases, the interaction between the filler surface and

the polymer phase decreases, and hence the elongation at break decreases. Another reason is as the filler loading increases, the matrix is filled by filler thereby decreasing the space available for polymer chains to stretch. As the filler content increases the stiffness of the rubber increases due to greater interaction between free polymer chain ends and filler.

7.3.3.3 Thermogravimetric analysis
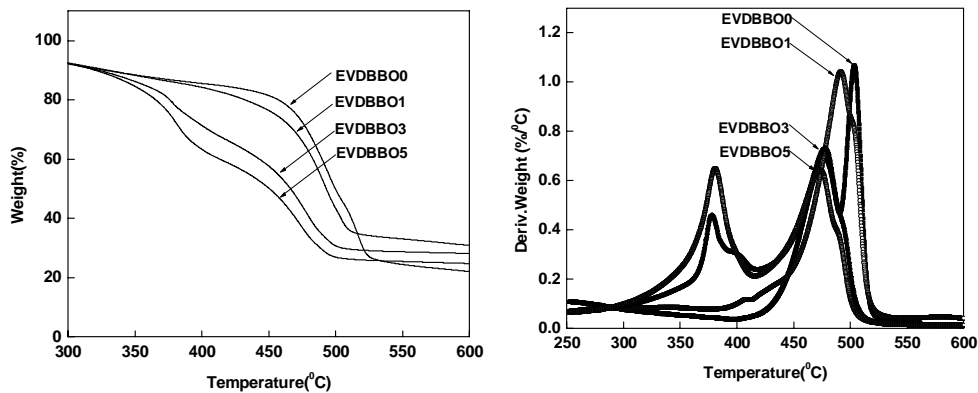
Fig. 7.21 The thermograms and derivative thermograms of EVDBBO series
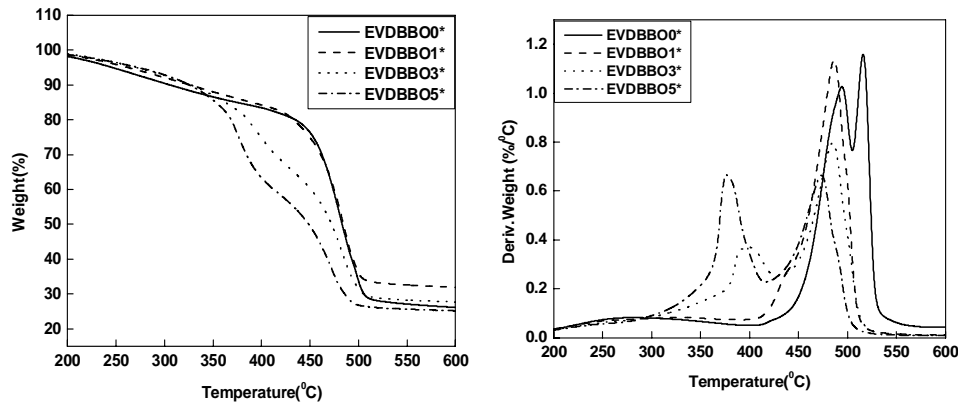
Fig. 7.22 The thermograms and derivative thermograms of EVDBBO* series

When the so-called flame retardant additives are incorporated into polymeric materials, the weight loss pattern of the polymers is altered. Fig. 7.21 and Fig. 7.22 show the TGA and DTG thermograms of DBBO

filled EPDM/FKM blends and the degradation data are listed in table 7.6. The difference in the degradation behavior of the EPDM/FKM containing various DBBO loading could be clearly seen from the derivative thermograms (DTG). Based on the numbers of peaks in the DTG thermograms, the weight loss processes of EPDM/FKM take place in several stages. Owing to the action of the flame retardants, very different degradation behavior is observed and different weight loss stages are found [17].

DBBO decreases the thermal stability (table 7.6) of the blends and introduces a second weight loss stage in which part of the bromine compound volatalizes. Introducing DBBO into EPDM/FKM causes a second stage mass loss. The initial decomposition temperature of EPDM/FKM blends is reduced. This might possibly result from the decomposition of C–Br bonds or the evaporation of DBBO. However, the weight loss of the DBBO containing EPDM/FKM at high temperatures region is less than that of unfilled EPDM/FKM. This is due to the fact that the decomposition of C–Br bonds or the evaporation of DBBO at relatively lower temperature protected the residues from heat. The residue percentage increases with increase in DBBO loading in both series.

Table 7.6 Thermal characteristics of DBBO filled EPDM/FKM blends

Sample name	Onset of degradation (T_0, ^{0}C)	Max. degradation (T_{max}, ^{0}C)	Residue (%)
EVDBBO0	422	490&504	24
EVDBBO1	Not identified	380&484	24
EVDBBO3	Not identified	380&480	27
EVDBBO5	Not identified	386&478	29
EVDBBO0*	435	486&506	26
EVDBBO1*	Not identified	380&487	28
EVDBBO3*	Not identified	388&482	31
EVDBBO5*	Not identified	382&479	33

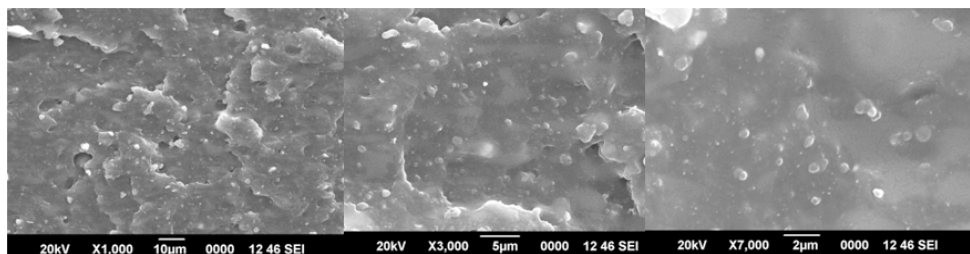### 7.3.3.4 Morphological studies
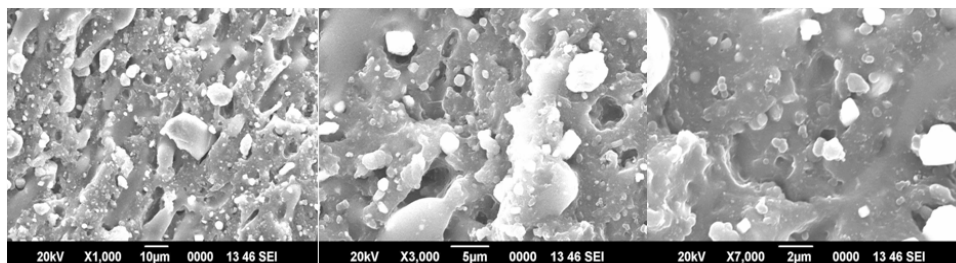
Fig. 7.23 SEM photographs of EVDBBO3 (25 phr DBBO filled blends at three different magnifications).
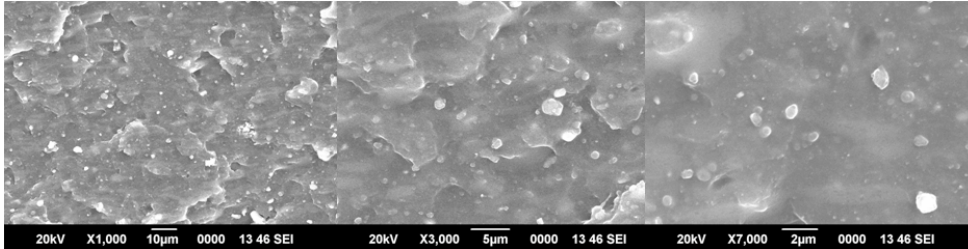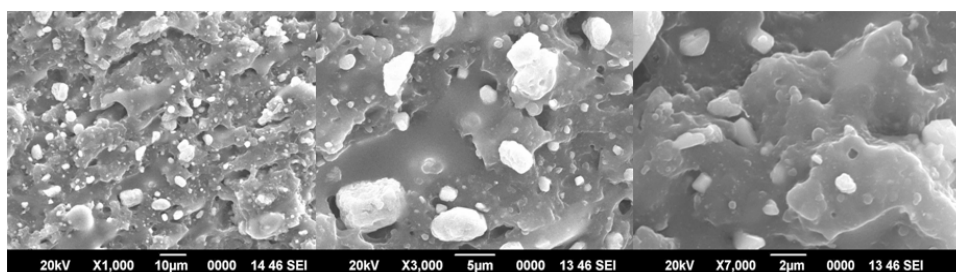

Fig. 7.24 SEM photographs of EVDBBO3* (25 phr ATH filled blends at three different magnifications)

The morphology of the tensile fractured surfaces of EPDM/FKM blends (25 phr DBBO filled blends at three different magnifications) in both series are given in Fig. 7.23 and 7.24 respectively. The morphology is not seen to be affected by compatibilization.

7.3.2.4 Sb_2O_3 filled EPDM/FKM rubber blends

Antimony trioxide (Sb_2O_3) is one of the most important and widely used flame retardant additives, more often in combination with halogen compounds. However, the future use of these flame retardants faces some challenges due to the environmental impact of recycling, toxicity, and combustion of certain halogenated flame retardants has become progressive [18,19]. The effect of Sb_2O_3 alone was studied.

7.3.4.1 Cure characteristics
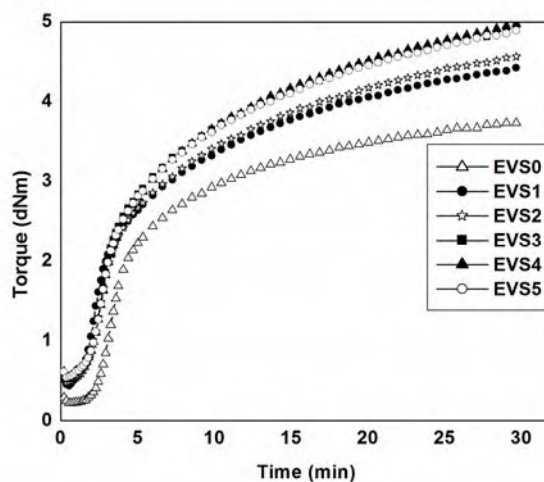
Fig. 7.25 Cure curves of Sb$_2$O$_3$ loaded EPDM/FKM blends
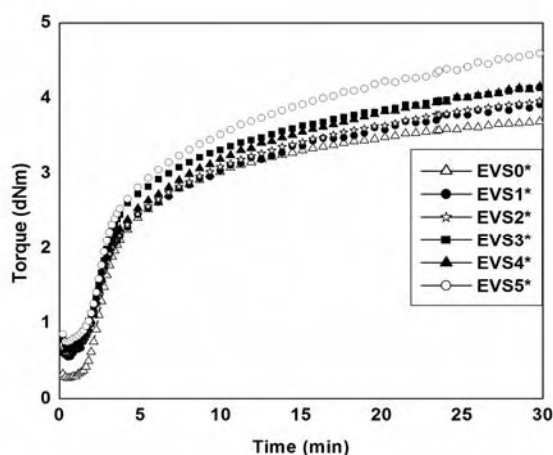
Fig. 7.26 Cure curves of Sb$_2$O$_3$ loaded EPDM/ FKM blends compatibilized with MA-g-EPDM

The cure curves of Sb$_2$O$_3$ loaded EPDM/FKM blends in both series are given in Fig. 7.25 and 7.26. Important cure characteristics are given in table 7.7. The trend obtained is same as that of DBBO filled systems. Increase in D$_{max}$ indicates higher degree of crosslinking. The cure time T$_{90}$ shows an increase on adding Sb$_2$O$_3$.

Table 7.7 **Cure characteristics of Sb$_2$O$_3$ filled compatibilized and uncompatibilized EPDM/FKM rubber blends**

Sample name	Minimum torque D$_{min}$ (dNm)	Maximum torque D$_{max}$ (dNm)	Scorch time T$_{10}$ (min.)	Optimum cure time T$_{90}$ (min.)
EVS0	0.32	3.79	2.37	17.60
EVS1	0.44	4.43	1.74	19.52
EVS2	0.48	4.58	2.04	19.92
EVS3	0.53	4.91	2.10	19.87
EVS4	0.54	5.01	2.13	20.77
EVS5	0.55	4.91	2.12	20.21
EVS0*	0.35	3.72	2.32	17.20
EVS1*	0.53	3.95	1.75	19.79
EVS2*	0.60	3.96	1.86	19.63
EVS3*	0.72	4.15	1.88	19.93
EVS4*	0.73	4.17	1.92	20.20
EVS5*	0.75	4.59	1.96	20.08

7.3.4.2 Stress-strain properties

The mechanical properties of composites are found to depend on many factors: the aspect ratio of the filler, the degree of dispersion of the filler in the matrix, and the adhesion at the filler–matrix interface. To assess the effect of the flame-retardant Sb$_2$O$_3$ on the mechanical properties of the blend, tensile strength, and elongation at break were measured; the results are numerated in Figs. 7.27 and 7.28.
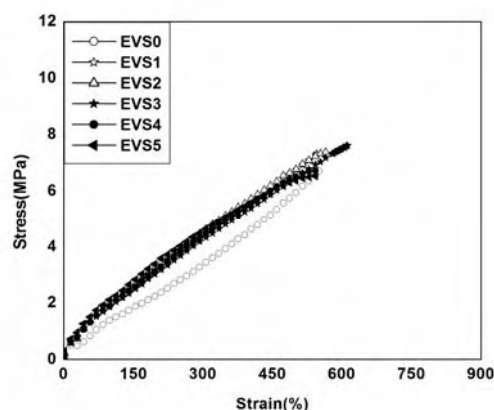
Fig. 7.27 Stress-strain behaviour of Sb$_2$O$_3$ filled EPDM/FKM blends (EVS series)
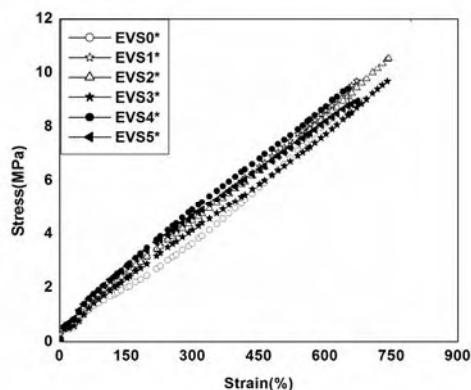
Fig. 7.28 Stress-strain behaviour of Sb$_2$O$_3$ filled EPDM/FKM blends compatibilized with MA-g-EPDM (EVS* series)

Filler loading up to 25 phr improved the tensile strength and elongation at break. A higher loading result in a reduction of both parameters. This reduction is due to the improper dispersion of filler particles. 45 phr Sb$_2$O$_3$ loading lowers tensile strength and elongation at break to rather lower value compared to that of gum vulcanizates. In compatibilized blends of EPDM/FKM, tensile strength increases by compatibilization with MA-g-EPDM as shown in Fig. 7.28. The increase in the tensile strength of compatibilized blend compared to uncompatibilized EPDM/FKM blends is due to the formation interfacial interactions between EPDM and FKM in the presence of compatibilizer, as confirmed by the morphological behavior (section 7.3.4.4). The presence of maleic anhydride groups makes a stronger interaction between EPDM and FKM in comparison to the blends without MA-g-EPDM.

7.3.4.3 Thermogravimetric analysis
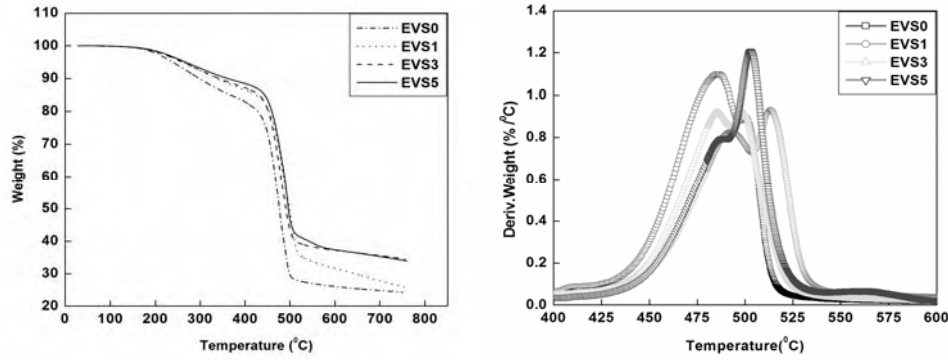
Fig. 7.29 The thermograms and derivative thermograms of EVS series
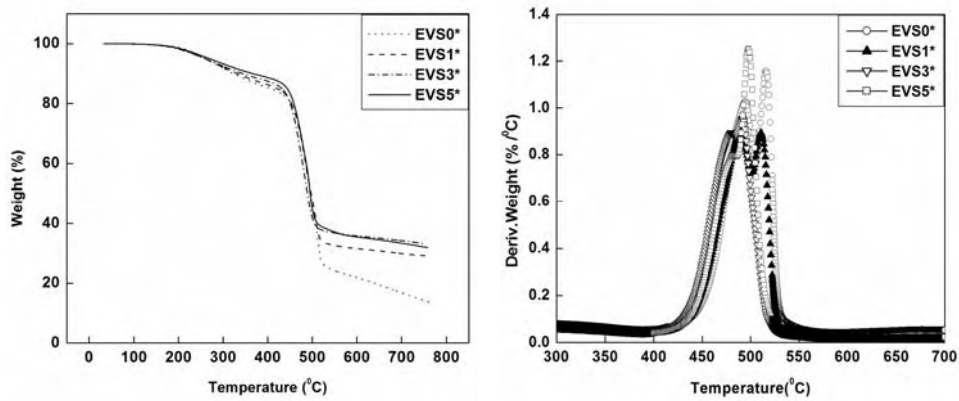
Fig. 7.30 The thermograms and derivative thermograms of EVS* series

The thermal behavior of all Sb_2O_3 formulations is shown in Fig. 7.29 and Fig. 7.30 and the thermal characteristics are reported in table 7.8.The comparison between ATH filled systems (table 7.2) shows that Sb_2O_3 is not as efficient as other metal oxides used in the present context. But it increases the amount of residue at the end of decomposition. This is related to the main gas phase action of this additive. The addition of Sb_2O_3 in blends does not essentially change the decomposition temperature but decreases decomposition rate of the main decomposition process.

Table 7.8 Thermal characteristics of Sb₂O₃ filled EPDM/FKM rubber blends

Sample name	Onset of degradation (T_0, ^{0}C)	Max. degradation (T_{max}, ^{0}C)	Residue (%)
EVS0	422	490&504	24
EVS1	419	483&504	26
EVS3	424	481&495	34
EVS5	425	482&496	35
EVS0*	435	486&506	26
EVS1*	415	482&506	29
EVS3*	417	484&495	33
EVS5*	428	479&497	36

7.3.4.4 Morphological studies

Scanning electron photograph of the tensile fractured surfaces EVS3 and EVS3* (a, b and c represents 25 phr Sb₂O₃ filled blends at three different magnifications) are given in Fig. 7.31.
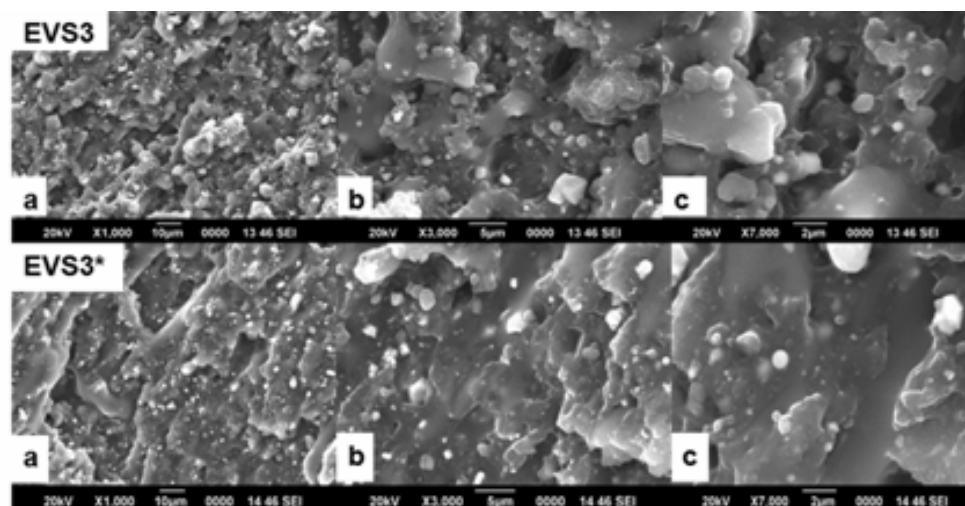
Fig. 7.31 SEM photographs of EVS3 and EVS3* (a, b and c represents 25 phr Sb₂O₃ filled blends at three different magnifications).

The SEM photographs of the un compatibilized blend containing 25 phr of Sb_2O_3 (EVS3) shows an irregular domain size and poor distribution of Sb_2O_3 in the matrix. This indicates low adhesion between the phases, giving rise to poor stress transfer across interface. In compatibilized blends (EVS3*), the compatibilizer improves interaction between phases and consequently enhancing the mechanical properties. Morphology studies of the blends are in good agreement with the variation in stress-strain properties.

7.3.5 Limiting oxygen index (LOI) of the composites

LOI is defined as the minimum concentration of oxygen required in the air mixture, just to support the downward burning (like candle) of a vertically placed strip specimen. High oxygen concentration requirement indicated the better flame retardancy of the specimen. The oxygen concentration is reported as volume percent.

Oxygen index methods, which describe the tendency of a material to sustain flame, are widely used as a tool to investigate the flammability of polymers. The sample testing using the LOI instrument is shown in Fig. 7.32. They provide a convenient reproducible means of determining numerical measures of flammability. A further attraction is that the test method uses inexpensive equipment and only requires small samples. These methods have been used to systematically investigate the relative flammabilities of fire retardant materials frequently comparing the effectiveness of fire retardants and fire retardancy mechanism.

In recent years, development of halogen-free flame retardant polymeric materials has become a potential trend. The limiting oxygen

index values of the composites are given in table 7.9. From the table it is clear that, ATH filled blends increase the LOI value from 22 % (unfilled) to 26 % (45 phr) in both series. Many investigations have demonstrated that aluminium hydroxide known as aluminium trihydrate (ATH) is a non-toxic and smoke suppressing halogen-free flame retardant additive. However, ATH more than 60 wt% ATH loading is required to meet flame retardant properties, which could be detrimental in obtaining mechanical properties of flame retardant materials. The flame retardancy of particulate composites ascribes the fact that particle size of inorganic flame retardants strongly influences its dispersion in polymer matrix. The good distributive dispersion and the small particle size tend to result in better flame retardancy [20]. ATH is usually considered to be an inert additive in flame retardant systems.

Fig. 7.32 Photograph showing sample testing procedure in an LOI instrument

Table 7.9 Limiting oxygen index (LOI) values of the prepared composites

Sample name	LOI (%)	Sample name	LOI (%)
Unfilled blend (uncompatibilized)	22	Unfilled blend (compatibilized)	22
EVATH1	22	EVATH1*	22
EVATH2	23	EVATH2*	22
EVATH3	23	EVATH3*	23
EVATH4	25	EVATH4*	25
EVATH5	26	EVATH5*	26
EVCPE1	22	EVCPE1*	22
EVCPE2	22	EVCPE2*	23
EVCPE3	22	EVCPE3*	23
EVCPE4	24	EVCPE4*	24
EVCPE5	26	EVCPE5*	26
EVDBBO1	23	EVDBBO1*	23
EVDBBO2	25	EVDBBO2*	25
EVDBBO3	27	EVDBBO3*	26
EVDBBO4	30	EVDBBO4*	29
EVDBBO5	33	EVDBBO5*	33
EVS1	24	EVS1*	24
EVS2	26	EVS2*	26
EVS3	27	EVS3*	28
EVS4	28	EVS4*	29
EVS5	29	EVS5*	30

The mechanism of the reduction in heat release rate is mainly due to the dehydration of water from ATH. The formation of the efficient char can prevent the heat mass transfer between the flame zone and the burning substrate, and thus protect the underlying materials from further burning and retard the pyrolysis of polymers. The higher residue amount found indicates an interaction between the polymer and the metal-oxide resulting in an increasing stability of the char [21].

The flame retardancy of polymers can be achieved according to three major mechanisms: (a) the gas phase mechanism, which is typical for

halogen based FR systems, (b) the condensed phase mechanism, which governs treatments based on phosphorus and sulphur derivatives and (c) the mechanism based on physical effects governing the endothermic processes (Mg and Al hydroxides). The objective of using flame retardants is to lower the blends inherent fire risk by lowering the combustion rate and flame spreading in the presence of fire.
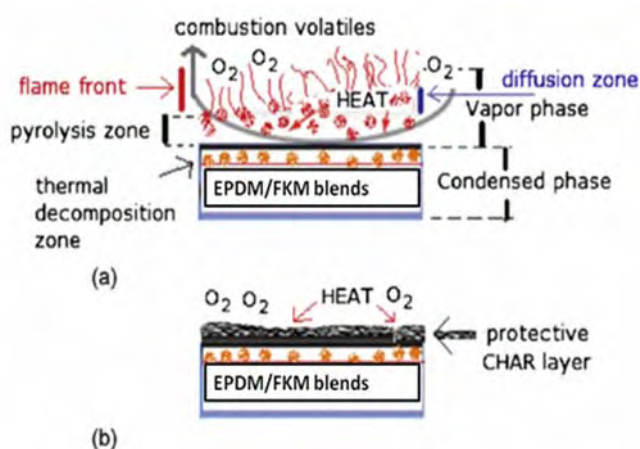
Fig. 7.33 A typical picture of blends (a) without flame retardant-resulting large heat release and (b) with flame retardant-resulting low heat release, showing the processes occurring during combustion. A low-density, high porosity char produces better flame retardancy

The flame retardance mechanism – the interference with the combustion process – can function either in the condensed phase (solid phase) or in the vapour phase (flame zone) through a physical mechanism, a chemical mechanism or a combination of these mechanisms. Combustion is a complex process and different mechanisms may be involved in the presence of different types of flame retardants. the incorporation of inorganic fillers dilute the polymer, produce a stable organic–inorganic interface, reduce the concentration of decomposition gases and increase the diffusion path barrier of the volatiles produced during the degradation process (Fig. 7.33).

The LOI tests are widely used to evaluate flame retardant properties of materials. The results for flammability (LOI) of CPE filled systems are summarized in table 7.9. The LOI value of unfilled EPDM/FKM blend is only 22 %. It can be observed from table 7.9 that the LOI value of sample EVCPE containing 45 phr ATH increases rapidly to 26 % from 22 % of original sample EVCPE0 without any additive. These results indicate that the addition of a suitable amount of CPE can increase the flame retardancy of EPDM/FKM composites. In thermal decomposition, they are thought to liberate halogen radicals and hydrogen halides, thereby serving both as free radical traps and as flame poisons.

Brominated and chlorinated compounds are most commonly employed, since organo-iodides are too unstable and the degradation products of fluorides are themselves too reactive. The organo-bromine and organo-chlorine retardants are stable at polymer processing temperatures but decompose below the temperature at which they pyrolyze. They are effective at low concentrations and thus their addition does not substantially change the properties of the polymer.

Nowadays, more and more attention is being paid to improve the flame retardant properties of polymer as it is an essential requirement for applications such as wire and cables, different household stuffs such as upholstered furniture and mattresses, aircraft interiors, fire-resistant coatings and clothes, etc. The driving forces for the development of flame retardant polymers include increasing safety awareness of consumers, environmental pollution generated during burning, and economic loss incurred due to burning of materials. The main approaches taken are to incorporate flame retardants either as additives or to incorporate reactive flame retardants into the formulation.

Additive type flame retardants (decabromo biphenyl, decabromo biphenyl oxide and its derivatives) are incorporated into the rubber by physical means, which may result in poor compatibility, leaching, as well as a inferior mechanical properties. On the other hand, reactive type flame retardants are mainly organic compounds having a flame retarding moiety as well as active functional groups that can form covalent bonds with rubbers. Reactive type flame retardants have the advantages of (a) increasing compatibility between polymer and the flame retardant, (b) not deteriorating the mechanical properties of the rubber, (c) possessing better compatibility as the flame retardant group is a part of the binder and (d) using small amount or low concentration for the enhancement of fire-retardancy [22].

The results (table 7.9) showed that unfilled EPDM/FKM had some resistance to combustion. After addition of DBBO, LOI value increased slightly. With increasing amounts of DBBO the value was raised from 22 to 33 %. It is well known that, DBBO acts as a flame retardant mainly by eliminating HBr, which when acts in the gas phase by replacing very active chain-propagating free radicals by less reactive Br-atoms.

The halogenated flame-retardant can produce poisonous gases. CO is the main component in gases formed in fire and it causes the worst danger to life according to US Fire Administration. In burning, an instantaneous char formed on the surface of the material acts as thermal insulation facilitating the extinguishion of the flame. It prevents combustible gases from feeding the flame and also separates oxygen from burning the material. The carbonaceous char can be formed and destroyed repetitively in burning. Therefore, the residue is the final char.

In general, Sb_2O_3 tends to give a slight positive effect with regard to delaying polymer ignition. Sb_2O_3 in EPDM/FKM is not active in reducing the combustion of blends. Generally, different flame retardants exhibit different mechanisms of flame resistance. The results of oxygen index for the Sb_2O_3 filled EPDM composites are presented in table 7.9. In the case of uncompatibilized blend, an increase in the concentration of Sb_2O_3 from 0 to 45 phr, increases the LOI from 22 to 29%. In compatibilized blends, it increases from 22 to 30 %. In all the above filled compatibilized systems, there is no much significant effect on flame-retardancy.

Generally Sb_2O_3 (synergist) is used along with halogenated flame-retardants. But the use of halogenated flame-retardants creates severe environmental problems. That is why we are using Sb_2O_3 alone in formulations. Though Sb_2O_3 has no perceptible flame-retardant effect on its own, it has been found to provide fire retardancy to polymer in some special cases; it was reported to be effective even in the absence of halogen [23]. The flame retardancy was accounted for simple physical dilution of the flammable substrate and formation of impermeable glassy layer or coating on the burning surface at ignition temperature [24].

7.4 Conclusions

Blending of EPDM rubber with FKM is found to be an effective way to improve the flame-retardancy of EPDM. In this work the flame retardancy mechanisms of halogenated and non-halogenated flame retardants are investigated for EPDM/FKM rubber blends. Fire behaviour has been analyzed by LOI tests.

From the analysis of the results of experiments, it is evident that untreated EPDM/FKM has low resistance to combustion. ATH, CPE, DBBO and Sb_2O_3 when used in formulation, produced improvement in the flame retardation. When metal oxides particles are added to blends, a higher residue amount is found, indicating an interaction between the polymer and the metal-oxide and resulting in an increasing stability of the char. The amount of char decreases in the order Al_2O_3> Sb_2O_3>DBBO>CPE. Adding flame retardant additives to EPDM/FKM blends promoted the formation of dense char during the burning process. The char can reduce the amount of combustible gases transported to the flame.

The incorporation of these fillers along with increasing flame retardancy, improves mechanical properties. Anyway, higher loading of flame retardant causes rapid decrease in the tensile strength and elongation at break. The thermal behavior of EPDM/FKM is altered by these flame retardants.

References

[1]   Fujimoto K, Oshimiya NY, Rubber Chem Technol 1968, 41, 1109.

[2]   Hess WM, Herd CR, Vegvars PC, Rubber Chem Technol 1993, 66, 329.

[3]   Utracki LK, Poly. Plast.Technol.Eng. 1984, 22, 27.

[4]   Imoto M, J.Assoc.Rubb.Ind.Japan 1969, 42, 439.

[5]   Hess WM, Vegvari PC, Rubber Chem. Technol. 1985, 58, 350.

[6]   Joseph R, George KE, Die Angewandte Makromolekulare Cheme. 1988, 163, 37.

[7]   Utracki LA, Hanser, New York, 1989.

[8]   So-go-chung-nam, Polymer Alloy: High molecule Society 1987, Japan, Chap. 1.

[9]   Suwa T, Takehisa M, Machi S, J. Appl. Polym.Sci. 1973, 17, 3253.

[10]   Yamaguchi S, Tatemoto M, Fine structure of fluorine elastomer emulsions, Sen'I

[11]   Gakkaishi 1994, 50, 414.

[12]   Zhang HY. Explosive 1993, 4, 26-33 [Chinese].

[13]   Chang YW, Yang Y, Polymer International 2002, 51, 319-24.

[14]   Junior, Kenneth E, US4600732, 1986.

[15]   Newman S. In: Paul DR, Newman S, editors. New York: Academic Press, 1978.

[16]   Xiao-Lin Xie, Robert Kwok-Yiu Li, Qing-Xi Liu, Yiu-Wing Mai. Polymer 2004, 45, 2793.

[17]   Li Yu, Wenjun Wang, Weidong Xiao. Polym degrad Stab 2004, 86, 69–73.

[18] Chuan Shao Wu, Ying Ling Liu, Yie Chan Chiu, Yie Shun Chiu. Polym Degrad Stab 2002, 78, 41–48.

[19] Montezin F, Lopez-Cuesta JM, Crespy A, Georlette P, Fire Mater 1997, 21, 245.

[20] Laachachi A, Cochez M, Ferriol M, Leroy E, Lopez Cuest JM. Oget N. Polym Degrad Stab 2004, 85, 641-646.

[21] Honghai Huang, Ming Tian, Li Liu, Wenli Liang, Liqun Zhang, J Appl Polym Sci 2006, 100, 4461–4469.

[22] Botelho G, Queiros A, Gijsman P, Polym Degrad Stab 2001, 73, 431435.

[23] Lu SY, Hamerton I, Prog Polym Sci 2002, 27, 1661–712.

[24] Karak N, Maiti S, J Appl Polym Sci 1998, 98, 927.

[25] Kuryla WC, Papa AJ, 1, Dekker, Ny, 1973.

.....ಞಐ.....

APPLICATION STUDIES OF THE COMPOSITES BASED ON EPDM AND EPDM/FKM BLENDS- INSULATION PROFILES

Contents

8A.1 Introduction
8A.2 Experimental
8A.3 Results and Discussion
8A.4 Conclusions

Formulations of EPDM (Keltan 7341A), and EPDM/FKM (80/20, Keltan 7341A/Viton A 401C) rubber blends containing mixtures of aluminum hydroxide (ATH) and calcium carbonate (CaCO$_3$) as fillers were developed, aiming to achieve a synergism in properties, for application as profiles, yet retaining the fire resistance. The cure characteristics and tensile properties of the extruded profiles were studied. Better aging tensile properties are obtained for profiles based on blends due to the improved thermal stability of FKM. The flammability of the developed profiles was measured using Limiting Oxygen Index (LOI). Scanning Electron Microscopic (SEM) studies of the cross section of the profiles were also carried out.

8A.1 Introduction

Polymeric materials have made an important role in engineering applications for long time, owing to their excellent insulation properties and mechanical properties. The application of polymeric materials in this field, however, requires special precautions because fire can be generated easily.

Thus the studies on flame-retarding polymeric materials become indispensable when these materials are widely used. There are four factors affecting the process of combustion, which are oxygen, heat, flammable materials and reaction of thermal degradation [1].

Brominated flame retardants, which stop the thermal degradation of composites by reacting with the polymers, are the most effective flame retardants [2-4] in markets that are adopted for most engineering polymers [5-7]. However, halogen flame retardants may release toxic gases when they are subjected to high temperatures. Environment friendly flame retardants, some brominated flame retardants begin to be replaced by some halogen-free flame retardants, particularly metallic hydroxide flame retardants such as magnesium hydroxide [8], aluminum trihydrate [9], hydrotalcite [10], magnesium hydroxide sulfate hydrate whisker [11]. In these metallic hydroxide flame retardants, aluminum trihydrate (ATH) is one of the most popular, safe, halogen-free and smoke suppressant. Other benefits include, low material cost, elimination of heavy metal promoters (e.g. antimony oxide) and absence of toxic fume generation [12,13]. Insulating compositions with fire resistant and flame retardant properties are made from polymers, such as polyethylene (PE), ethylene-propylene rubber (EPR), ethylene-propylene-diene rubber (EPDM), silicon elastomer, etc.

Ethylene-propylene-diene rubber (EPDM) has been the one of the fastest growing synthetic rubbers on market for both general purpose and special applications. Ethylene propylene diene monomer (EPDM) is the polymer prepared from ethylene, propylene, and ethylidene norbornene or 1, 4-hexadiene or dicyclopentadiene monomers. EPDM composite is a

good internal insulating material for solid rocket motors by virtue of various advantageous features, such as low density (0.87-0.89 g/cm^3), low ablation rate, high thermal decomposition temperature, high specific heat, low brittle temperature, good aging resistance, and good air-tightness, and its tensile strength and elongation are in full accord with those required for this application [14]. Elastomeric materials have numerous applications in all major sectors, including industries, automotive, aerospace, defense and biomedical due to their elasticity, stretchability and durability [15, 16].

Fluorocarbon rubbers, specialty polymer are also widely used in many industrial applications. A primary variable in FKM grades is the level of fluorine content in the elastomer molecule, FKMs being fluorohydrocarbons. In general, fluoroelastomers have excellent resistance to oxidation, ozone, fuels and petroleum oils and are resistant to most mineral acids at high concentrations. Although FKM has good resistance to many chemicals, excessive swelling occurs in some polar solvents such as low molecular weight ethers, esters and ketones. Chemicals such as alkalis and amines should be used with caution, with standard fluorocarbon grades, especially at higher temperatures because alkalis harden the general purpose FKM, which will eventually embitter and then crack. FKM has a tendency to self extinguish when a flame is removed. Polymer blends have received a lot of attention in recent years due to the possibility of obtaining compounds with novel and/or different properties through proper combination of the properties of the respective components. EPDM blended with FKM produces materials with better overall properties. So these can be used safely in many applications such as automotive insulation materials, roof sealing sheets, playground mat, sealing profile for windows, cars etc. Internal insulating materials are used to

meet various requirements, such as moderate tensile strength, high elongation at break, low density, good thermal stability, and effective heat insulation. Present study has been carried out on the applicable utility of the extruded EPDM and EPDM/FKM blend based profiles for high temperature insulation purposes.

8A.2 Experimental

8A.2.1 Materials

The materials used are given in section 2.1.

8A.2.2 Methods

The methods used are given in section 2.6. Extrusion of the rubber samples are done as described under section 2.6.4 and vulcanization of the expanded profiles as described in section 2.6.5.

Table 8A.1 The formulations of mixes used for extrusion

Serial No.	Ingredients	E_{mix}	EV_{mix}
1	EPDM	100	80
2	FKM mix.* (A401C)	-	22
3	ATH	50	50
4	$CaCO_3$	50	50
5	SRF	12	12
6	Praffinic Oil	30	30
7	DOA	-	20
8	PEG	2	2
9	ZnO	6.5	6.5
10	Stearic acid	4	4
11	Zinc stearate	-	15
12	ADC	30	30
13	ZDBC	4.7	3.76
14	ZDEC	2.2	1.76
15	S	2	2
* FKM mix = FKM-100, $Ca(OH)_2$-6.0, MgO-4, MT black-20			

8A.3 Results and discussions
8A.3.1 Cure characteristics

During rubber profile extrusion unvulcanized rubber blends (prepared as per the formulations given in table 8A.1) are pressed through a die (diameter= 10mm) with a specified geometry. The vulcanization process (140 ^{0}C for 40 min and 150 ^{0}C for 20 min) is completed in a hot air oven. This is the most frequently used method of vulcanizing extrusions.

Table 8A.2 Cure characteristics of the extruded samples from RPA

Sample name	Minimum Torque (D_{min}, dNm)	Maximum Torque (D_{max}, dNm)	Scorch time (T_{10}, min)	Cure time (T_{90},min)
E_{mix}	0.11	0.44	0.55	12.29
EV_{mix}	0.33	0.64	0.64	14.33

The cure characteristics of the prepared compounds are given in table 8A.2. From table 8A.2, the minimum torque, maximum torque and scorch time are not affected by the addition of FKM. But the optimum cure time shows slight increase by the incorporation of FKM. The photograph of extruded sample is given in Fig. 8A.1. Photographs of the expanded E_{mix} and EV_{mix} profiles are given in Figs. 8A.2 and 8A.3 respectively.

Fig. 8A.1 Extruded profiles (E_{mix})

Fig. 8A.2 Expanded EPDM (E$_{mix}$) extruded sample

Fig. 8A.3 Expanded EPDM/Viton blend (EV$_{mix}$, 80:20) extruded sample

8A.3.2 Density calculation by specific gravity method

Table 8A.3 Density of the prepared profiles

Sample name	Density (g/cm^3)
E$_{mix}$	0.29
EV$_{mix}$	0.36

The density of the prepared profiles is given in table 8a.3. From this it is clear that, the addition of FKM donot have much influence on the density.

8A.3.3 Tensile properties of profiles

Measuring the tensile properties after aging at 150, 170,190 and 210 ^{o}C for 24 h in an air oven assessed resistance of the sample to aging is shown in the below, table 8A.4.

Table 8A.4 Tensile properties of the profiles before and after aging (150^{0}C, 170^{0}C, 190^{0}C, 210^{0}C for 22h)

Ageing Temperature (^{0}C)	Emix			EVmix		
	Tensile Strength (MPa)	Elongation at Break (%)	Modulus (100%)	Tensile Strength (MPa)	Elongation at Break (%)	Modulus (100%)
Unaged	5.45	679.45	2.00	5.69	659.89	2.66
150^{0}C	5.97	251.08	4.02	6.33	239.43	4.15
170^{0}C	6.45	142.50	5. 45	7.16	137.45	6.22
190^{0}C	5.49	37.62	0.98	5.64	32.06	1.02
210^{0}C	2.06	19.04	1.00	4.55	11.47	0.99

The tensile properties (table 8A.4) after aging show that better retention in properties of EPDM/FKM blends compared to EPDM profile. This is due to the thermal stability of fluorocarbon rubber compared to EPDM. After aging process at 210^{0}C, EPDM/FKM blend based profile shows tensile strength of 4.55 MPa and that for EPDM is 2.06 MPa. The elongation at break decreases with increase in aging temperature. This decrease is due to the formation of crosslinked structure. However, at higher crosslink density the network is so dense that there is little energy dissipation in the matrix and the energy supplied is utilized for breaking the bonds. At higher crosslink density, the segments of macromolecules become immobile, the system becomes stiffer and the elasticity decreases.

8A.3.4 Foam morphology

Azodicarbonamide is a predominant exothermic chemical foaming agent (CFA). Pure ADC is a yellow-orange powder with a decomposition temperature of 205^{0}C. Upon complete decomposition, its residues are white to off-white in colour. It is one of the most efficient CFA's,

generating 210-220 cc of gas per gram of product. The gas is mainly nitrogen with lesser amounts CO, CO_2, and NH_3 also given off. The decomposition temperature may be reduced by the addition of metal salts (activators). Metal salts containing Zinc and Lead are especially effective. These blowing agents are usually used in closed cell products. Scanning electron microscopy (SEM) was used to investigate the cell structure of foam. SEM photomicrographs (Fig. 8A.3 and Fig. 8A.4) show foam morphology of compounds with their blowing takesplace at their curing cycle.

Fig. 8A.3 presents the SEM micrographs of razor cut surfaces of EPDM. From Fig. 8A.3, cell morphology of expanded EPDM (EPDM foam) sows that ADC in EPDM allowing the EPDM matrix to expand freely without collapsing and merging of the foam cells under the heat. This statement was substantiated by SEM micrographs of the EPDM foamed by ADC (see Fig. 8A.3).
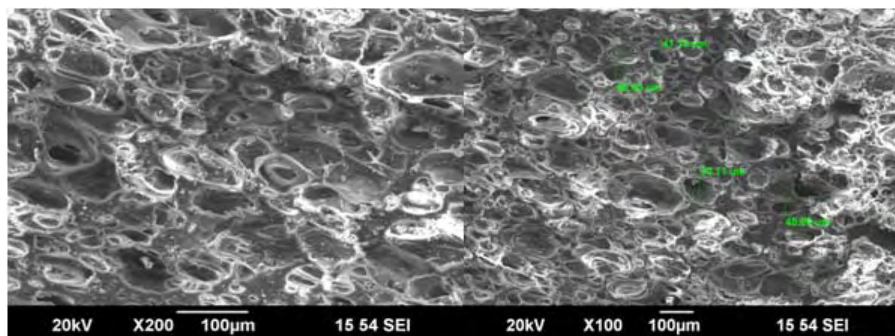
Fig. 8A.3 SEM photographs of razor cut surfaces of EPDM foam

The cell morphology of 80/20 EPDM/FKM blend is given in Fig. 8A.4. The two-phase morphology could not be found in the blends with FKM. From Fig. 8A.4, it is clear that closed cells with thicker

walls. But in Fig. 8A.3, many of small cells are observed. This might be explained from two ways-the viscosity and modulus of the rubber matrix. When the blowing agents begins to release gas, the modulus of the matrix are relatively weak, so that the gas pressure easy to break the cell walls and the gas would be drained out in lower viscosity, then form a small cells.
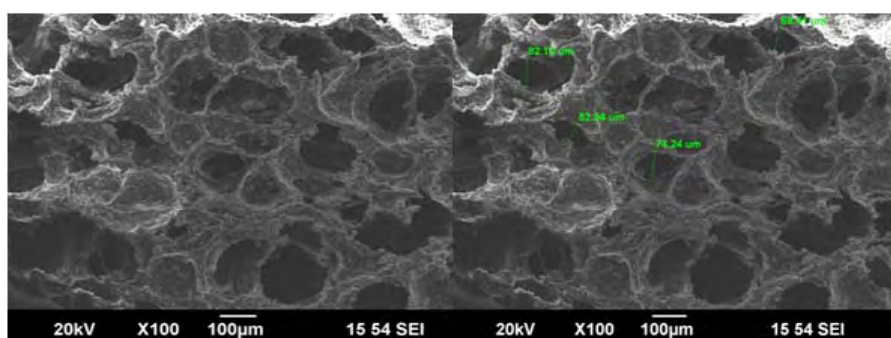
Fig. 8A.4 SEM photographs of razor cut surfaces of EPDM/FKM rubber foam

8A.3.5 Limiting Oxygen Index

The relative performance of hydrated fire retardant fillers in polymers strongly depends on the nature and the origin of the filler type and the chemical characteristics of the host polymer, in particular, its decomposition mechanism. In this connection, specific interactions may exist between certain polymers and fillers, which influence their mechanism of action [17].

The flame retardancy mechanism of ATH is based on its thermal decomposition between 200 ^{0}C and 400 ^{0}C. During this endothermic reaction, ATH releases its chemically bonded water (34.6 wt %), while aluminum oxide remains in the char residue. The water removes the heat energy from the burning zone by changing into vapor, and surrounds the

compound surface to lower the concentration of oxygen and burnable gases. Meanwhile, the aluminum oxide provides a protective layer on the surface of the burning material, preventing oxygen and heat reaching it. However, the decomposing temperature of ATH is as low as 220 ^{0}C and the efficiency of flame retardancy of ATH is low. So ATH can only be used in those polymers processed at low temperature, and in polyolefin, the overall ATH loading must be higher than 50 wt% to achieve useful flame-retarding properties, which will ruin the mechanical properties of whole material.

However, compared to alternative fire retardants, including halogen containing formulations, hydrated fillers are relatively ineffective, requiring addition levels of up to 50 wt % in order to achieve acceptable combustion resistance [18].

Table 8A.5 Limitting oxygen index of the prepared profiles

Sample name	LOI(%)
E_{mix}	46
EV_{mix}	48

The LOI of the prepared samples are given in table 8A.5. So from table 8A.5, it could be concluded that the char layer formed during the combustion process of EPDM/FKM blends based profiles had better structural strength and thermal stability, was effective in preventing heat transfer, hindered the spread of decomposition products to the flame region, and slowed down the rate of production of volatiles. Hence, the physical barrier was enhanced, which resulted in an enhancement of the flame-retarding properties.

8A.4 Conclusions

Blending of EPDM with FKM is found to be an effective way to improve the hot air aging resistance of EPDM. This method cannot only increase flame retardancy, but also improve heat–resistance. The experimental results indicated that the ADC blowing agent was more effective to produce EPDM and EPDM/FKM foam with more uniform cell structure and better cell distributions. The curing properties show that the optimum cure time (t_{90}) increased with the 20 phr replacement of EPDM by FKM. The addition of FKM does not have much influence on the density of EPDM. The addition of FKM into EPDM improved the mechanical properties of the EPDM. The optimum tensile properties of EPDM/FKM (80/20), suitable candidate for many applications such as: roof sealing sheets, playground mat, sealing profile for windows etc. LOI results confirmed that the blends have better flame resistance than EPDM. The formed char layer was effective in preventing heat transfer, hindered the spread of decomposition products to the flame region, and slowed down the rate of production of volatiles; hence the physical barrier was enhanced. The char can reduce the amount of combustible gases transported to the flame.

References

[1] Grand AF, Wilkie CA, 1st ed. New York: Marcel Dekker, 2000 [chapter 2].

[2] Chigwada G, Jash P, Jiang DD, Wilkie CA, Polym Degrad Stab 2005, 88, 382-93.

[3] Finberg I, Yaakov YB, Georlette P, Polym Degrad Stab 1999, 64, 465-70.

[4] Rosa ADL, Recca A, Carter JT, McGrail PT, Polymer 1999, 40, 4093-8.

[5] Smith R, Georlette P, Finberg I, Reznick G, Polym Degrad Stab 1996, 54, 167-73.

[6] Liaw DJ, Chang P, Polymer 1997, 38, 5545-50.

[7] Georlette P, Plast Addit Compound 2001, 3, 28-33.

[8] Hippi U, Mattila J, Korhonen M, Seppala, J. Polymer 2003, 44, 1193-201.

[9] Pinto UA, Visconte LLY, Nunes RCR, Eur Polym J 2001, 37, 1935-7.

[10] Du L, Qu B, Xu Z. Polym Degrad Stab 2006, 91, 995-1001.

[11] Lu H, Hu Y, Yang L, Wang Z, Chen Z, Fan W. Macromol Mater Eng 2004, 289, 984-9.

[12] Zilberman J, Hull TR, Price D, Milnes GJ, Keen F, Fire Mater 2000, 24, 159-64.

[13] Lynch TJ, Chen T, Riley D, Reinf Plast 2003, 47, 44-6.

[14] Zhang HY, Explosive 1993, 4, 26-33.

[15] Allcock HR, Lampe FW, James E, 3rd edn., 690. Mark, Pearson Education 2003, Inc., Indiana, USA.

[16] Yasin T, Ahmed S, Yoshii F, Makuuchi K, React. Funct. Polym. 2003, 57, 113–118.

[17] Hornsby PR, Macromol. Symp. 1996, 108, 203.

[18] Hornsby PR, Watson CL, Plast. Rubber. Process. Appl., 1989, 11, 45-51.

.....�saఇ.....

Chapter **9**

SUMMARY AND CONCLUSIONS

A detailed description on the major findings of the work done is reported in this chapter. The scope of future work is also mentioned.

In the manufacture of rubber products, the blending of rubbers produces new materials with a wide range of properties. When compared with the economical and technical uncertainties associated with synthesizing new polymeric materials, these blends have the potential to combine the attractive properties of the components present. EPDM is one of the fastest growing elastomers on industrial level as it is more stable than other conventional elastomers such as silicon rubber, butadiene rubber, butyl rubber, acrylo nitrile rubber, natural rubber and isoprene rubbers. It is amorphous and exhibit weak physico-mechanical properties. Reinforcing fillers and other additives are added to enhance the physico-mechanical properties of EPDM. One of the most important characteristics of EPDM is its ability to accommodate large quantities of fillers and other additives without affecting processability and without creating unnecessary instability in the composite structure. Apart from its applications in automotives, building, constructions, roof-sheeting, seals and for electrical purposes, EPDM is widely used for fabricating blends with general-purpose or specialty rubbers with a view to improve the properties.

For the past fifty years, fluroelastomers (FKM) are materials of choice to designers for specialized products, as it shows the best resistance of all rubbers to the attack of heat, chemicals and solvents. It finds

applications in aerospace, automotive, chemical and petroleum industries. EPDM is the material that has excellent thermal stability, weatherability and resistance to oxidation and ozone. Blending of EPDM with FKM is a potential measure to prepare materials with better overall properties. Even though a great deal of work has been carried out on EPDM based blends, a survey of literature reveals that the studies on EPDM/FKM blends are rather scarce. Present venture aims to prepare EPDM/FKM blends and evaluate their properties. However, the high incompatibility between FKM and EPDM restricts the attainment of the best properties because the properties of blends depend strongly on the compatibility of the components. Maleic anhydride grafted EPDM (MA-g-EPDM) was used as compatibilizer in EPDM/FKM blends and the properties of compatibilized blends were also studied.

Polymer composites find wide applications in various industrial sectors because of their light weight, design flexibility and processability. Flame retardants are chemical substances used in rubbers, thermoplastics, thermosets, textiles and coatings that inhibit or resist the spread of fire. In this work, attention was paid to evaluate the effect of different flame retardant fillers like ATH, CPE, DBBO, EG and Sb_2O_3 on the flammability, physico-mechanical and thermal properties of EPDM and EPDM/FKM blends, both compatibilized and uncompatibilized.

DC electrical conductivity studies were carried out for the composites containing EG. Dielectric parameters of the composites are required to assess their suitability for use in telecommunications, dielectric wave guides, lenses and microwave integrated circuits (MICs). With this view, the dielectric properties at microwave frequencies were studied for the

elastomeric composites containing EG and ATH. Recently, electronic devices and components have been rapidly developing and advancing. Thus, with increased usage of electronic devices, electromagnetic waves generated by electronic systems can potentially create serious problems such as malfunctions of medical apparatus and industry robots and can even cause harm to the human body. Therefore, in this work the utility of the EG based composites as electromagnetic interference (EMI) shielding material was also investigated. The major conclusions drawn from the study are summarized below:-

It is found that the best balance properties can be obtained by blending EPDM and FKM preferably in 50:50 (w/w) ratios. The morphological studies revealed the incompatibility of the blends. Still the mechanical properties of EPDM were improved with FKM addition. The thermal stability was found to be maximum for blends containing highest percentage of FKM. MA-g-EPDM was used as a compatibilizer for EPDM/FKM blends. The evaluation of mechanical properties and thermal stability of the compatibilized blends shows that the best properties were obtained when 5 phr of MA-g-EPDM was used.

The characterization of rubber blends, both compatibilized and uncompatibilized were also done with the help of dynamic mechanical analysis. The T_g of a polymer depends on the structure and co-operative mobility of the chain segments. For uncompatible and compatible EPDM/FKM blends, the tan δ versus temperature curve shows two damping peaks corresponding to the glass transition temperatures of individual polymers. From DMA studies, it is concluded that the individual rubbers followed their own behavior. Phase morphology is one of the significant properties of polymer blends. The morphological studies of the

blends revealed that incorporation of compatibilizer stabilized the morphology against coalescence and improved the interfacial adhesion by reducing the interfacial energy of the phases. It is concluded that the system is technologically compatible.

Studies of EPDM based composites with different fillers showed that cure characteristics of EPDM remain unaffected on addition of ATH, CPE, DBBO and EG. EPDM vulcanizates containing 25 phr ATH showed maximum tensile strength which indicates the high reinforcing effect of ATH on EPDM matrix. From the thermal analysis it is evident that ATH and CPE imparted maximum thermal stability to the composites. Flame retardant studies revealed that all fillers significantly retarded the process of burning. EG and DBBO are better flame retardants compared to ATH and CPE. SEM analysis revealed even distribution of ATH in the EPDM matrix which contributed to improvement in mechanical properties.

The cure characteristics, mechanical properties, DC electrical conductivity, thermal and dielectric properties of the composites based on compatibilized and uncompatibilized EPDM/FKM (50/50; w/w) blends filled with increasing amounts of expanded graphite (EG) were evaluated. The cure time decreased at higher loading due to the increased thermal transition of the matrix in presence of EG. The tensile properties of all the composites, especially those with compatibilizer, increased with aging. The AC and DC conductivities increased with increase in EG loading, due to the formation of enhanced conductive networks by EG platelets. The dielectric permittivity and dielectric loss of the composites at microwave frequencies increased with increase in frequency and with EG loading. The flammability and thermal characteristics improved by the addition of EG.

The cure characteristics, thermal stability and microwave characteristics of EPDM/ATH, FKM/ATH and EPDM/FKM blend/ATH systems were investigated. The reinforcing effect of ATH on EPDM, FKM and their blends was also explored in detail. The addition of ATH does not affect the cure characteristics of EPDM while there is substantial reduction in cure time of FKM rubber with increase in concentration of ATH. Tensile properties of both EPDM and FKM improved by the addition of ATH. The thermal stability of EPDM increased with the addition of ATH while decreased in the case of FKM. Storage modulus increased with the addition of ATH, reached a maximum and then decreased for both the matrices.

Blending of EPDM rubber with FKM is found to be an effective way to improve the flame-retardancy of EPDM. Flame retardancy mechanisms of halogenated and non-halogenated flame retardants were also investigated for EPDM/FKM rubber blends. It is found that compared to pure EPDM/FKM blends, their composites showed much improvement in flame retardation. Adding flame retardant additives to EPDM/FKM blends promoted the formation of dense char during the burning process. The char can reduce the amount of combustible gases transported to the flame. This method can not only increase flame retardancy, but also improve mechanical properties. Blending of EPDM with FKM was also found to be an effective way to improve the hot air aging resistance of EPDM.

Rubber composites have significant role in engineering applications owing to their excellent insulation properties and mechanical properties. Flame retardancy is a major criterion for such applications. The flame retardant additives filled EPDM and EPDM/FKM (80/20) blend based insulation profiles were developed and the important parameters discussed.

The prepared composites are found to have good microwave absorption properties. Therefore in the last part, the EMI shielding effectiveness of the composites based on EG was explored in the frequency range 8-12 GHz. The samples were found to have appreciable shielding effectiveness depending on loading of EG and in turn, the conductivity.

Future scope of the work

1) **Fabrication of useful products:** The prepared composite can be used safely in many applications such as automotive insulation materials, roof sealing sheets, playground mat, sealing profile for windows, cars etc.

2) **Studies on the effect of different compatibilizers on the properties of EPDM/FKM blends:** In the present study only one compatibilizer was employed for the preparation of blends. The effect of other compatibilizers may be investigated.

3) **Reinforcing mechanism:** In the case of FKM/ATH composites, the reinforcing mechanism of ATH filler particles can be studied. The reduction of cure time holds promise for reduction of the moulding cycles. Studies have to be made to commercially employ this result.

4) **Replacement of halogenated flame retardants by non-halogenated ones:** To develop more and more environmental friendly flame retardants filled rubber composites, to replace toxic halogenated flame retardants by keeping better flame resistance.

5) **Studies on the development of new or modified flame retardant materials**: The strategy for this can be two-fold: existing flame retardant materials can be modified to get materials of improved mechanical properties and second approach is engineering polymers can be modified by blending or co-reacting with thermally stable materials.

6) **Oil absorption studies:** Since this particular EPDM/FKM blend system is aimed at developing oil resistant materials, the swelling studies can be extended to various oils under accelerated conditions.

.....ೞೞ.....

Abbreviations and Symbols

ASTM	American Society for Testing and Materials
$CaCO_3$	Calcium Carbonate
CNT	Carbon nano tube
CS	Crystallite size
DMA	Dynamic Mechanical Analysis
DSC	Differential Scanning Calorimetry
FTIR	Fourier Transform Infrared
LOI	Limiting Oxygen Index
MHz	Mega Hertz
PP	Polypropylene
PVA	Polyvinyl alcohol
SEM	Scanning Electron Microscopy
SWNT	Single walled carbon nanotube
TGA	Thermo gravimetric analysis
ZnO	Zinc oxide
ACN	Acrylonitrile content
AFM	Atomic Force Microscopy
BR	Butadiene rubber
CB	Carbon black
CPE	Chlorinated polyethylene
CR	Chloroprene rubber
CRI	Cure Rate Index
DBP	Dibutyl phthalate
DMTA	Dynamic Mechanical Thermal Analysis
DTG	Derivative thermogravimetry
EM	Electron Microscopy
ENR	Epoxidised natural rubber
EPDM	Ethylene-propylene-diene-monomer
EPR	Ethylene–propylene rubber
HAF	High abrasion furnace
IIR	Isoprene-co-isobutylene rubber
IR	Infrared spectroscopy
ISAF	Intermediate super abrasion furnace
M100	Modulus at 100% elongation
MA	Maleic anhydride

MA-g-EPDM	Maleic anhydride-grafted -EPDM
MBTS	Mercaptobenzothiazyl disulphide
MWCNT	Multi walled carbon nanotubes
NBR	Nitrile rubber
NMR	Nuclear Magnetic Resonance
NR	Natural Rubber
PEO	Poly (ethylene oxide)
PHEPDM	Phenol hydroxy EPDM
phr	Parts per hundred rubber
PUR	Polyurethane rubber
SAXS	Small-angle X-ray Scattering
SBR	Styrene-butadiene rubber
SEM	Scanning Electron Microscopy
SMR L	Standard Malaysian rubber latex
SRF	Semi reinforcing furnace
TEM	Transmission Electron Microscopy
TS	Tensile strength
UFPR	Ultra-fine full-vulcanized powdered rubber
XNBR	Carboxylated nitrile rubber
XSBR	Carboxylated styrene-co-butadiene rubber
ENB	5-Ethylidene-2-norbornene
HD	1, 4-Hexadiene
DCPD	Dicyclopentadiene
PO	Peroxide
MBT	Mercaptobenzothiazole
DPG	Diphenyl guanidine
FKM	Fluoroelastomers
PTFE	Polytetrofluoroethylene
VF_2	Vinylidine fluoride
CTFE	Chlorotrifluoroethylene
HFP	Hexafluoropropylene
CCl_4	Carbon tetrachloride
HF	Hydrogen fluoride
MgO	Magnesium oxide
CaO	Calcium oxide
$Ca(OH)_2$	Calcium hydroxide
PbO	Litharge (Lead oxide)
MT	Medium thermal

$BaSO_4$	Barium sulphate
PET	Pentaerytritol stearate
SiC	Silicon carbide
HFFR	Halogen free flame retardant
GC	Gas chromatography
SANS	Small-angle neutron scattering
ToF-SIMS	Time-of-flight secondary ion mass spectroscopy
IBR	Isoprene–butadiene rubber
ISAF	Intermediate super abrasion furnace black
D	Diffusivity
DIPTRI	Bis (diisopropyl) thiophosphoryl trisulfide
DIPTET	Bis (diisopropyl) thiophosphoryl tetrasulfide
UFNBRPR	Ultra-fine full vulcanized powdered NBR rubber
TS	Tensile strength
CFCs	Chlorofluorocarbons
CO	Carbon monoxide
UV	Ultraviolet
CF	Carbon fiber
MICs	Microwave-integrated circuits
EMI	Electromagnetic interference
LRU	Line replaceable unit
MU	Mooney unit
ATH	Aluminium hydroxide
DBBO	Decabromo biphenyl oxide
EG	Expanded Graphite
Sb_2O_3	Antimony trioxide
CBS	N-Cyclohexyl-2-benzothiazolesulfenamide
TMTD	Tetramethylthiuram disulfide
ZDEC	Zinc diethyldithiocarbamate
ZDBC	Zinc dibutyldithiocarbamate
ZBEC	Zinc dibenzyldithiocarbamate
VGC	Viscosity gravity constant
CPW	Chlorinated paraffin wax
CaO	Calcium oxide
PEG	Polyethylene glycol
ADC	Azodicarbonamide
MEK	Methyl ethyl ketone
RPA	Rubber Process Analyser

OI	Oxygen index
BR	Burning rate
HB	Horizontal burning
MVQ	Methyl vinyl silicone rubber
EB	Elongation at break
GICs	Graphite intercalation compounds
RF	Radio frequency
IFRs	Intumescent flame retardants
MPa	Mega pascal
CFAs	Chemical foaming agent
AC	Alternating current
ML	Mooney viscosity -large rotor
SE	Shielding effectiveness
XRD	X-ray diffraction analysis
POSS	Polyhedral oligomeric silsesquioxane
E	Apparent degradation activation energy
dB	Decibels
R	Universal gas constant
%	Percentage
ΔT	Temperature change
GPa	Giga Pascal
kJ/mol	Kilo Joule per mole
mm/min	Milli meter per minute
N/mm^2	Newton per millimetre square
cm^3	Centimeter cube
μm	Micrometer
Mw	Molecular weight
MPa	Mega Pascal
m^2g^{-1}	Meter square gram inverse
nm	Nanometer
T_g	Glass transition temperature
wt %	Weight percentage
ºC	Degree celcius
ΔG_{mix}	Gibb's free energy of mixing
ΔH_{mix}	Enthalpy of mixing
ΔS_{mix}	Entropy of mixing
T	Absolute temperature
E_f	Young's modulii of filled vulcanizates

E_g	Young's modulii of gum vulcanizates
φ_A	Volume fraction of polymer A
φ_B	Volume fraction of polymer B
χ_A	Degrees of polymerization of polymer A
χ_B	Degrees of polymerization of polymer B
χ_{AB}	Interaction parameter of polymer A & B
δ_A	Solubility parameter of the polymer A
δ_B	Solubility parameter of the polymer B
'χ'	Interaction parameter
D_{min}	Minimum torque
D_{max}	Maximum torque
T_{10}	Scorch time
T_{90}	Optimum cure time
G'	Storage modulus
G''	Loss modulus
$G*$	Complex modulus
V_r	Volume fraction of rubber
M_s	Mass of solvent sorbed
MM_s	Molar mass of solvent
M_p	Mass of polymer
Q	Ratio of swollen weight to original weight
W_1	Weight of the sample before swelling
W_2	Weight of the sample after swelling
M_c	Number-average molecular weight between crosslinks
F	Weight fraction of insoluble components
A_0	Weight of the absorbed solvent corrected for the Swelling increment
ρ_r	Density of rubber
ρ_s	Density of the solvent
'σ'	Electrical conductivity
'I'	Current through the electrode in amperes
'V'	Voltage in volts
'l'	Thickness of the sample in centimeters
'A'	Area of contact of the electrodes with the sample in centimeter square
GHz	Gega hertz
α	Decomposed fraction

η_r	Relative viscosity
M_r	Relative modulus
m_f	Mass of filler in the compound
α_f	Specific constant for the filler
T_0	Onset degradation temperature
r	Correlation coefficient
S/cm	Siemens per centimeter
'λ'	Wavelength of X ray
'β'	Full width at half maximum of diffraction peak (FWHM)
'Θ'	Angle corresponding to the peak
d	Average size of crystallites
$\tan \delta$	Loss tangent
V_c	Volume of the cavity
V_s	Volume of sample
ε^*	Complex permittivity
ε'	Real part of complex permittivity
ε''	Imaginary part of complex permittivity
π	pi

.....ಬಂ.....

List of Publications

Publications in international/national journals

[1] **Ajalesh Balachandran Nair**, Philip Kurian, Rani Joseph. Effect of expanded graphite on thermal, mechanical and dielectric properties of ethylene-propylene-diene terpolymer/hexa fluoropropylene-vinylidinefluoride dipolymer rubber blends. *European Polymer Journal,* Volume 49, 2013, p 247-260. DOI: 10.1016/j.eurpolymj.2012. 08.014.

[2] **Ajalesh Balachandran Nair**, Ullas G Kalappura, Philip Kurian, Rani Joseph. Dielectric behavior of aluminium hydroxide filled oil-extended ethylene-propylene-diene-monomer rubber composites in microwave fields. *Polymer Engineering and Science*, Volume 53, 2012, p 699-706. DOI: 10.1002/pen.23314.

[3] **Ajalesh Balachandran Nair**, Philip Kurian, Rani Joseph. Ethylene–propylene–diene terpolymer/hexa fluoropropylene–vinylidinefluoride dipolymer rubber blends: Thermal and mechanical properties. *Materials & Design*, Volume 36, 2012, p 767-778. DOI: 10.1016/j.matdes.2011.11.062.

[4] **Ajalesh Balachandran Nair**, Philip Kurian, Rani Joseph. Effect of aluminium hydroxide, chlorinated polyethylene, decabromobiphenyl oxide and expanded graphite on thermal, mechanical and sorption properties of oil-extended ethylene–propylene–diene terpolymer rubber. *Materials & Design*, Volume 40, 2012, p 80-89. DOI: 10.1016/j.matdes.2012.03.032.

[5] **Ajalesh Balachandran Nair**, Rani Joseph. Novel technologically compatibilized ethylene-propylene-diene terpolymer/fluorocarbon rubber blend: Cure characteristics and mechanical properties- Part 1, *polymer SOCIETY*, Volume 5, 2012, p 36-39.

[6] **Ajalesh Balachandran Nair**, Rani Joseph. Polymer blends and composites from non-polar/polar systems. *Journal of Rubber Research.* Indian Rubber Board. India (in press).

[7] **Ajalesh Balachandran Nair**, Rani Joseph. Novel technologically compatibilized ethylene-propylene-diene terpolymer/fluorocarbon rubber blend: Solvent sorption and thermogravimetric analysis- Part 2, *polymer SOCIETY*, Volume 6, 2013, p 15-18.

[8] **Ajalesh Balachandran Nair**, Philip Kurian, Rani Joseph. Studies on EPDM/FKM blends: Effect of MA-g-EPDM as a compatibilizer. *Journal of Polymer materials: An international journal*, Volume 30, 2013, p 37-51.

[9] **Ajalesh Balachandran Nair**, Sreekala P S, Rani Joseph. Electromagnetic interference shielding effectiveness of expanded graphite filled ethylene-propylene-diene terpolymer and ethylene-propylene-diene terpolymer/hexa fluoropropylene-vinylidinefluoride dipolymer rubber blends (Communicated).

[10] **Ajalesh Balachandran Nair**, Philip Kurian, Rani Joseph. Dielectric behaviour of expanded graphite filled oil-extended ethylene-propylene-diene-monomer rubber composites in microwave fields (Communicated).

[11] **Ajalesh Balachandran Nair**, Rani Joseph. Effect of aluminium tri-hydroxide in hexa fluoropropylene-vinylidinefluoride dipolymer rubber: Thermal and mechanical properties (Communicated).

[12] **Ajalesh Balachandran Nair**, Rani Joseph. Effect of antimony trioxide on thermal, mechanical and flame retardant properties of ethylene-propylene-diene terpolymer/fluorocarbon rubber blends (Communicated).

[13] **Ajalesh Balachandran Nair**, Dhanya Vijayan, Rani Joseph. Preparation, characterization and use of aluminum tri-hydroxide as reinforcing filler in ethylene-propylene-diene terpolymer rubber (Communicated).

[14] **Ajalesh Balachandran Nair**, Rani Joseph. Effect halogenated flame retardants in ethylene-propylene-diene terpolymer/fluorocarbon rubber blends: Thermal and mechanical properties (Communicated).

[15] **Ajalesh Balachandran Nair**, Rani Joseph. Morphology and dynamic mechanical analysis of ethylene-propylene-diene terpolymer/fluorocarbon rubber blends (Communicated).

Presentations in Conferences

[1] **Ajalesh Balachandran Nair**, Dhanya Vijayan, Rani Joseph. Reinforcing effect of aluminium hydroxide: in ethylene-propylene-diene terpolymer rubber and fluorocarbon rubber. INDIA rubber expo 2013, Mumbai, p 89-92.

[2] **Ajalesh Balachandran Nair**, Dhanya Vijayan, Rani Joseph. Preparation and use of aluminum tri-hydroxide as novel filler in Viton, EPDM and NBR. International conference on rubber and rubber like materials (ICRRM- 2013), Indian Institute of Technology (IIT), Kharagpur, p 37.

.....ఴఴ.....

Curriculum Vitae

Ajalesh Balachandran Nair
Kochu moothedathu house
U.C.College (P.O)
E.Kadungalloor, Aluva-2
Eranakulam (Dist.),
Kerala, India.

Tel: 0484-6595732
Ph: +91-9249512906
E mail: ajilesh4kannan@gmail.com

Personal Details

Nationality	:	Indian
Sex and Marital Status	:	Male, Single
Language Proficiency	:	English, Hindi, Malayalam
Present Address	:	Research Scholar Department of Polymer Science and Rubber Technology, Cochin University of Science and Technology (CUSAT), Cochin, Pin: 682022 Kerala, India. Ph: +91-4842575723 E mail: ajilesh@cusat.ac.in
Educational qualifications:		M.Sc. Chemistry, Mahatma Gandhi University, Kerala, India
		Post Graduate Diploma offered by Indian Rubber Institute & Indian Institute of Technology (IIT), Kharagpur
Research experience	:	Five years in Polymer Science and Rubber Technology and one year and three months in Inorganic and Analytical chemistry
Teaching experience	:	Two Years (Engineering Chemistry)

List of other research publications

Book Chapters

1. **Ajalesh Balachandran Nair**, P. Sivasubramanian, M. S. Sreekala. *Environmental Effects, Biodegradation and Life Cycle Analysis of Fully Biodegradable "Green" Composites* (Chapter-15), *Biocomposites*, Vol-3, p 531-586, 2013, Wiley-VCH Verlag & Co. KGaA, Germany.

2. **Ajalesh Balachandran Nair**, Rani Joseph. *Eco-friendly biocomposites of natural rubber and natural fiber* (Chapter-12), *Chemistry, manufacture and applications of natural rubber,* Woodhead Publishing Ltd., Cambridge, UK, September 2012 (in press).

3. **Ajalesh Balachandran Nair**, Rani Joseph. *Use of coir fibers in polymer products*. "ICAR publication on coconut fibre". National Institute for Research on Jute and Allied Fibre Technology, ICAR, Kolkata, India (in press).

4. **Ajalesh Balachandran Nair**, Rani Joseph. *Effect of hybrid fillers in the non linear viscoelasticity of rubber composites and nanocomposites, Non-linear viscoelasticity of rubber composites and nanocomposites* (Series title: Advances in Polymer Science), Springer (Under preparation).

Other publications in International Journals

5. D. S. Pramila Devi, **Ajalesh. B. Nair**, T. Jabin, Sunil K. N. Kutty. Mechanical, Thermal, and Microwave Properties of Conducting Composites of Polypyrrole/Polypyrrole-Coated Short Nylon Fibers with Acrylonitrile Butadiene Rubber. *J. Appl. Polym. Sci*. 2012, 126: 1965-1976.

   DOI: 10. 1002/ app. 36924.

6. Preetha K Nair, **Ajalesh Balachandran Nair,** Rani Joseph. Carboxylated acrylo nitrile butadiene rubber latex/kaolin clay nanocomposites (submitted to *Applied Clay Science*).

7. Saisy K Esthappan, **Ajalesh Balachandran Nair,** Rani Joseph. Crystallization, mechanical, thermal and flow properties of polypropylene/ zinc oxide nanocomposites. *Composites Part B: Engineering (in press)*.

8. A. P. Susamma, N.M. Claramma, **Ajalesh. B. Nair**, A.P Kuriakose. New Binary Systems Containing TMTD-Amidino Phenyl Thiourea and CBS–Amidinophenyl Thiourea for the Vulcanization and Rheological Behavior of Natural Rubber Latex. *J. Appl. Polym. Sci*. 2009, 115: 2310-2316.

   DOI: 10.1002/app.31360

Other Presentations in International/National Conferences

1. **Ajalesh Balachandran Nair**, K. Girish Kumar. Potentiometric determination of Copper ions using 5, 10, 15, 20-tetrakis (3-methoxy-4-hydroxy phenyl) porphyrin modified carbon paste electrode (Matcon-2010), conducted by Dept. of Applied Chemistry, CUSAT, Kerala, India.

2. A. P Susamma, Alexander Bismark**, Ajalesh B Nair,** E. M. Mohammed. Rubber nanocomposites with nickel ferrite- rubber nanocomposites with nickel ferrite-preparation, mechanical and electrical characterization (Matcon-2010) conducted by Dept. of Applied Chemistry, CUSAT, Kerala, India.

3. **Ajalesh Balachandran Nair**, A. P Susamma. Participated and presented a paper in the International Conference on Materials Science Research and Nanotechnology (ICMSRN-2008) at the Mother Teresa Women's University, Kodaikanal during 27-29 Feb 2008.

4. A. P Susamma, **Ajalesh Balachandran Nair.** Effective use of ecofriendly waste materials like rice husk and coir pith as fillers and oil from refinery sludge as process aid in the vulcanization of rubber. International Conference on Biodiversity Conservation and Management (BIOCAM-2008), 3-6th February 2008, Cochin, p 227-228.

5. **Ajalesh B Nair**, Susamma A P. Novel accelerator system in the vulcanization of NR-SBR blends. National Symposium "Polymers-Prospects and Challenges" held at National Institute of Technology, Calicut, 4-5th April 2008.

6. **Ajalesh B Nair**, Susamma A P. Effective use of oil from refinery sludge as process aid in the vulcanization of Natural rubber and their blends. 7th National Seminar on Current Advances in Chemical Science- ACS 2008, 26th to 27th November 2008, Cochin, p 42-44.

7. Vidya Francis, **Ajalesh Balachandran Nair,** Aswathy N. S, Eby Thomas Thachil**.** Modification of LDPE with Casein. 7th National Seminar on Current Advances in Chemical Science- ACS 2008, 26th to 27th November 2008, Cochin, p 95-98.

.....౸౸.....